[redacted]

Copy 690

NASA TM X-494

Declassified by authority of NASA
Classification Change Notices No. 113
Dated ** 6/28/67

NASA TM X-494

TECHNICAL MEMORANDUM

X-494

STATIC LONGITUDINAL STABILITY CHARACTERISTICS OF VARIOUS MERCURY ESCAPE CONFIGURATIONS AND OF A PROPOSED ALTERNATE ESCAPE CONFIGURATION FOR MACH NUMBERS OF 0.05 TO 9.60

By Robert P. Smith and William C. Moseley, Jr.

Space Task Group
Langley Field, Va.

GPO PRICE $ _____

CFSTI PRICE(S) $ _____

Hard copy (HC) 3.00

Microfiche (MF) .65

ff 653 July 65

[redacted]

FACILITY FORM 602

N67 [illegible] (ACCESSION NUMBER)

(THRU)

180 (PAGES)

1 (CODE)

TMX-494 (NASA CR OR TMX OR AD NUMBER)

31 (CATEGORY)

NATIONAL AERONAUTICS AND SPACE ADMINISTRATION

WASHINGTON July 1961

[redacted]

[redacted] Downgrade [redacted]

[redacted] 12 years

Declassified by authority of NASA
Classification Change Notices No. 113
Dated ** 6/28/67

DECLASSIFIED

NATIONAL AERONAUTICS AND SPACE ADMINISTRATION

TECHNICAL MEMORANDUM X-494

STATIC LONGITUDINAL STABILITY CHARACTERISTICS OF VARIOUS MERCURY ESCAPE CONFIGURATIONS AND OF A PROPOSED ALTERNATE ESCAPE CONFIGURATION FOR MACH NUMBERS OF 0.05 TO 9.60*

By Robert P. Smith and William C. Moseley, Jr.

SUMMARY

This paper presents a summary of the available wind-tunnel results on the static longitudinal stability characteristics of the basic Mercury escape configuration and modifications made to the basic escape configuration up to, but not including, present production configurations. The investigations were made at the National Aeronautics and Space Administration Langley Research Center and the U.S. Air Force Arnold Engineering and Development Center. The tests covered a Mach number range from 0.05 to 9.60 at Reynolds numbers from 0.14×10^6 to 14.5×10^6 (based on capsule maximum diameter). Results are also presented for tests on a proposed alternate escape configuration.

The basic escape configuration was stable near an angle of attack of 0° throughout the Mach number range investigated (0.05 to 9.60). However, in the transonic speed range the configuration was stable over a limited angle range (up to about 15°), and in the supersonic speed range the configuration was stable up to an angle of attack of about 30°. The addition of igniter strips and associated conduits and junction boxes resulted in a further decrease in the static stability in the transonic speed range. The addition of a turning vane at the base of the escape rocket and/or a flow separator at the base of the escape tower resulted in improved stability in the subsonic, transonic, and low supersonic speed ranges.

The finned-adapter configuration with the various tail fins was unstable in the high subsonic Mach number range and became stable at a Mach number of about 1.00. As the Mach number was increased above a Mach number of 1.00, the stability of the configuration decreased until at a Mach number of 6.86 the configuration was neutrally stable.

*Title, Unclassified.

[redacted]

INTRODUCTION

One of the primary concepts of the Project Mercury program is pilot safety under any and all conditions. The capsule design incorporates an escape system that will safely remove the capsule and its occupant from the booster in the event of a malfunction. The escape system consists of a tubular tower-rocket structure attached to the capsule and the resulting combination is referred to as the escape configuration. The escape system is unique in that it adds very little drag to the configuration and it can be jettisoned when no longer needed and thereby reduce the orbital weight. The configuration on which the early wind-tunnel tests were made is referred to as the basic escape configuration. (See, for example, refs. 1 to 4.) As the research and development program of Project Mercury progressed, many modifications and additions were made to the basic escape configuration before the present production configuration was determined. The purpose of this paper is to present a summary of the results of wind-tunnel tests made during the development of the Mercury escape configuration up to but not including the final production configuration. The results of wind-tunnel tests of the static longitudinal stability characteristics of the production escape configuration are given in reference 5. Also included in this paper is a summary of the results of wind-tunnel tests of a proposed alternate escape configuration.

The tests were made by personnel of the NASA Langley Research Center and the U.S. Air Force Arnold Engineering Development Center to determine the necessary aerodynamic characteristics. The tests were made at Mach numbers from 0.05 to 9.60 at angles of attack from 0° to 120°.

SYMBOLS

The data are referred to both the body and stability systems of axes and are presented in the form of standard coefficients of forces and moments. Figure 1 indicates the positive direction of the forces, moments, and angular displacements. Pitching-moment coefficients for the Mercury escape configurations are presented about a center of gravity, located 65 inches from the maximum diameter of the capsule. Pitching-moment coefficients for the finned-adapter escape configuration are presented about a center of gravity which is located 55.70 inches from the base of the adapter.

[redacted]

DECL[redacted]IFIED

C_A	axial-force coefficient, $\frac{\text{Axial force}}{qS}$
C_D	drag coefficient, $C_A \cos \alpha + C_N \sin \alpha$
$C_{D,\alpha=0^\circ}$	drag coefficient at $\alpha = 0^\circ$
C_L	lift coefficient, $C_N \cos \alpha - C_A \sin \alpha$
C_l	rolling-moment coefficient, $\frac{\text{Rolling moment}}{qSd}$
C_m	pitching-moment coefficient, $\frac{\text{Pitching moment}}{qSd}$
C_N	normal-force coefficient, $\frac{\text{Normal force}}{qS}$
C_n	yawing-moment coefficient, $\frac{\text{Yawing moment}}{qSd}$
C_Y	side-force coefficient, $\frac{\text{Side force}}{qS}$
C_{L_α}	lift-curve slope per degree at $\alpha = 0^\circ$, $\frac{\partial C_L}{\partial \alpha}$
C_{m_α}	pitching-moment curve slope per degree at $\alpha = 0^\circ$, $\frac{\partial C_m}{\partial \alpha}$
C_{N_α}	normal-force curve slope per degree at $\alpha = 0^\circ$, $\frac{\partial C_N}{\partial \alpha}$
d	maximum diameter of capsule, ft
M	free-stream Mach number
p	free-stream static pressure, lb/sq ft
q	free-stream dynamic pressure, $0.7\ pM^2$, lb/sq ft
R	Reynolds number based on maximum diameter of capsule
S	maximum capsule cross-sectional area, sq ft

[redacted]

α angle of attack of model center line, deg

ϕ roll angle simulated by location of rocket igniter-cable fairing on the escape rocket (positive with a clockwise rotation looking upstream), deg

TEST FACILITIES

The tests were made at the Langley Research Center and at the Arnold Engineering and Development Center (AEDC). The following facilities were utilized: the Langley free-flight tunnel, the Langley 8-foot transonic pressure tunnel, the Langley 4-foot supersonic pressure tunnel, the Langley Unitary Plan wind tunnel, the Langley high Mach number jet, the Langley 20-inch hypersonic tunnel, the Langley 11-inch hypersonic tunnel, and the AEDC 16-foot transonic propulsion wind tunnel. More complete descriptions of the facilities can be found in references 6 to 12. A summary of the test conditions in the various facilities is given in table I.

MODELS

Full-scale dimensions of the basic escape configuration are shown in figure 2. The basic configuration was the configuration on which the early wind-tunnel tests were made. The modifications made to the basic escape configuration are given in figures 3 to 5. Figure 3 shows the basic escape configuration with three different sets of rocket igniter-cable fairings that are attached to the escape rocket. A comparison of the basic escape configuration shown in figure 2 with the configuration shown in figure 3 shows that the parachute-housing diameter was increased from 30 inches to 32 inches. Junction boxes were also added to this configuration at the base of the escape rocket.

Additional modifications made to the escape configuration are shown in figure 4. The modifications included tangential igniter-cable fairings and associated straps and clamps attached to the escape rocket, and igniter-cable conduits and junction boxes attached to the base of the escape tower. Configurations which were modified with turning vanes are denoted by numbers; for example, in the configuration 22.75D-30.00° the diameter of the turning vane is 22.75 inches and the afterbody angle of the turning vane is 30.00°. Also the following stability improving devices were tested: (1) original clamp ring, (2) 4 flow separators, and (3) 7 turning vanes.

Shown in figure 5 is the original basic escape configuration with rocket igniter-cable conduit, junction boxes, 45° flow separator, and various rocket-face cant angles. It should be noted that this configuration was tested with the 30-inch-diameter parachute housing and without an aerodynamic spike on the front of the escape rocket.

Figure 6 shows full-scale dimensions of the proposed alternate escape configuration. This particular configuration will be referred to as the finned-adapter escape configuration throughout this paper. The various configurations tested in the tunnels are described in table II.

PRESENTATION OF RESULTS

Estimates of the accuracy of the data are given in table III. These estimates were based on balance calibrations and repeatability of data measurements. The data are presented as follows:

	Figure
Aerodynamic characteristics of basic escape configuration	7 to 10
Aerodynamic characteristics of escape configuration with 1.72 inch by 1.40 inch rocket igniter-cable fairings at Mach numbers from 0.50 to 1.50. $R \approx 6 \times 10^6$	11
Effect of Reynolds number on the aerodynamic characteristics of the escape configuration with 1.72 inch by 1.40 inch rocket igniter-cable fairings. M = 0.50 to 1.50	12
Effect of rocket igniter-cable fairings on the aerodynamic characteristics of the escape configuration. M = 0.50 to 1.50; $R \approx 6 \times 10^6$	13 to 14
Effect of rocket-face cant angles on the aerodynamic characteristics of the escape configuration. M = 0.50 to 2.01	15
Effect of turning-vane afterbody angles on the aerodynamic characteristics of the escape configuration. M = 0.50 to 1.50	16
Effect of turning-vane diameter on the aerodynamic characteristics of the escape configuration. M = 0.50 to 1.50	17

[redacted]

Figure

Effect of escape rocket turning-vane exit area on the aerodynamic characteristics of the escape configuration. M = 0.50 to 1.50. 18
Effect of various flow separators on the aerodynamic characteristics of the escape configuration (without turning vane). M = 0.50 to 1.50. 19
Effect of various flow separators on the aerodynamic characteristics of the escape configuration (with turning vane). M = 0.50 to 1.50. 20
Effect of turning vanes and flow separators on the aerodynamic characteristics of the escape configuration 21
Comparison of the aerodynamic characteristics of various escape configuration modifications. M = 0.50 to 1.50 . . . 22
Effect of ramp size at the base of the escape rocket on the aerodynamic characteristics of the escape configuration. M = 0.50 to 1.50 23
Effect of fin area and nose shape on the aerodynamic characteristics of the finned-adapter escape configuration . . . . . 24 to 30
Effect of fin area and fin orientation on the aerodynamic characteristics of the finned-adapter escape configuration. . . . . 31 to 34
Effect of fin area on the aerodynamic characteristics of the finned-adapter escape configuration. . . . . 35 to 37
Summary of the longitudinal stability characteristics of the basic escape configuration 38
Summary of the longitudinal stability characteristics of the escape configuration with and without rocket igniter-cable fairings. 39
Summary of the longitudinal stability characteristics of the escape configuration with and without various rocket-face cant angles 40
Summary of the longitudinal stability characteristics of the escape configuration with various turning-vane afterbody angles. 41
Summary of the longitudinal stability characteristics of the escape configuration with various turning-vane diameters 42
Summary of the longitudinal stability characteristics of the escape configuration with various flow separators (with and without turning vanes) 43
Summary of the longitudinal stability characteristics of the escape configuration with various configuration modifications 44

CONF[redacted]L

Figure

Summary of the longitudinal stability characteristics of the finned-adapter escape configuration 45

AERODYNAMIC CHARACTERISTICS OF ESCAPE CONFIGURATION

Basic Configuration

The variation of pitching-moment coefficient with angle of attack (shown in figs. 7 to 10) indicates that the basic Mercury escape configuration is statically stable near $\alpha = 0^{\circ}$ throughout the Mach number range investigated. However, for subsonic and transonic Mach numbers ($M = 0.05$ to $M = 1.14$), the configuration is stable over a limited α range (up to $\alpha = 15^{\circ}$ at $M = 0.05$ and up to $\alpha = 16^{\circ}$ at $M = 1.14$). The symbol change on the Langley 8-foot tunnel data (fig. 7) denotes a change in tunnel sting or support arrangement, since a single arrangement did not allow testing through the entire angle-of-attack range desired.

Data presented in figure 10 for $M = 9.60$ show the effects of rotating the tower 180° about the longitudinal axis. The normal position (flat down) refers to tower legs being subjected to the free-stream velocity when the escape configuration is at a positive angle of attack. (See section C-C of fig. 2.) As seen from these data, rotation of the escape tower 180° produced little or no effects on all coefficients for this particular Mach number.

Configuration With and Without Various Rocket Igniter-Cable Fairings

In order to determine the aerodynamic effects of adding external rocket igniter-cable fairings to the basic escape configuration, a limited investigation was conducted in the Arnold Engineering Development Center's 16-foot transonic propulsion wind tunnel. (See ref. 13.) During this investigation, three different sets of fairings were tested (two rectangular and one cylindrical) to evaluate the effects of size and shape of external fairings on the longitudinal stability characteristics. (See fig. 3.) The Mach number range that was covered varied from 0.50 to 1.50.

The larger set of the rectangular fairings (1.72 inch by 1.40 inch) was tested through an angle-of-attack range of 0° to 115° at $R \approx 6 \times 10^{6}$, and through an angle-of-attack range of 0° to 46° at $R = 10.90 \times 10^{6}$ to 12.70×10^{6}. Results obtained from this particular phase of the

investigation are presented in figures 11 and 12. Comparison of the pitching-moment coefficients for the escape configuration with the 1.72 inch by 1.40 inch rectangular fairings (fig. 11) to the basic escape configuration without fairings (fig. 7) indicates the longitudinal stability was reduced at low angles of attack with the addition of the fairings. The escape configuration with the 1.72 inch by 1.40 inch rectangular fairings was tested at higher Reynolds numbers between 10.90×10^6 and 12.70×10^6. The data show little or no effect of varying the Reynolds number (fig. 12) on the longitudinal aerodynamic characteristics.

Also, the data of figures 11 and 12 show that at an angle of attack of about 35° there were large effects on the lateral coefficients C_n, C_Y, and C_l. These effects were attributed to the asymmetrical location of the fairings. In an attempt to determine the effect of fairing size, tests were made with $\frac{1}{2}$-size fairings and with fairings removed. Results from these tests are presented in figure 13. The data on this figure indicate that the escape configuration with fairings removed resulted in low lateral coefficients at $\alpha = 65^\circ$ to $\alpha = 80^\circ$. The $\frac{1}{2}$-size fairings produced almost the same effects as the large 1.72 inch by 1.40 inch rectangular fairings.

Since all the igniter-cable fairings appeared to have large effects on the lateral stability coefficients at $\alpha = 65^\circ$ to $\alpha = 80^\circ$, it was decided to investigate the effect of removing the fairings at low angles of attack. Results of these tests are presented in figure 14. These tests showed a reduction in longitudinal stability caused by the large 1.72 inch by 1.40 inch rectangular fairings; rod fairings were therefore tested. The rod fairings also resulted in a considerable reduction in the longitudinal stability near $\alpha = 0^\circ$.

Configuration With Various Flow Separators and Escape Rocket Turning Vanes

In an effort to improve the stability of the escape configuration at subsonic and transonic speeds and to evaluate the effect of various modifications and additions made to the escape configuration, an investigation was conducted in the 16-foot transonic propulsion wind tunnel of the Arnold Engineering Development Center (ref. 14). The Mach number range that was covered varied from 0.50 to 1.50. Shown in figure 4 is the escape configuration with and without a combination of the following devices that were tested during this investigation: (1) original clamp ring, (2) four various flow separators, (3) seven various escape rocket turning vanes, and (4) two different ramps located at the base of the escape rocket.

Also shown in figure 4 are the production modifications and additions made to the escape configuration. These modifications are the necessary additions for escape rocket ignition and include: (a) igniter-cable conduits and junction boxes located at the base of the escape tower, (b) tangential igniter-cable fairings located on the escape rocket, and (c) straps and clamps on the escape rocket.

Effects of turning-vane afterbody angles.- Results shown in figure 16 indicate the effects of varying the turning-vane afterbody angles on the longitudinal aerodynamic characteristics of the escape configuration equipped with an original clamp ring and a 27.56-inch-diameter turning vane. Turning-vane afterbody angles of 30°, 40°, and 50° were tested during this particular phase of the investigation. Also shown in figure 16 for comparative purposes are the results obtained for the escape configuration with the original clamp ring (fig. 4) but without a turning vane.

The data of figure 16 indicate that the addition of the turning vanes resulted in an appreciable increase in the stability of the configuration; however, there was little effect of varying the turning-vane afterbody angle.

Effects of turning-vane diameter.- The effects of turning-vane diameter on the longitudinal aerodynamic characteristics of the escape configuration at Mach numbers varying from 0.50 to 1.50 are shown in figure 17. During this particular phase of the investigation, it was anticipated that increasing the diameter of the turning vane would result in an increase in the longitudinal stability of the escape configuration at subsonic, transonic, and low supersonic Mach numbers without an increase in longitudinal stability at higher supersonic Mach numbers (above $M = 2.0$). Data presented in figure 17 show that increasing the turning-vane diameter produced increases in the longitudinal stability at subsonic and transonic Mach numbers with little change in normal-force coefficient. The data in figure 17 give no indication of a dropoff in the longitudinal stability increment caused by the addition of the turning vane as the Mach number is increased into the supersonic region. Axial-force coefficients increased slightly because of the increase in the turning-vane diameter.

Effects of turning-vane exit area.- The effects of turning-vane exit area on the longitudinal aerodynamic characteristics of the escape configuration are shown in figure 18. Two escape configurations were tested during this particular phase of the investigation, one without a choked turning vane (fig. 4(b)) and the other with a choked turning vane (fig. 4(c)). As previously stated it was desired to improve the stability in the subsonic and transonic speed regions without increasing the stability in the supersonic region. The variation of pitching-

moment coefficient with angle of attack for the choked turning vane (fig. 18) indicates that there was an increase in the stability at subsonic and transonic speeds with no apparent reduction in stability up to the highest Mach number tested ($M = 1.50$). Axial-force coefficient increased with decrease in turning-vane exit area.

Effects of various flow separators (without turning vanes).- The effects of various flow separators on the aerodynamic characteristics of the escape configuration (without turning vanes) are shown in figure 19. The flow separators were developed as stability-improving devices when it was found that the addition of the original clamp-ring fairing resulted in an improvement in the stability. (See fig. 22.) The improved stability was assumed to be a flow phenomena caused by the projection of the explosive bolt covers into the airstream. By then extending this projection all the way around the clamp, further improvement was obtained. In an attempt to find a flow separator which provided the most optimum improvement in stability, tests were made with flow separators of various cross section. (See fig. 4(a) for details of flow separators tested.) The data of figure 19 indicate that the 45° flow separators produced the largest improvement in stability. Also, it should be noted that there was no measurable effect of adding the 45° flow separator on either the normal-force or drag coefficients of the configuration. This condition would indicate that the increased stability was caused by a rearward shift in the center of pressure of the configuration caused by the addition of the 45° flow separator. Another advantage of the flow separator is its simplicity of construction and ease of installation, and this modification has been incorporated into the production configuration.

Effects of various flow separators (with turning vanes).- Shown in figures 20 and 21 are the effects of various combinations of turning vanes and flow separators. The data of figure 20 show the effects of various flow separators in combination with the 32-inch-diameter 50° exit turning-vane angle. Three flow separators were investigated: the airfoil flow separator, the 30° flow separator, and the 30°-45° flow separator. (See fig. 4(a).) The data indicate the combination of 32.00D-50° turning vane and 30°-45° flow separator results in the largest increase in stability. A brief check on the effect of Reynolds number was made with this configuration at $M = 0.90$ and indicated that, for the range of the tests, Reynolds number has little or no effect.

Further effects of the turning vanes and flow separators are given in figures 21 and 22. These data indicate that the increases in stability due to turning vanes and flow separators are two independent phenomena and indications are that the effect of the two devices in combination is a summation of the two independent effects.

Effect of ramp size at base of escape rocket.- The effect of ramp size at the base of the escape rocket is given in figure 23. (See fig. 4(d) for ramp details.) The data indicate that ramp size has no effect for these Mach numbers.

Configuration With Various Rocket-Face Cant Angles

In the event of an abort, the escape configuration must be laterally displaced away from the booster so that the booster will not collide with the escape configuration. One means for obtaining the necessary separation distance makes use of the inherent aerodynamics of the configuration providing some simple method of shifting the trim angle of attack can be found.

An investigation was conducted in the Langley 8-foot tunnel and in the Langley 4-foot tunnel in an attempt to shift the trim angle of attack by varying the cant angle on the face of the escape rocket. The Mach number range through which the tests were conducted varied from 0.50 to 2.01. The configuration that was used during the investigation was the basic escape configuration equipped with igniter-cable conduit, junction boxes, 45° flow separator, and various rocket-face cant angles. Full-scale dimensions of this configuration are shown in figure 5.

Results of this investigation are shown in figure 15. The variation of pitching-moment coefficient shown in figure 15 indicates there is little or no effect at subsonic and transonic Mach numbers; whereas, at the supersonic Mach number ($M = 2.01$) the trim angle of attack varies appreciably with rocket-face cant angle.

Finned-Adapter Escape Configuration

The results obtained from the wind-tunnel investigations of the finned-adapter escape configuration are presented in figures 24 to 37. The data on these figures show the effect of fin area, nose shape, and fin orientation on the aerodynamic characteristics of the finned-adapter escape configuration. The finned-adapter configuration with the various tail fins is unstable in the high subsonic Mach number range and becomes stable at a Mach number of about 1.00. As the Mach number is increased above a Mach number of 1.00, the stability of the configuration decreases until at a Mach number of 6.86 the configuration is neutrally stable (figs. 24 to 37). The loss in stability in the high subsonic speed region ($M \approx 0.8$ to 1.0) was believed to be the result of flow separation over the fins caused by the capsule-adapter clamp ring. Also, from the data presented it can be seen that changing the nose shape produced little or no effect on the stability of the configuration.

[redacted]

LONGITUDINAL STABILITY CHARACTERISTICS OF ESCAPE CONFIGURATION

Basic Configuration

Presented in figure 38 is a summary plot of the longitudinal stability characteristics of the basic escape configuration as a function of Mach number. The results presented in this figure indicate C_{N_α} is generally constant with Mach number except for a slight decrease in the vicinity of $M = 1.00$.

The data also show the drag coefficient at $\alpha = 0^\circ \left(C_{D,\alpha=0^\circ}\right)$ increases throughout the transonic Mach number range, the maximum value occurring at $M = 1.10$. Above $M = 1.10$, further increase in Mach number resulted in a decrease in the drag coefficient.

The variation of C_{m_α} with Mach number indicates the basic Mercury escape configuration is statically stable near $\alpha = 0^\circ$ throughout the Mach number range investigated; however, the stability extends only over a limited angle-of-attack range.

Configuration With and Without Various Rocket Igniter-Cable Fairings

Shown in figure 39 is a summary of the longitudinal stability characteristics of the escape configuration with and without rocket igniter-cable fairings. The data in this figure indicate C_{N_α} is generally constant with increasing Mach number.

The data also indicate the configuration is statically stable near $\alpha = 0^\circ$ for all the Mach numbers investigated. Although the data indicate that the addition of the fairings had no effect on the C_{m_α} of the escape configuration, there is a considerable reduction in the maximum negative value of C_m, and the angle of attack where instability occurs is lower.

Drag coefficient at $\alpha = 0^\circ$ for all the fairings tested increases with increasing Mach number up to a Mach number of about 1.14. Above $M = 1.14$, $C_{D,\alpha=0^\circ}$ for the rod fairings and the full-size fairings decreases with increasing Mach number.

[redacted]

Configuration With and Without Rocket-Face Cant Angles

The data shown in figure 40 is a summary of the longitudinal stability characteristics of the escape configuration with and without rocket-face cant angles. The data shown in figure 40 indicate that varying the cant angle on the face of the escape rocket had little or no effect on the stability parameters presented; however, the trim angle of attack was found to be proportional to the rocket-face cant angle at $M = 2.01$.

Configuration With Various Turning-Vane Afterbody Angles

Presented in figure 41 is a summary of the longitudinal stability characteristics of the escape configuration with various turning-vane afterbody angles. Also given is the effect of the choked vane on the longitudinal stability characteristics. Increasing the turning-vane exit angle results generally in a decrease in the stability parameter C_{m_α}, while the effect on C_{N_α}, C_{L_α}, or $C_{D,\alpha=0^\circ}$ is small. The effect of the choked-vane configuration on C_{m_α}, C_{N_α}, and C_{L_α} is generally negligible whereas $C_{D,\alpha=0^\circ}$ is increased slightly.

Configuration With Various Turning-Vane Diameters

Presented in figure 42 is a summary of the longitudinal stability characteristics of the escape configuration with various turning-vane diameters. From this data it can be seen that increasing the diameter of the turning vane increased C_{m_α} for all Mach numbers investigated. The other parameters C_{N_α}, C_{L_α}, and $C_{D,\alpha=0^\circ}$ are generally not affected by increase in turning-vane diameter.

Configuration With Various Flow Separators With and Without Turning Vanes

Figure 43 presents a summary of the longitudinal stability characteristics of the escape configuration with various flow separators with and without turning vanes. The data presented in this figure indicate the various flow separators produce the same general level of C_{m_α} throughout the Mach number range investigated. It should be noted that, because of the nonlinear variation of C_m with α, the parameter C_{m_α}

is not a true indication of the stability. The combination of flow separator and turning vane results in a further improvement in stability. The parameters C_{N_α}, C_{L_α}, and $C_{D,\alpha=0^\circ}$ show that the combination of flow separator and turning vane results in a reduced lift-curve slope.

Configuration With Various Modifications

The data shown in figure 44 are a summary of the longitudinal stability characteristics of the escape configuration with various modifications. Shown is a comparison of the production configuration with the original tower clamp and the basic or clean configuration. Also included is the effect of the addition of the 45° flow separator and the 32-inch-diameter 50° turning vane. The comparison shows little difference between the production and clean configurations but there are large effects on the stability due to adding the 45° flow separator and the turning vane. There was little or no effect on C_{N_α} or C_{L_α} due to adding the 45° flow separator and the turning vane; thus, these additions shift the center of pressure rearward to produce the stabilizing effect.

Finned-Adapter Escape Configuration

The data shown in figure 45 are a summary of the longitudinal stability characteristics of the finned-adapter configuration. The finned-adapter configuration with the various tail fins is unstable in the high subsonic Mach number range and becomes stable at a Mach number of about 1.00. As the Mach number is increased above a Mach number of 1.00, the stability of the configuration decreases until at a Mach number of 6.86 the configuration is neutrally stable. (See figs. 24 to 37.)

CONCLUDING REMARKS

Wind-tunnel tests have been made to determine the static longitudinal stability characteristics of the basic Mercury escape configuration and also to determine the effects of the various additions and modifications made to the configuration during its development.

The basic escape configuration was stable near an angle of attack of 0° throughout the Mach number range of the tests (0.05 to 9.60). However, in the transonic speed range the configuration was stable over

a limited angle-of-attack range and became unstable at angles of attack of about 15°. The addition of rocket igniter strips and associated conduits and junction boxes resulted in a further decrease in the static stability in the transonic speed range. The addition of a turning vane at the base of the escape rocket and/or a flow separator at the base of the escape tower resulted in improved stability in the subsonic, transonic, and low supersonic speed ranges.

The finned-adapter configuration with the various tail fins is unstable in the high subsonic Mach number range and becomes stable at a Mach number of about 1.00. As the Mach number is increased above a Mach number of 1.00, the stability of the configuration decreases until at a Mach number of 6.86 the configuration is neutrally stable.

Space Task Group,
National Aeronautics and Space Administration,
Langley Field, Va., March 3, 1961.

REFERENCES

1. Pearson, Albin O.: Wind-Tunnel Investigation at Mach Numbers From 0.50 to 1.14 of the Static Aerodynamic Characteristics of a Model of a Project Mercury Capsule. NASA TM X-292, 1960.

2. Shaw, David S., and Turner, Kenneth L.: Wind-Tunnel Investigation of Static Aerodynamic Characteristics of a $\frac{1}{9}$-Scale Model of a Project Mercury Capsule at Mach Numbers From 1.60 to 4.65. NASA TM X-291, 1960.

3. Rittenhouse, Lewis E., and Kaupp, Harry, Jr.: Transonic Wind Tunnel Tests To Determine Some Aerodynamic Characteristics of Two Proposed Escape Configurations for Project Mercury. AEDC-TN-59-76 (Contract No. AF40(600)-800), Arnold Eng. Dev. Center, July 1959.

4. Everhart, Philip E., and Bernot, Peter T.: Measurements of the Surface Flows, Heat Transfer, Pressure Distribution, and Longitudinal Stability of a Mercury Capsule Model at Mach Numbers of 6.9 and 9.6. NASA TM X-458, 1961.

5. Brown, Steve W., and Moseley, William C., Jr.: Summary of Wind-Tunnel Investigations of the Static Longitudinal Stability Characteristics of the Production Mercury Configurations at Mach Numbers From 0.05 to 20. NASA TM X-491, 1961.

6. Shortal, Joseph A., and Osterhout, Clayton J.: Preliminary Stability and Control Tests in the NACA Free-Flight Wind Tunnel and Correlation With Full-Scale Flight Tests. NACA TN 810, 1941.

7. Anon.: Propulsion Wind Tunnel. Vol. 3 of Test Facilities Handbook, second ed., Arnold Eng. Dev. Center, Jan. 1959.

8. Anon.: Manual for Users of the Unitary Plan Wind Tunnel Facilities of the National Advisory Committee for Aeronautics. NACA, 1956.

9. Ulmann, Edward F., and Lord, Douglas R.: An Investigation of Flow Characteristics at Mach Number 4.04 Over 6- and 9-percent Circular-Arc Airfoils Having 30-Percent-Chord Trailing-Edge Flaps. NACA RM L51D30, 1951.

10. Ashby, George C., Jr., and Fitzgerald, Paul E., Jr.: Longitudinal Stability and Control Characteristics of Missile Configurations Having Several Highly Swept Cruciform Fins and a Number of Trailing-Edge and Fin-Tip Controls at Mach Numbers From 2.21 to 6.01. NASA TM X-335, 1961.

11. McLellan, Charles H., Williams, Thomas W., and Bertram, Mitchel H.: Investigation of a Two-Step Nozzle in the Langley 11-Inch Hypersonic Tunnel. NACA TN 2171, 1950.

12. McLellan, Charles H., Williams, Thomas W., and Beckwith, Ivan E.: Investigation of the Flow Through a Single-Stage Two-Dimensional Nozzle in the Langley 11-Inch Hypersonic Tunnel. NACA TN 2223, 1950.

13. Rittenhouse, Lewis E., and Kaupp, Harry, Jr.: Experimentally Determined Static Stability and Drag Characteristics for NASA's Project Mercury Manned Orbital Capsule at Transonic Speeds. AEDC TN-59-130 (Contract No. AF40(600)-800), Arnold Eng. Dev. Center, Oct. 1959.

14. Rittenhouse, Lewis E., and Kaupp, Harry, Jr.: The Effect of Several External Modifications on the Static Stability Characteristics of the NASA Project Mercury Escape Configuration at Transonic Speeds. AEDC TN-60-50 (Contract No. AF 40(600)-800), Arnold Eng. Dev. Center, Mar. 1960.

[redacted]

TABLE I.- TEST CONDITIONS

Configuration	Facility	Mach number	Stagnation pressure, lb/sq in. abs	Dynamic pressure, lb/sq ft	Stagnation temperature, °F	Reynolds number[1]
Basic escape	Langley free-flight tunnel	0.05	14.7	2 to 15	75	0.35×10^6 to 0.65×10^6
	Langley 8-foot tunnel	0.50	14.7	312	125	2.42×10^6
		.60	14.7	418	125	2.77
		.70	14.7	524	125	3.06
		.80	14.7	623	125	3.30
		.90	14.7	710	125	3.50
		.95	14.7	750	125	3.56
		.98	14.7	770	125	3.60
		1.00	14.7	783	125	3.61
		1.03	14.7	801	125	3.62
		1.14	14.7	858	125	3.68
	AEDC 16-foot tunnel	0.50	6.14	133	120	2.3×10^6
		.50	27.40	588	120	10.4
		.70	6.53	234	120	3.1
		.70	26.70	954	120	12.7
		.80	20.50	870	120	10.5
		.90	6.72	325	120	3.6
		.90	13.05	632	120	7.0
		.90	20.50	990	120	11.0
		.90	25.70	1,241	120	13.8
		.95	25.70	608	120	14.0
		1.00	6.63	352	120	3.7
		1.00	12.60	671	120	7.0
		1.00	25.95	689	120	14.5
		1.10	6.56	375	120	3.7
		1.10	12.35	707	120	7.0
		1.10	24.30	690	120	13.8
		1.30	6.53	403	120	3.7
		1.30	12.38	760	120	7.1
		1.40	12.85	797	130	7.1
		1.40	16.65	636	140	8.9
	Langley Unitary Plan tunnel	1.60	14.6	885	125	2.69×10^6
		2.06	16.2	805	150	2.50
		2.87	24.7	678	150	2.39
		2.87	38.0	1,051	150	3.67
		3.94	55.8	624	175	2.20
		4.65	55.0	343	175	2.05
	Langley 20-inch tunnel	5.98	295	687	410	1.8×10^6
	Langley 11-inch tunnel	6.72	162	212	675	0.26×10^6
		9.60	412	113	1,200	.14
		9.60	676	193	1,200	.23
Escape with various rocket igniter-cable fairings	AEDC 16-foot tunnel	0.50	16.05	340	120	6.0×10^6
		.50	29.20	620	120	10.9
		.70	12.70	450	120	6.0
		.70	26.75	950	120	12.7
		.90	11.20	540	120	6.0
		.90	21.85	1,055	120	11.7
		1.14	10.60	620	120	6.0
		1.14	21.20	1,235	120	12.0
		1.30	10.60	650	120	6.0
		1.30	18.20	1,115	120	10.4
		1.50	5.70	350	140	3.0
		1.50	11.35	700	140	6.0

[1]Based on capsule maximum diameter.

[redacted]

TABLE I.- TEST CONDITIONS - Concluded.

Configuration	Facility	Mach number	Stagnation pressure, lb/sq in. abs	Dynamic pressure, lb/sq ft	Stagnation temperature, °F	Reynolds number[1]
Escape with various rocket-face cant angles	Langley 8-foot tunnel	0.50	14.70	313	125	2.42×10^6
		.80	14.70	625	125	3.30
		.90	14.70	712	125	3.50
		1.00	14.70	785	125	3.61
		1.14	14.70	861	125	3.68
	Langley 4-foot tunnel	2.01	14.70	748	100	2.48×10^6
Escape with various flow separators and various turning vanes	AEDC 16-foot tunnel	0.50	16.05	344	120	6.0×10^6
		.70	12.65	452	120	6.0
		.90	11.20	540	120	6.0
		1.14	10.60	620	120	6.0
		1.30	10.65	654	120	6.0
		1.50	10.40	644	120	6.0
Finned adapter	Langley 8-foot tunnel	0.50	14.7	313	125	1.90×10^6
		.80	14.7	623	125	2.57
		1.00	14.7	785	125	2.80
		1.14	14.7	857	125	2.87
	Langley 4-foot tunnel	2.01	5.0	255	100	0.78×10^6
	Langley high Mach number jet tunnel	4.00	175.0	1,800	63	3.30×10^6
	Langley 11-inch tunnel	6.86	151.0	210	650	0.26×10^6
	AEDC 16-foot tunnel	0.50	16.65	355	120	6.2×10^6
		.70	13.08	468	120	6.2
		.80	12.15	517	120	6.2
		.90	11.54	556	120	6.2
		1.00	11.54	596	120	6.2
		1.10	10.95	627	120	6.2
		1.40	11.60	721	120	6.2

[1]Based on capsule maximum diameter.

TABLE II.- CONFIGURATIONS TESTED

Facility	Escape configuration	Scale of model	Material used for model	Remarks
Langley free-flight tunnel	Basic	$\frac{1}{4}$	Wood	M = 0.05
Langley 8-foot tunnel	Basic	$\frac{1}{7}$	Aluminum with steel escape tower	
Langley 8-foot tunnel	With various rocket-face cant angles	$\frac{1}{7}$	Capsule and noses of aluminum; escape tower, steel	Interchangeable noses, constructed of aluminum, were attached to the escape rocket to provide various cant angles.
Langley 8-foot tunnel	Finned adapter	$\frac{1}{9}$	Steel and aluminum	
AEDC 16-foot transonic propulsion wind tunnel	Basic	32%	Steel, wood, and aluminum	
AEDC 16-foot transonic propulsion wind tunnel	With rocket igniter-cable fairings	32%	Steel, wood, and aluminum	
AEDC 16-foot transonic propulsion wind tunnel	With escape rocket-turning vanes	32%	Steel, wood, and aluminum	
AEDC 16-foot transonic propulsion wind tunnel	With flow separators	32%	Steel, wood, and aluminum	
AEDC 16-foot transonic propulsion wind tunnel	Finned adapter	32%	Steel, wood, and aluminum	
Langley Unitary Plan wind tunnel	Basic	$\frac{1}{9}$	Aluminum and steel	
Langley 20-inch hypersonic tunnel	Basic	5.37%	Steel	
Langley 11-inch hypersonic tunnel	Basic	3.02%	Aluminum and steel	
Langley 11-inch hypersonic tunnel	Finned adapter	3.02%	Steel	Same model tested in Langley high Mach number jet.
Langley 4-foot supersonic pressure tunnel	With rocket-face cant angles	$\frac{1}{9}$	Aluminum and steel	Interchangeable noses, constructed of aluminum, were attached to the escape rocket to provide various cant angles.
Langley 4-foot supersonic pressure tunnel	Finned adapter	10%	Aluminum and steel	
Langley high Mach number jet	Finned adapter	3.02%	Steel	Model tested with and without three sets of four interchangeable tail fins and two interchangeable noses.[1]

[1]The tail fins have the same geometric characteristics except that the fin tips have been dropped chordwise and spanwise. The effective planform area of the large fins was 7.5 square feet; for the medium fins, 6.5 square feet; and for the small fins, 5.5 square feet. The cross section of the fins was wedge shaped. The noses which were attached to the antenna canister were either hemispherical or flat plate (blunt).

Table III.- ACCURACY OF DATA

Configuration	Facility	M	Accuracy of –								
			M	α, deg	C_m	C_N	C_A	C_L	C_D	C_n	C_Y
Basic escape	Langley 8-foot tunnel	0.50 1.14	±0.010 ±.004	±0.2 ±.2	±0.008 ±.014	±0.040 ±.014	±0.040 ±.014	±0.040 ±.014	±0.040 ±.014	- -	- -
	AEDC 16-foot tunnel	0.50 1.40	±0.01 ±.01	±0.1 ±.1	±0.005 ±.005	±0.020 ±.020	±0.01 ±.01	±0.020 ±.020	±0.01 ±.01	- -	- -
	Langley Unitary tunnel	1.60 2.06 2.87 3.96 4.65	±0.05 ±.05 ±.05 ±.05 ±.05	±0.1 ±.1 ±.1 ±.1 ±.1	±0.005 ±.005 ±.005 ±.005 ±.005	±0.024 ±.024 ±.024 ±.024 ±.024	±0.021 ±.021 ±.021 ±.021 ±.021	±0.024 ±.024 ±.024 ±.024 ±.024	±0.021 ±.021 ±.021 ±.021 ±.021	- - - - -	- - - - -
	Langley 20-inch tunnel	5.98	±0.02	±0.1	±0.005	±0.010	±0.02	±0.010	±0.02	-	-
	Langley 11-inch tunnel	6.86 9.60	±0.03 ±.03	±0.1 ±.1	±0.007 ±.007	±0.020 ±.020	±0.008 ±.008	±0.020 ±.020	±0.008 ±.008	- -	- -
Escape with various rocket igniter-cable fairings	AEDC 16-foot tunnel	0.50 .50 .90 .90 1.50	±0.003 ±.003 ±.004 ±.004 ±.005	±0.1 ±.1 ±.1 ±.1 ±.1	±0.007 ±.004 ±.003 ±.002 ±.003	±0.011 ±.009 ±.006 ±.005 ±.005	±0.018 ±.016 ±.013 ±.012 ±.010	±0.011 ±.009 ±.006 ±.005 ±.005	±0.017 ±.015 ±.012 ±.011 ±.009	±0.007 ±.004 ±.003 ±.002 ±.003	±0.011 ±.009 ±.006 ±.005 ±.005
Escape with various rocket-face cant angles	Langley 8-foot tunnel	0.50 1.14	±0.010 ±.004	±0.1 ±.1	±0.008 ±.003	±0.040 ±.014	±0.040 ±.014	±0.040 ±.014	±0.040 ±.014	- -	- -
	Langley 4-foot tunnel	2.01	±0.01	±0.1	±0.005	±0.02	±0.02	±0.02	±0.02	-	-
Escape with various flow separators and various turning vanes	AEDC 16-foot tunnel	0.50 .90 1.50	±0.003 ±.004 ±.005	±0.1 ±.1 ±.1	±0.007 ±.003 ±.003	±0.011 ±.006 ±.005	±0.018 ±.013 ±.010	- - -	- - -	±0.007 ±.003 ±.003	±0.011 ±.006 ±.005
Finned adapter	Langley 8-foot tunnel	0.50 1.14	±0.010 ±.004	±0.2 ±.2	±0.0155 ±.0056	±0.060 ±.022	±0.060 ±.022	±0.060 ±.022	±0.060 ±.022	- -	- -
	Langley 4-foot tunnel	2.01	±0.015	±0.1	±0.0021	±0.0073	±0.0017	±0.001	±0.0017	-	-
	Langley high Mach number jet	4.00	±0.005	±0.1	±0.020	±0.006	±0.010	±0.010	±0.013	-	-
	Langley 11-inch tunnel	6.86	±0.01	±0.2	±0.007	±0.014	±0.004	±0.014	±0.004	-	-
	AEDC 16-foot tunnel	0.50 .80 1.10 1.40	±0.01 ±.01 ±.01 ±.01	±0.1 ±.1 ±.1 ±.1	±0.007 ±.002 ±.002 ±.002	±0.011 ±.006 ±.007 ±.006	±0.018 ±.013 ±.010 ±.009	±0.011 ±.006 ±.007 ±.006	±0.017 ±.012 ±.010 ±.009	- - - -	- - - -

[redacted]

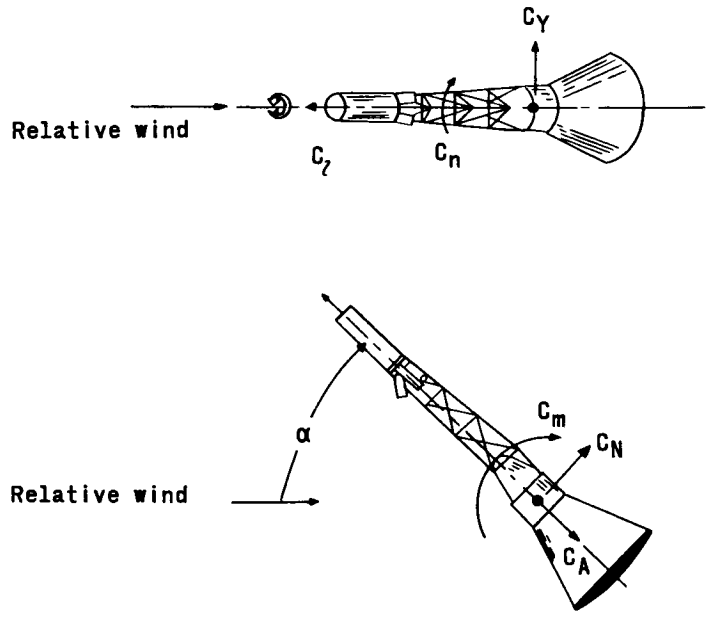

(a) Body axis.

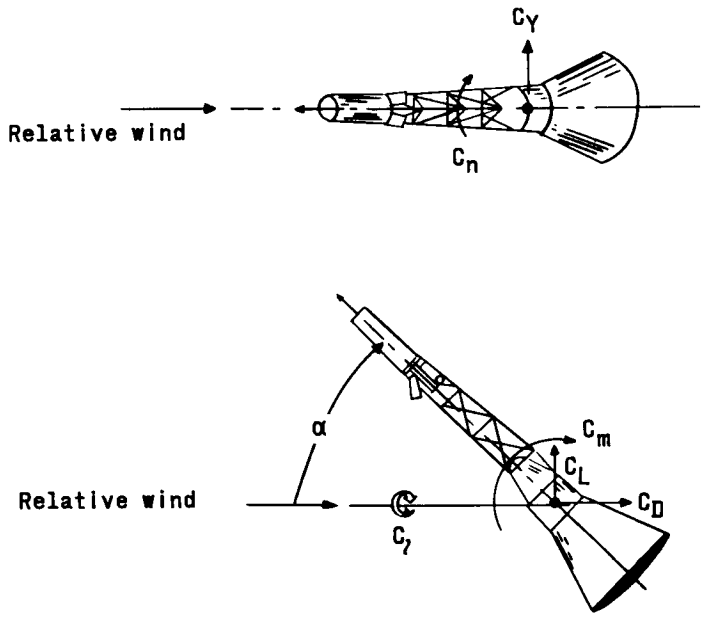

(b) Stability axis

Figure 1.- Axes system with arrows indicating positive direction of forces, moments, and angular deflections.

[redacted]AL

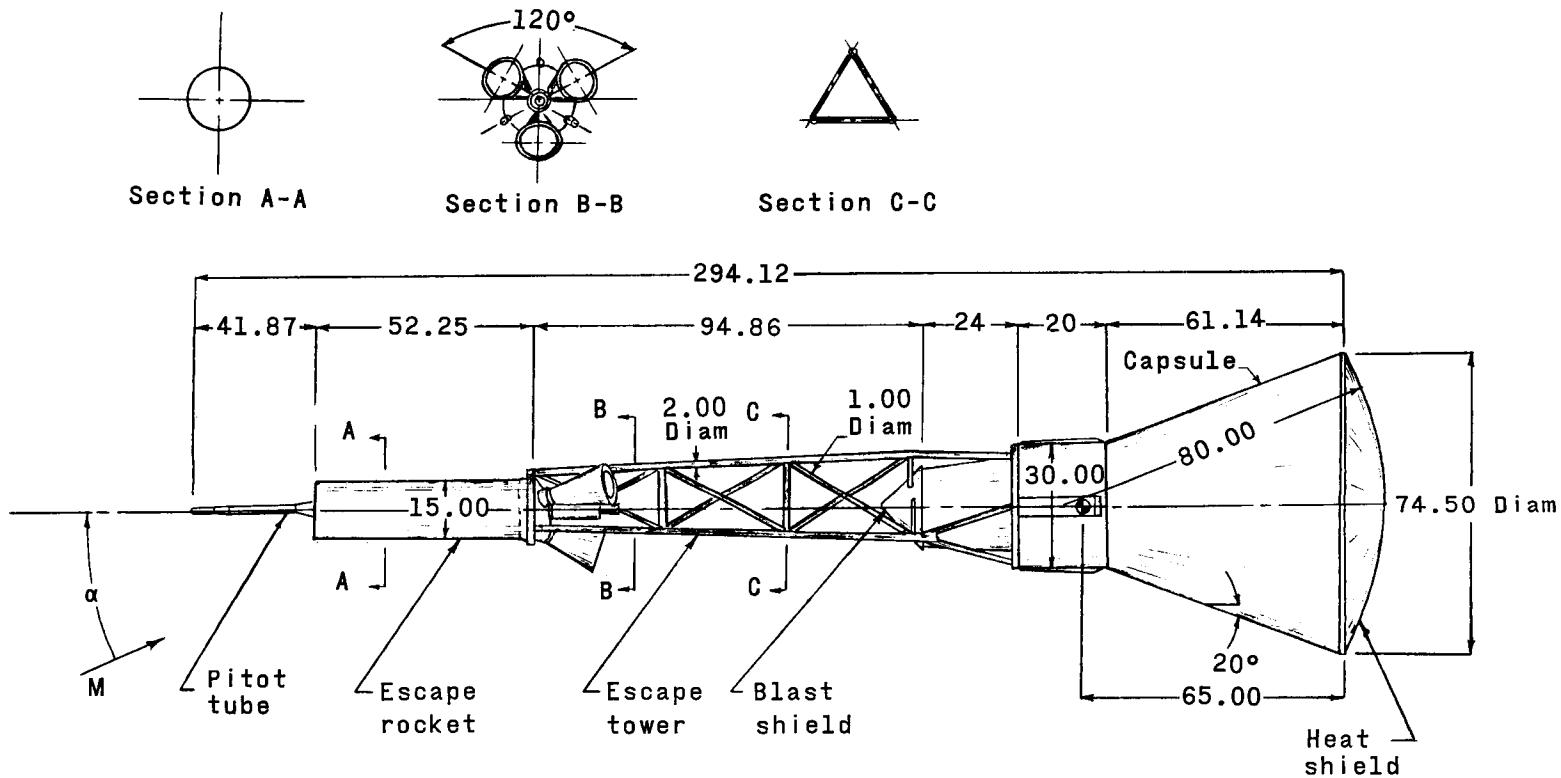

Figure 2.- Full-scale dimensions of basic escape configuration. All dimensions are in inches unless otherwise noted.

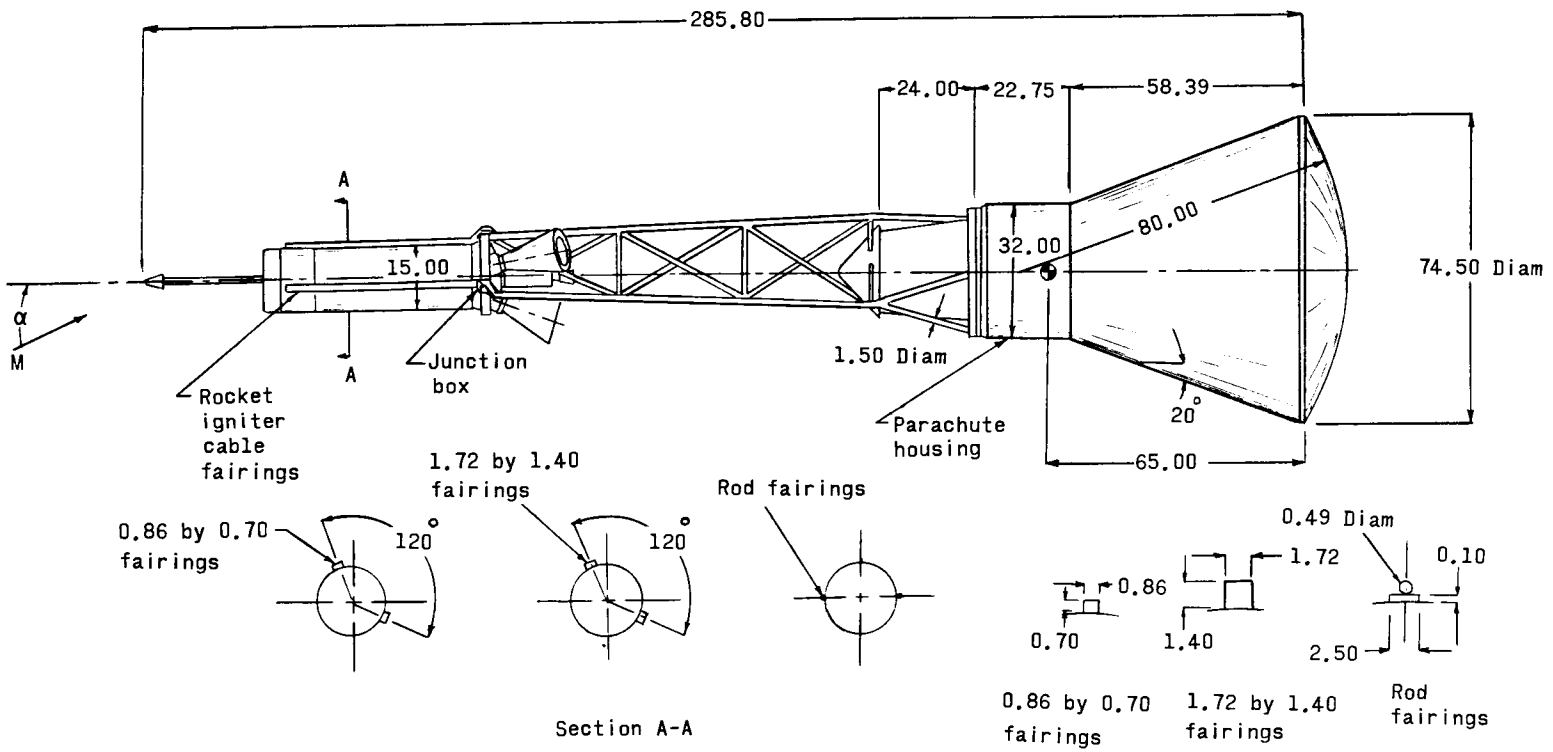

Figure 3.- Escape configuration with various rocket igniter-cable fairings. All dimensions are in inches unless otherwise noted.

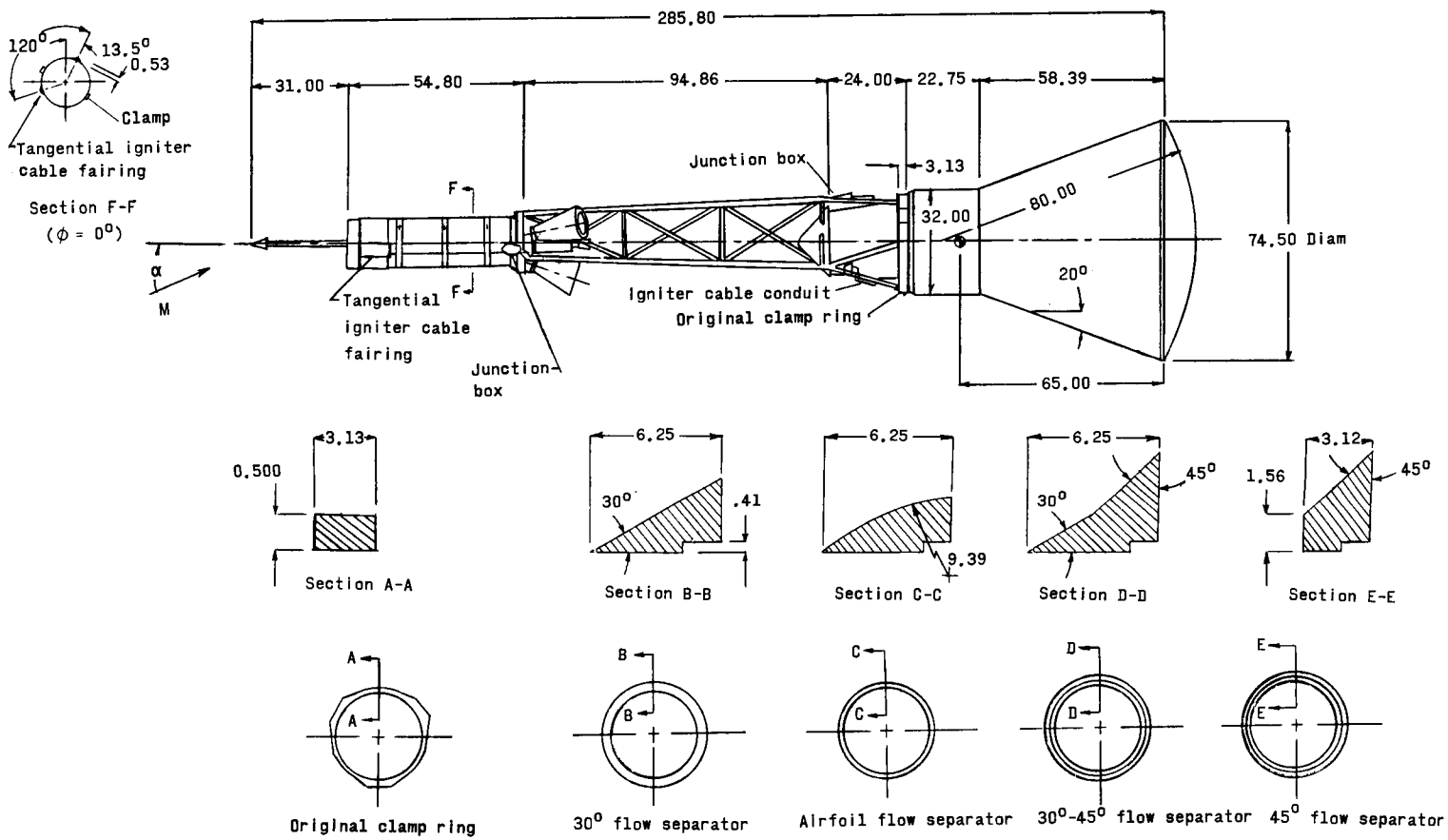

(a) Detailed dimensions of flow separators.

Figure 4.- Escape configuration with igniter-cable conduit, junction boxes, rocket igniter-cable fairings, various flow separators, and various turning vanes. All dimensions are in inches unless otherwise noted.

[redacted]

Configuration	Diam "A"	"B"	"C"	Angle "D"
22.75 D-30.00°	22.75	3.50	5.47	30.00°
25.00 D-30.00°	25.00	4.13	4.88	30.00°
27.56 D-30.00°	27.56	4.38	4.38	30.00°
27.56 D-40.00°	27.56	4.56	4.19	40.00°
27.56 D-50.00°	27.56	4.69	3.88	50.00°
32.00 D-50.00°	32.00	5.25	4.69	50.00°

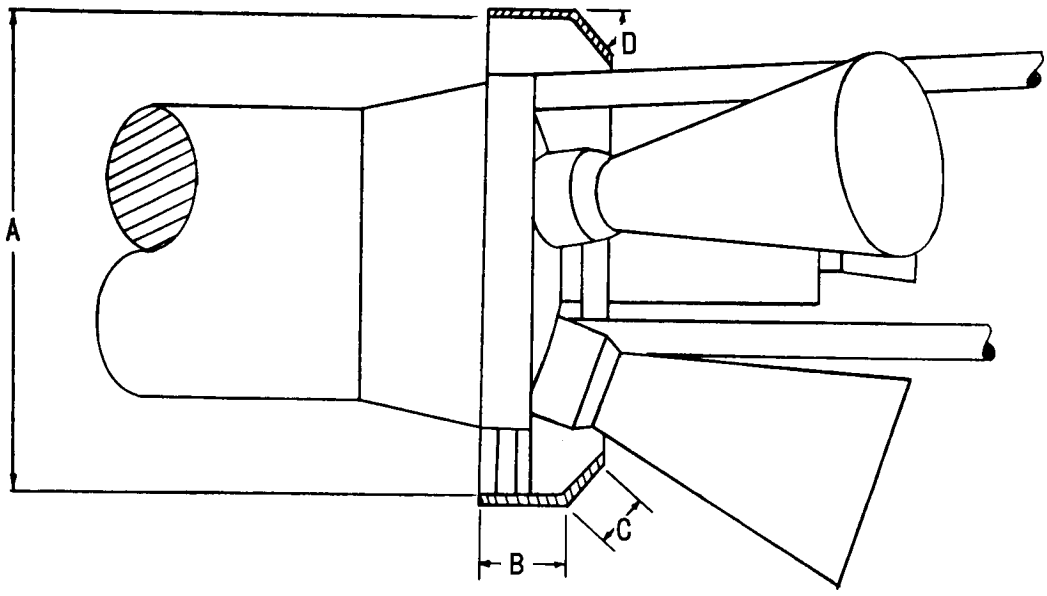

(b) Detailed dimensions of turning vanes.

Figure 4.- Continued.

[redacted]

Configuration	Diam "A"	"B"	Angle "C"
32.00 D-50°	32.00	5.25	50°

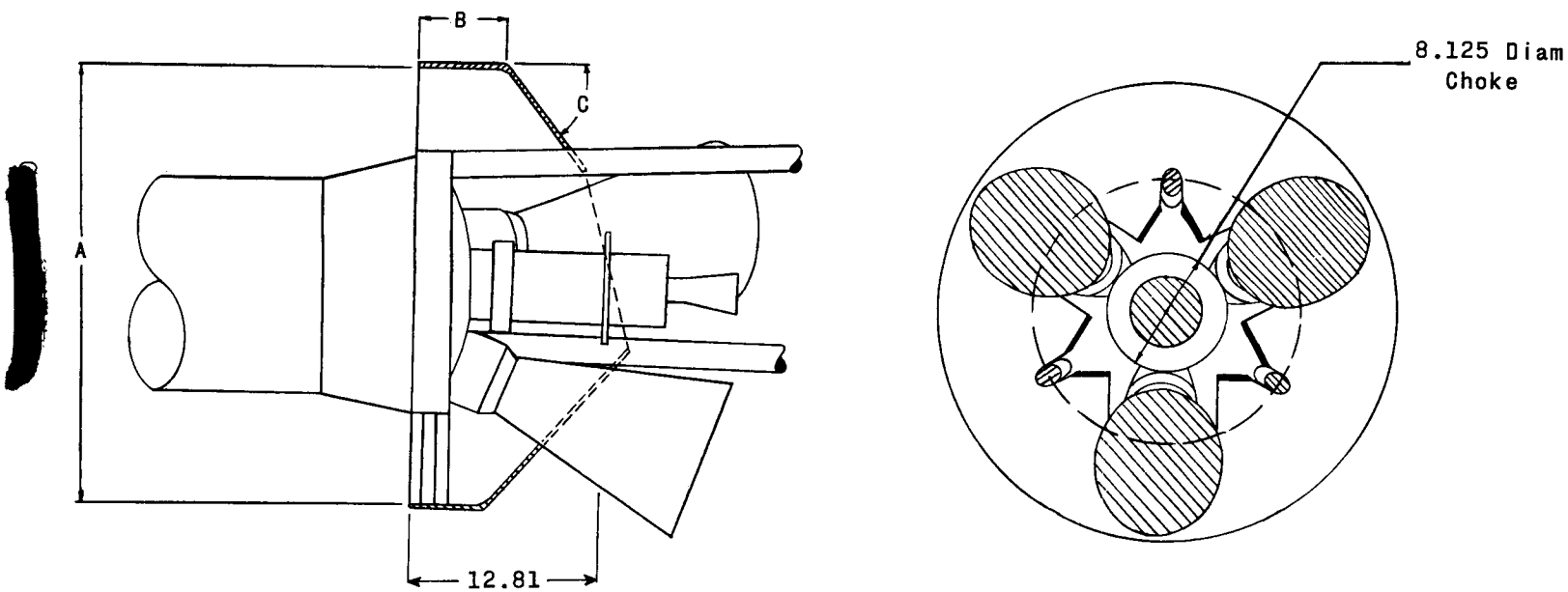

(c) Detailed dimensions of turning vane. Choked configuration.

Figure 4.- Continued.

[redacted]

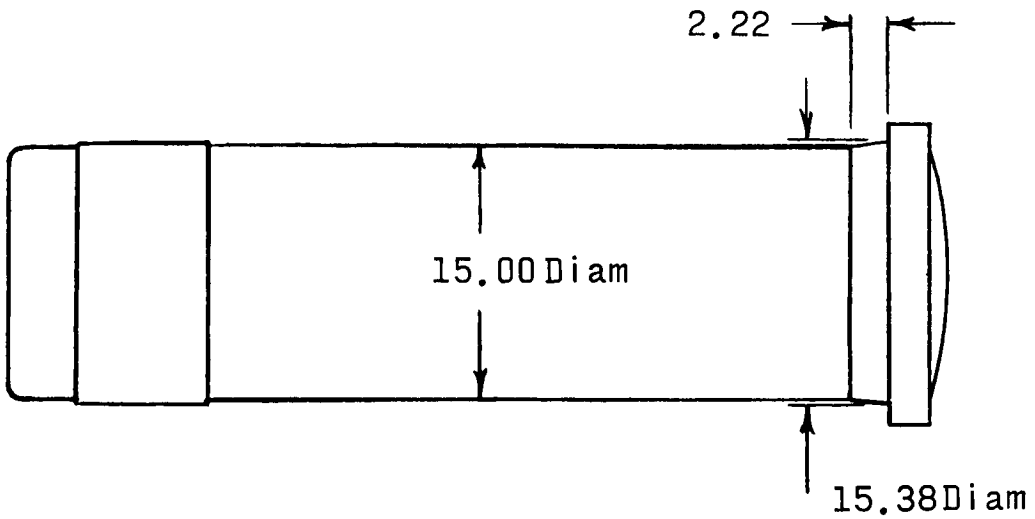

Small ramp

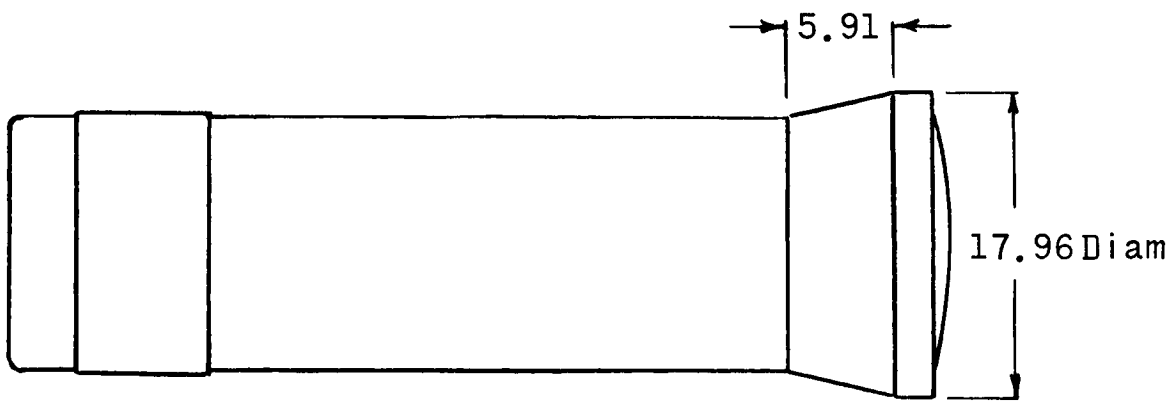

Large ramp

(d) Detailed dimensions of escape rocket ramps.

Figure 4.- Concluded.

[redacted]

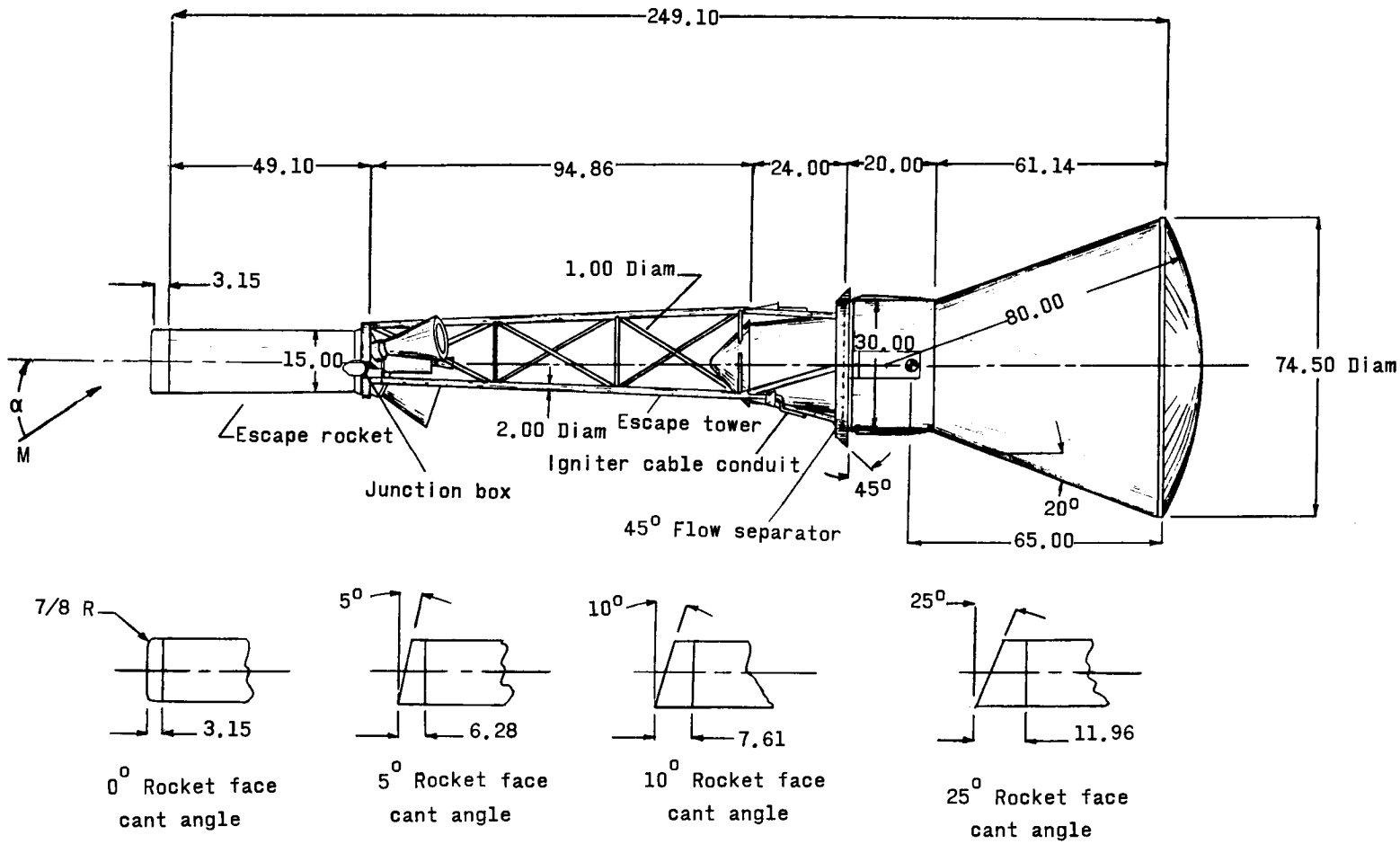

(a) Full-scale dimensions of model.

Figure 5.- Escape configuration with igniter-cable conduit, junction boxes, 45° flow separator, and various rocket-face cant angles. All dimensions are in inches unless otherwise noted.

CONFIDENTIAL

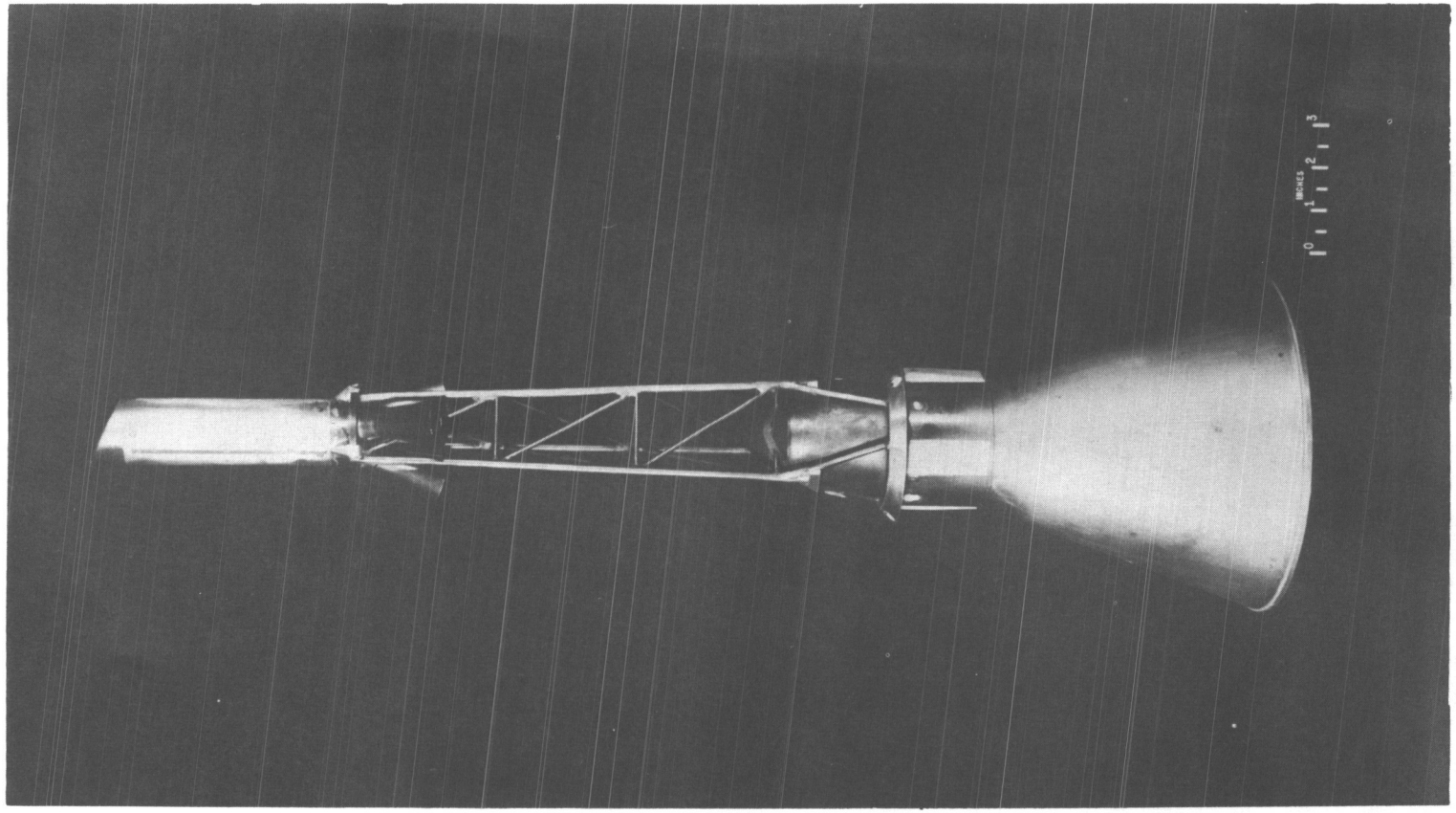

(b) Photograph of $\frac{1}{9}$-scale model tested in Langley 4-foot tunnel. G-61-15

Figure 5.- Concluded.

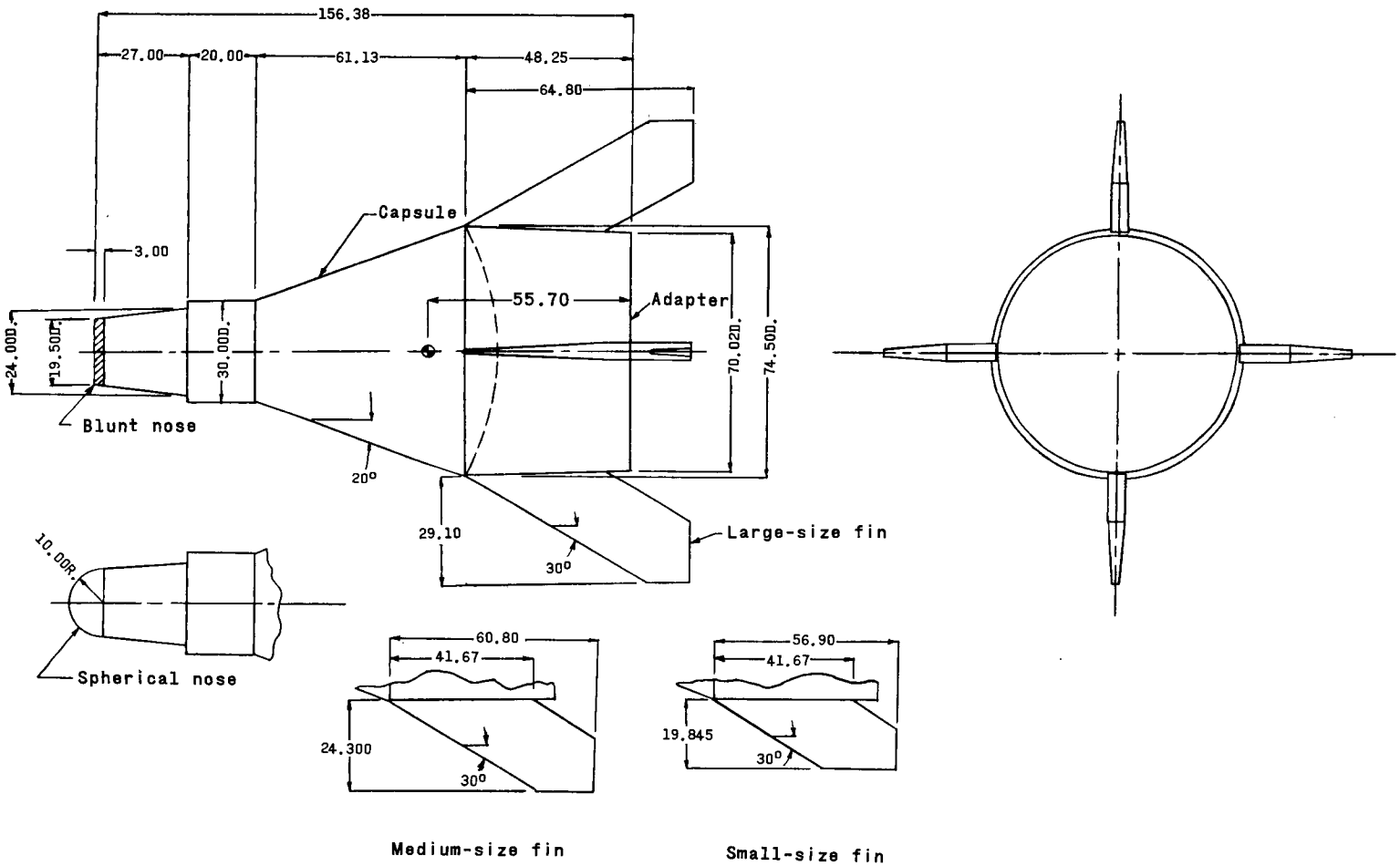

Figure 6.- Finned-adapter escape configuration. All dimensions are in inches unless otherwise noted.

[redacted]

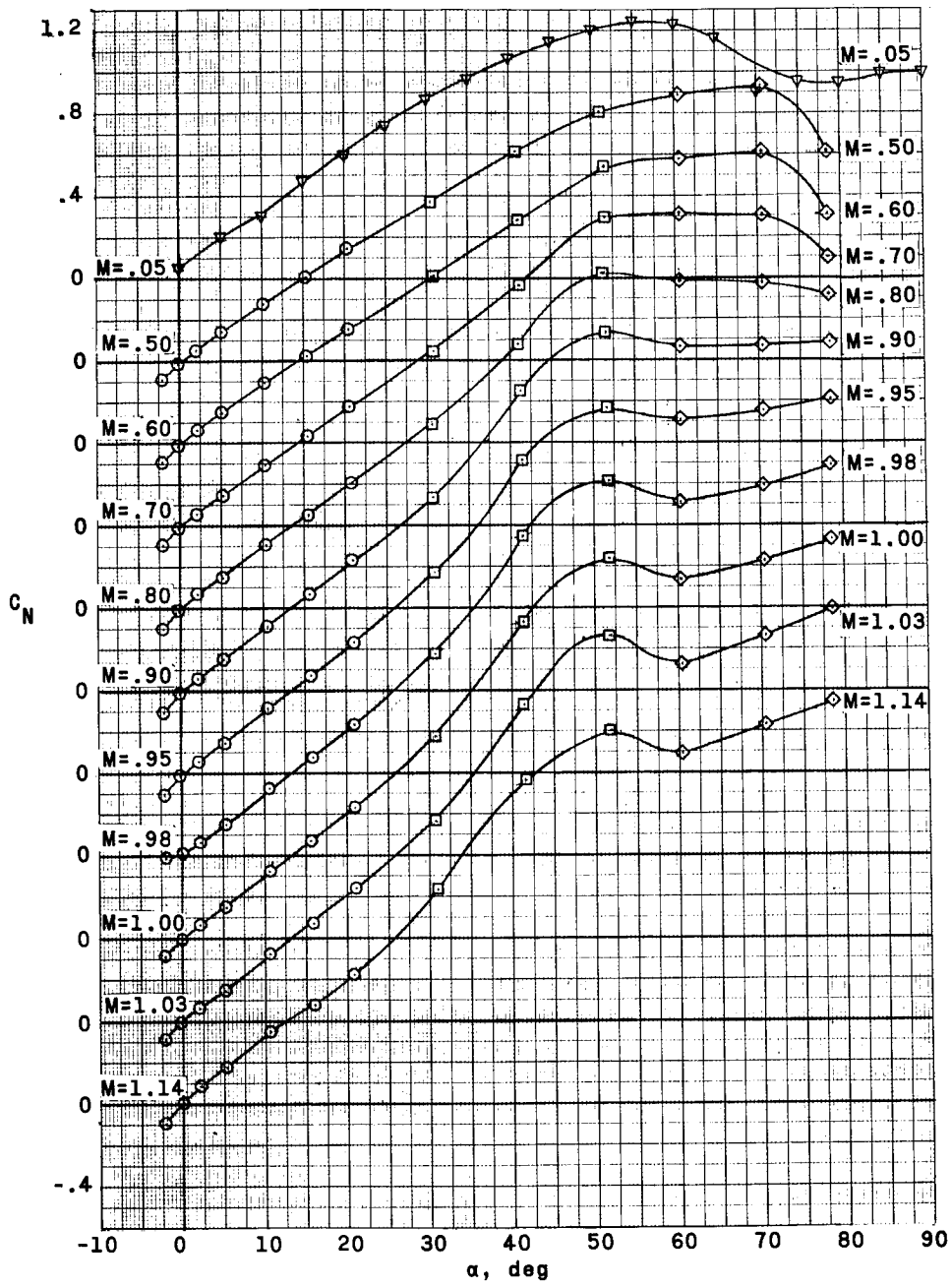

Figure 7.- Aerodynamic characteristics of basic escape configuration at Mach numbers from 0.05 to 1.14. Symbol change denotes change in sting or support arrangement.

G
6

[redacted]

DE[redacted]SIFIED

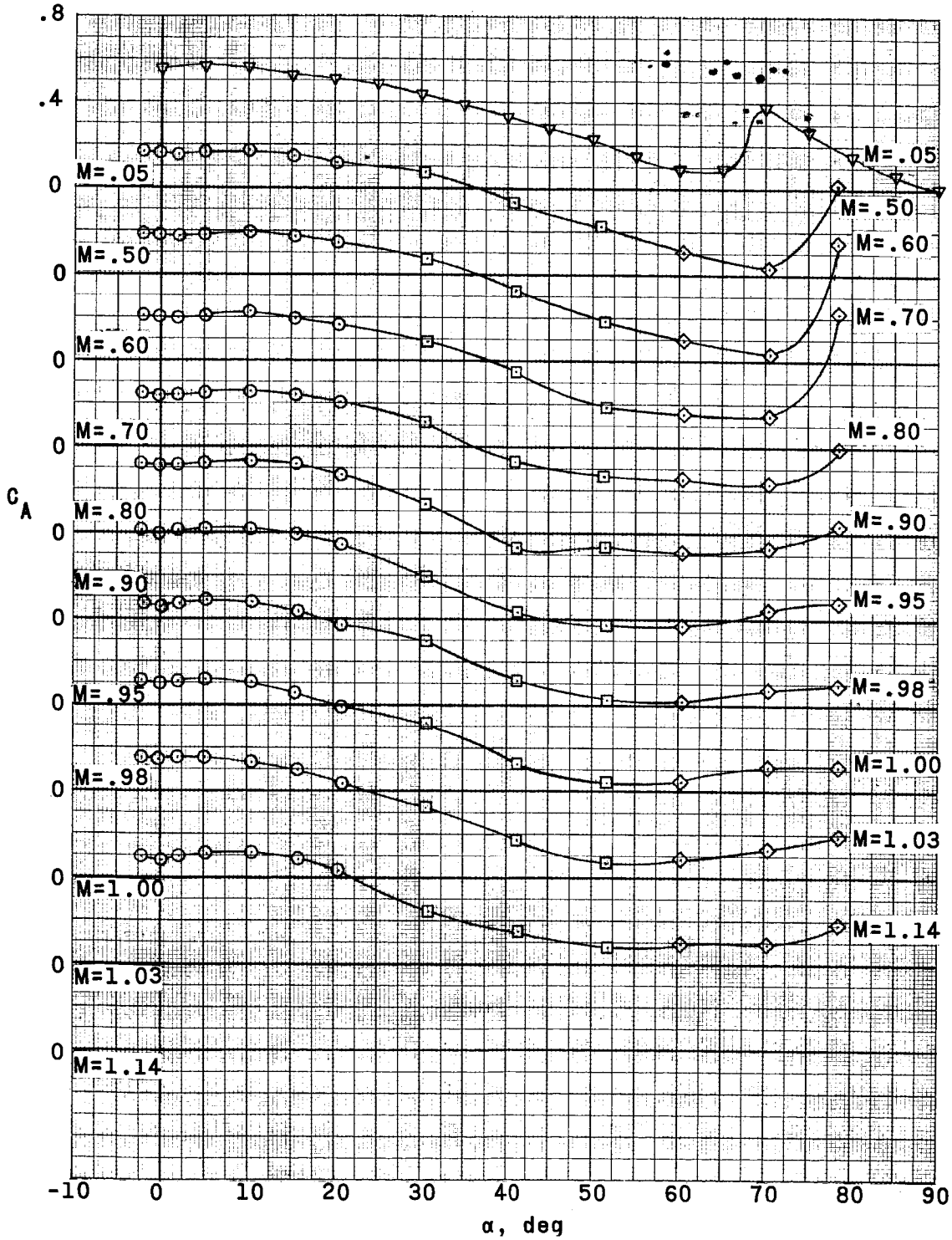

Figure 7.- Continued.

[redacted]

DECLASSIFIED

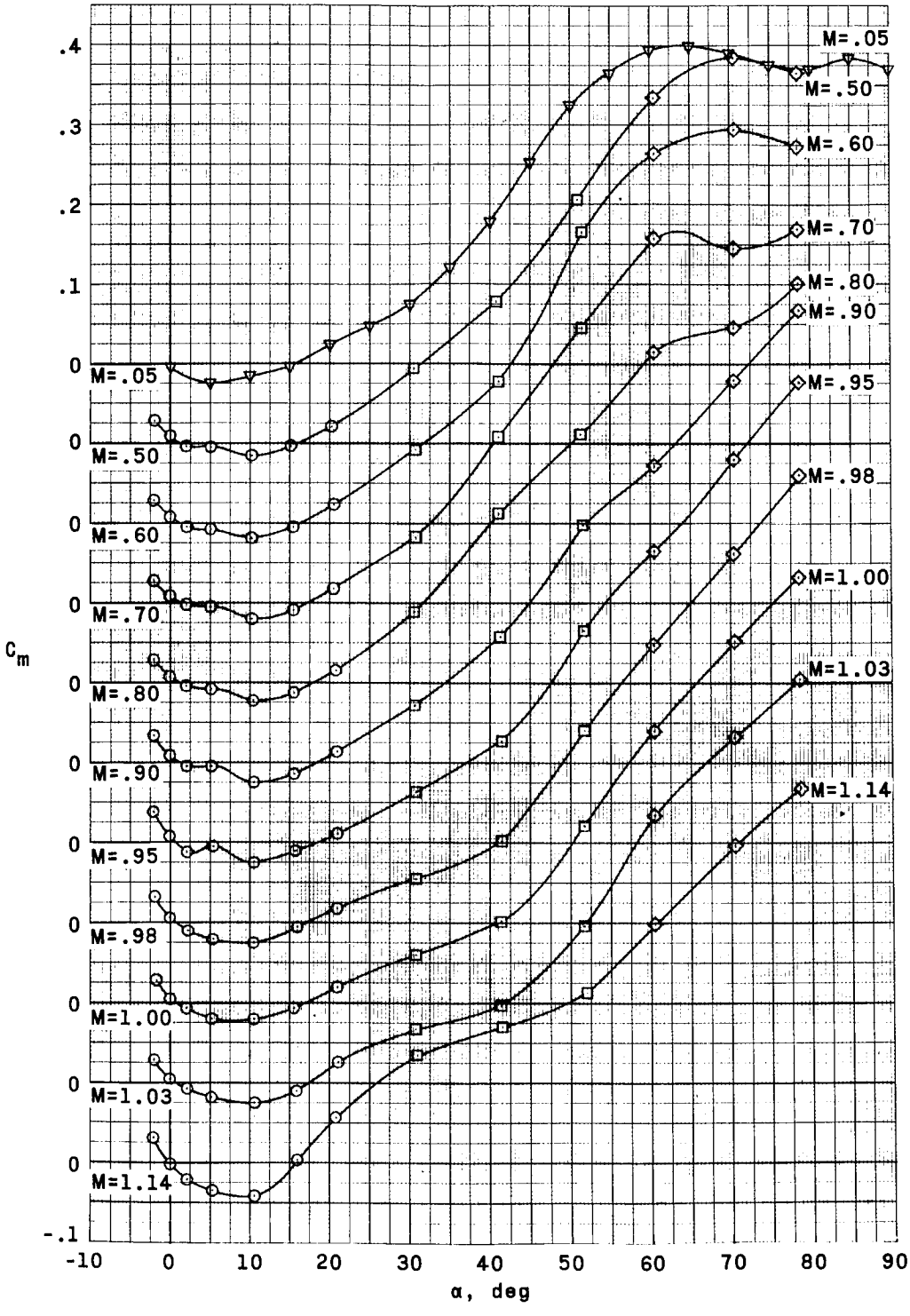

Figure 7.- Continued.

CONFIDENTIAL

DE[redacted]IFIED

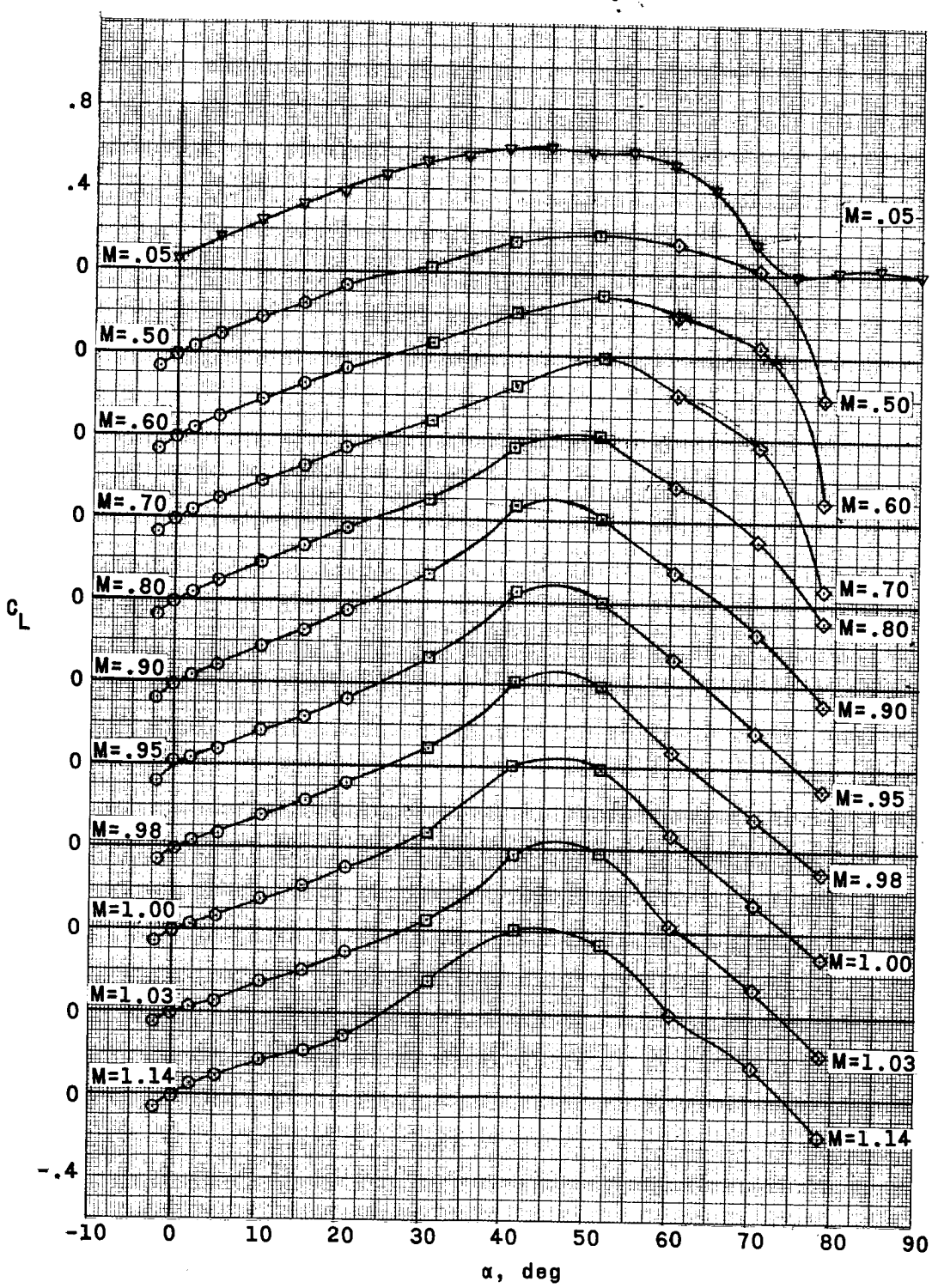

Figure 7.- Continued.

[redacted]

[redacted]

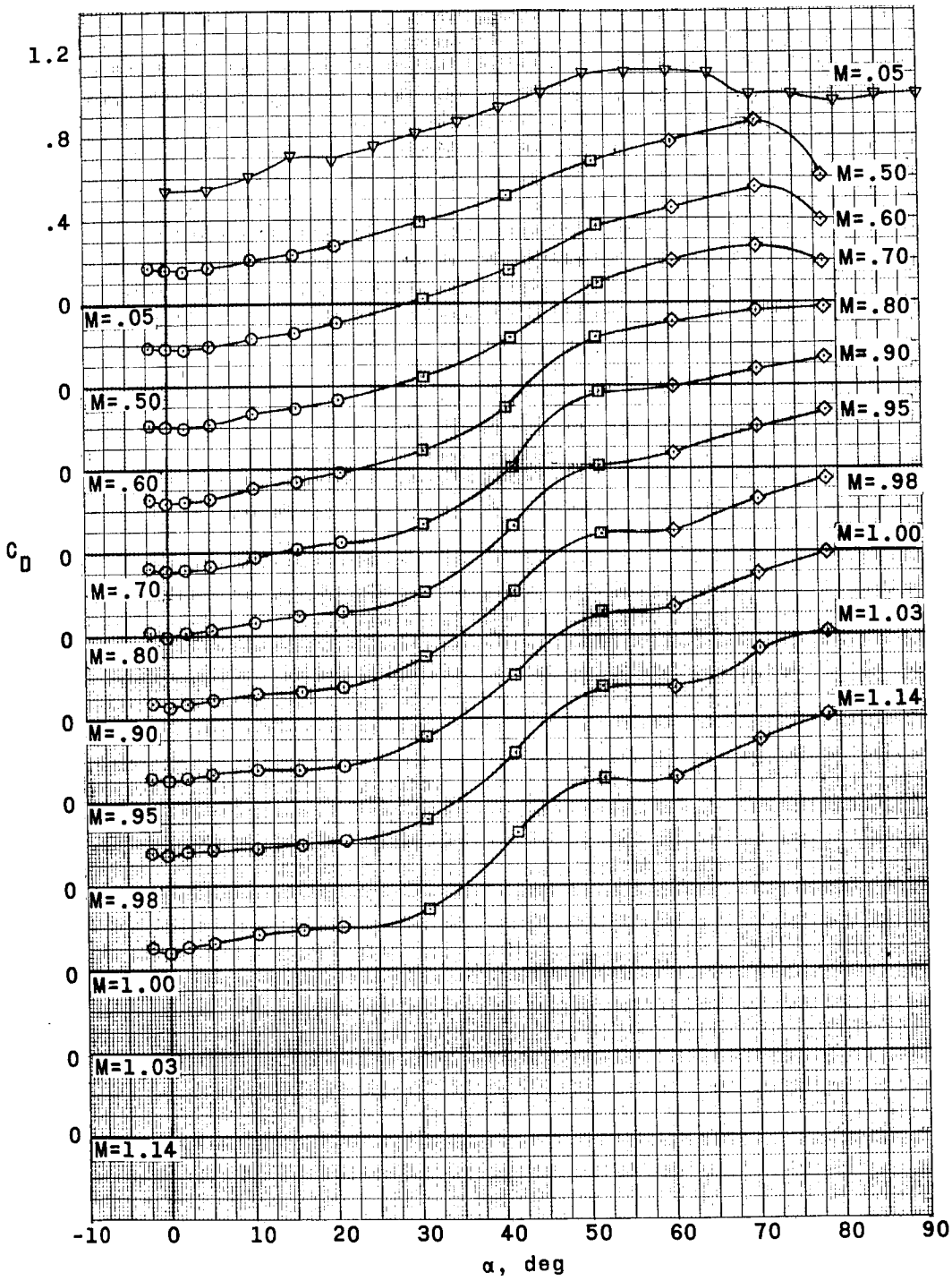

Figure 7.- Concluded.

[redacted]

[redacted]
DECLASSIFIED

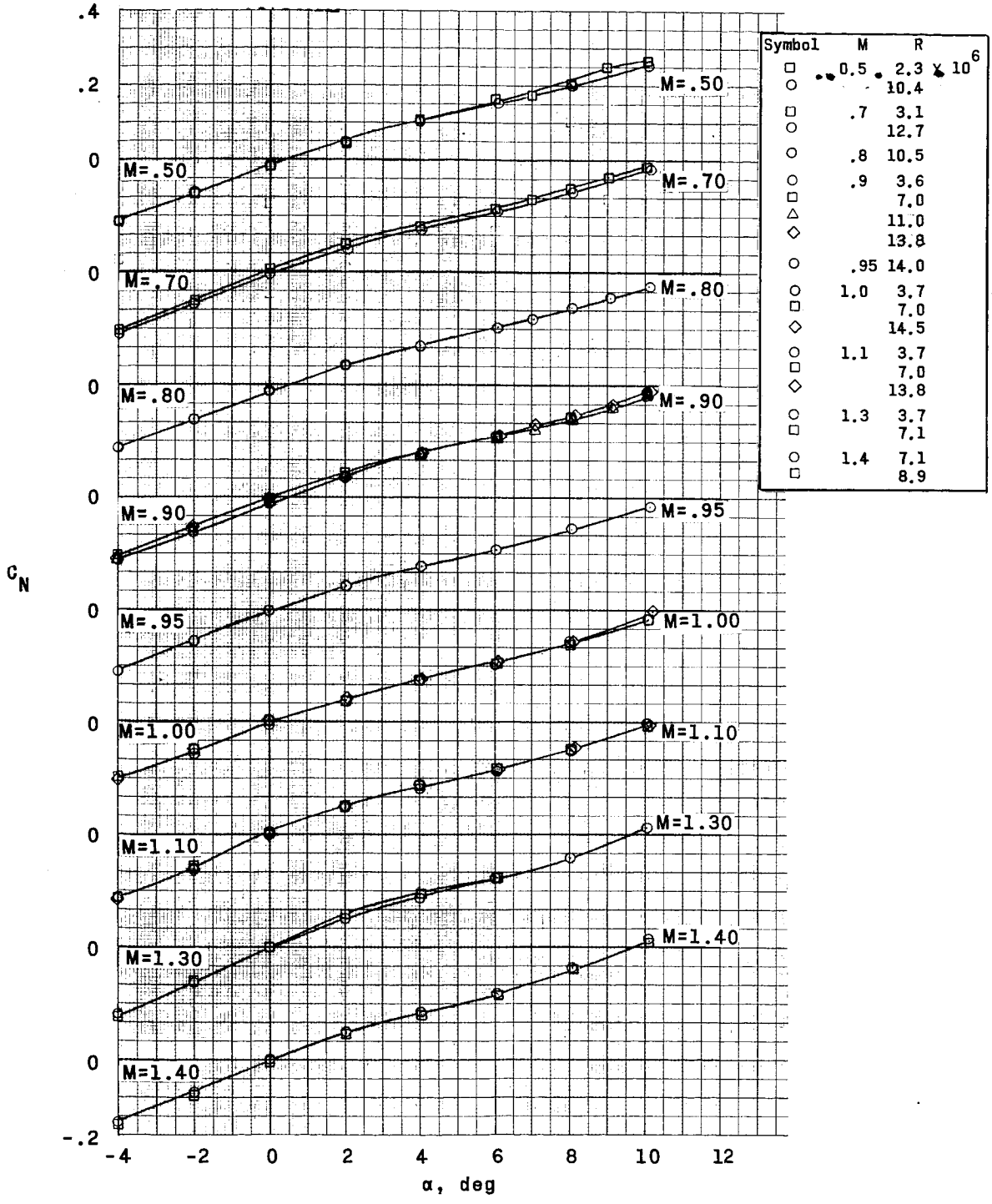

Figure 8.- Aerodynamic characteristics of basic escape configuration at Mach numbers from 0.50 to 1.40.

[redacted]

[redacted]

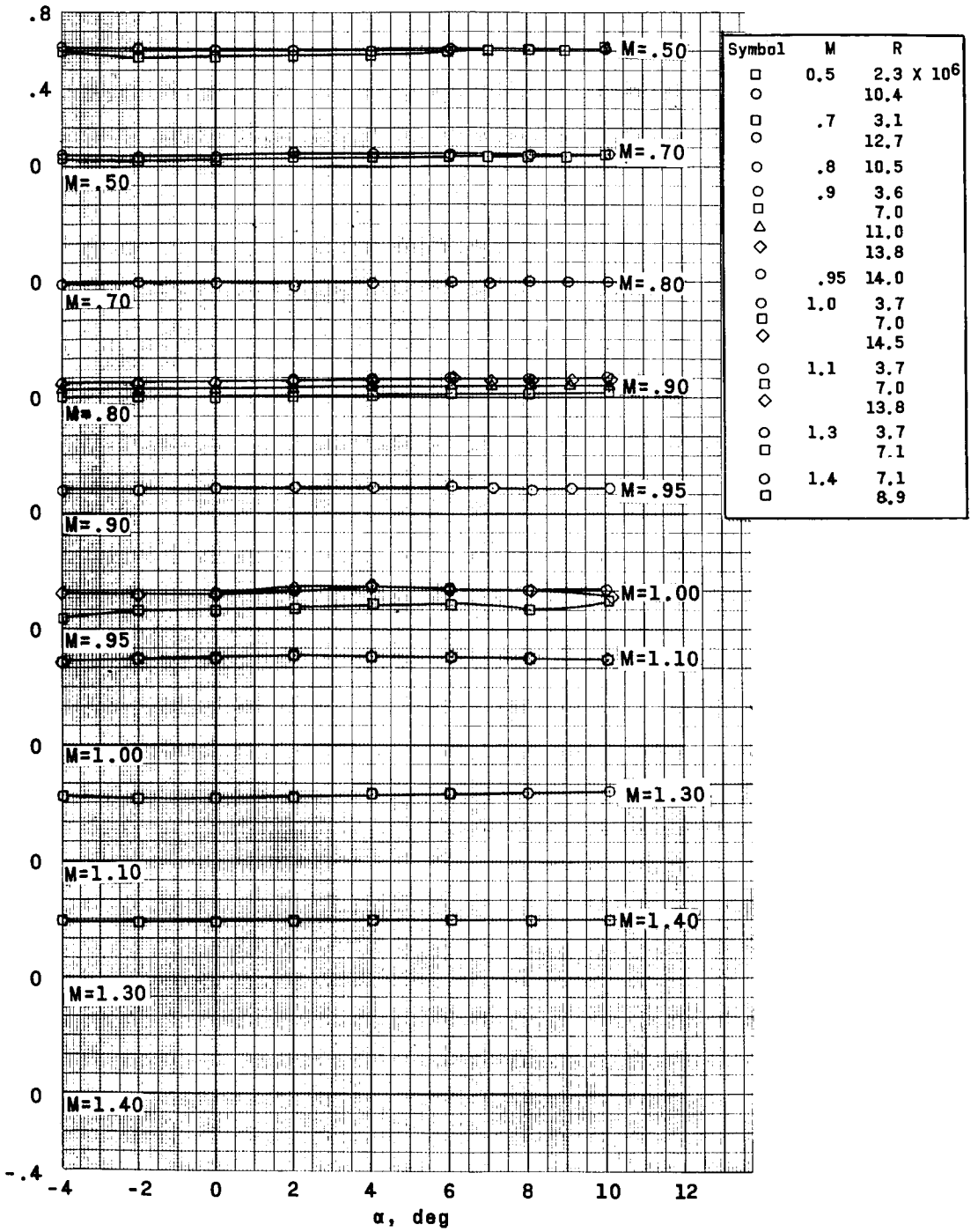

Figure 8.- Continued.

[redacted]

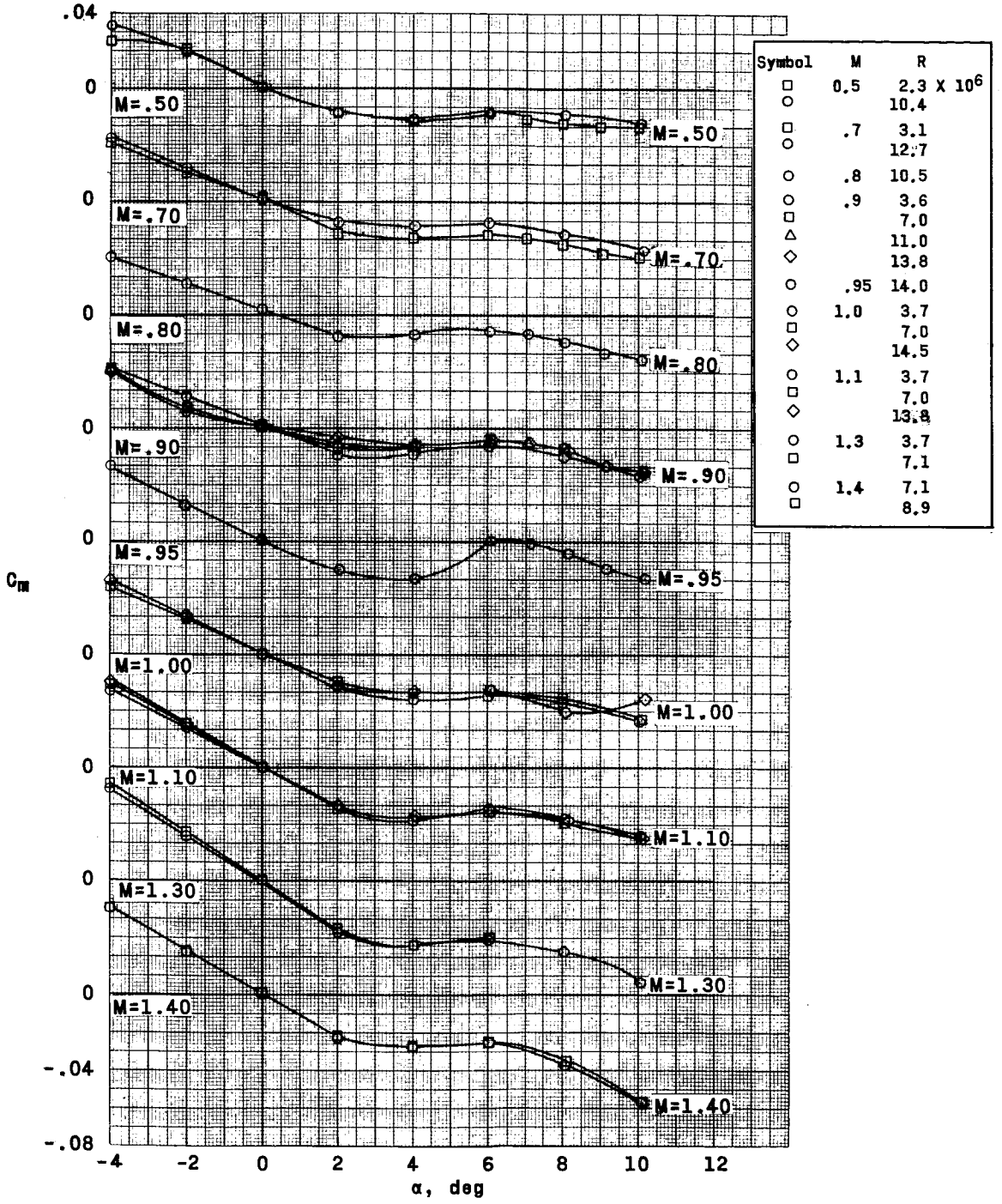

Figure 8.- Continued.

[redacted]

[redacted]

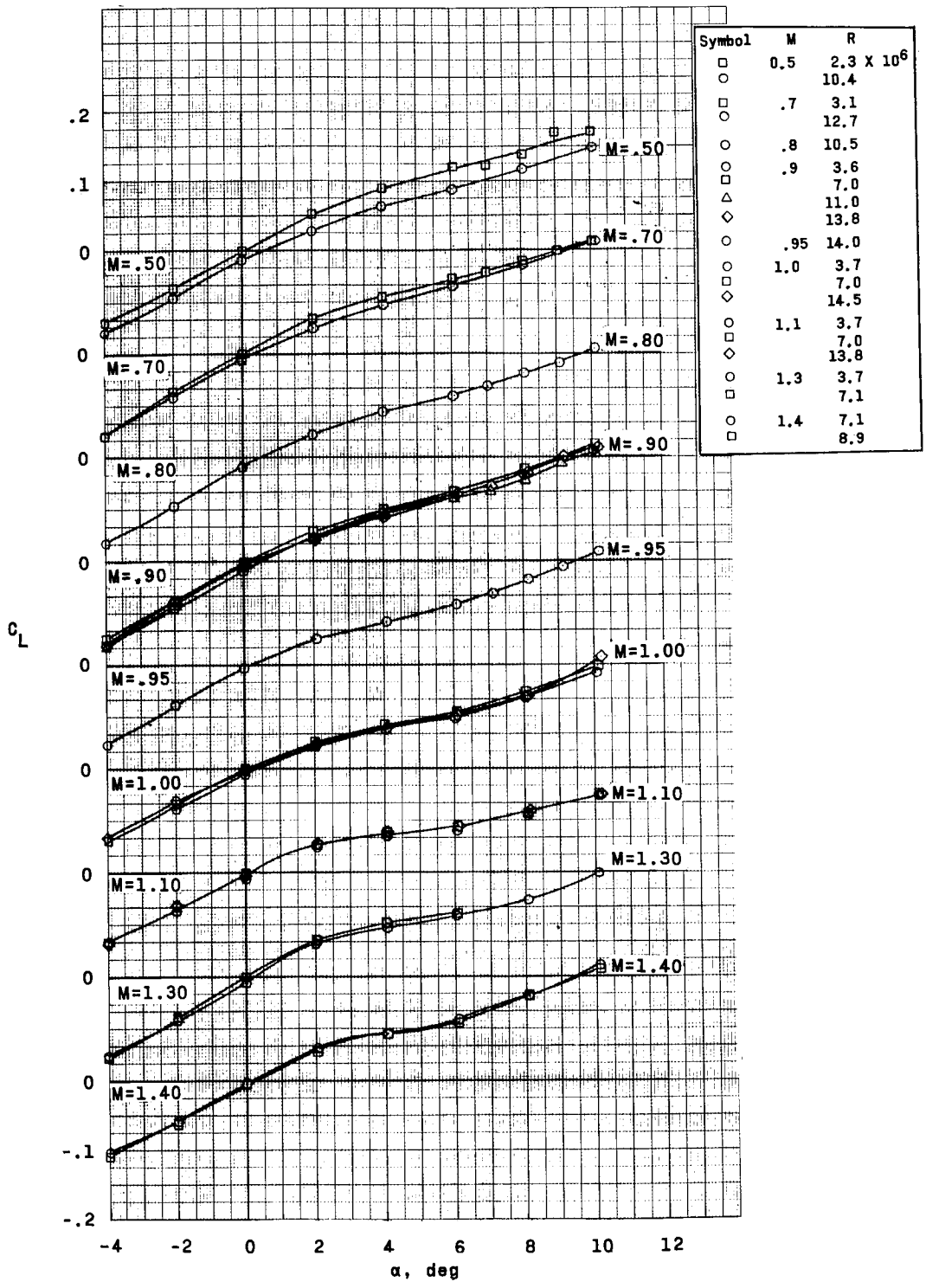

Figure 8.- Continued.

[redacted]

DECLASSIFIED

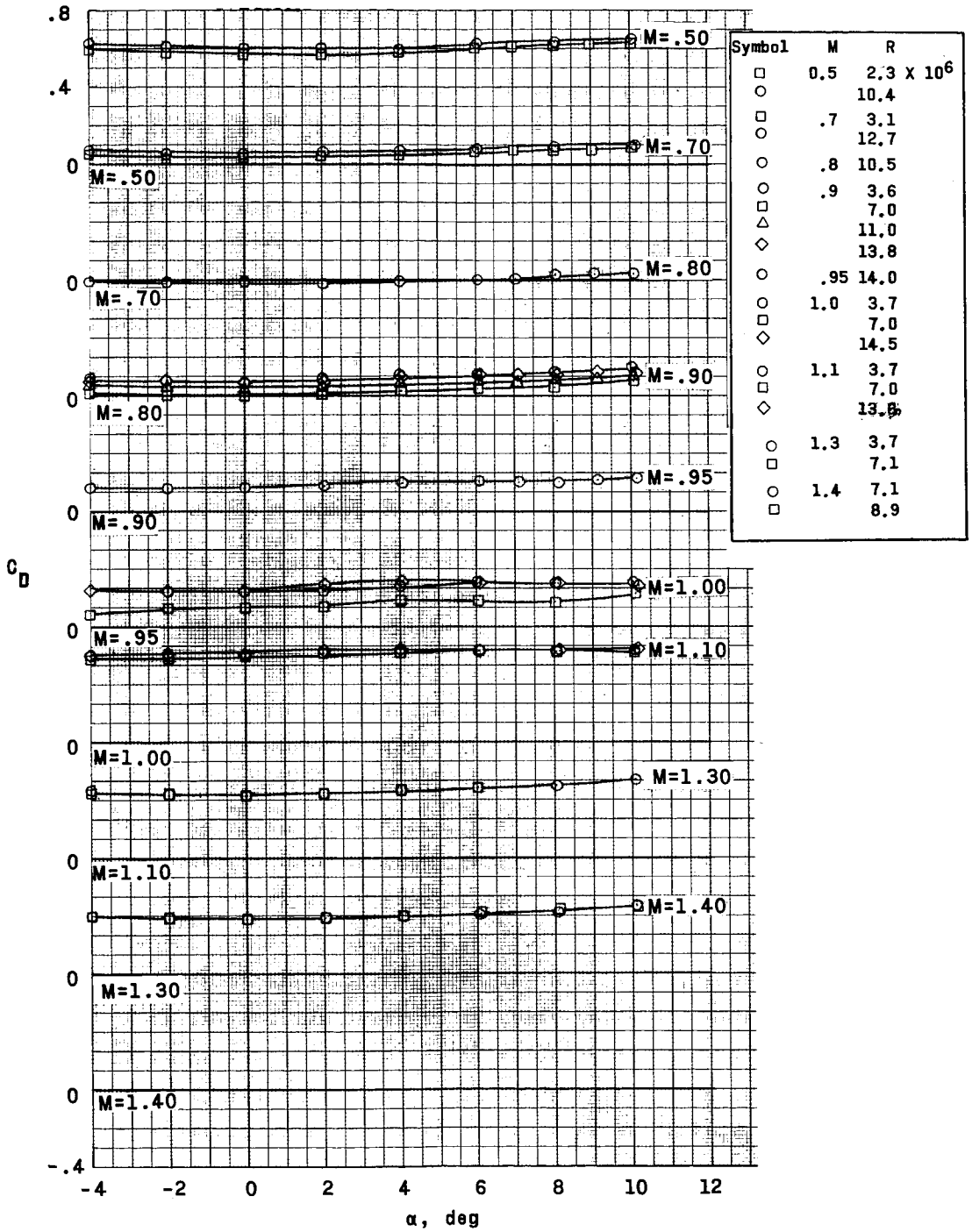

Figure 8.- Concluded.

[redacted]

[redacted]

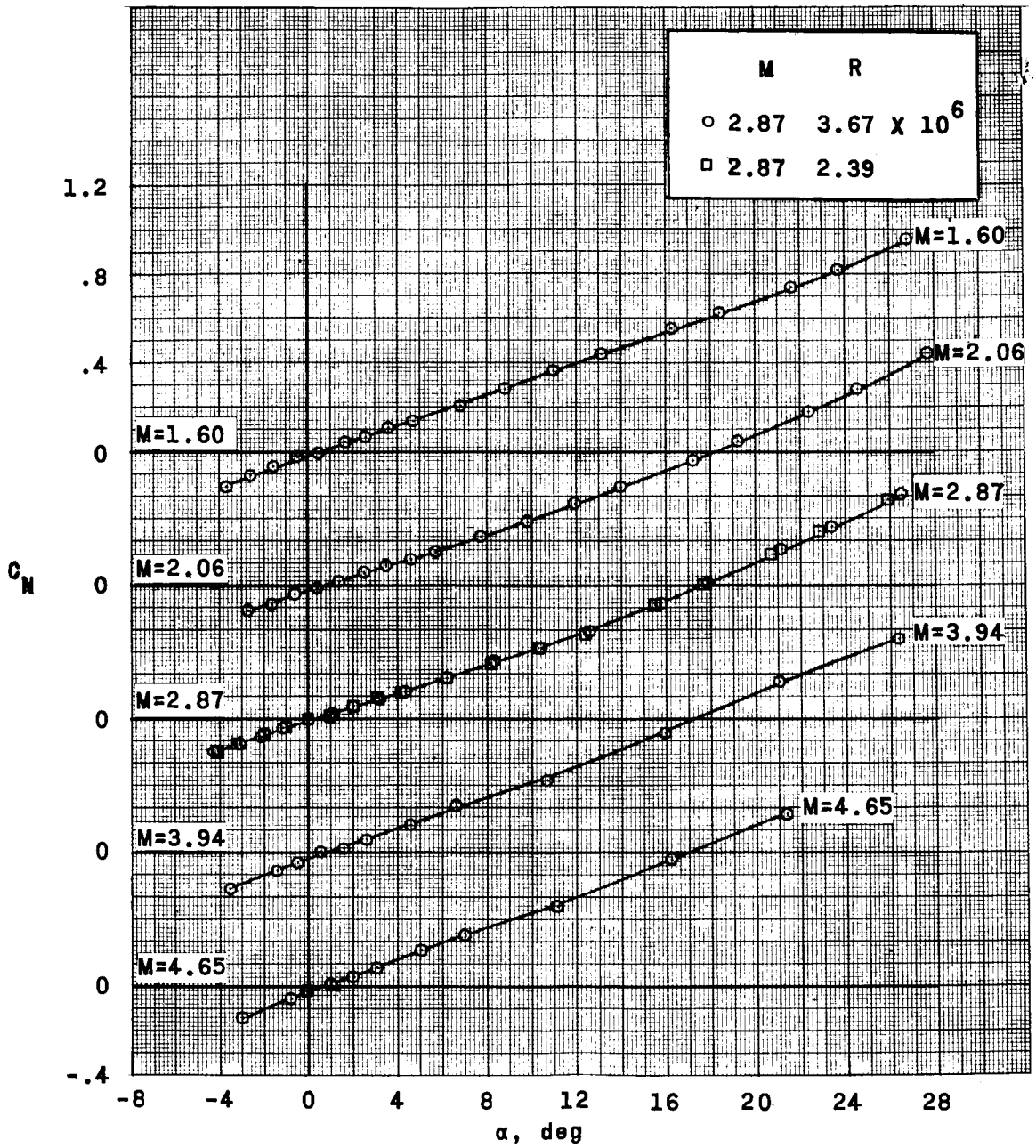

Figure 9.- Aerodynamic characteristics of basic escape configuration at Mach numbers from 1.60 to 4.65.

[redacted]

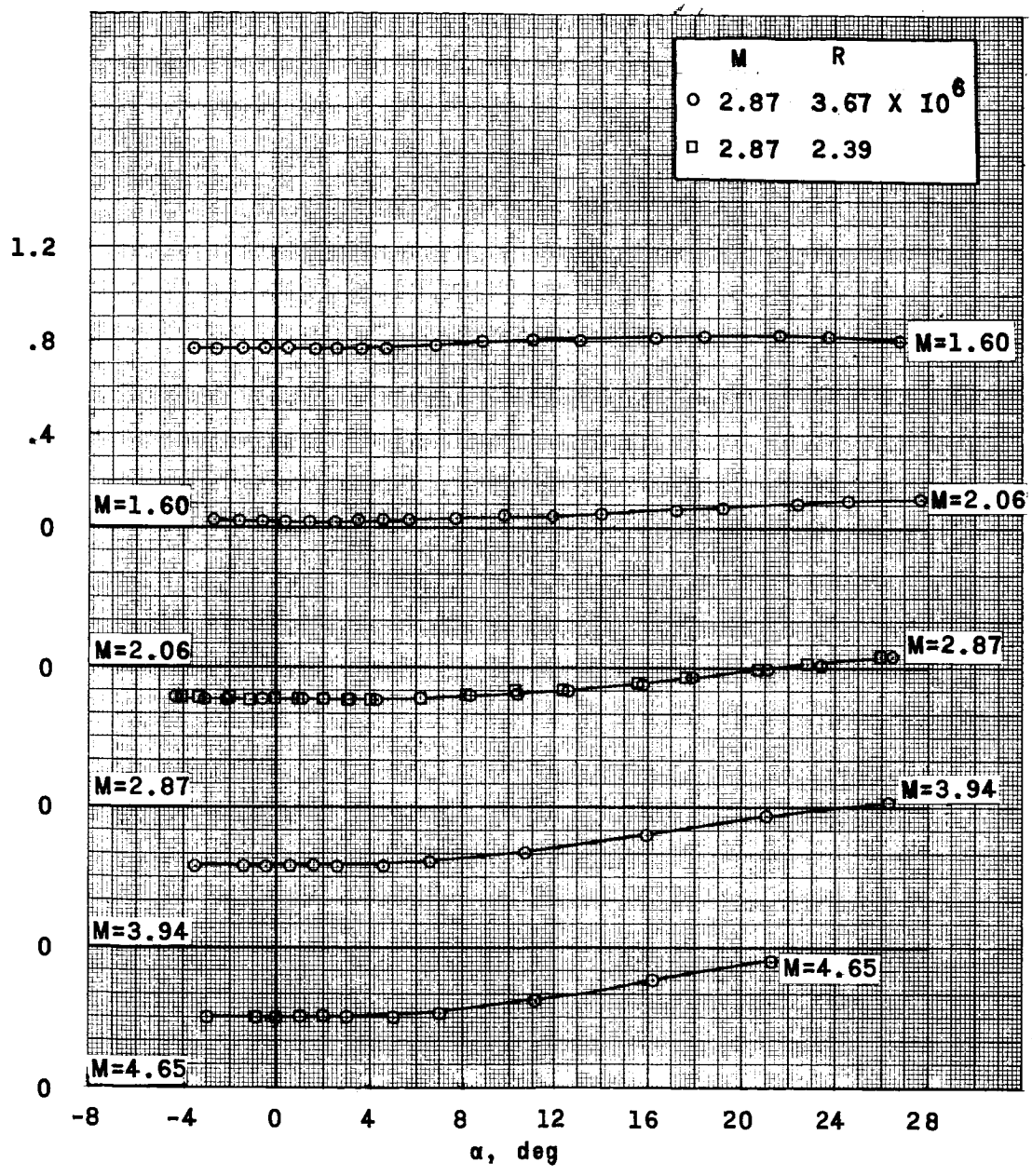

Figure 9.- Continued.

[redacted]

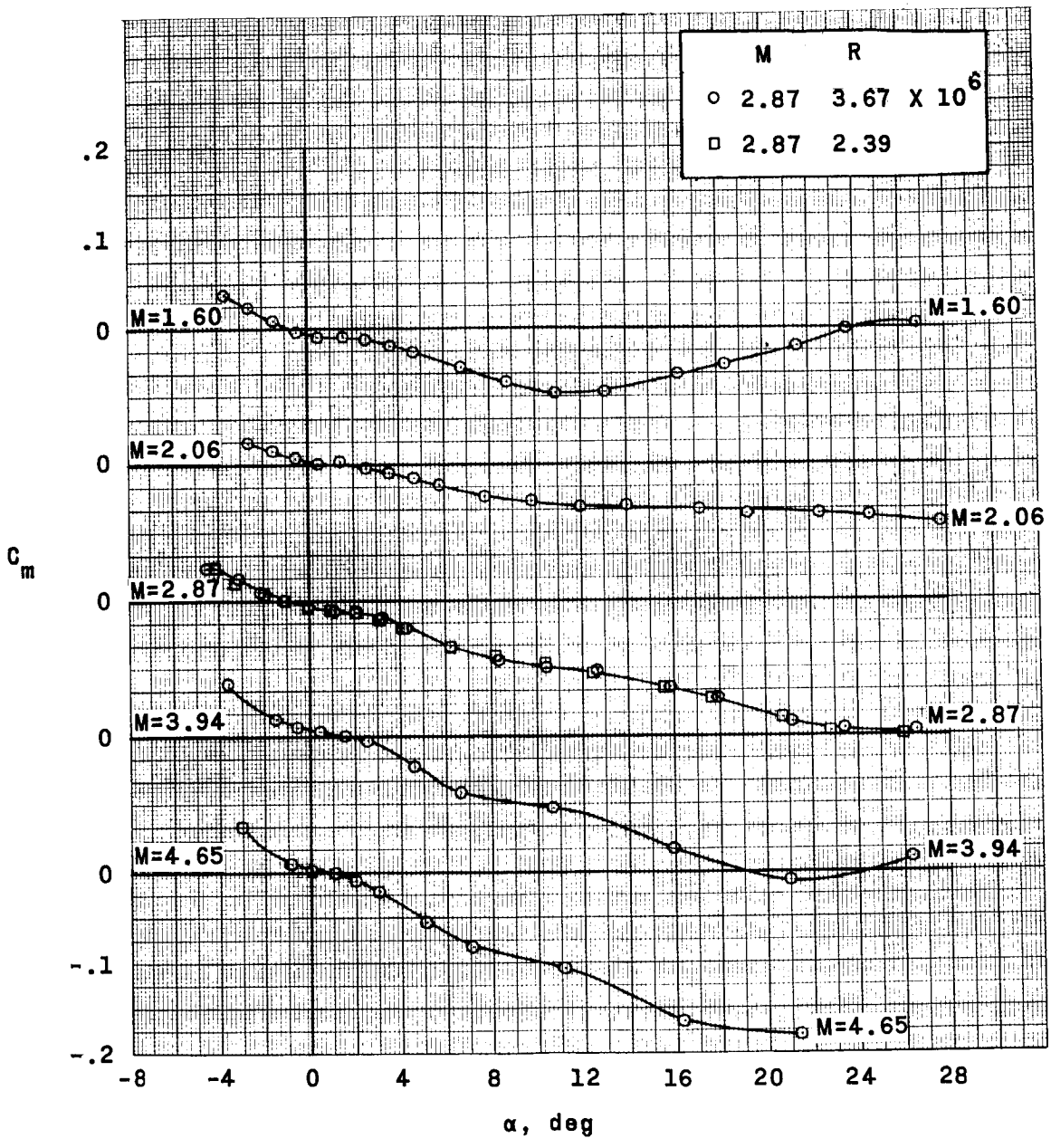

Figure 9.- Continued.

[redacted]

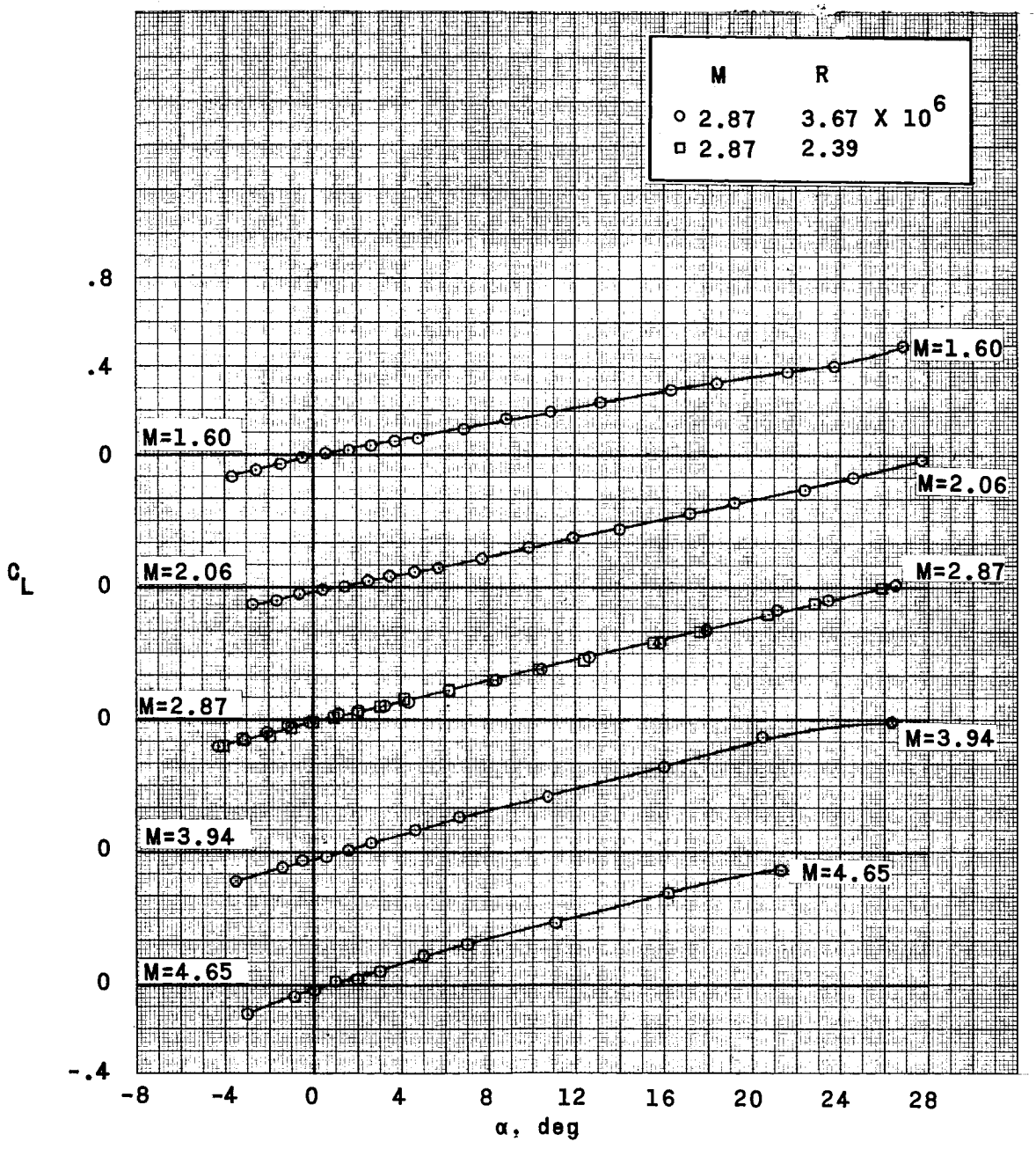

Figure 9.- Continued.

G
6

[redacted]

[redacted]

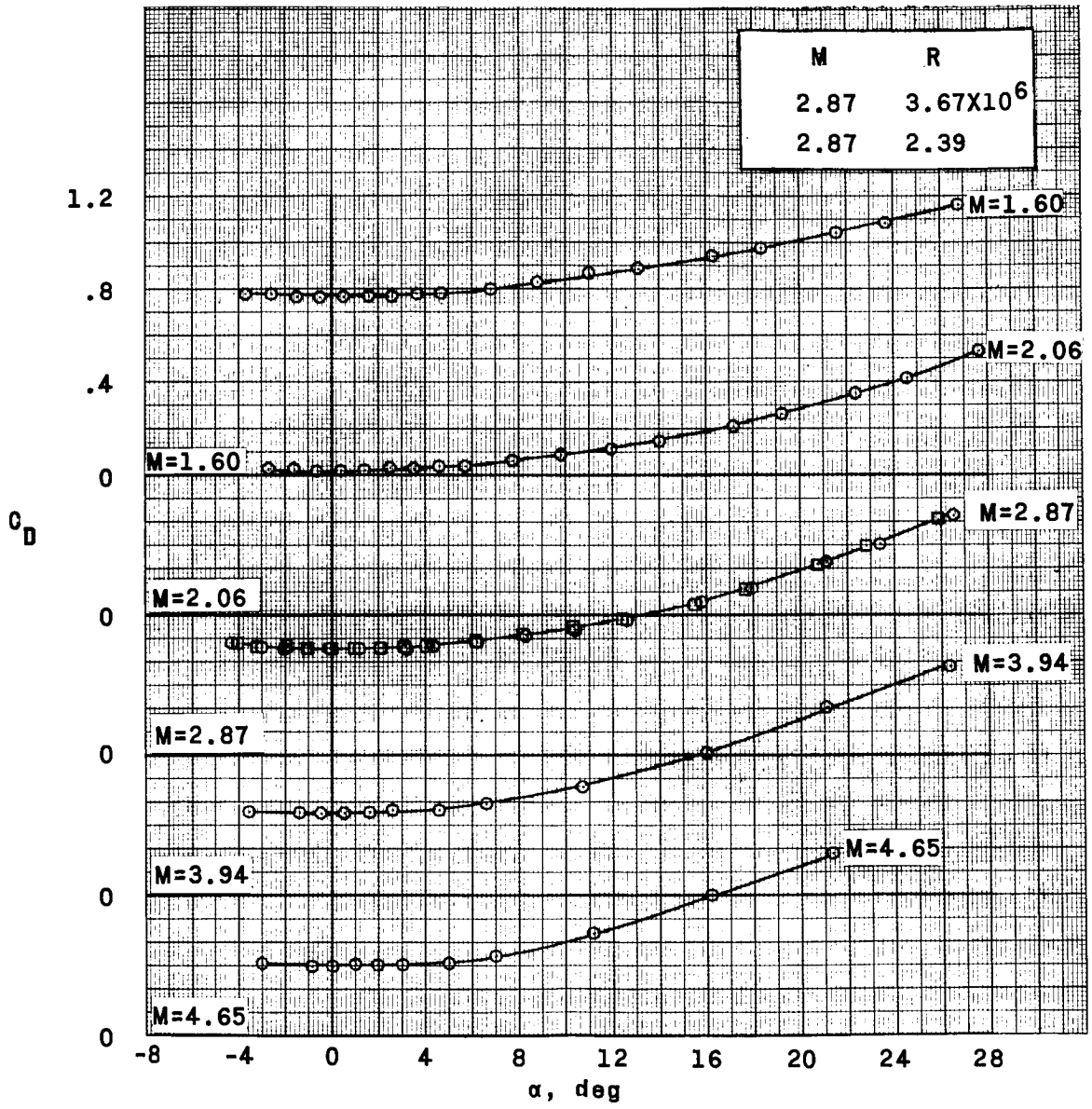

Figure 9.- Concluded.

[redacted]

G
6

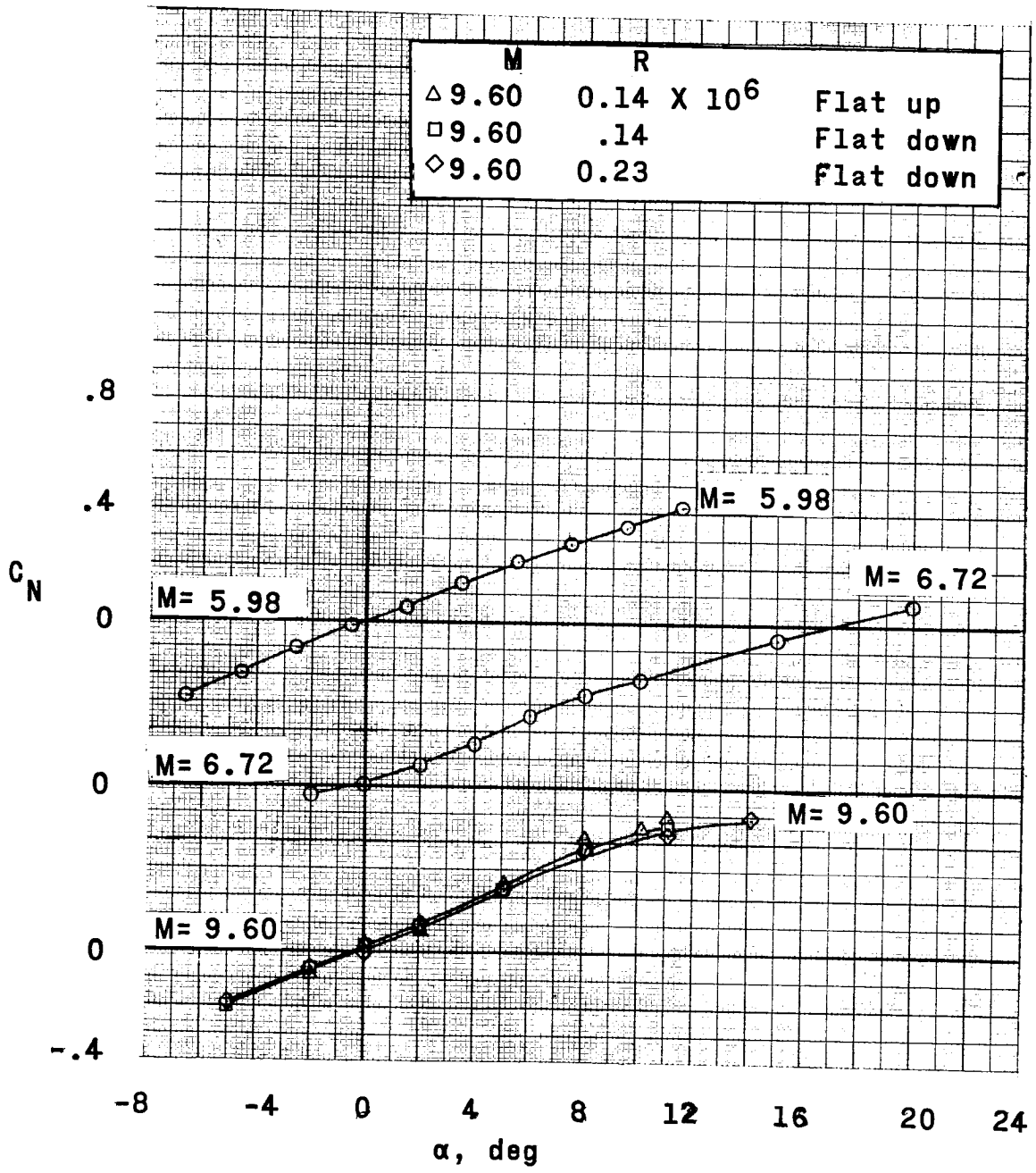

Figure 10.- Aerodynamic characteristics of basic escape configuration at Mach numbers from 5.98 to 9.60.

[redacted]

[redacted]

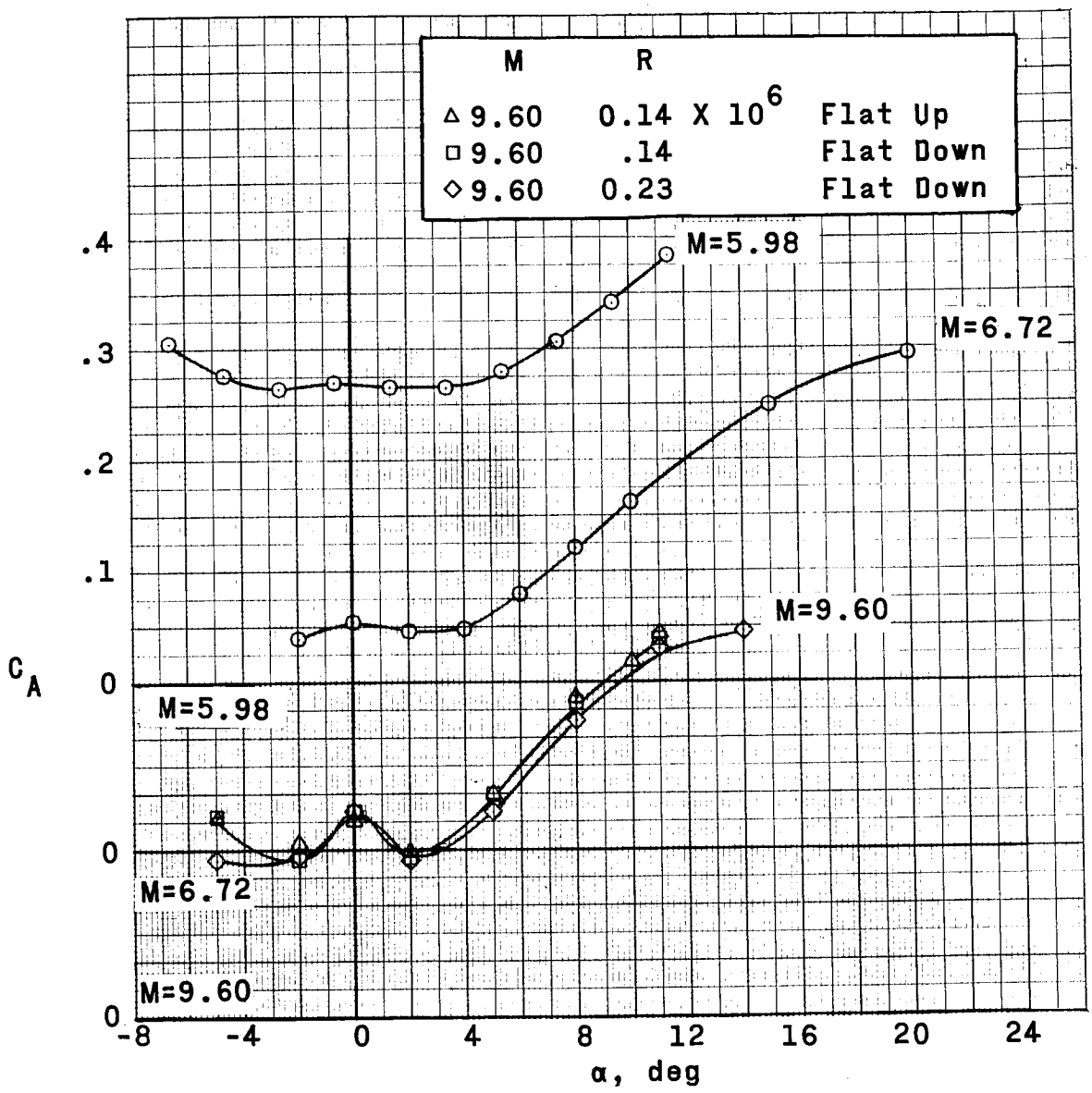

Figure 10.- Continued.

[redacted]

DE[redacted]SIFIED

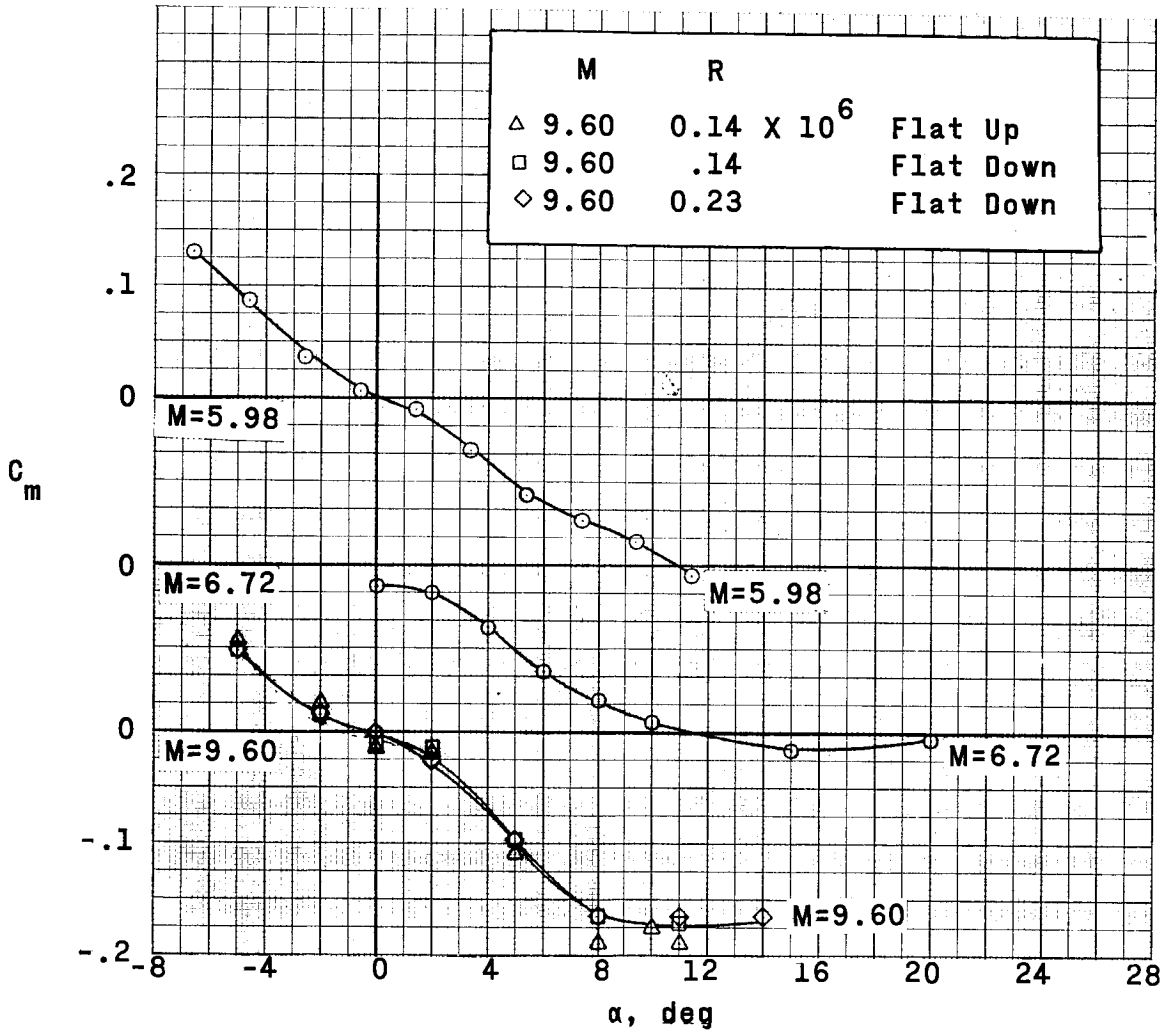

Figure 10.- Continued.

[redacted]

[redacted]

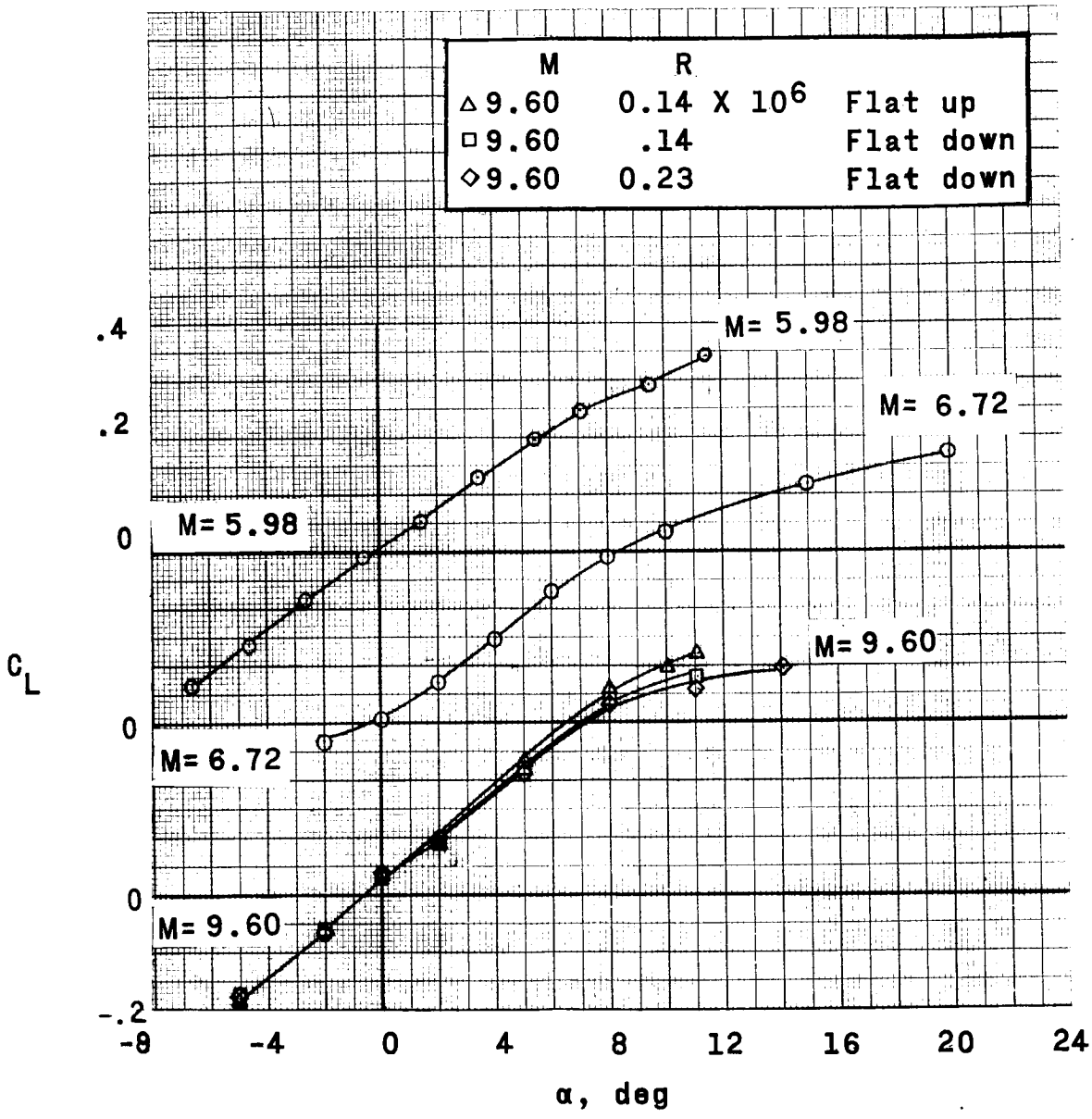

Figure 10.- Continued.

[redacted]

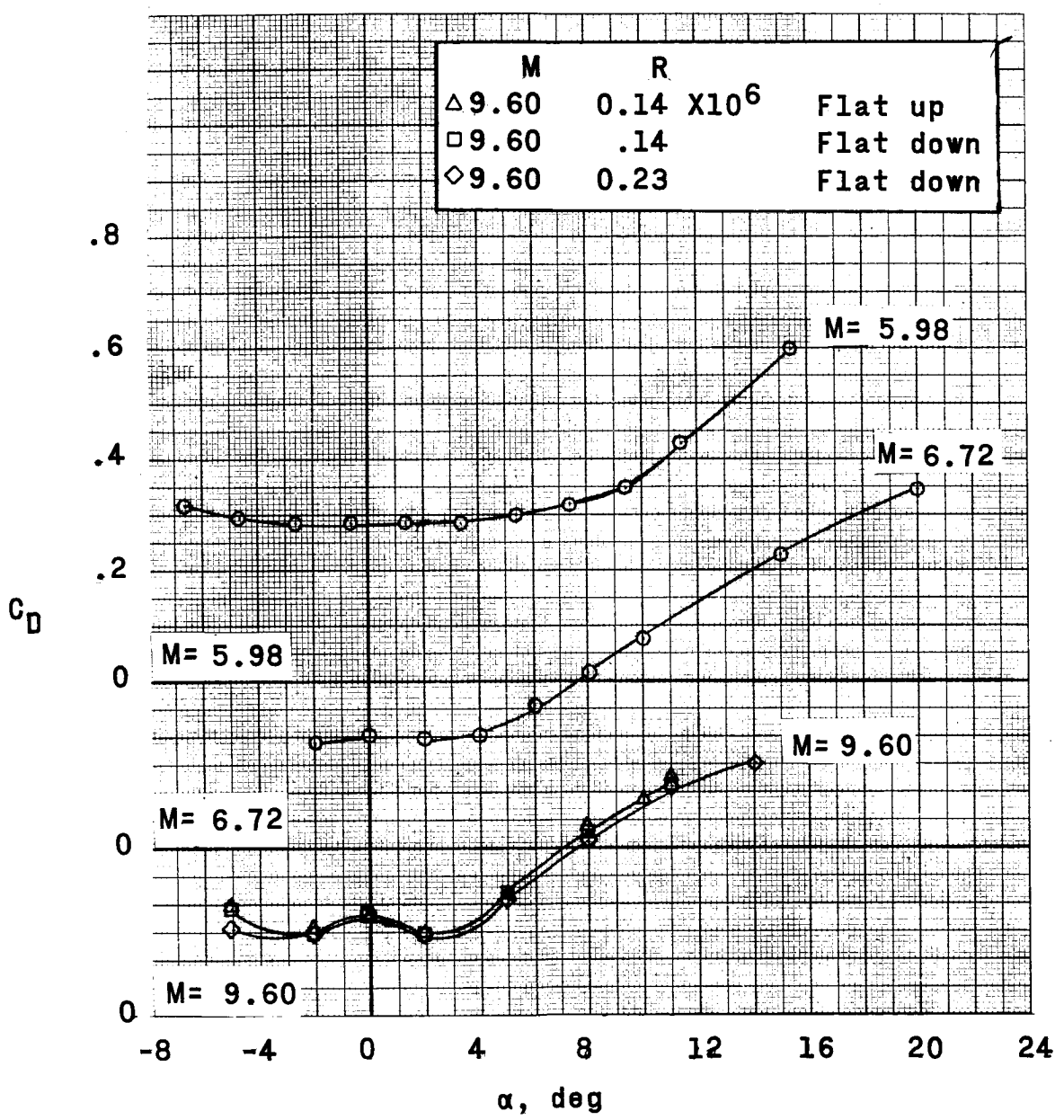

Figure 10.- Concluded.

[redacted]

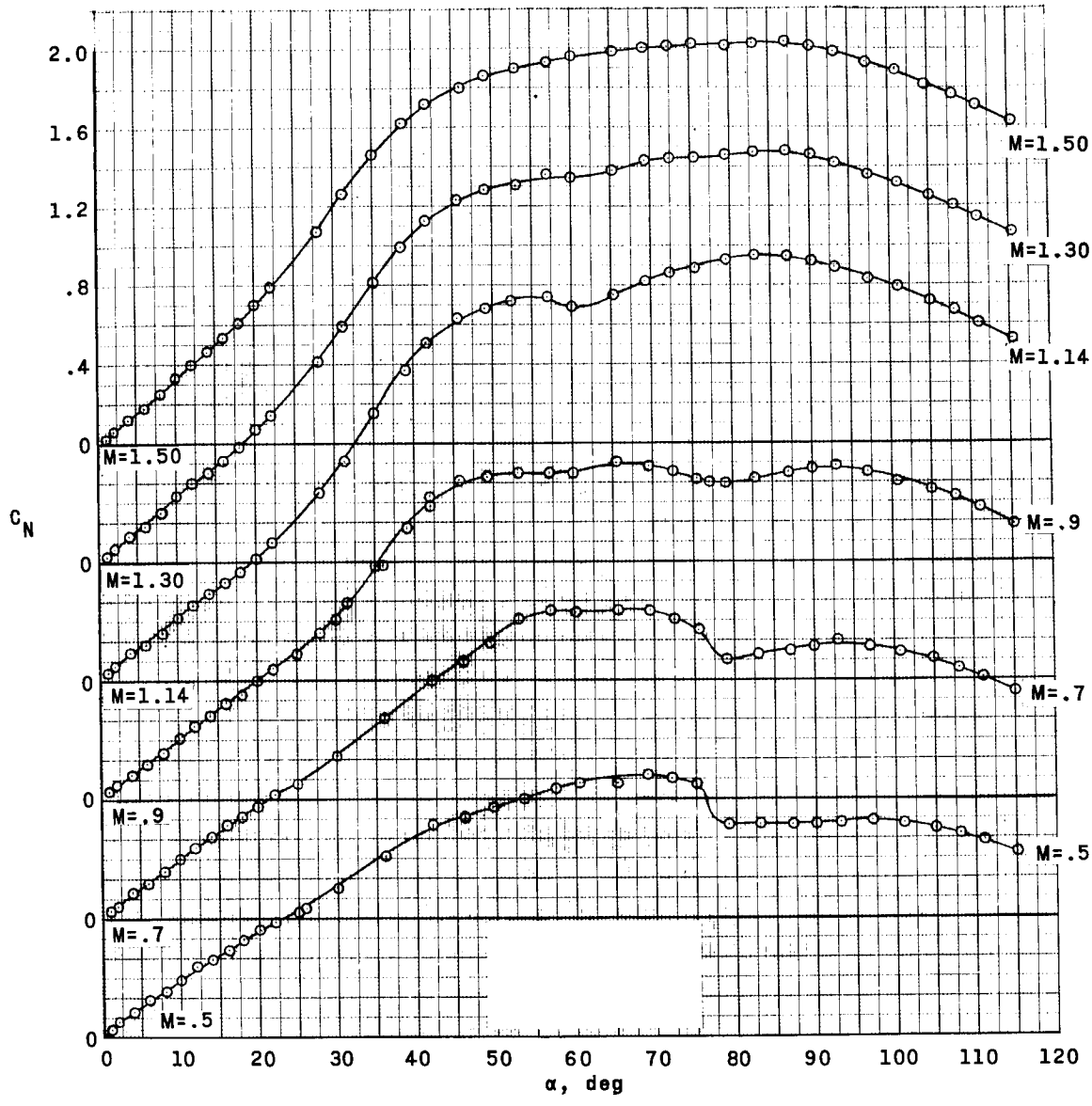

Figure 11.- Aerodynamic characteristics of escape configuration with 1.72 inch by 1.40 inch rocket igniter-cable fairings at Mach numbers from 0.50 to 1.50. $R \approx 6 \times 10^6$.

[redacted]

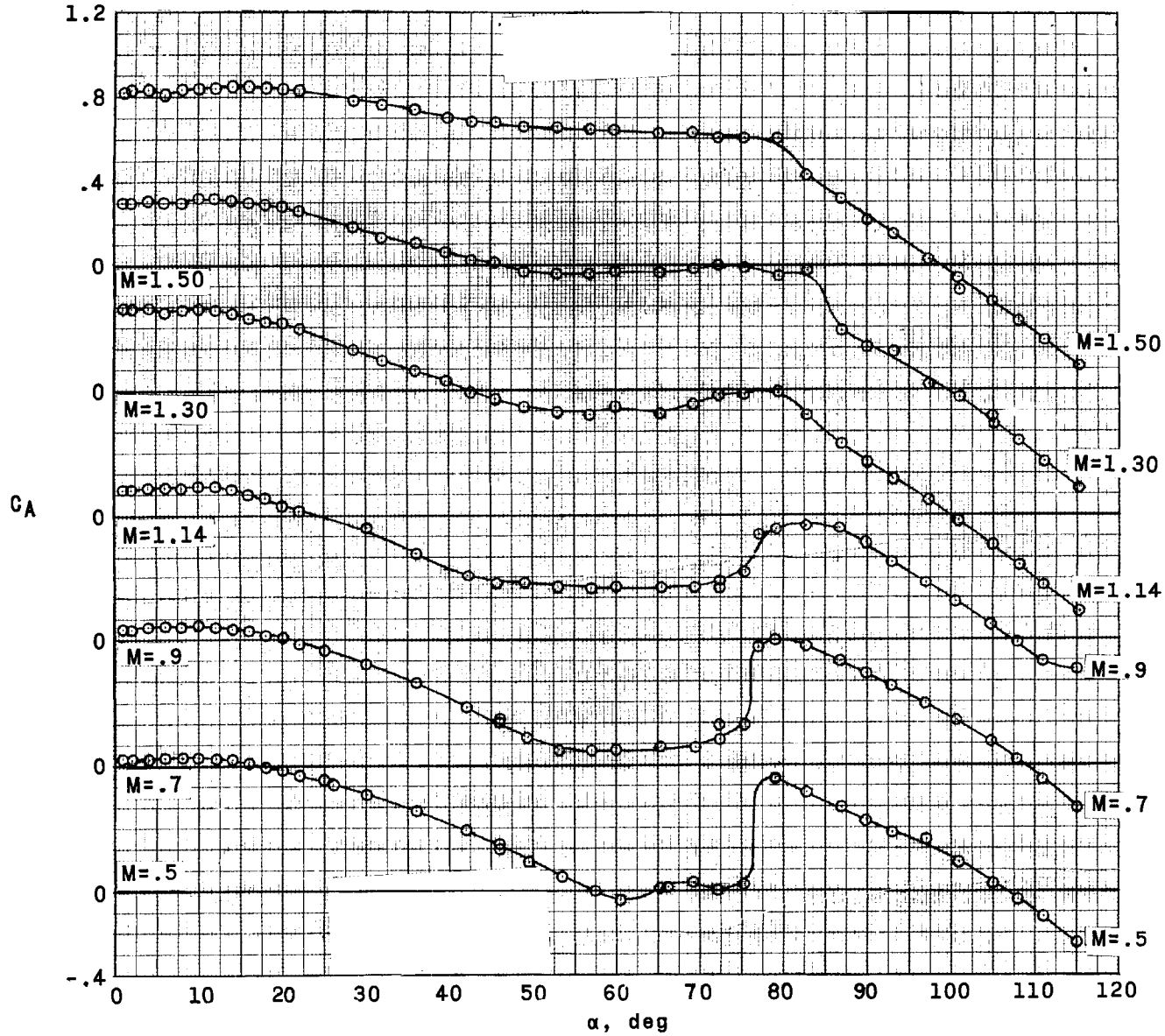

Figure 11.- Continued.

[redacted]

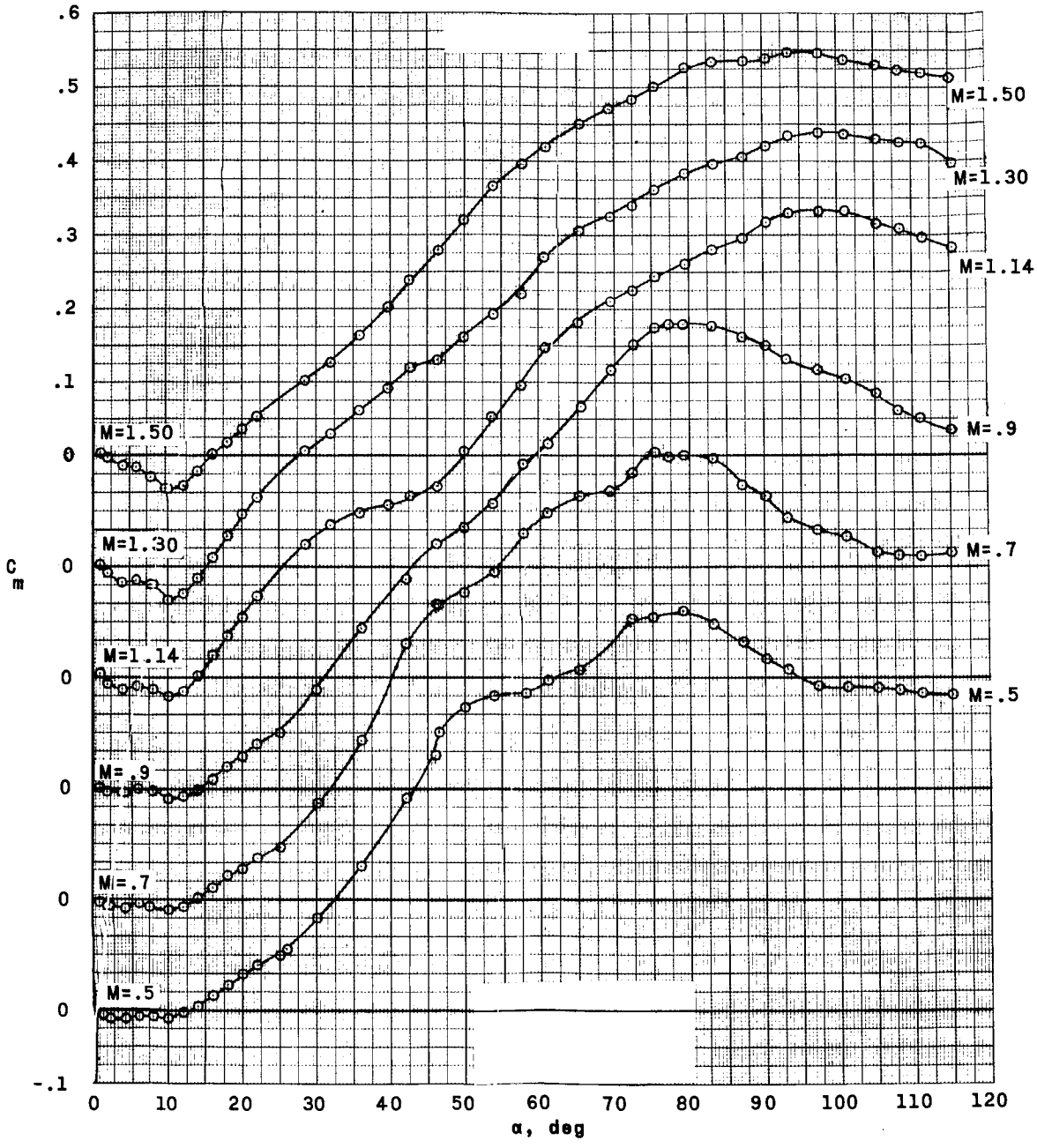

Figure 11.- Continued.

[redacted]

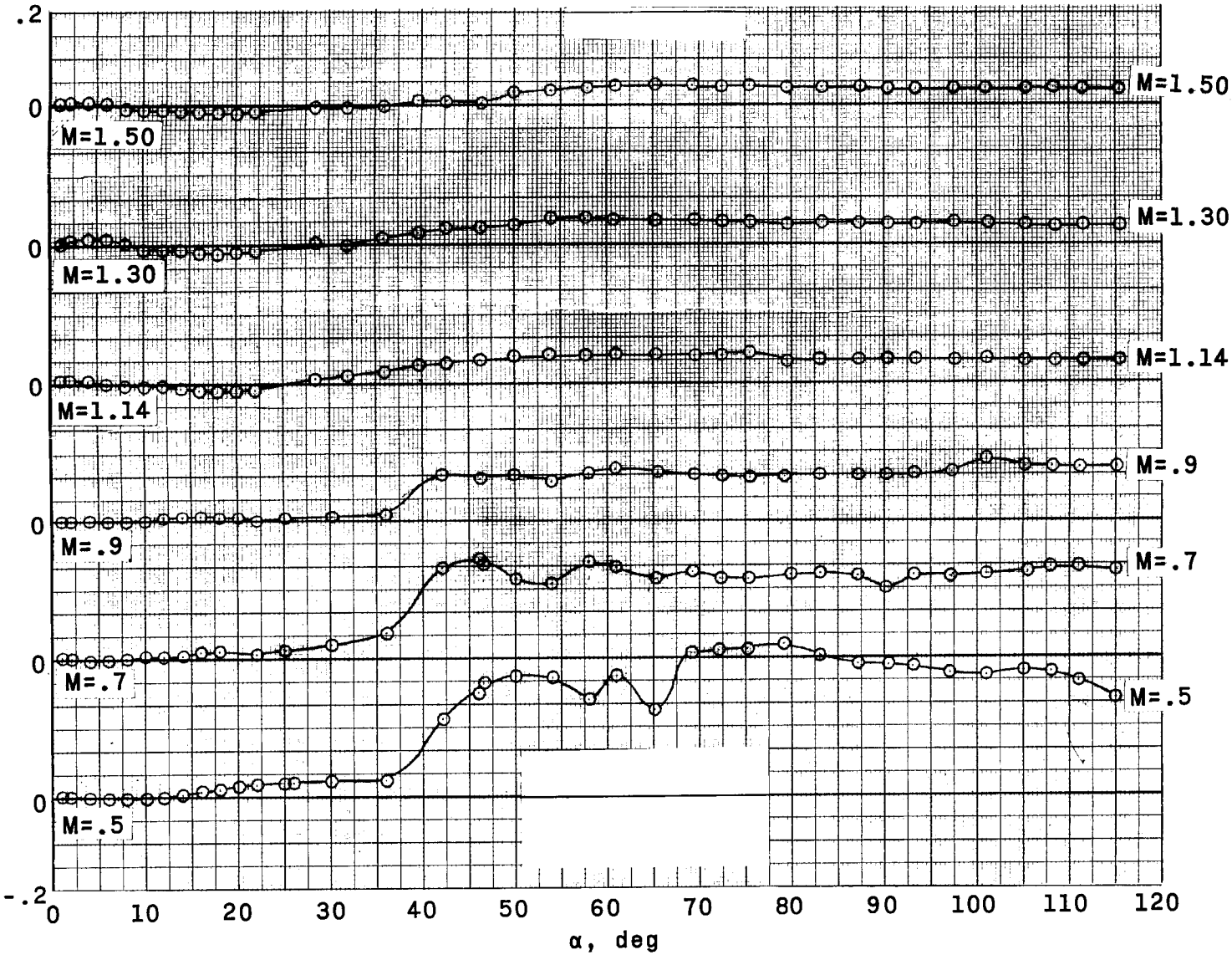

Figure 11.- Continued.

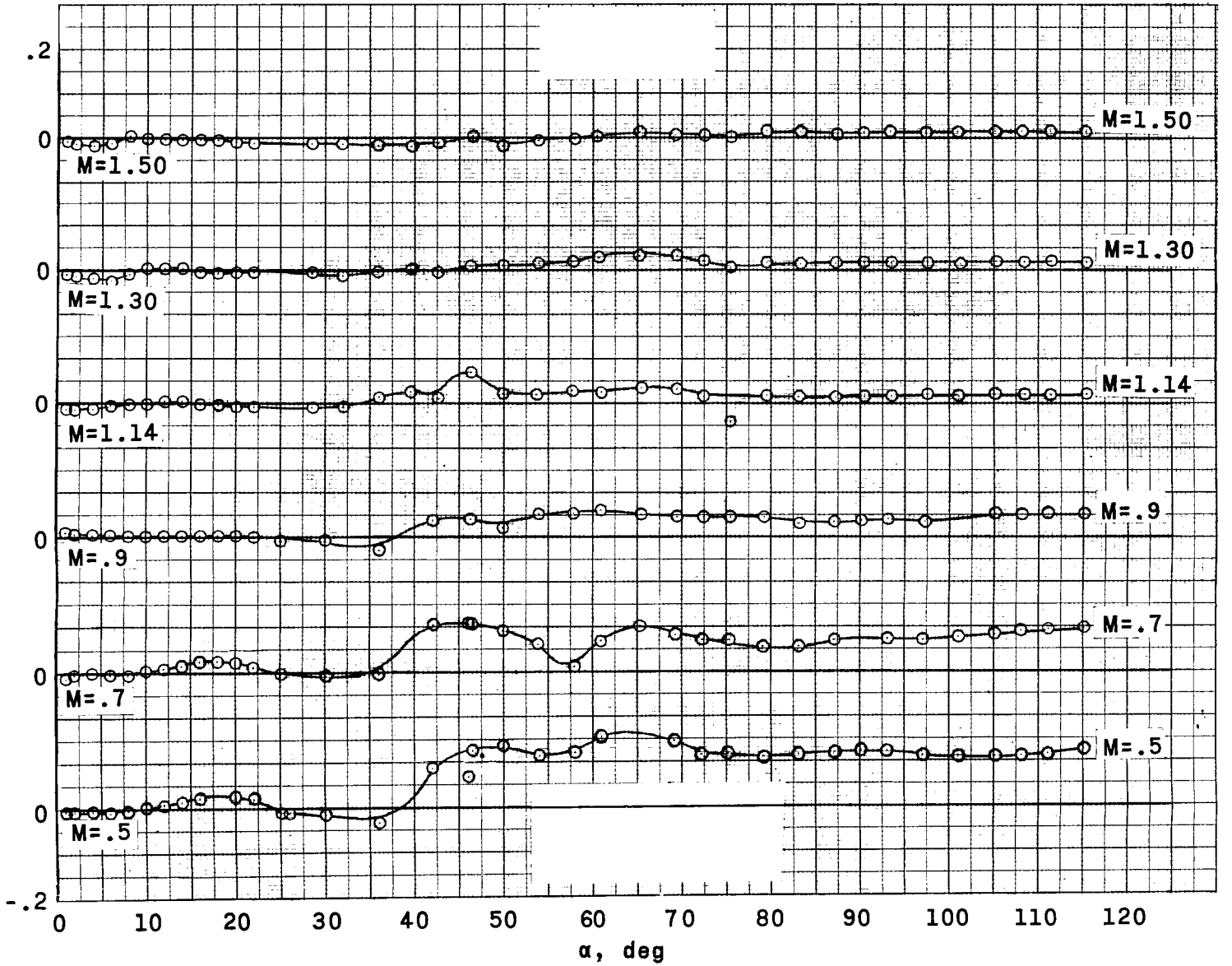

Figure 11.- Continued.

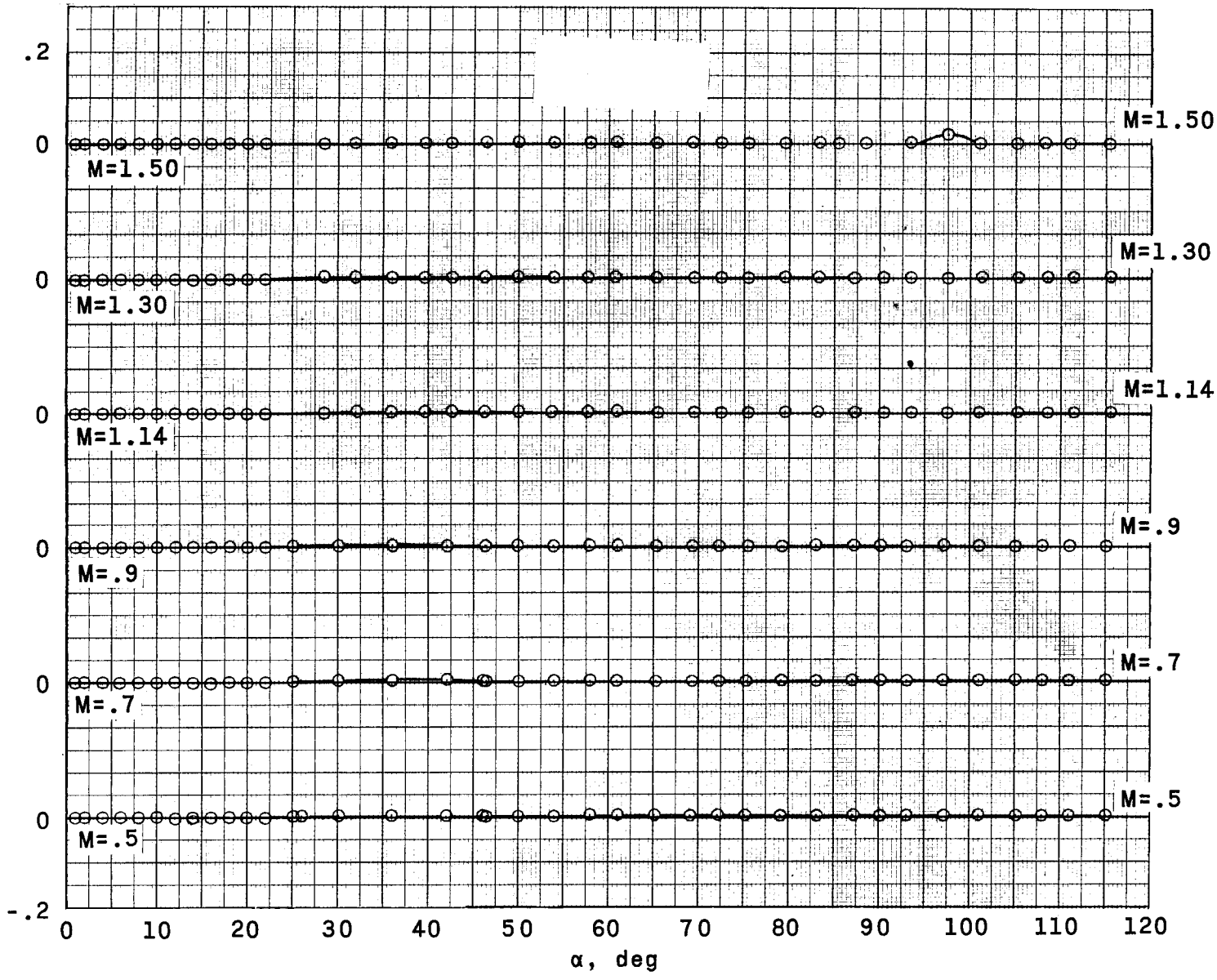

Figure 11.- Continued.

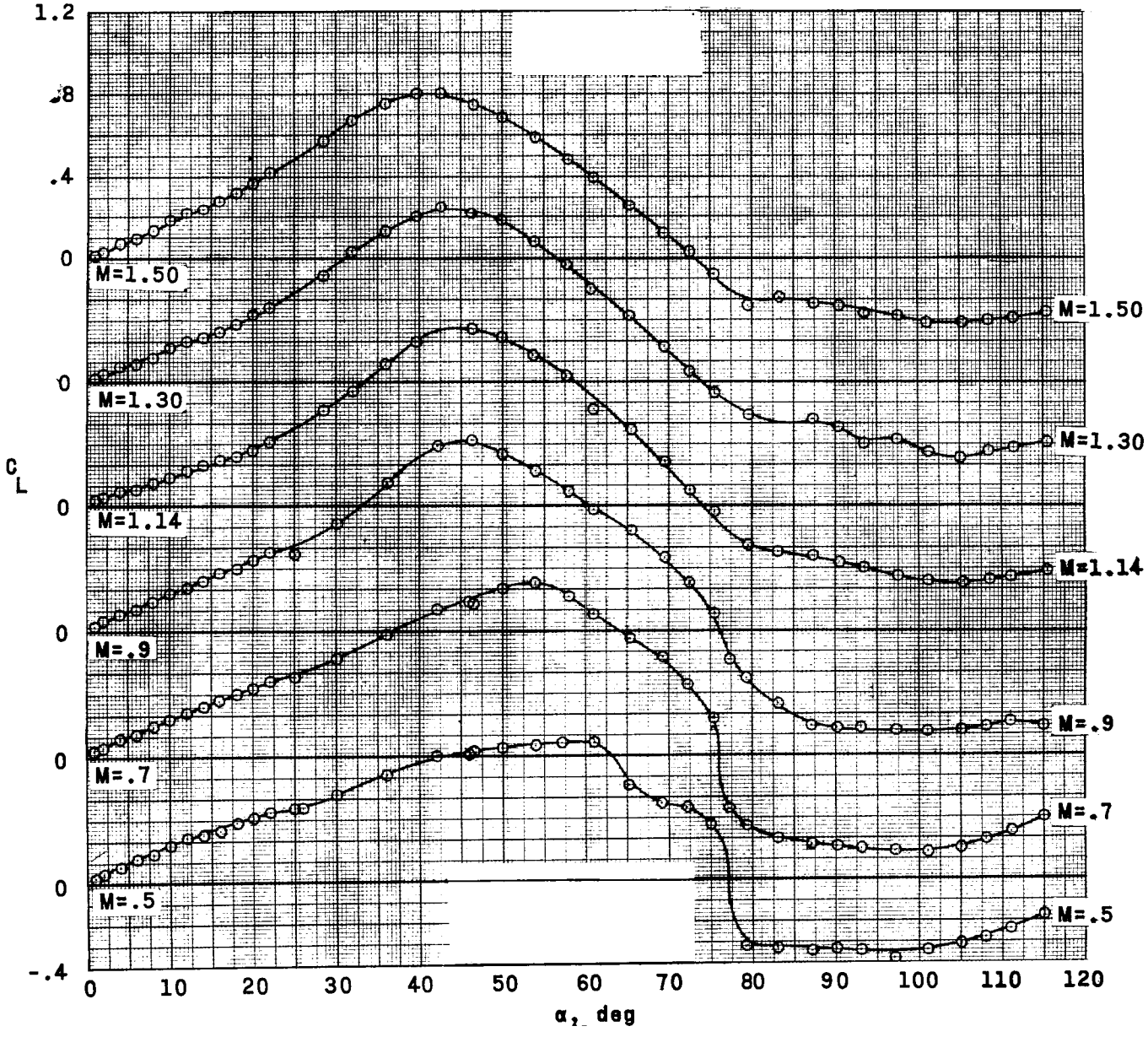

Figure 11.- Continued.

[redacted]

[redacted]

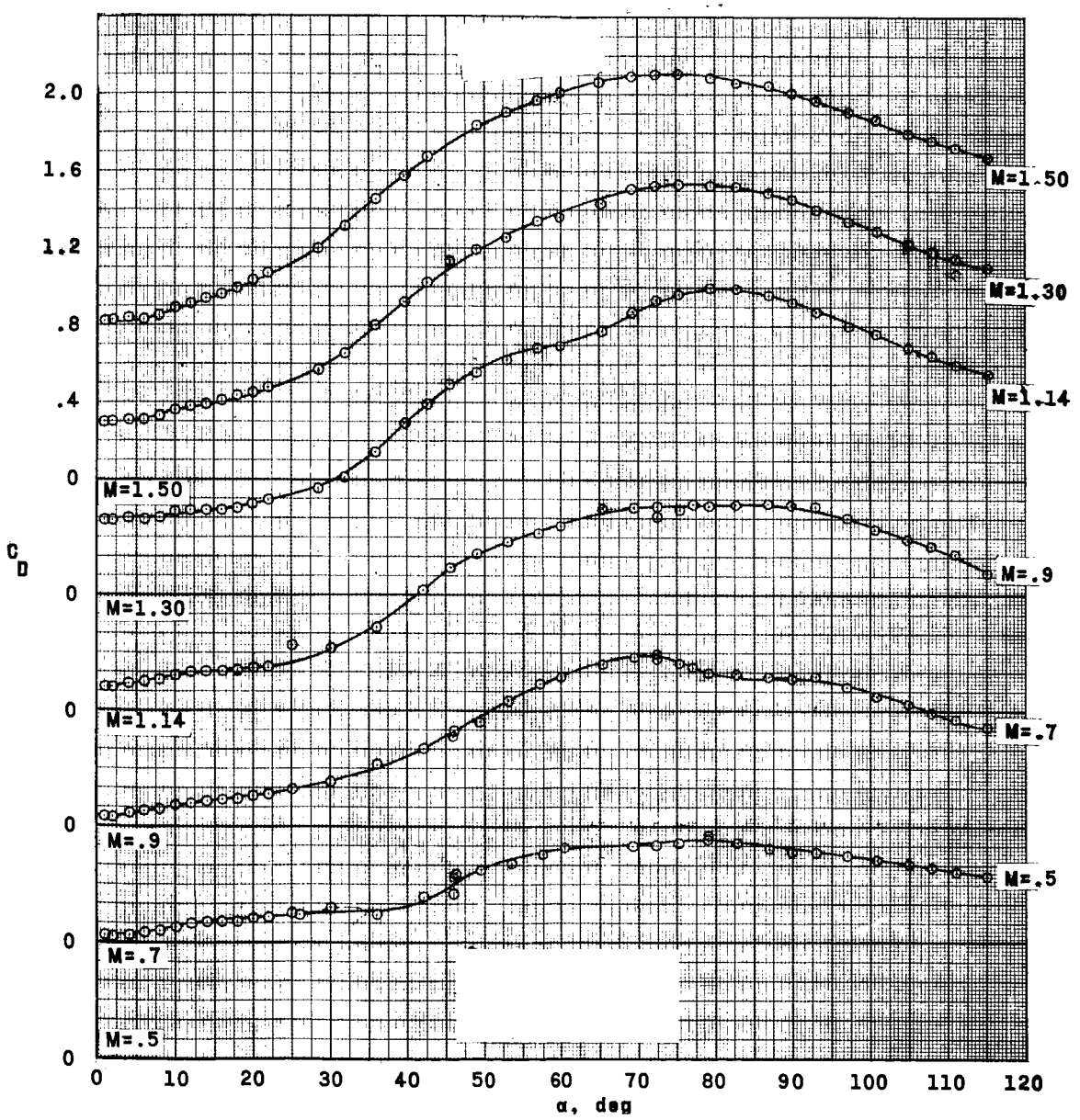

Figure 11.- Continued.

[redacted]

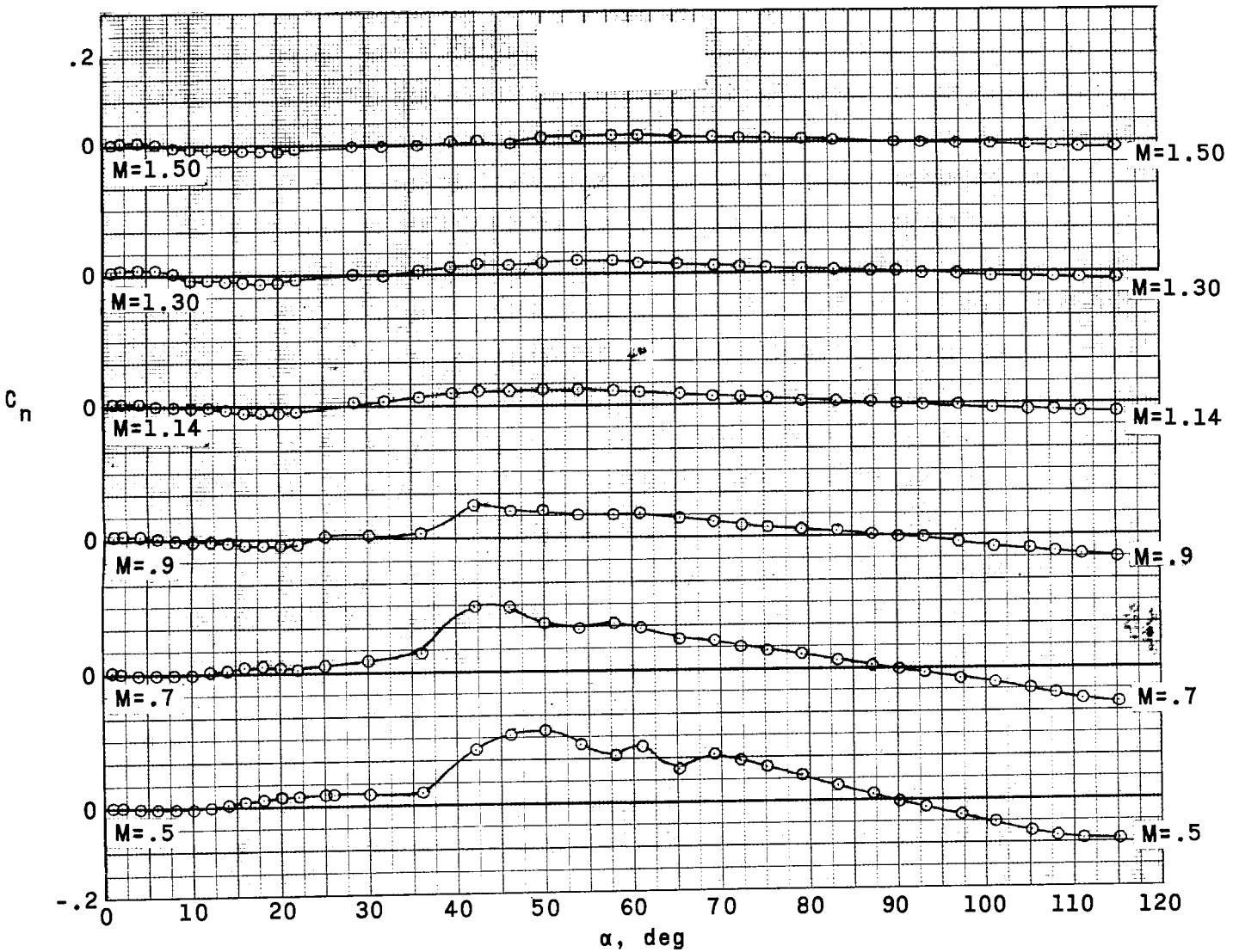

Figure 11.- Continued.

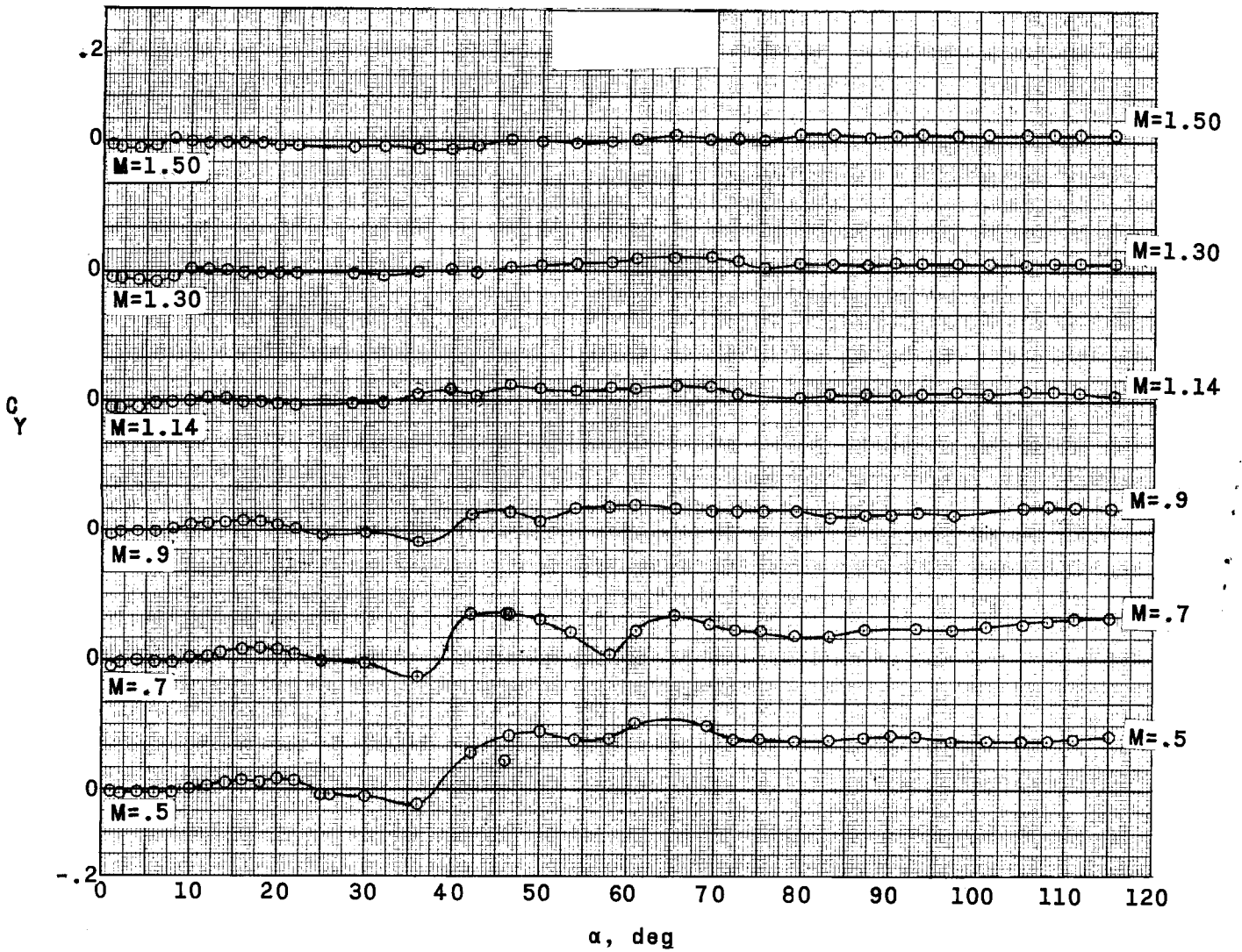

Figure 11.- Continued.

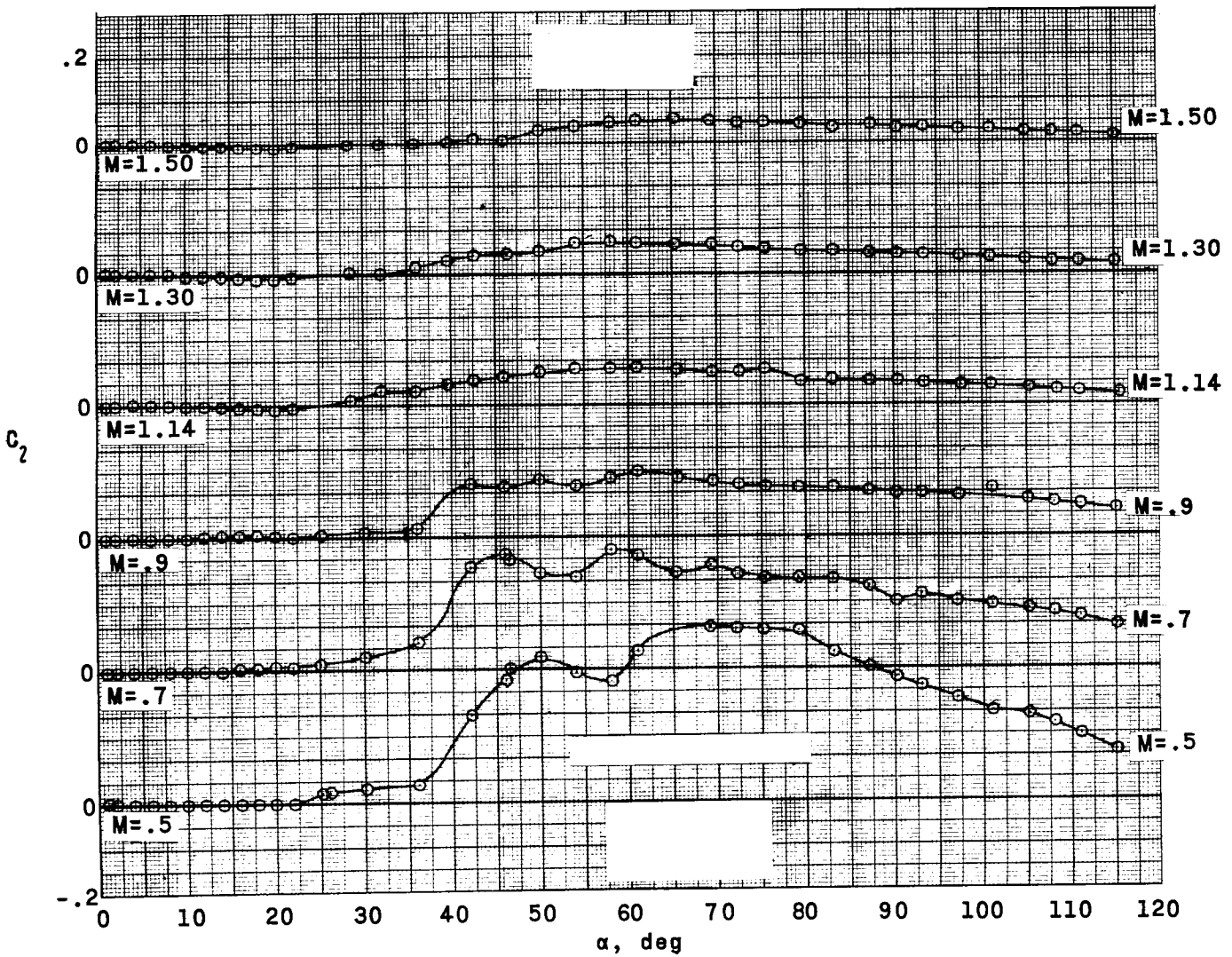

Figure 11.- Concluded.

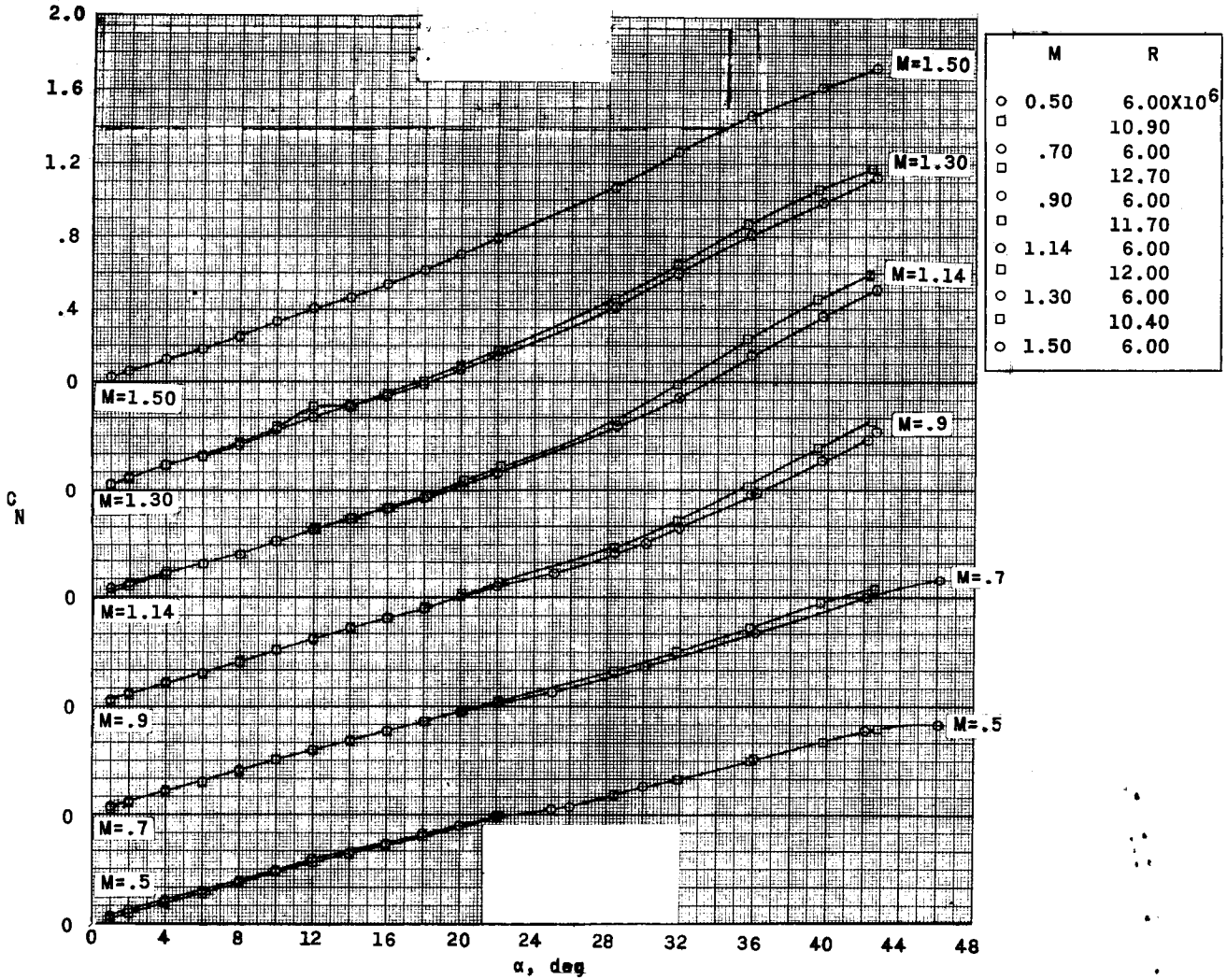

Figure 12.- Effect of Reynolds number on the aerodynamic characteristics of the escape configuration with 1.72 inch by 1.40 inch rocket igniter-cable fairings. M = 0.50 to 1.50.

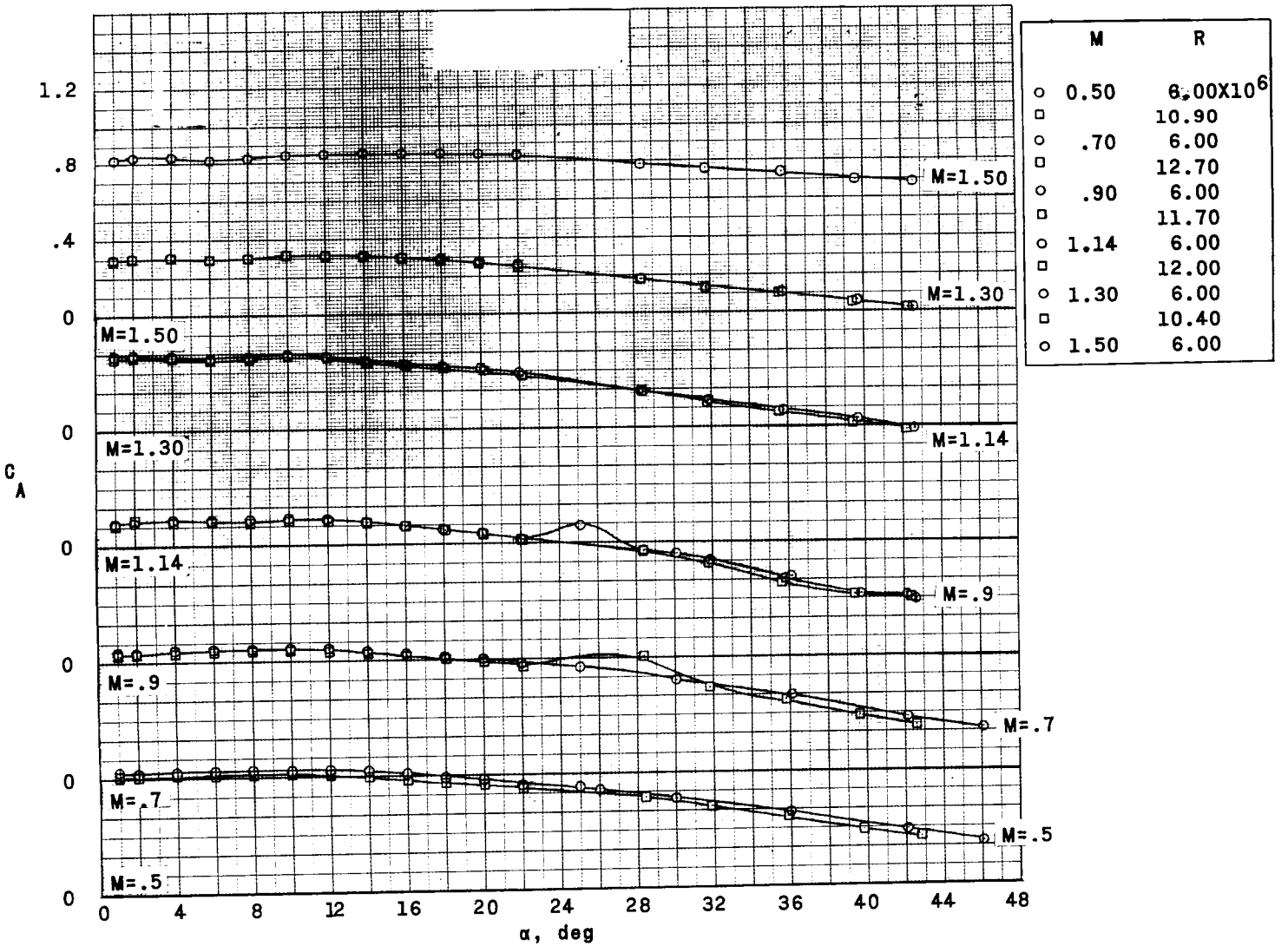

Figure 12.- Continued.

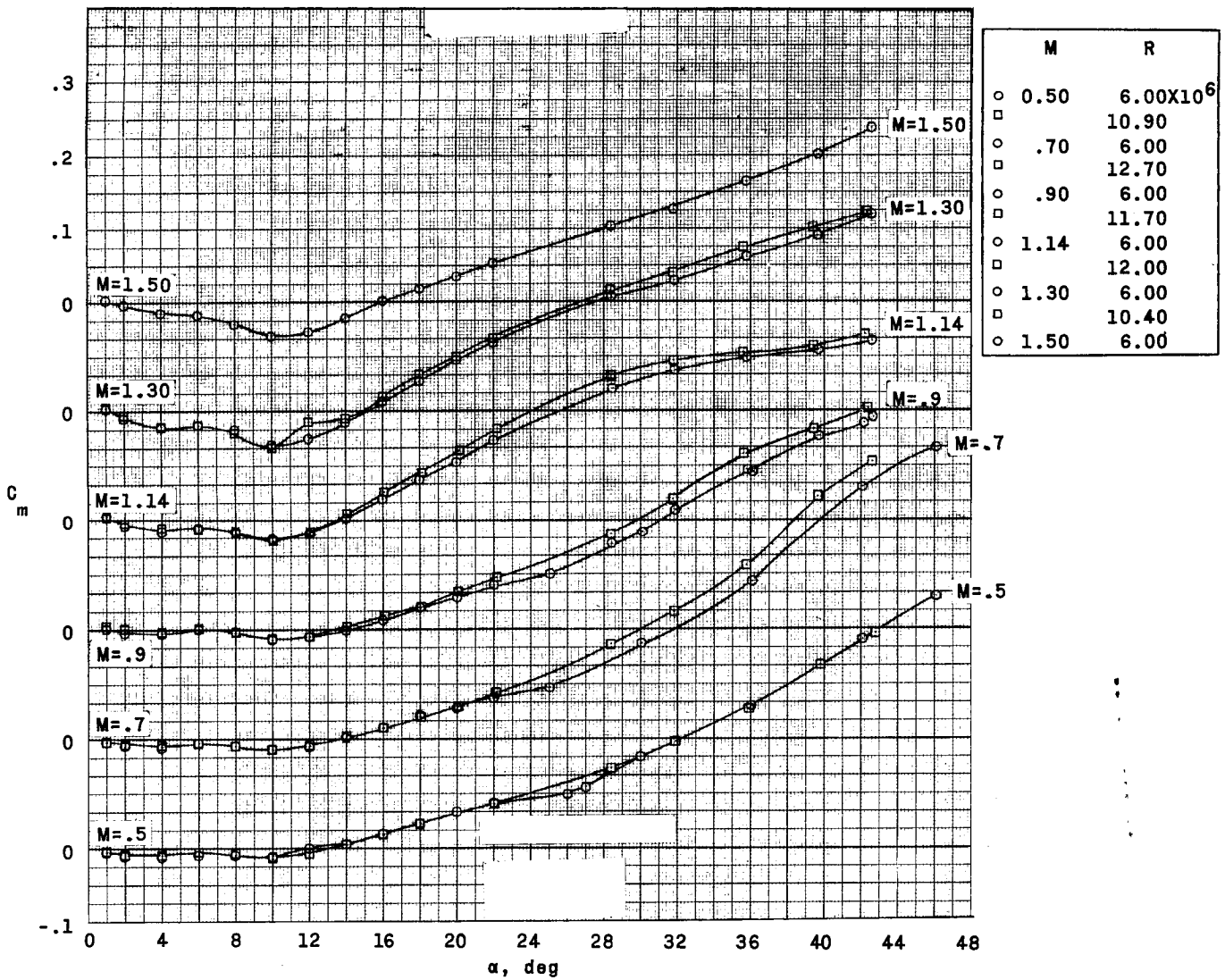

Figure 12.- Continued.

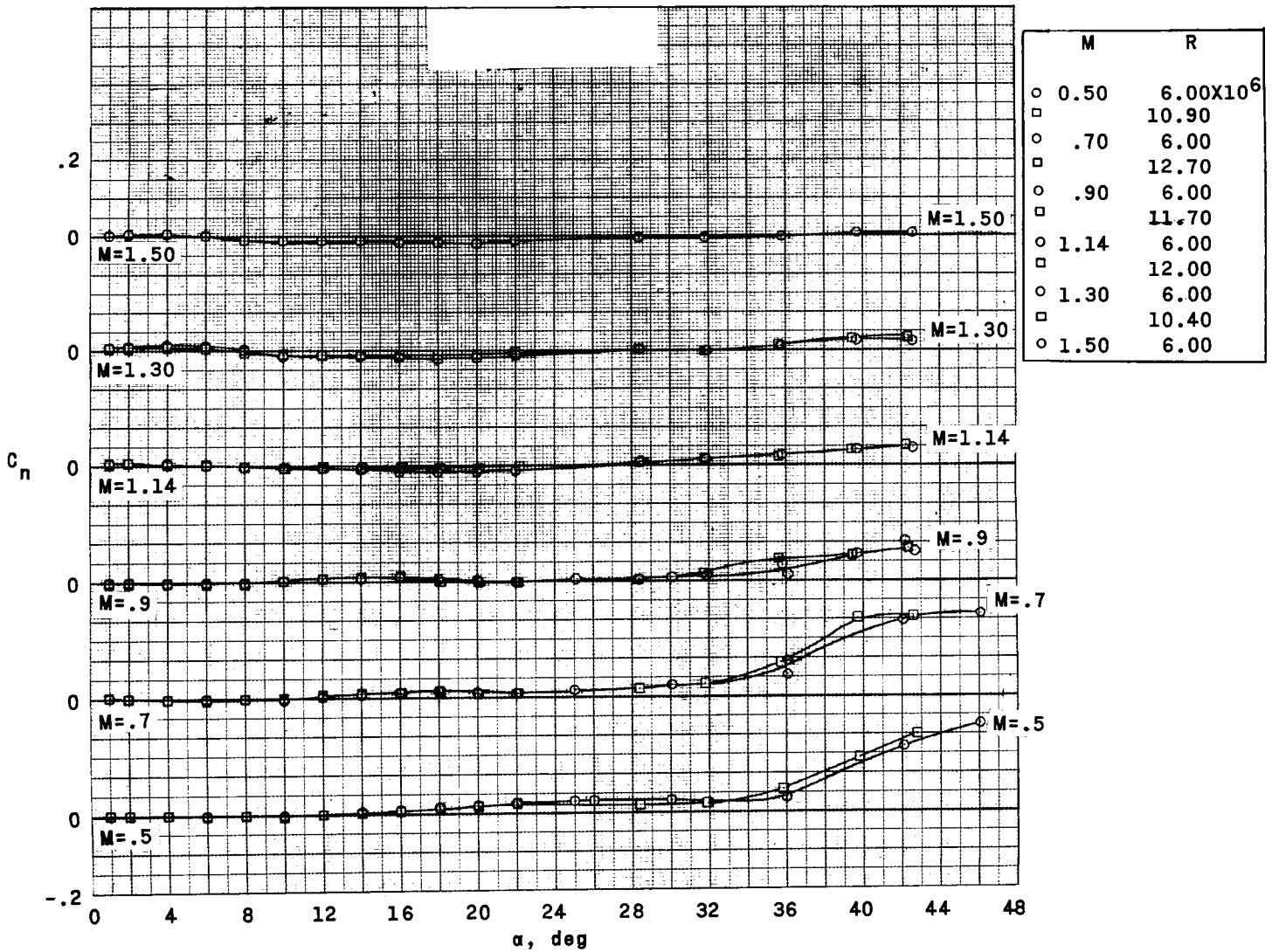

Figure 12.- Continued.

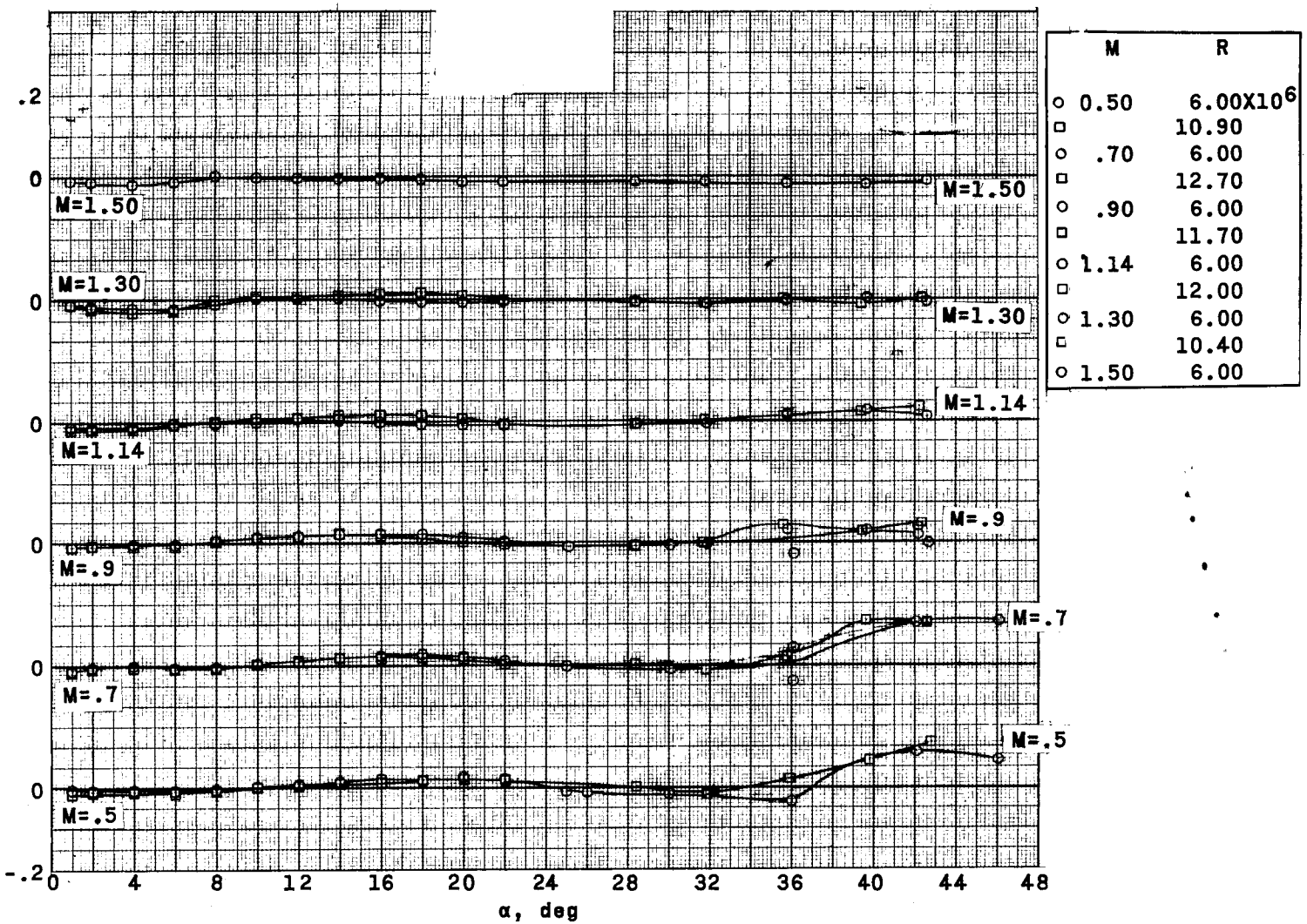

Figure 12.- Continued.

[redacted]

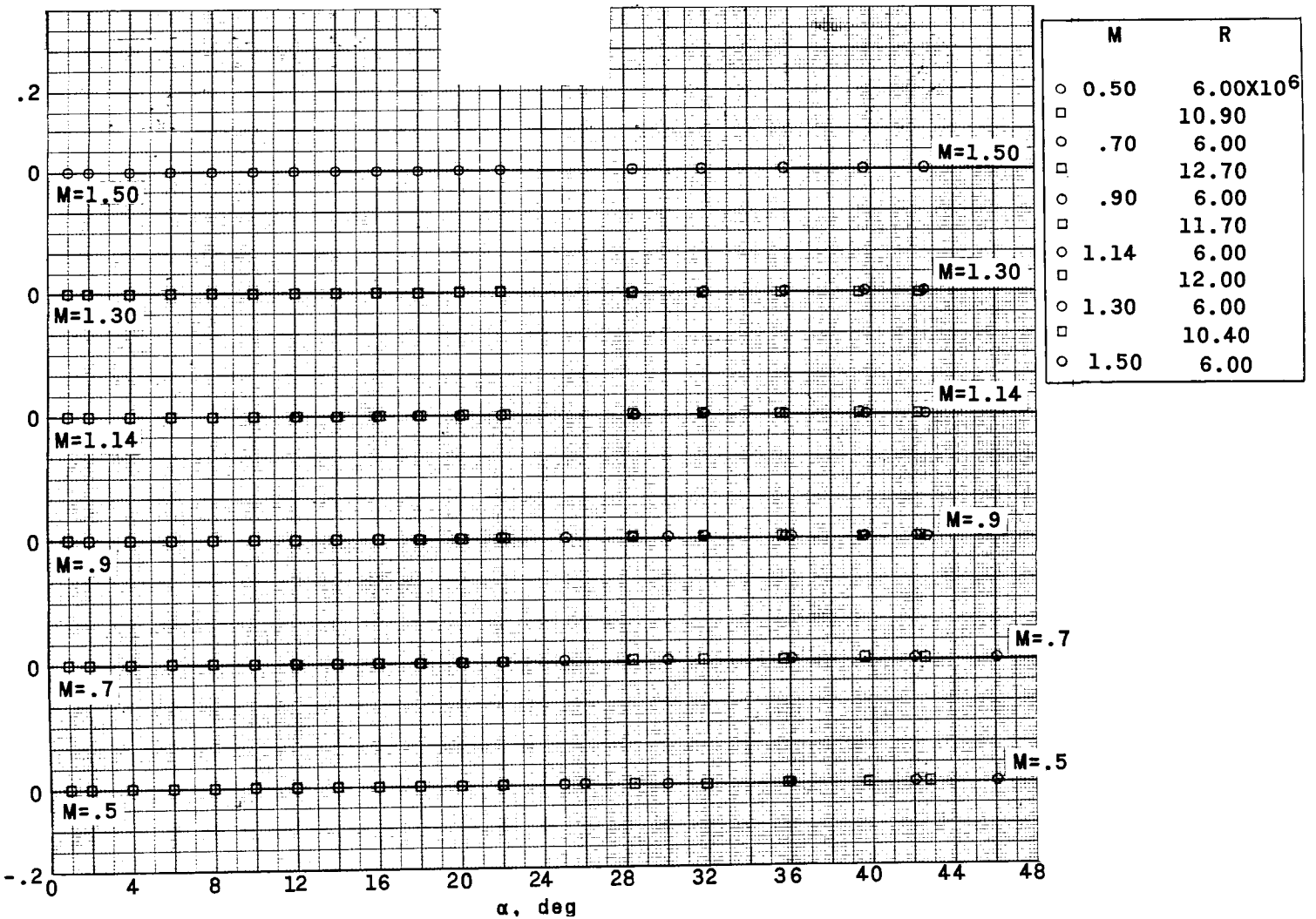

[redacted]

Figure 12.- Continued.

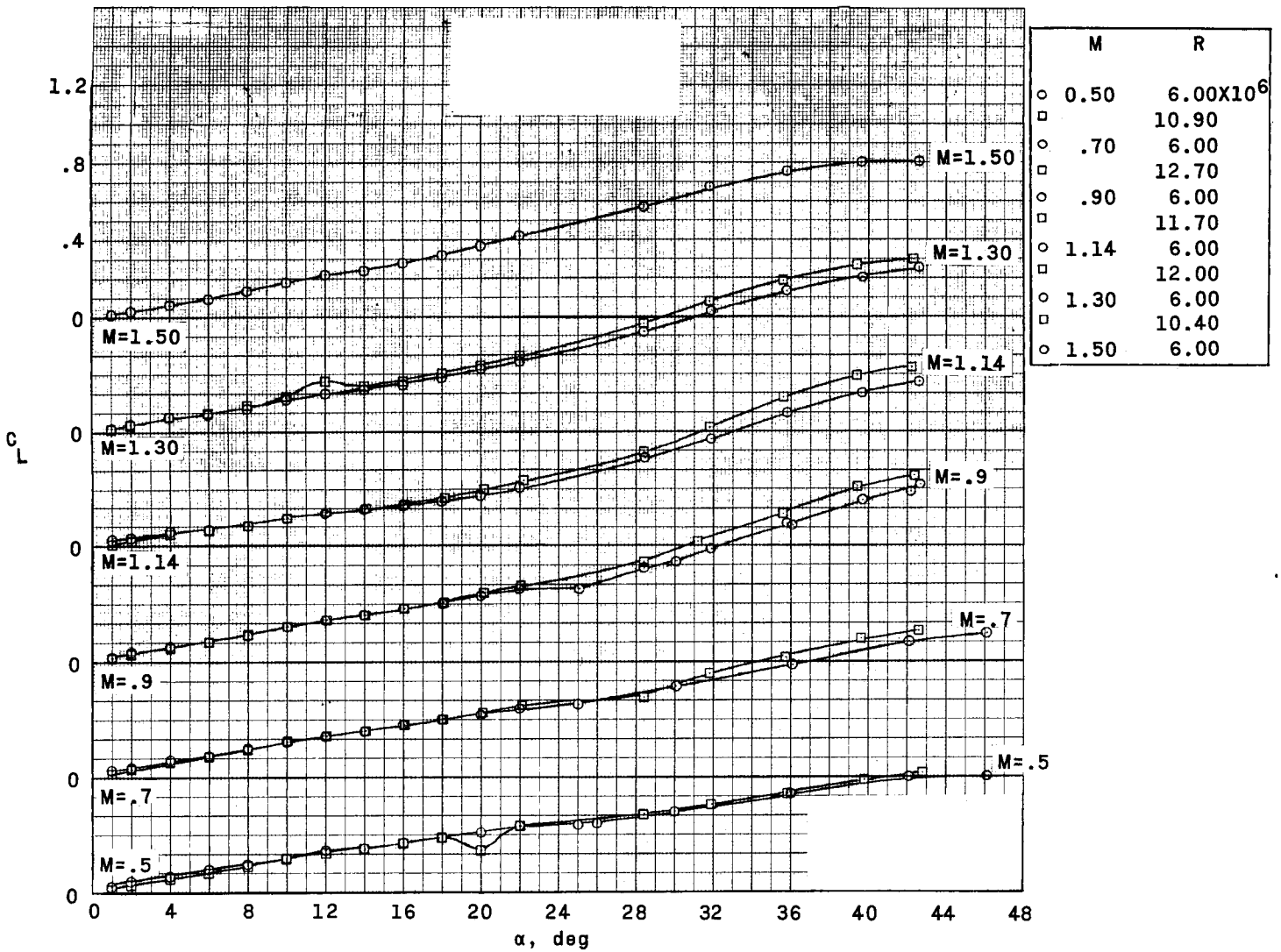

Figure 12.- Continued.

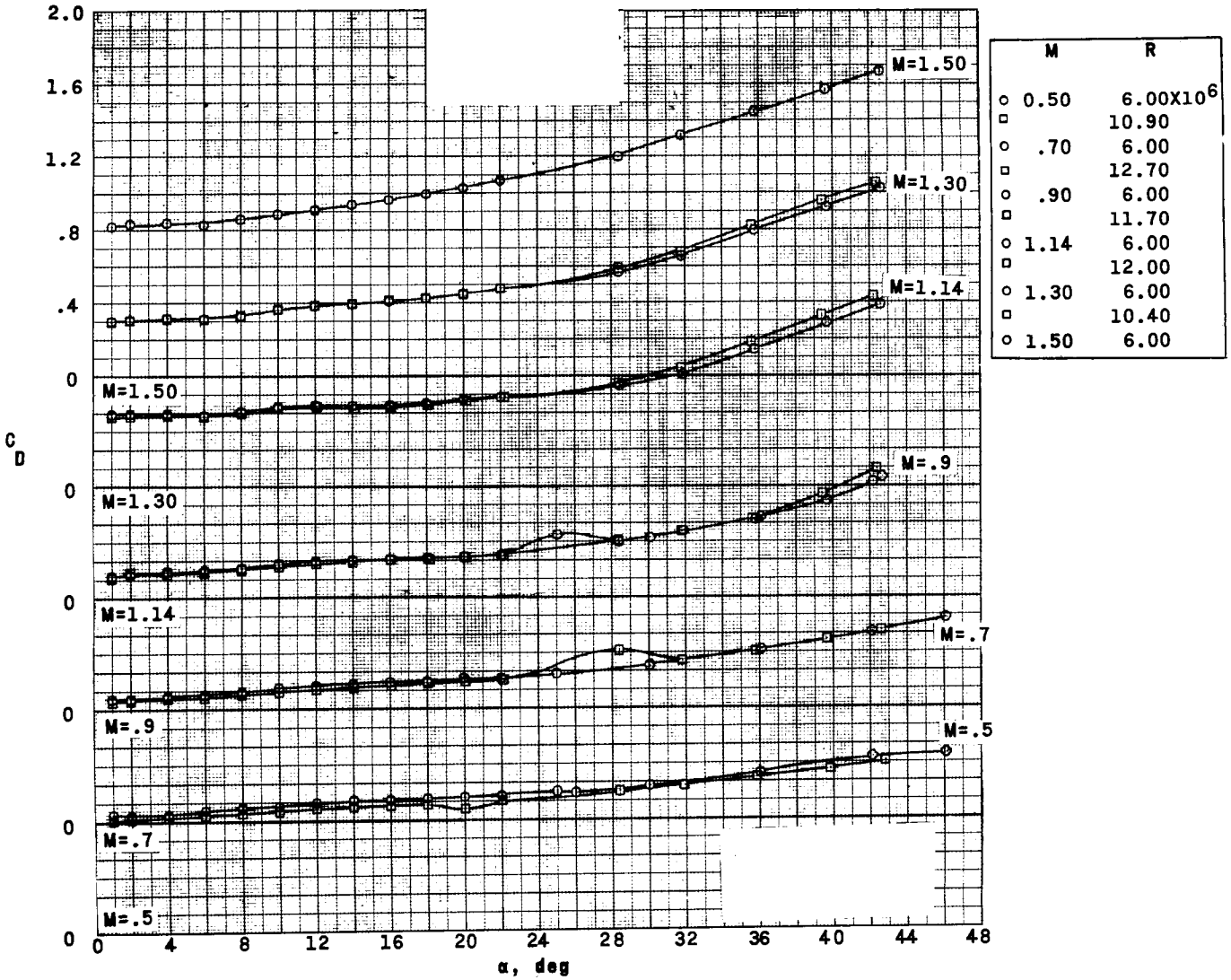

Figure 12.- Continued.

CONFIDENTIAL

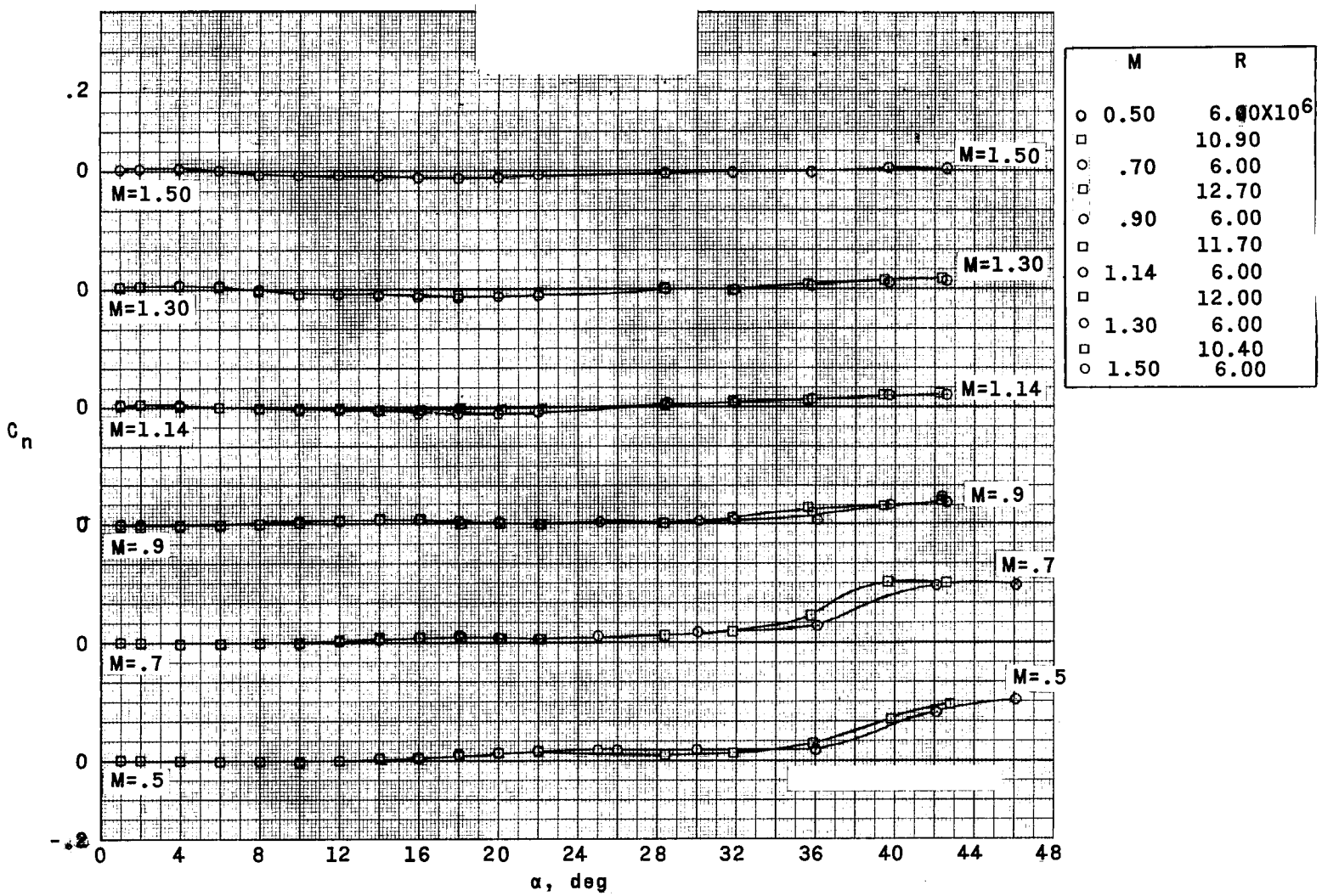

Figure 12.- Continued.

CONFIDENTIAL

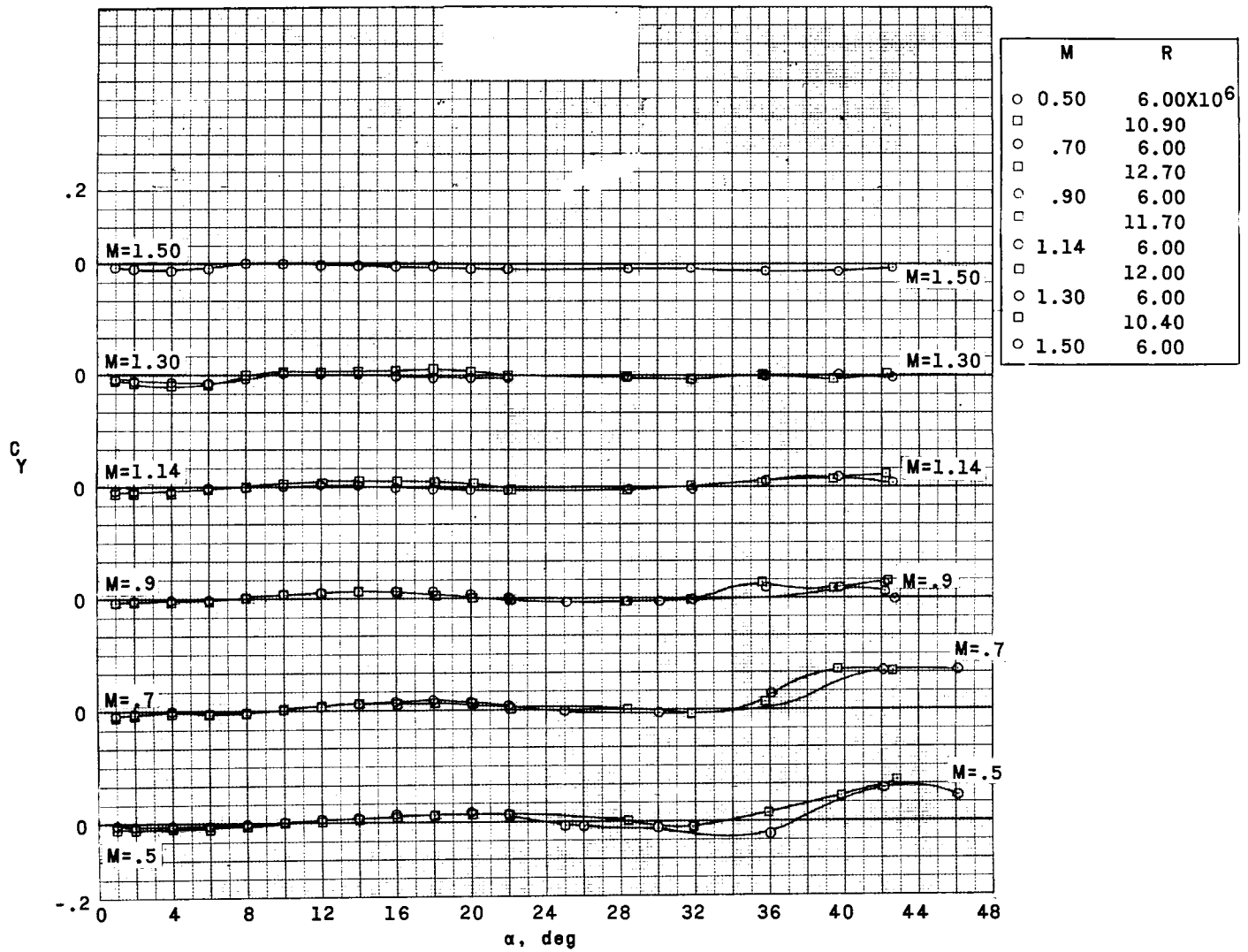

Figure 12.- Continued.

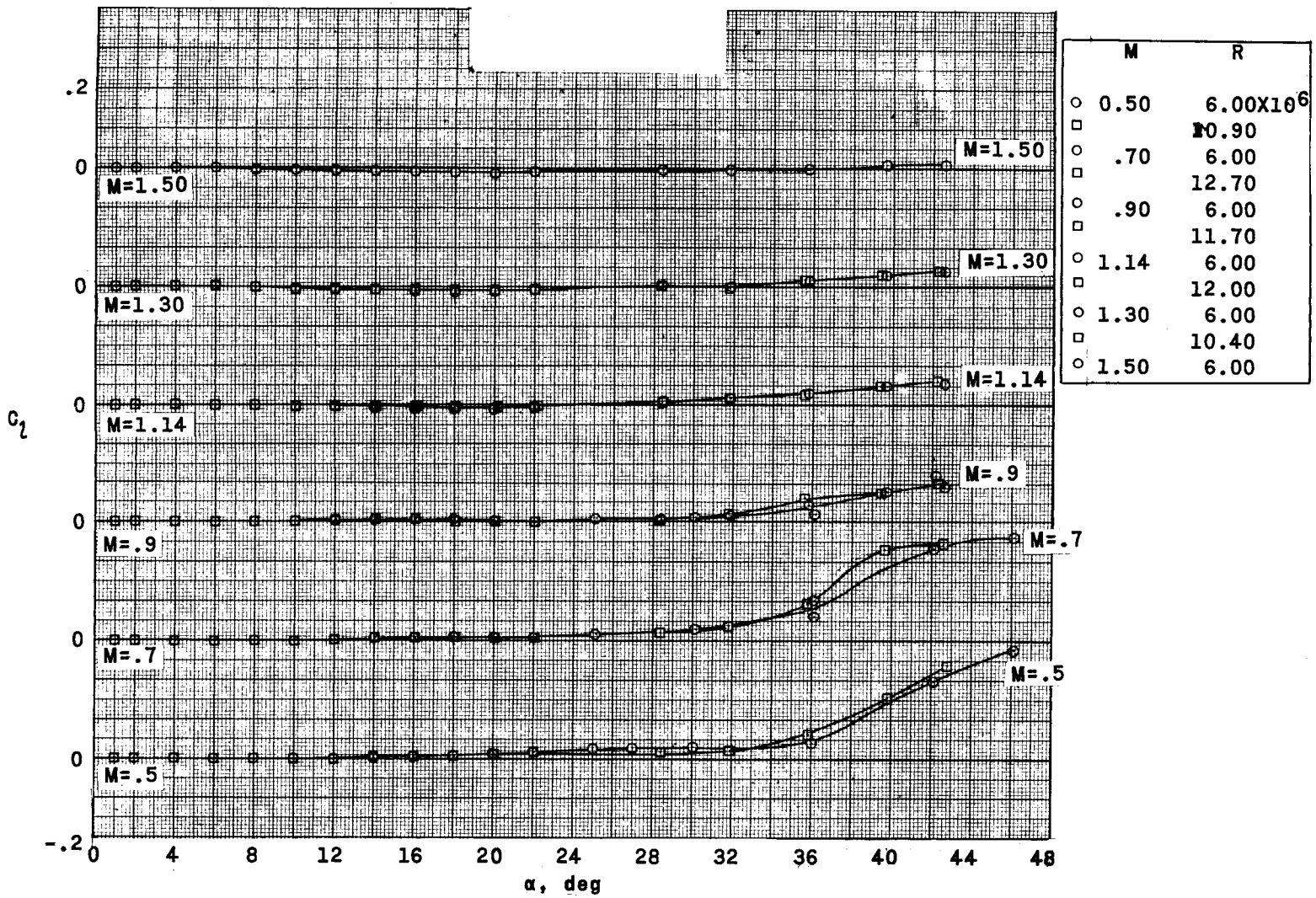

Figure 12.- Concluded.

[redacted]

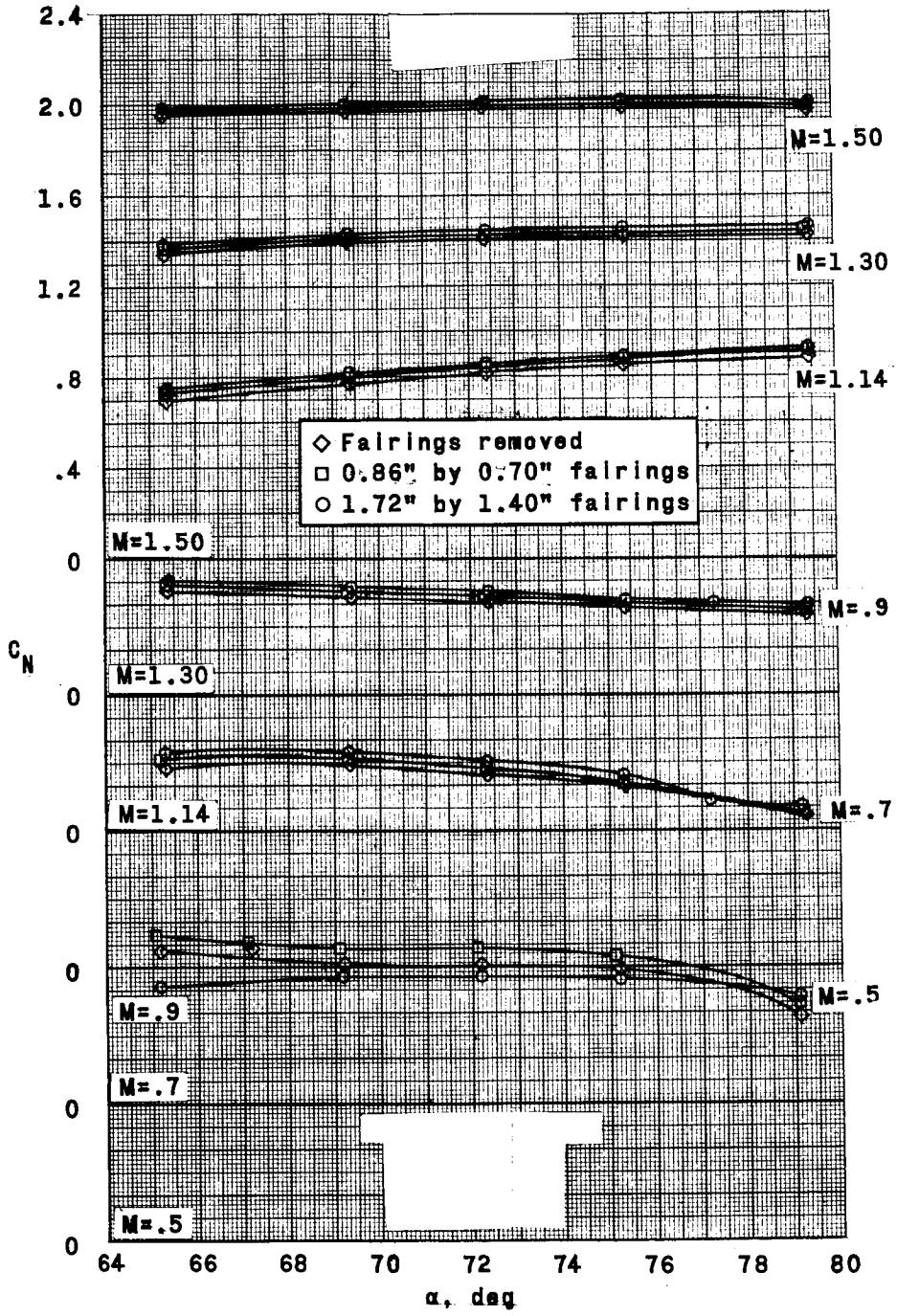

Figure 13.- Effect of rocket igniter-cable fairings on the aerodynamic characteristics of the escape configuration. M = 0.50 to 1.50; $R \approx 6 \times 10^6$.

[redacted]

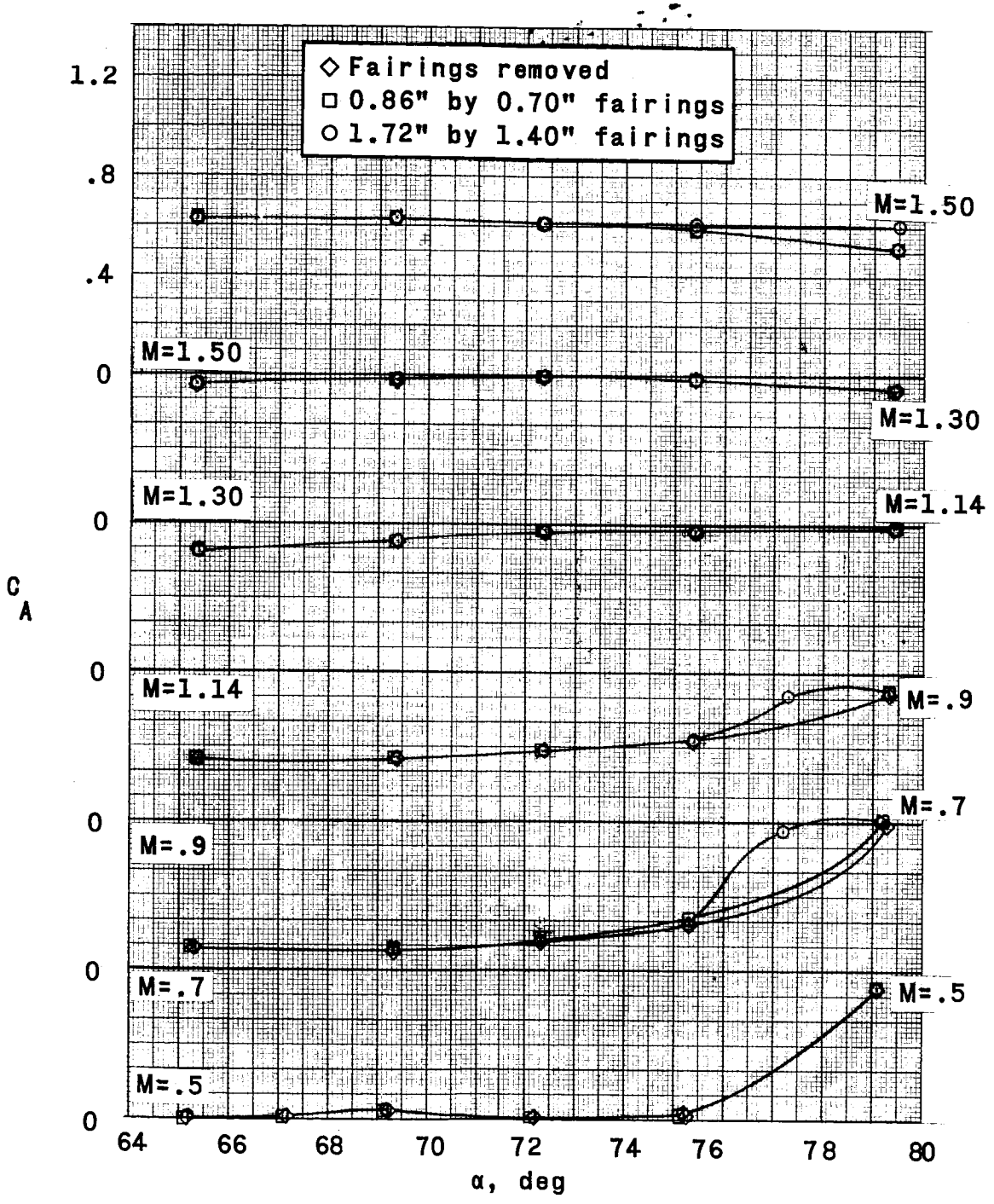

Figure 13.- Continued.

[redacted]

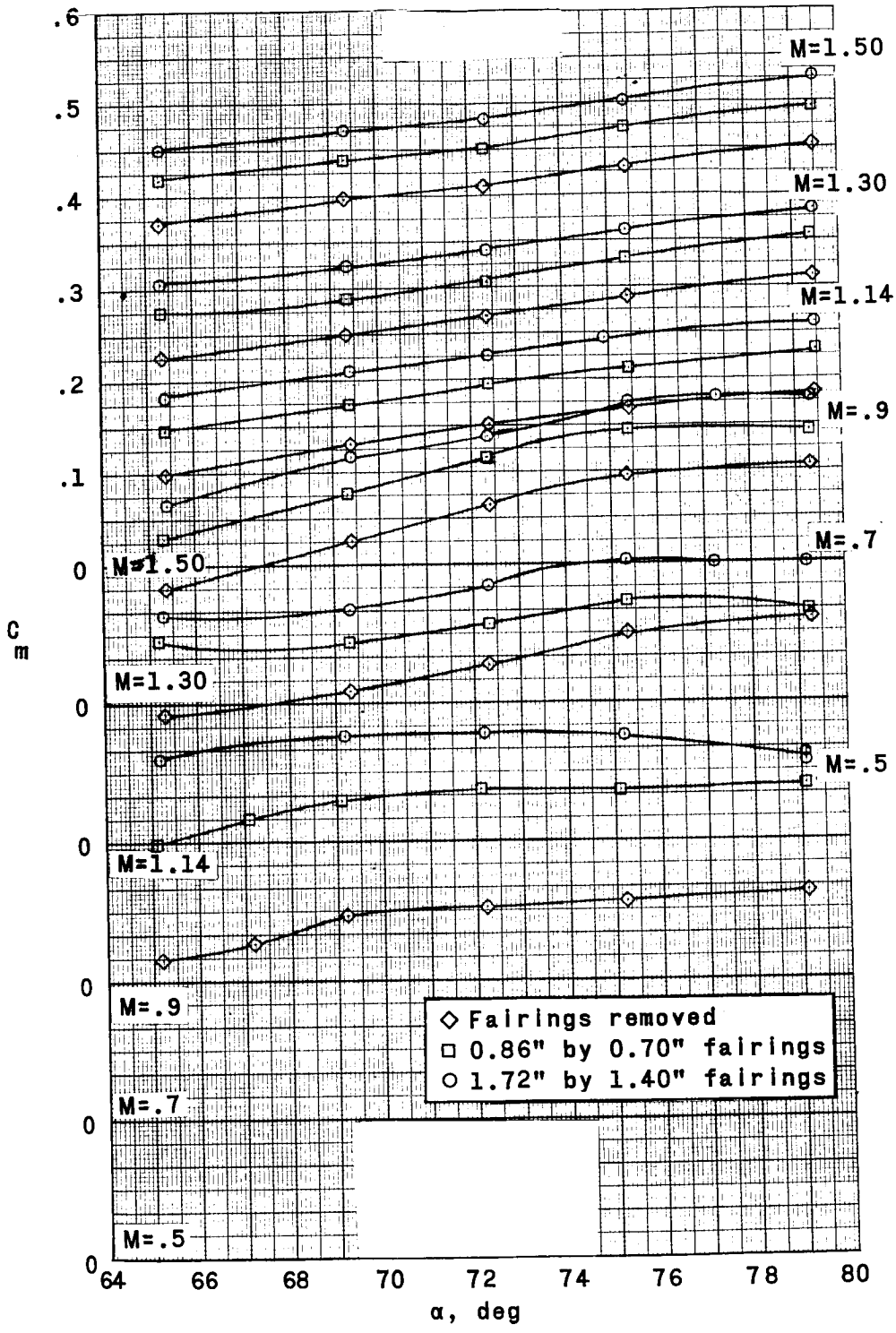

Figure 13.- Continued.

[redacted]

DE[redacted]SIFIED

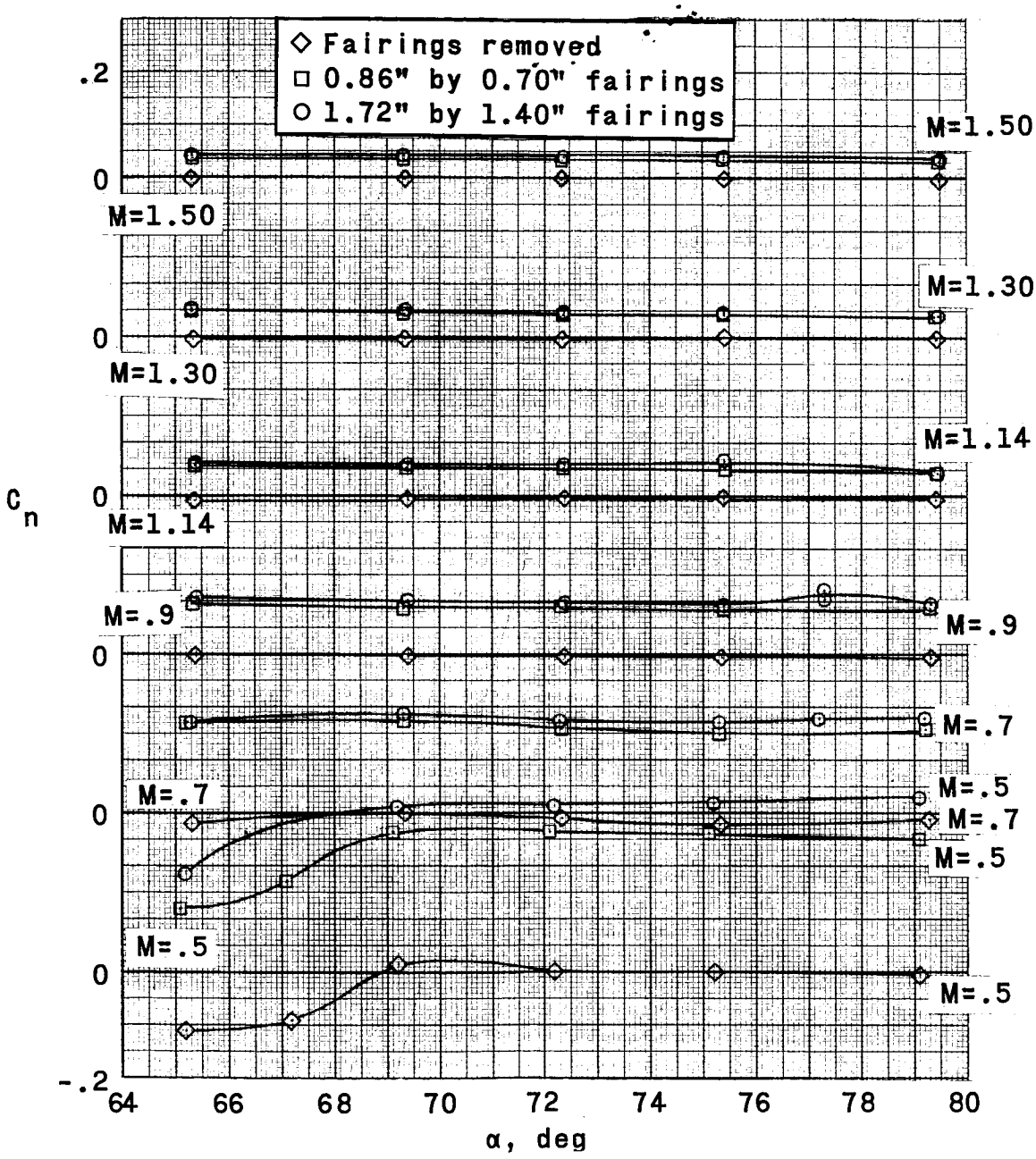

Figure 13.- Continued.

[redacted]

[redacted]

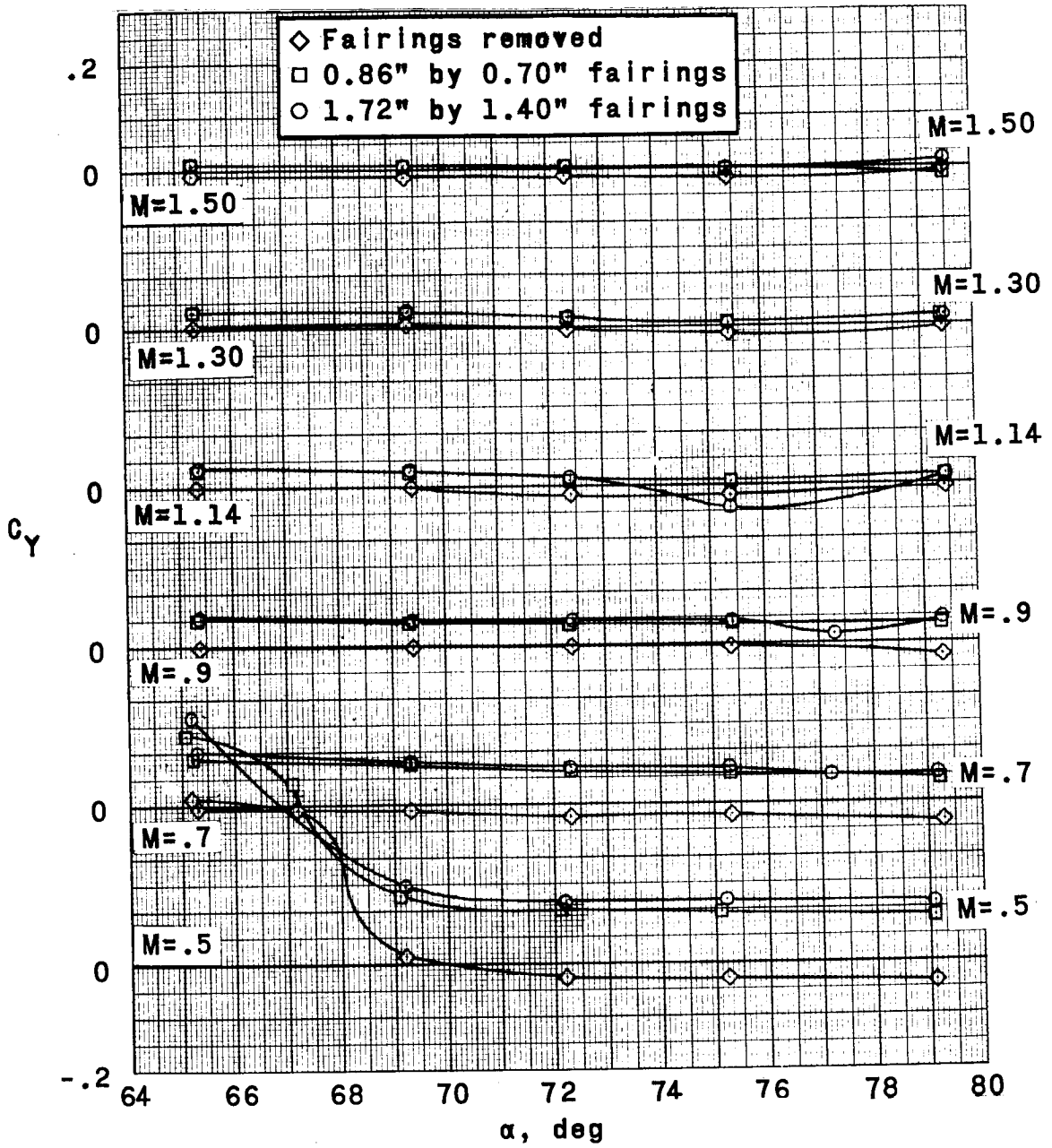

Figure 13.- Continued.

[redacted]

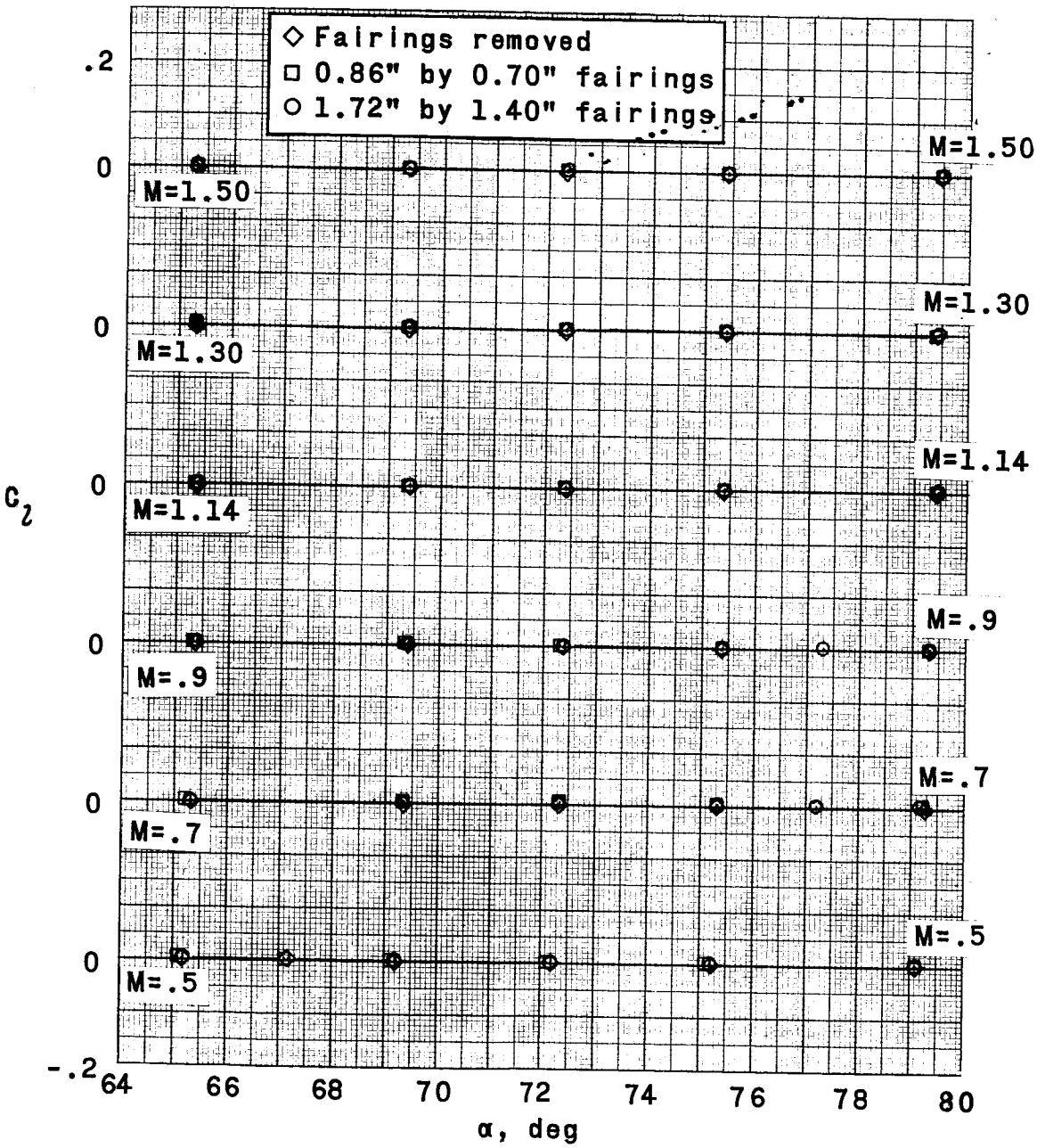

Figure 13.- Continued.

[redacted]

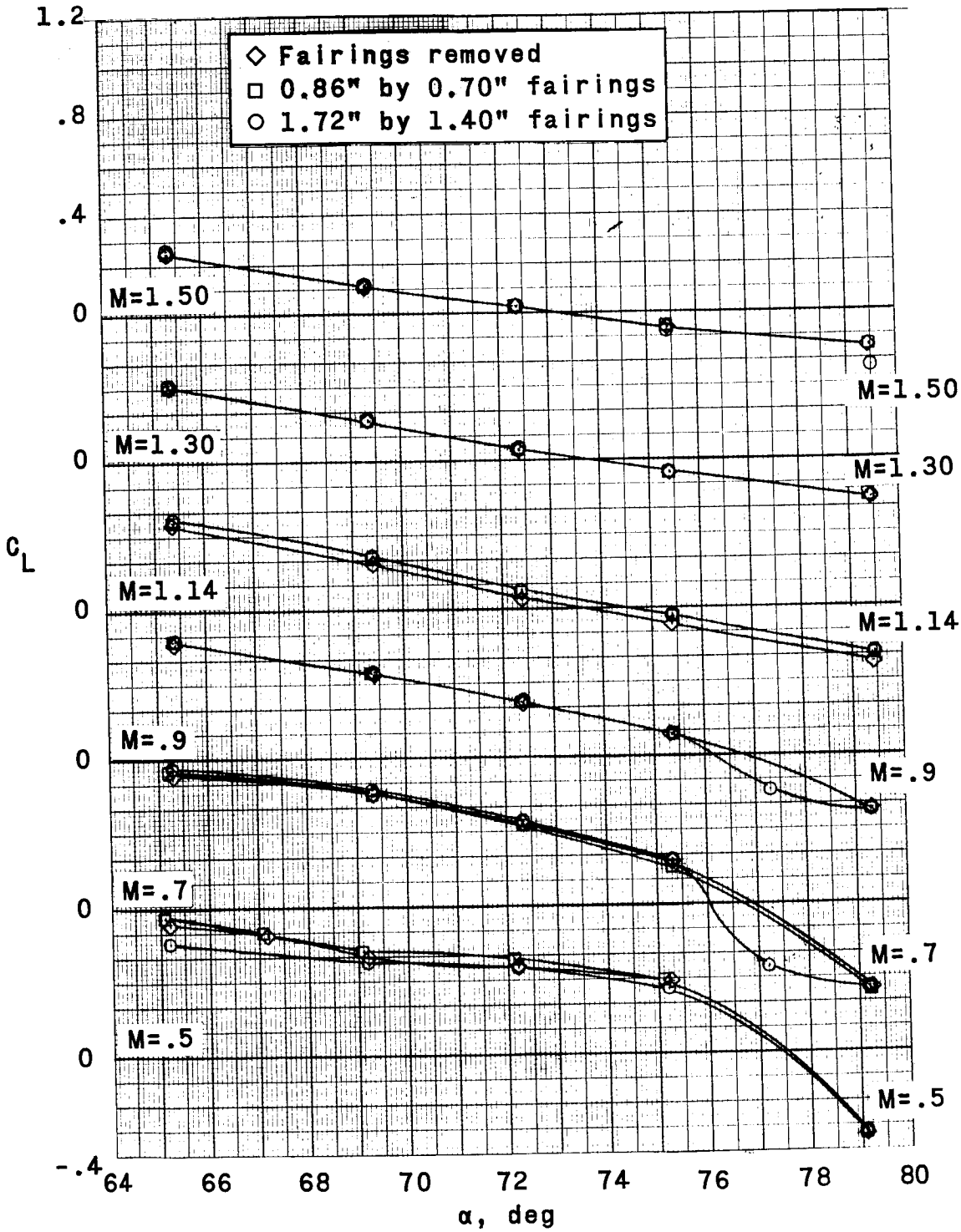

Figure 13.- Continued.

[redacted]

[redacted]SIFIED

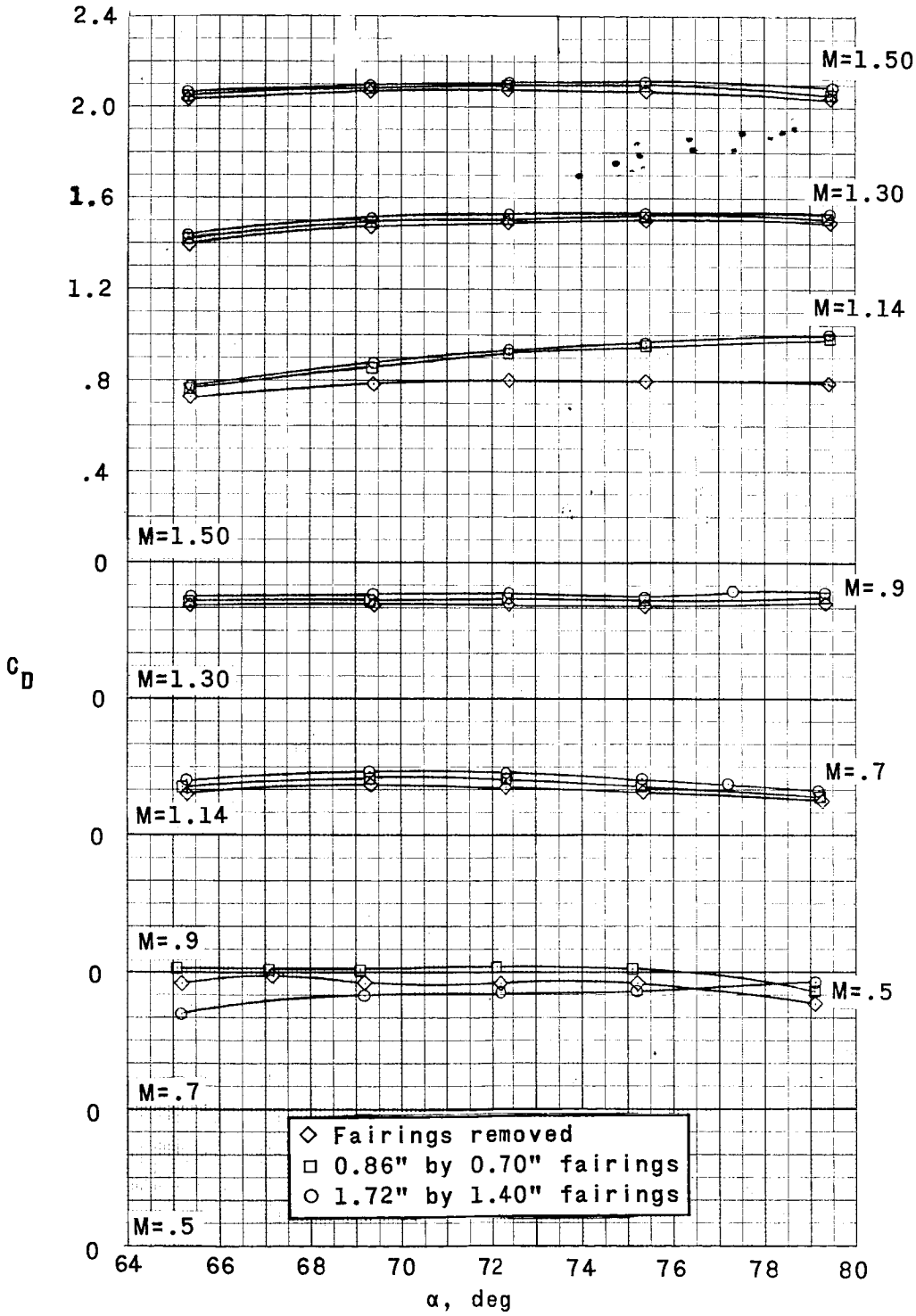

Figure 13.- Continued.

[redacted]

[redacted]

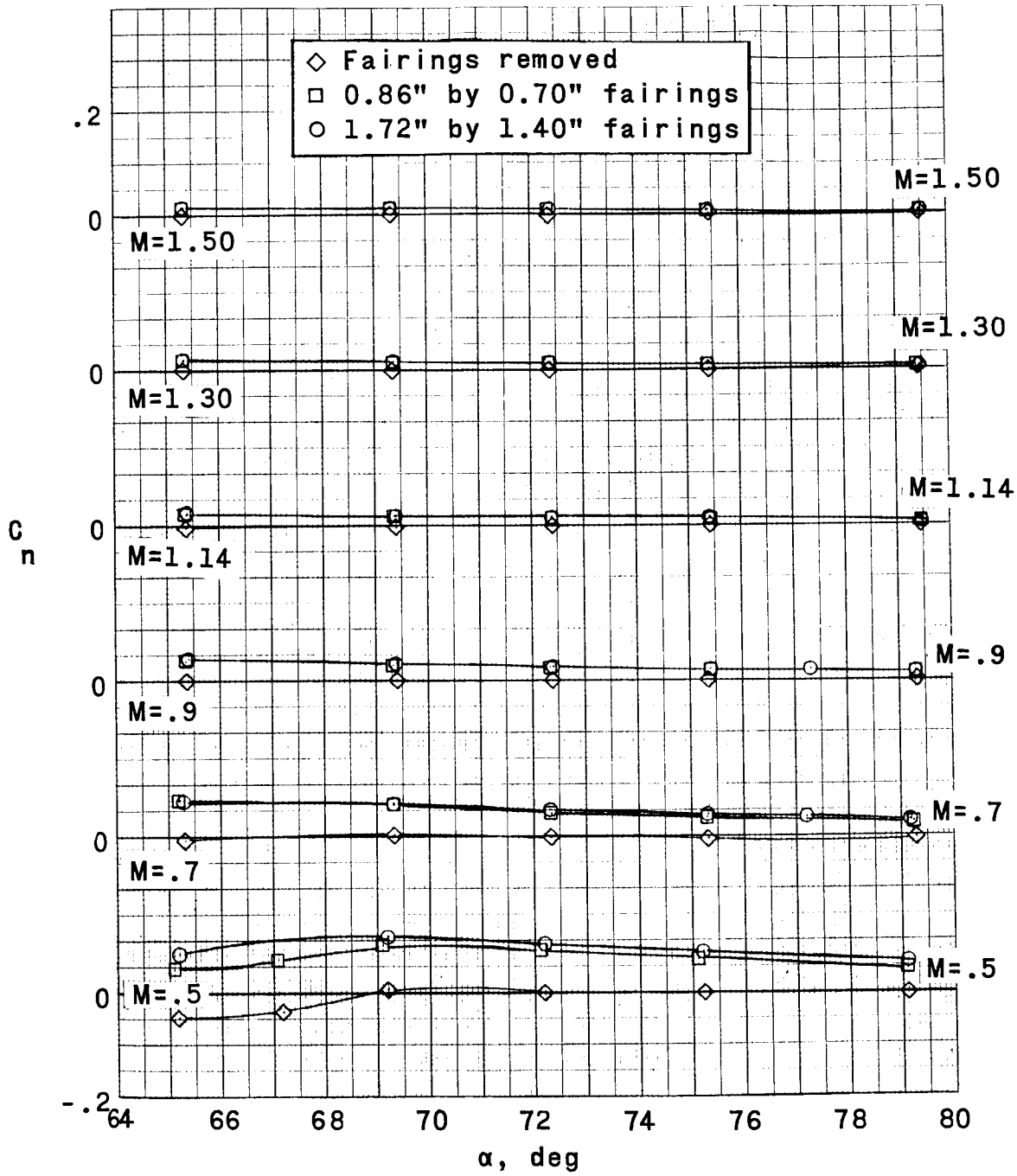

Figure 13.- Continued.

[redacted]

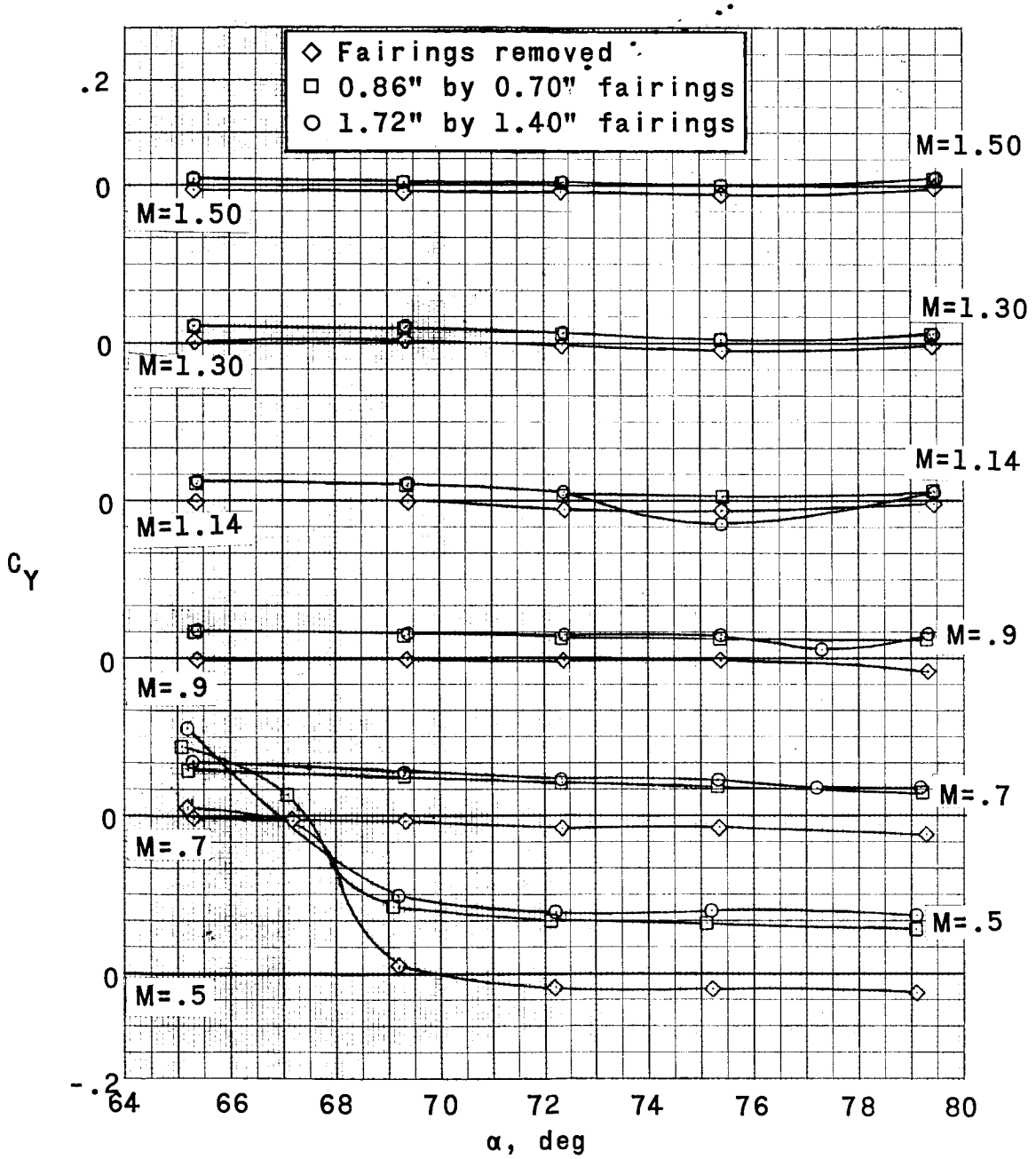

Figure 13.- Continued.

[redacted]

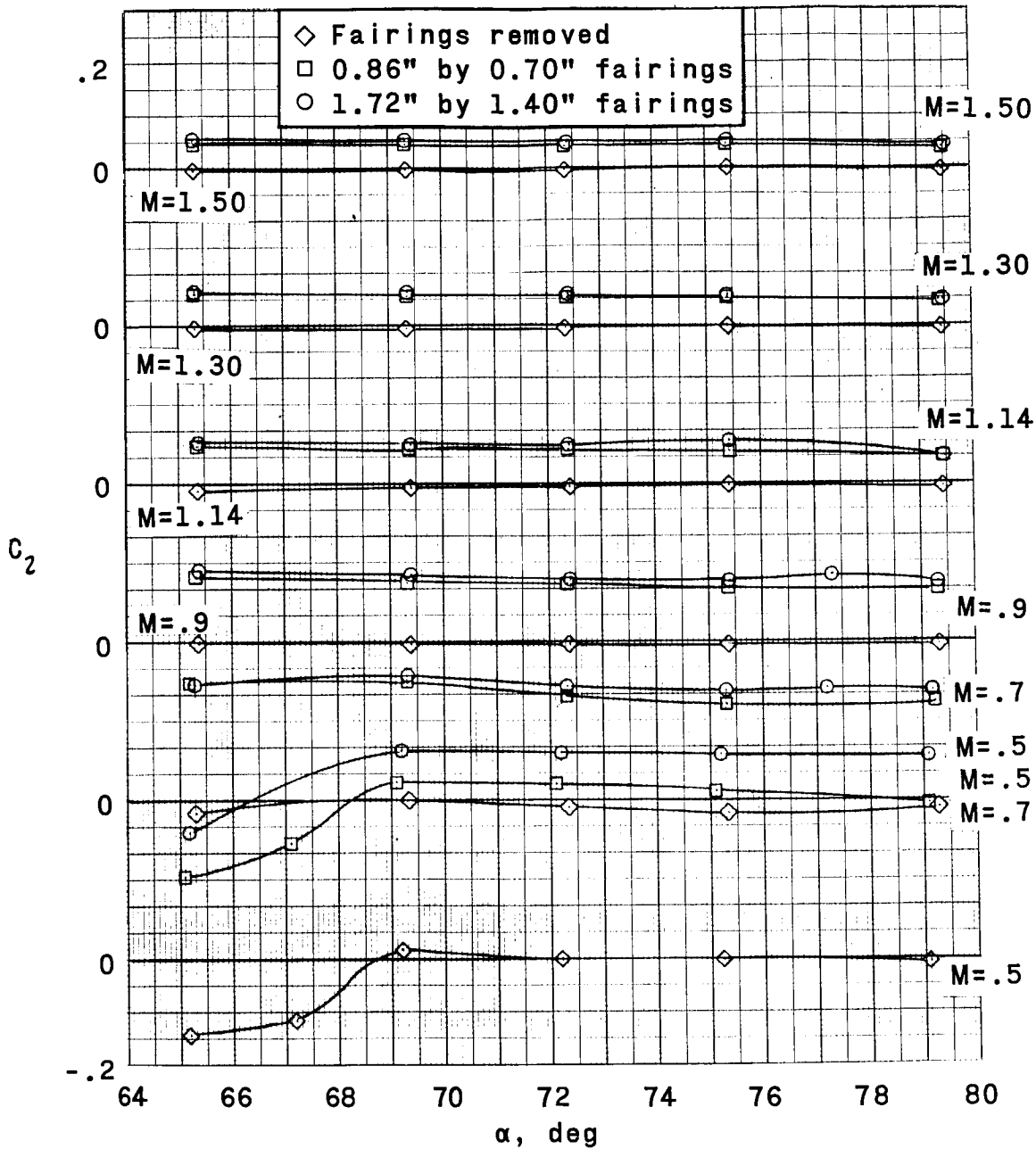

Figure 13.- Concluded.

[redacted]

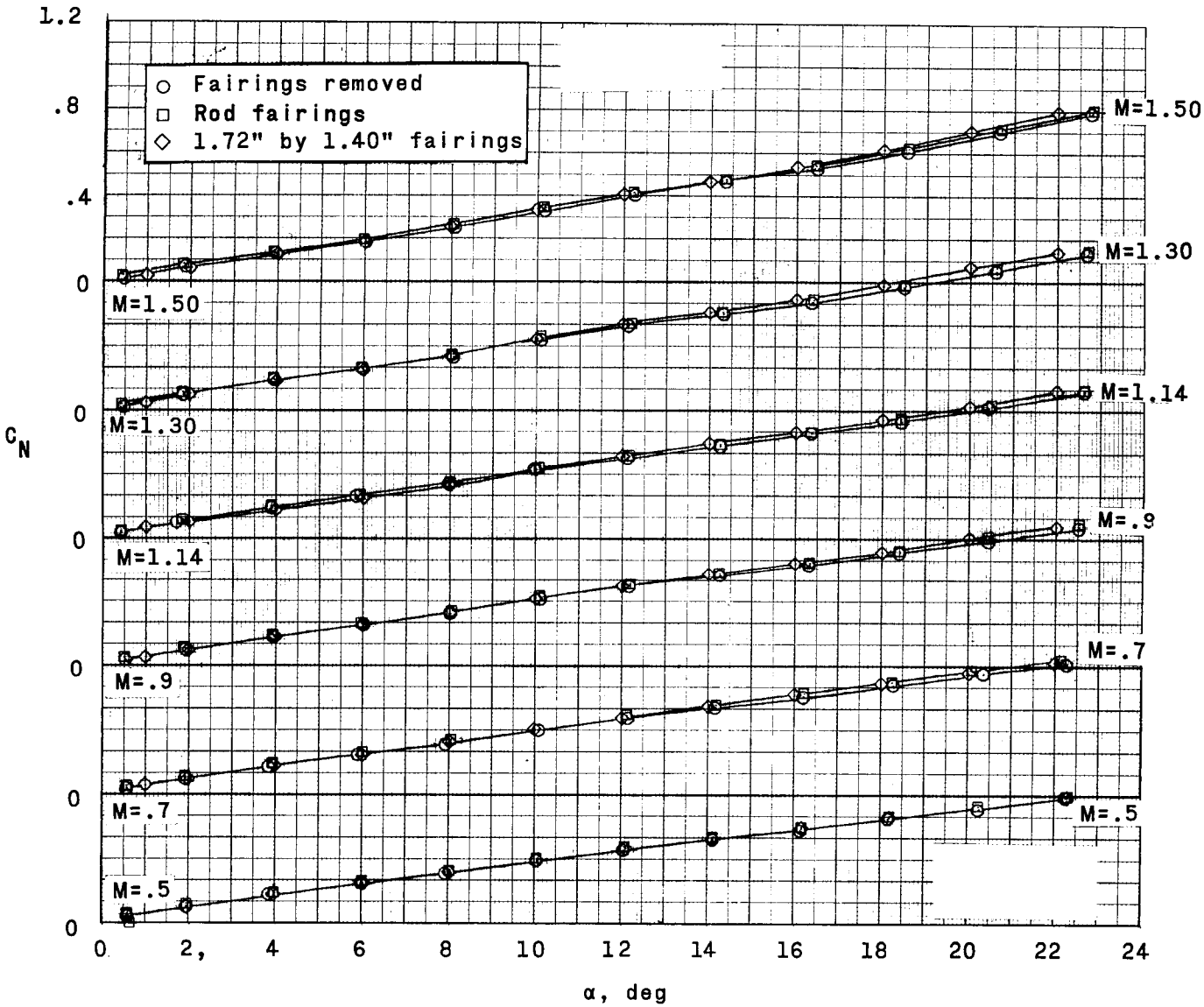

Figure 14.- Effect of rocket igniter-cable fairings on the aerodynamic characteristics of the escape configuration. M = 0.50 to 1.50; $R \approx 6 \times 10^6$.

[redacted]

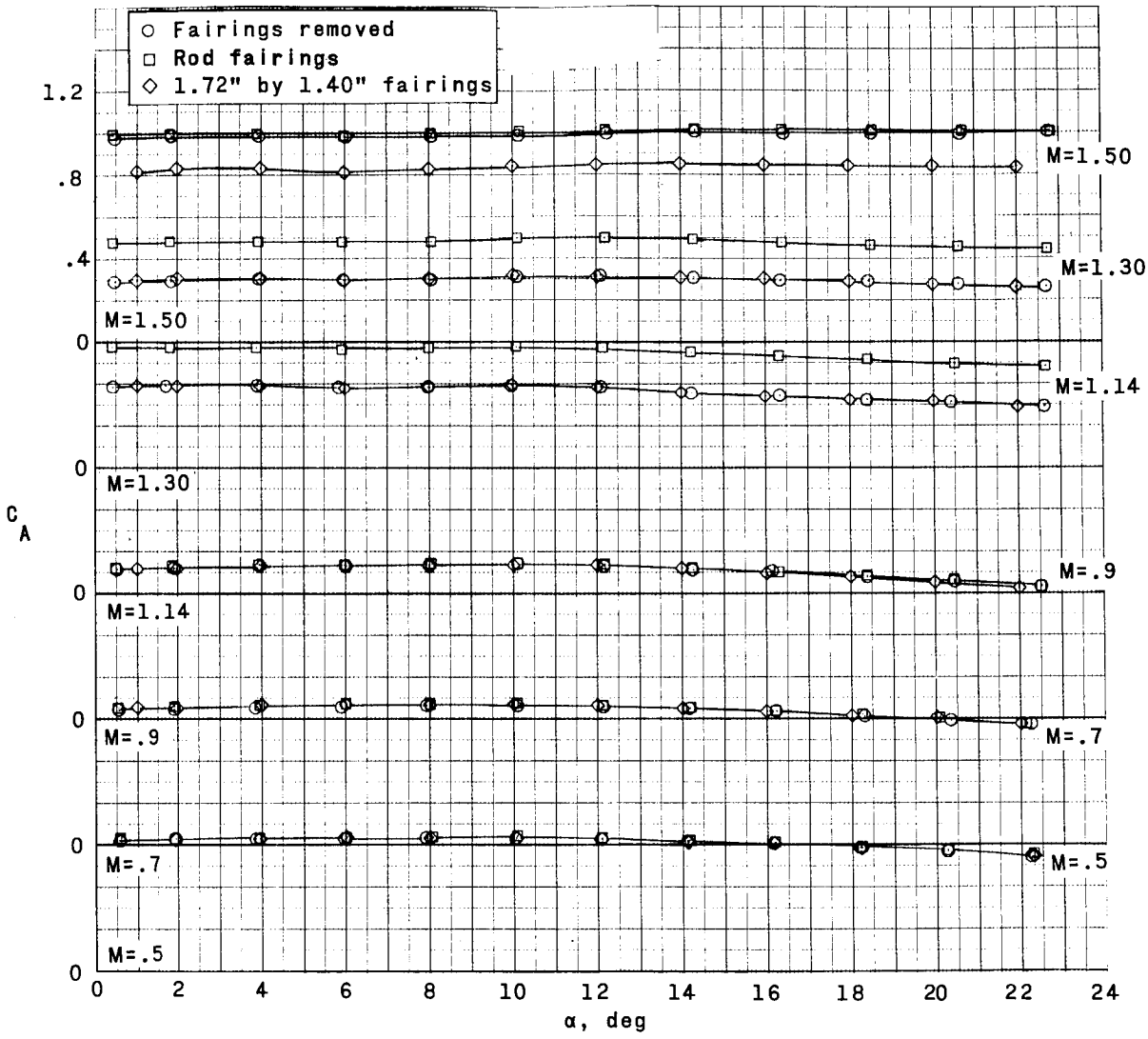

Figure 14.- Continued.

[redacted]

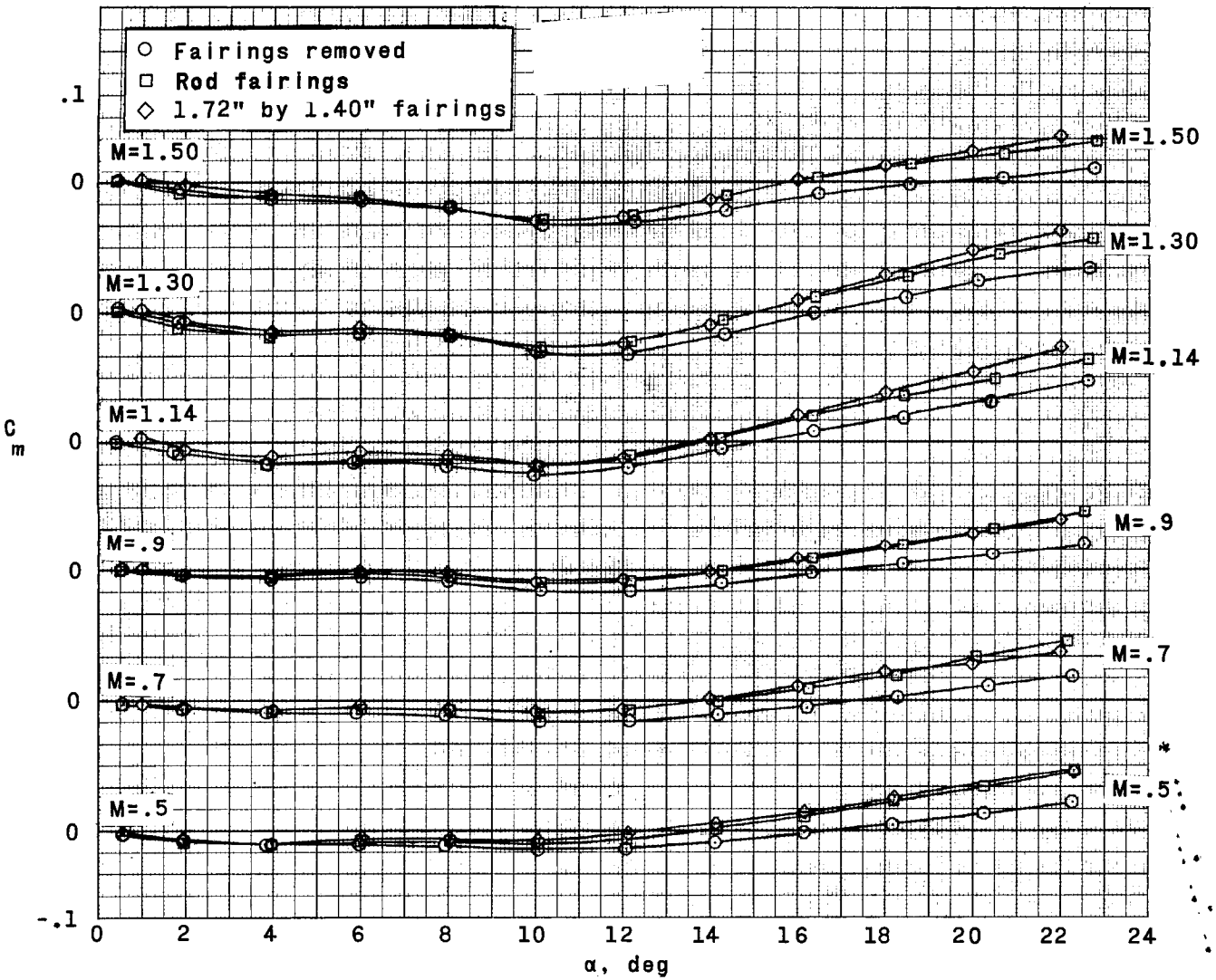

Figure 14.- Continued.

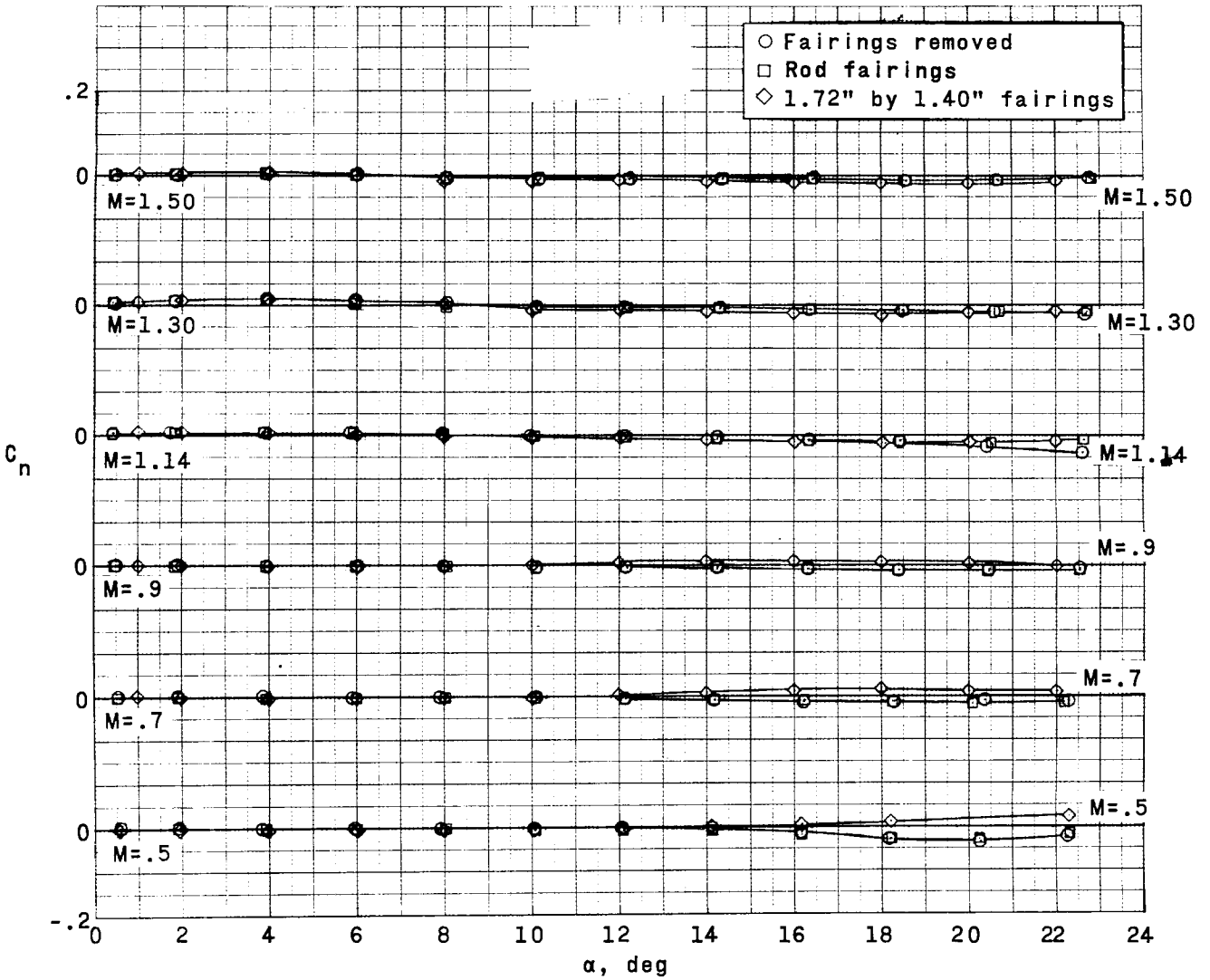

Figure 14.- Continued.

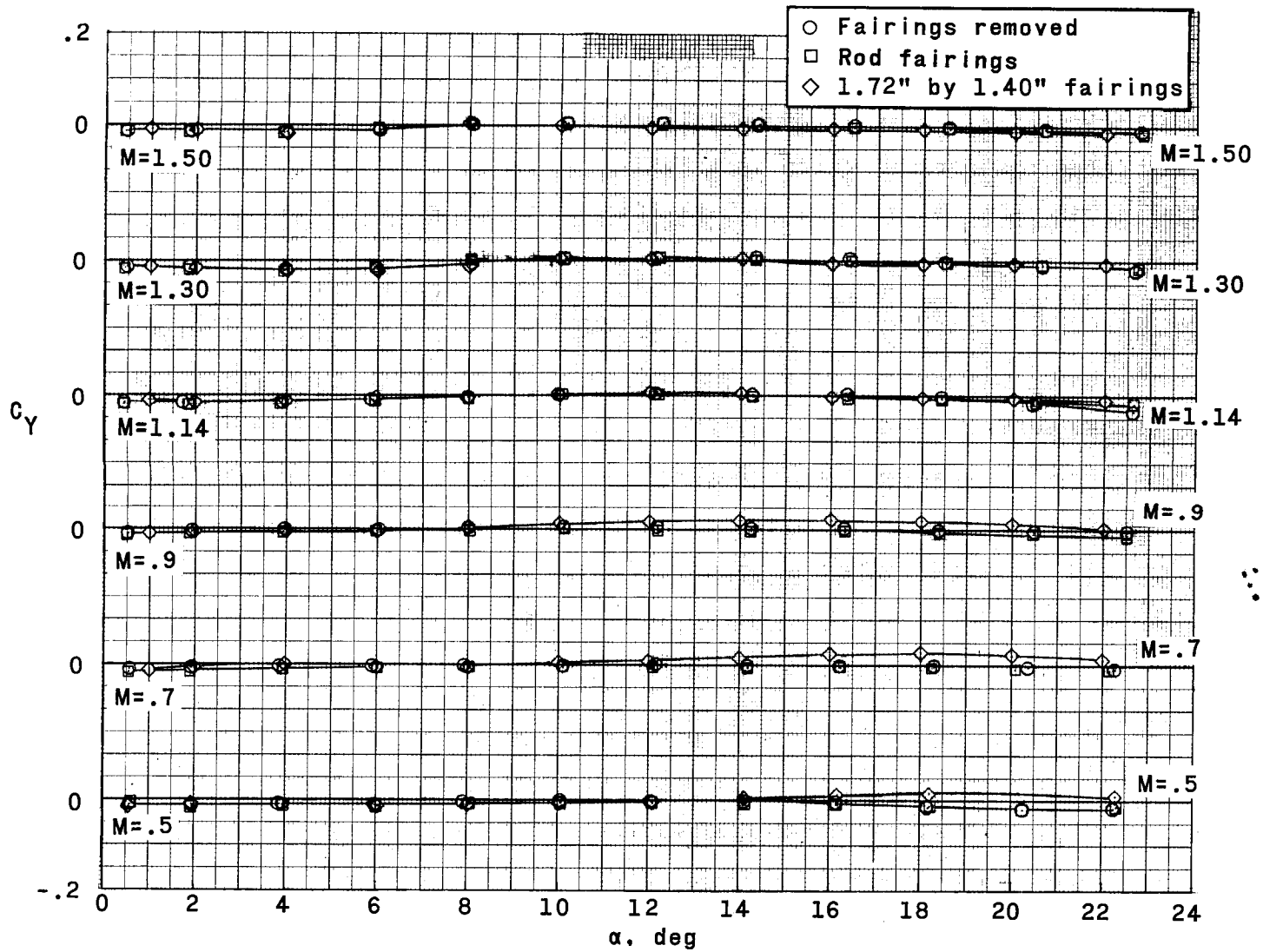
○ Fairings removed
□ Rod fairings
◇ 1.72" by 1.40" fairings
C_Y
.2
0
-.2
M=1.50
M=1.30
M=1.14
M=.9
M=.7
M=.5
0
2
4
6
8
10
12
14
16
18
20
22
24
α, deg

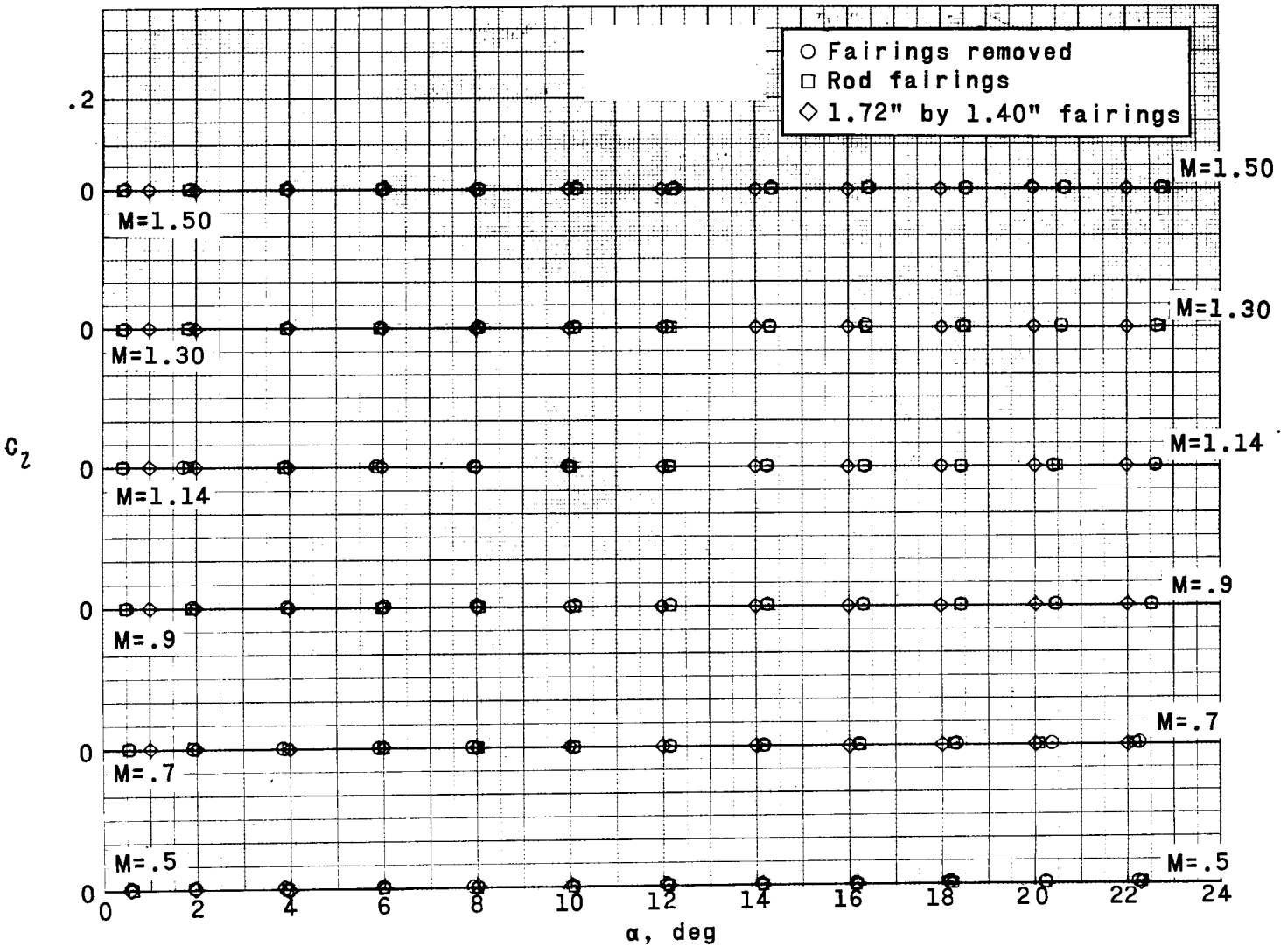

Figure 14.- Continued.

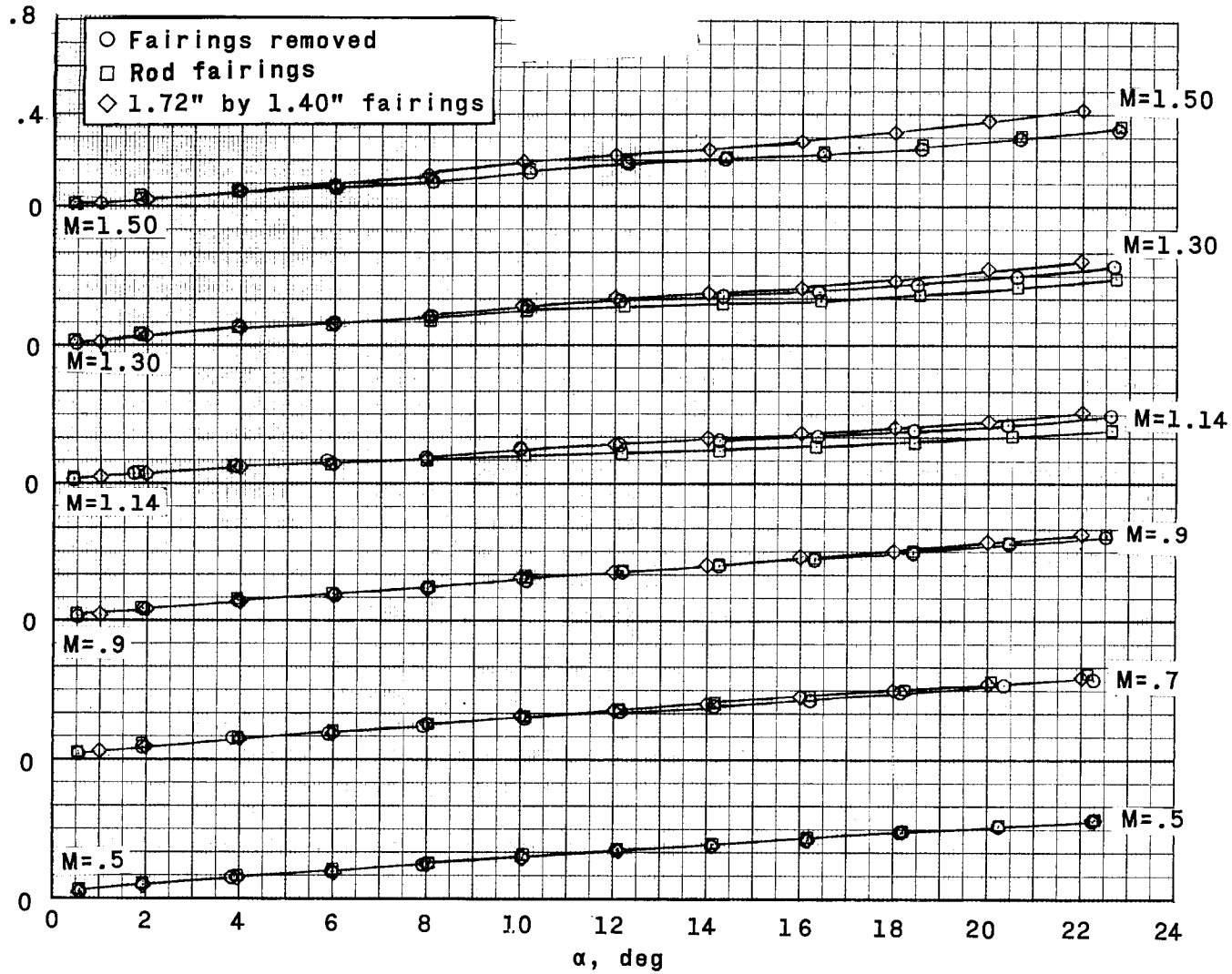
○ Fairings removed
□ Rod fairings
◇ 1.72" by 1.40" fairings
M=1.50
M=1.30
M=1.14
M=.9
M=.7
M=.5
C_L
.8
.4
0
0
2
4
6
8
10
12
14
16
18
20
22
24
α, deg

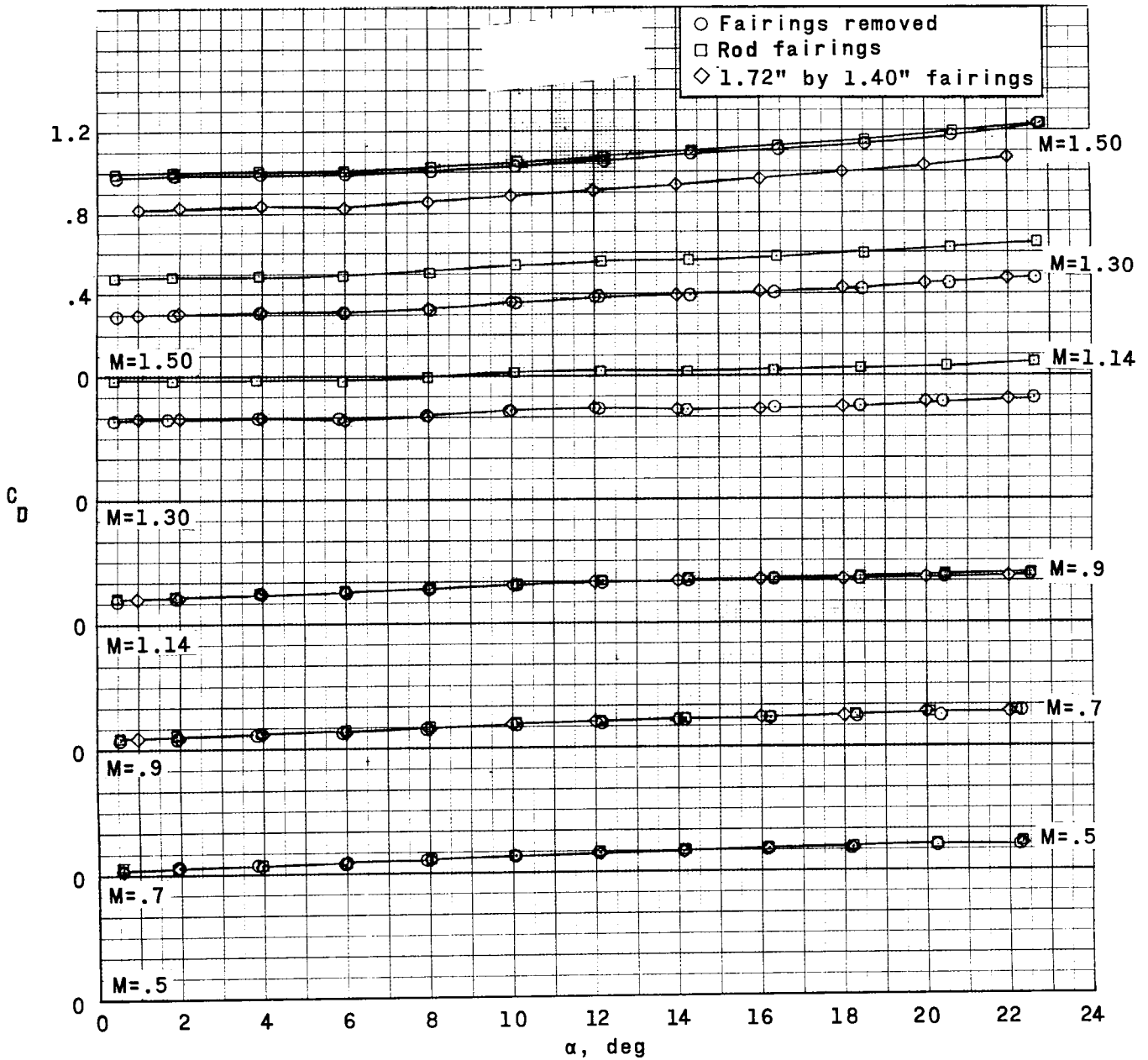

Figure 14.- Continued.

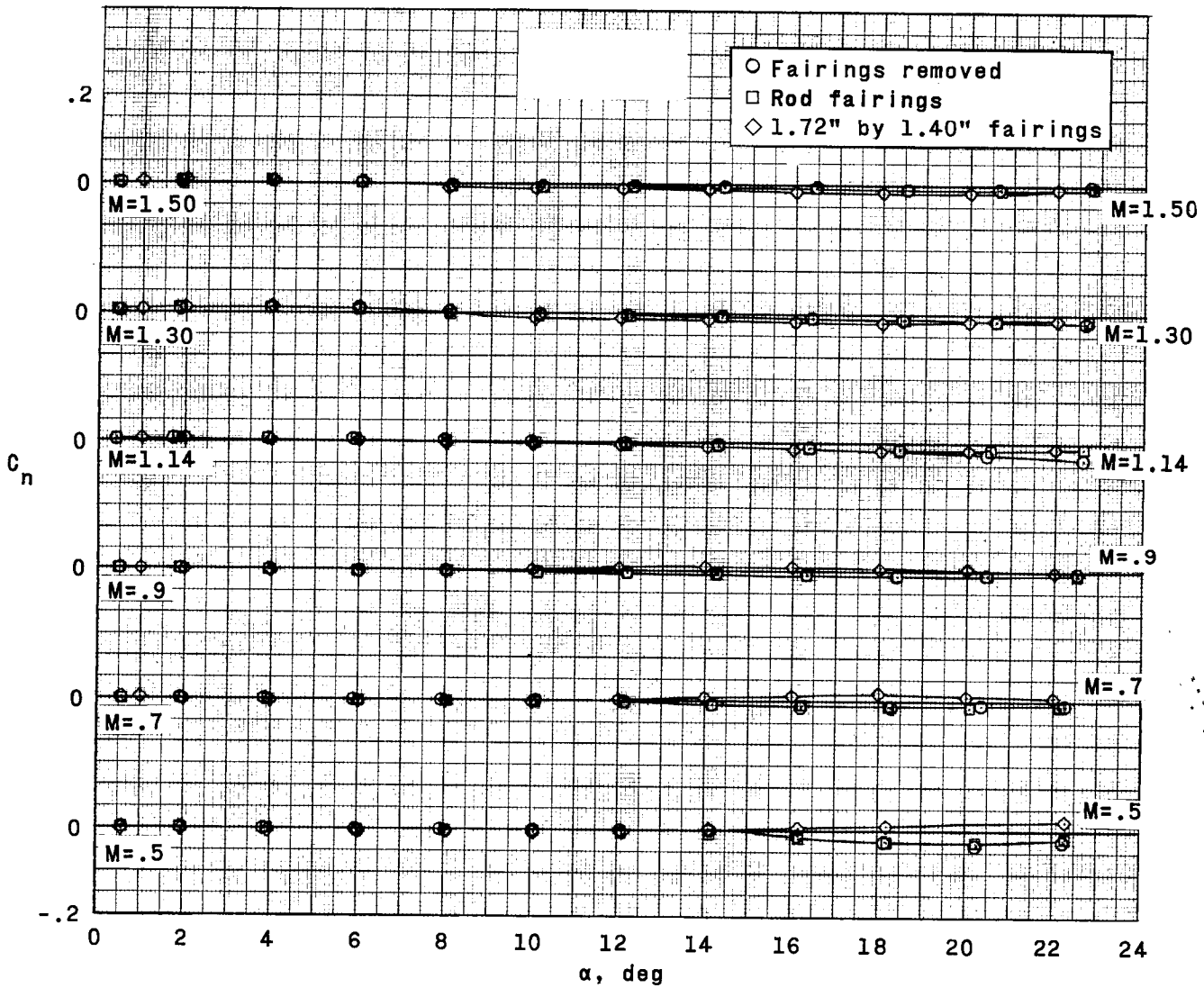

Figure 14.- Continued.

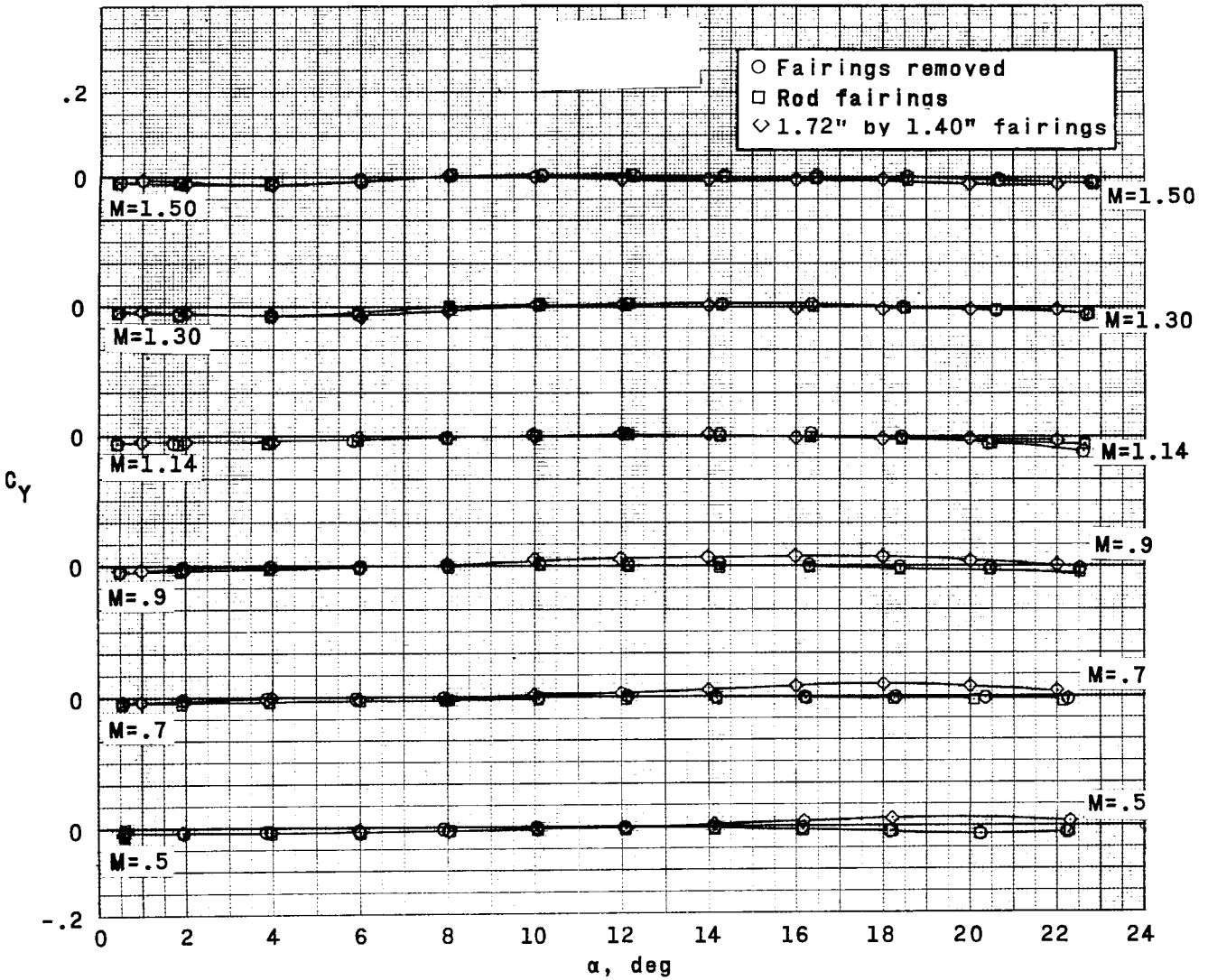

Figure 14.- Continued.

[redacted]

[redacted]

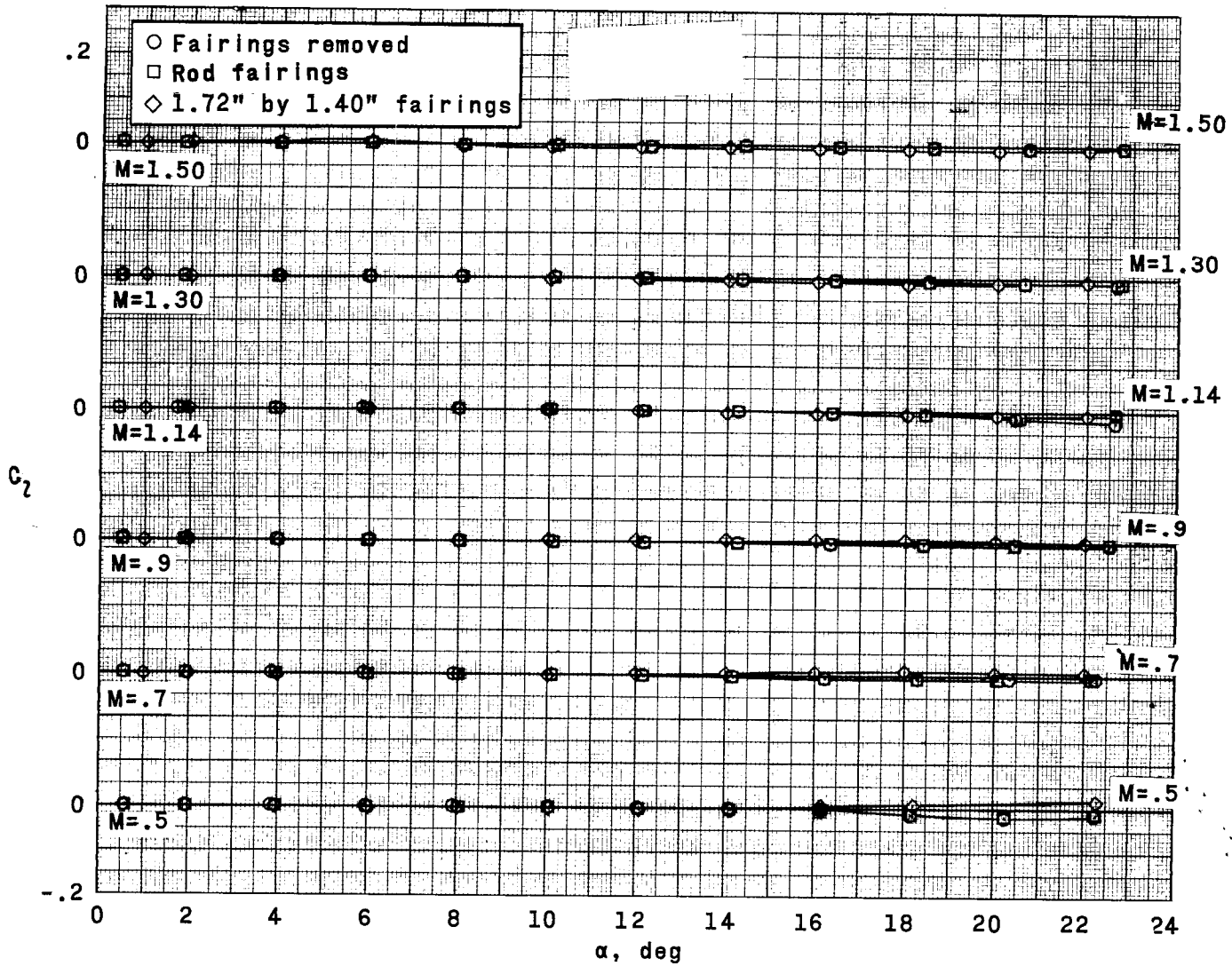

Figure 14.- Concluded.

DECLASSIFIED

[redacted]

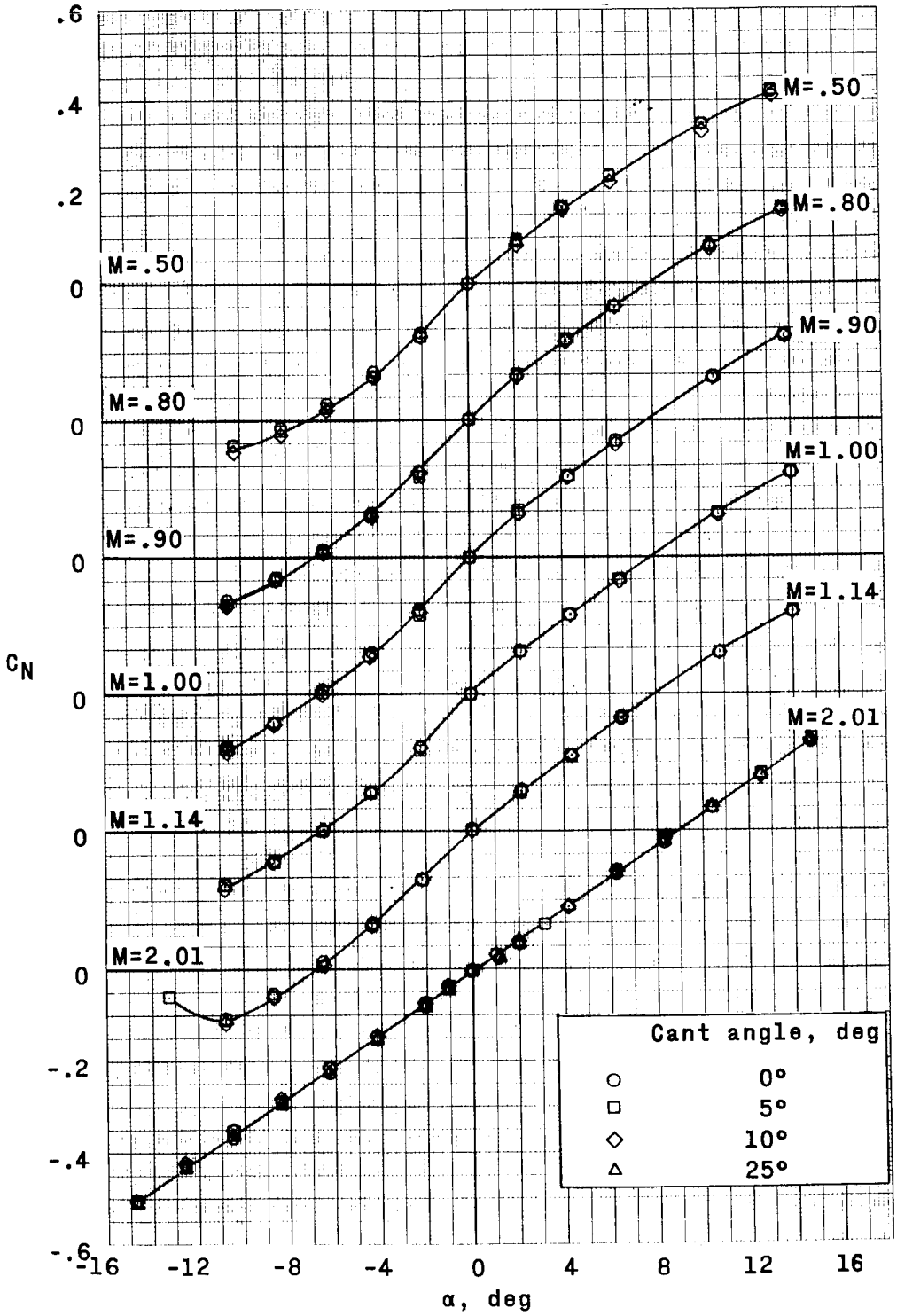

Figure 15.- Effect of rocket-face cant angles on the aerodynamic characteristics of the escape configuration. M = 0.50 to 2.01.

[redacted]

[redacted]

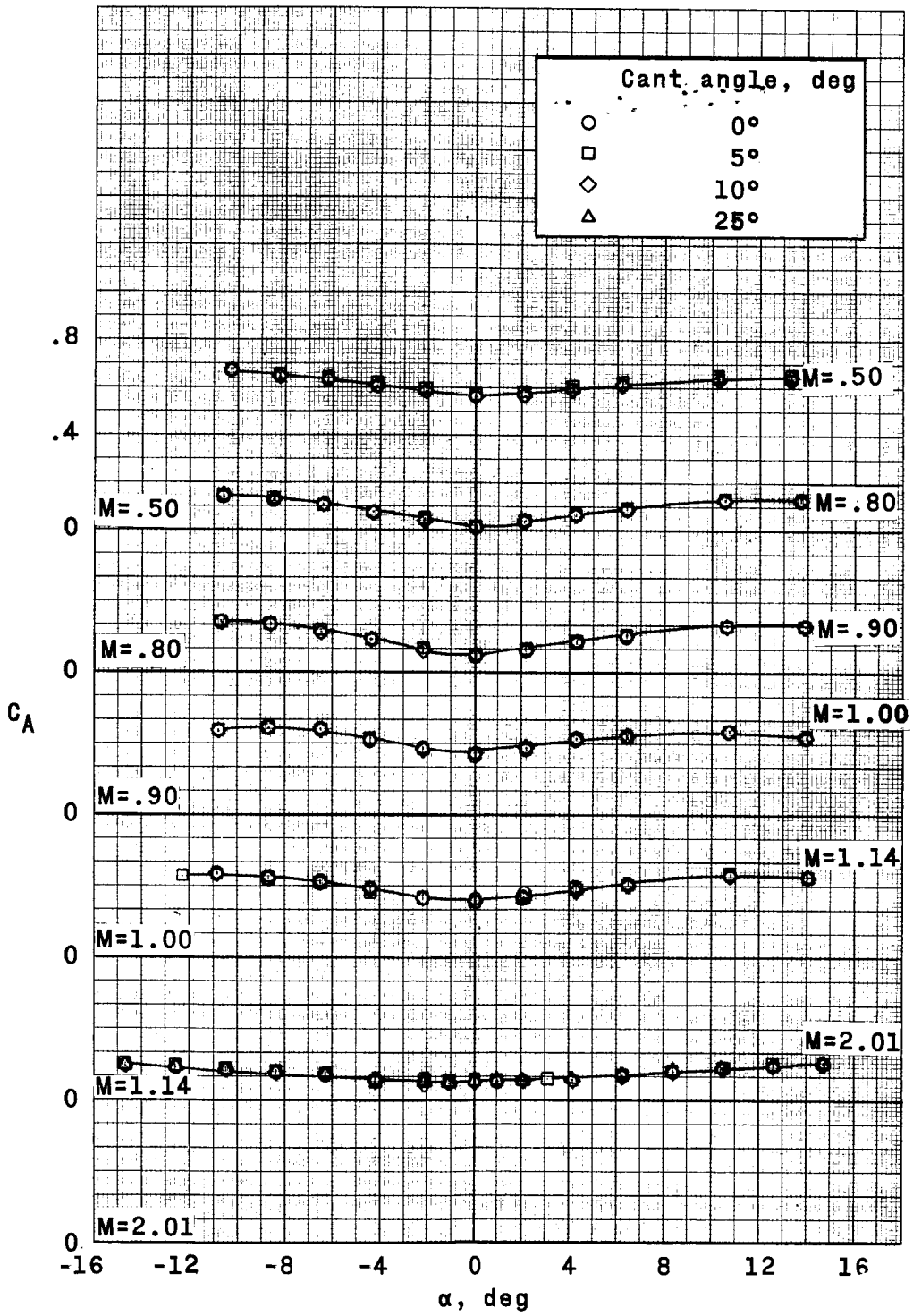

Figure 15.- Continued.

[redacted]

[redacted]

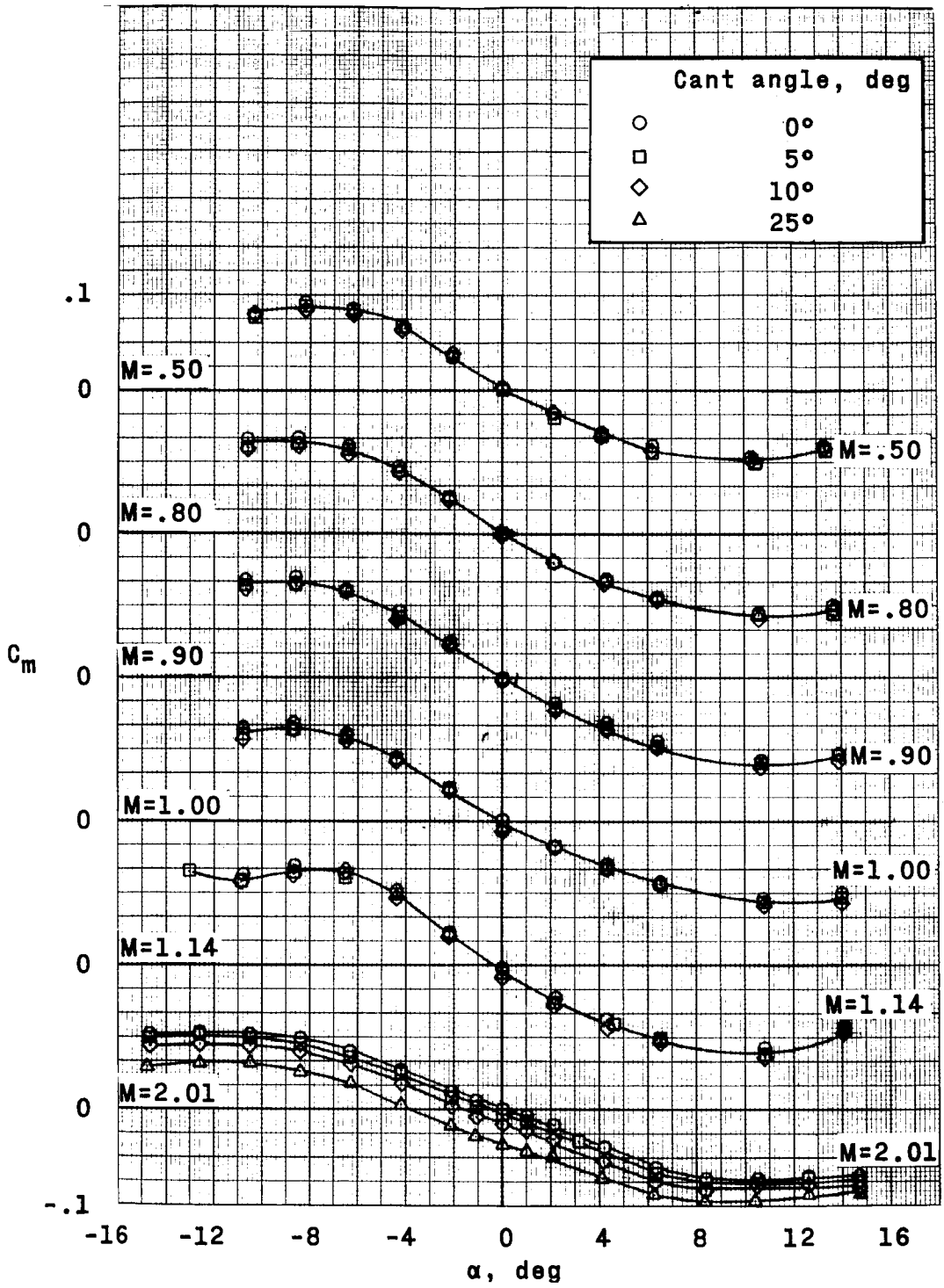

Figure 15.- Continued.

[redacted]

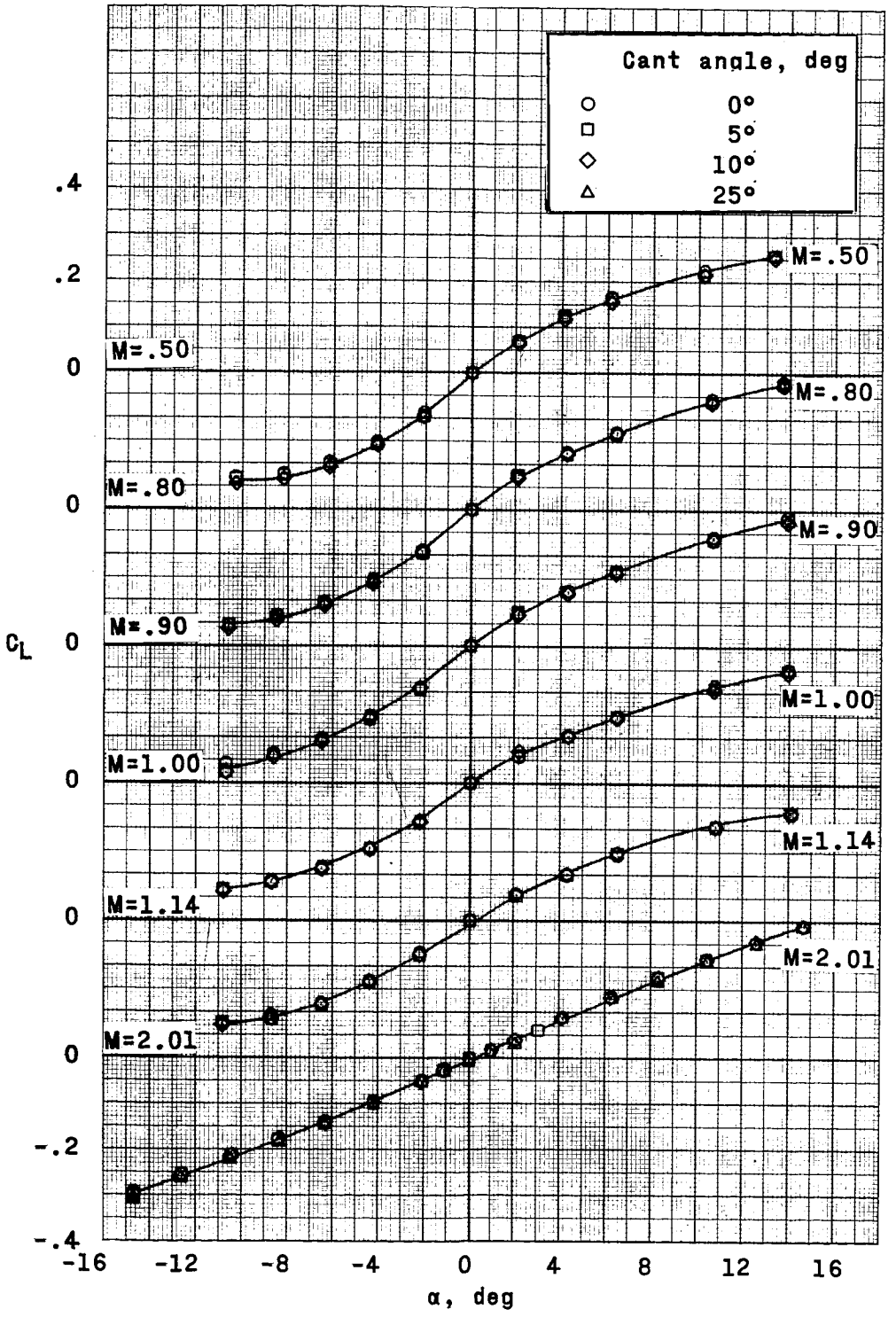

Figure 15.- Continued.

[redacted]

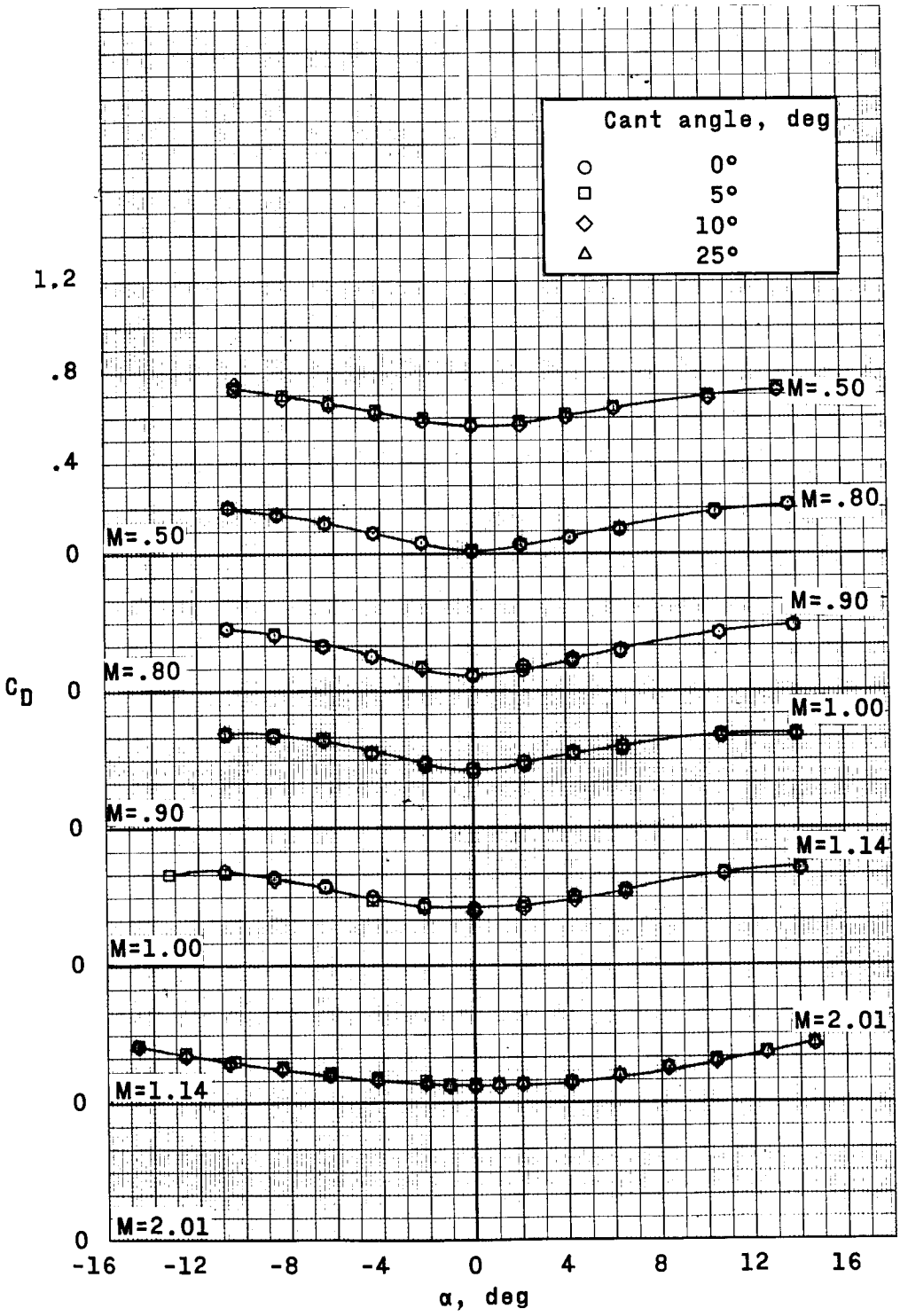

Figure 15.- Concluded.

[redacted]

DECLASSIFIED
[redacted]

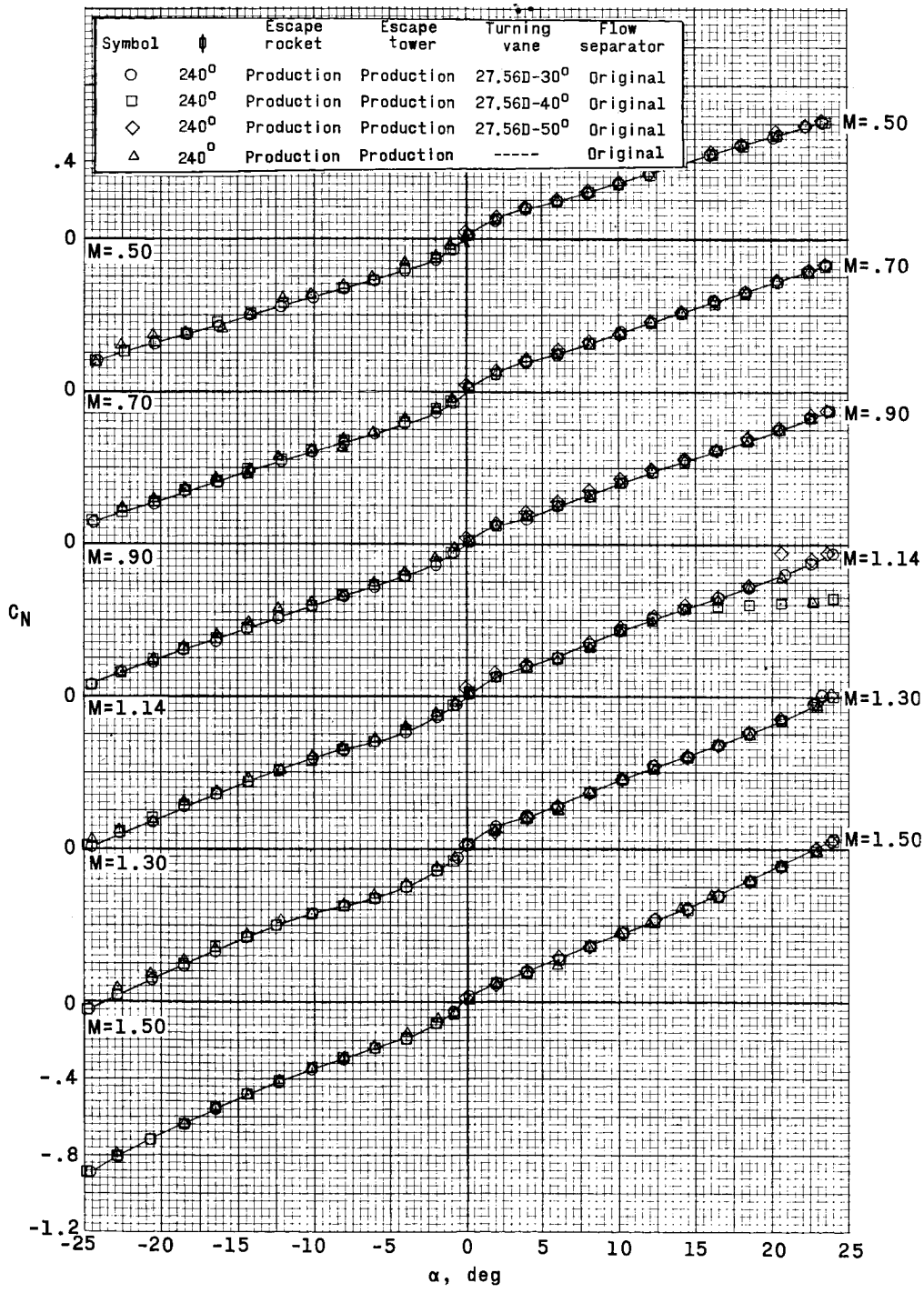

Figure 16.- Effect of turning-vane afterbody angles on the aerodynamic characteristics of the escape configuration. M = 0.50 to 1.50.

[redacted]

CONFIDENTIAL

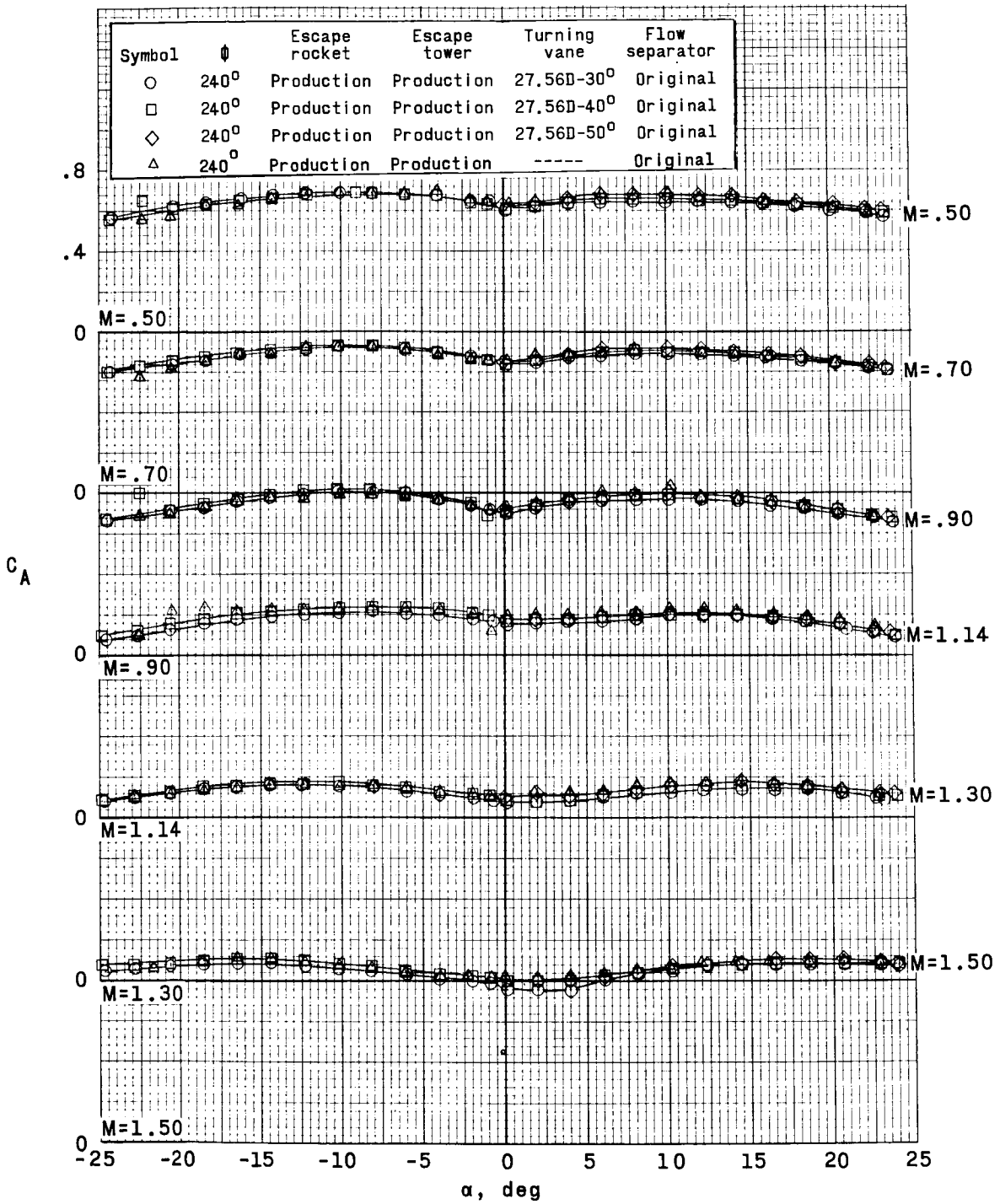

Figure 16.- Continued.

CONFIDENTIAL

DECLASSIFIED

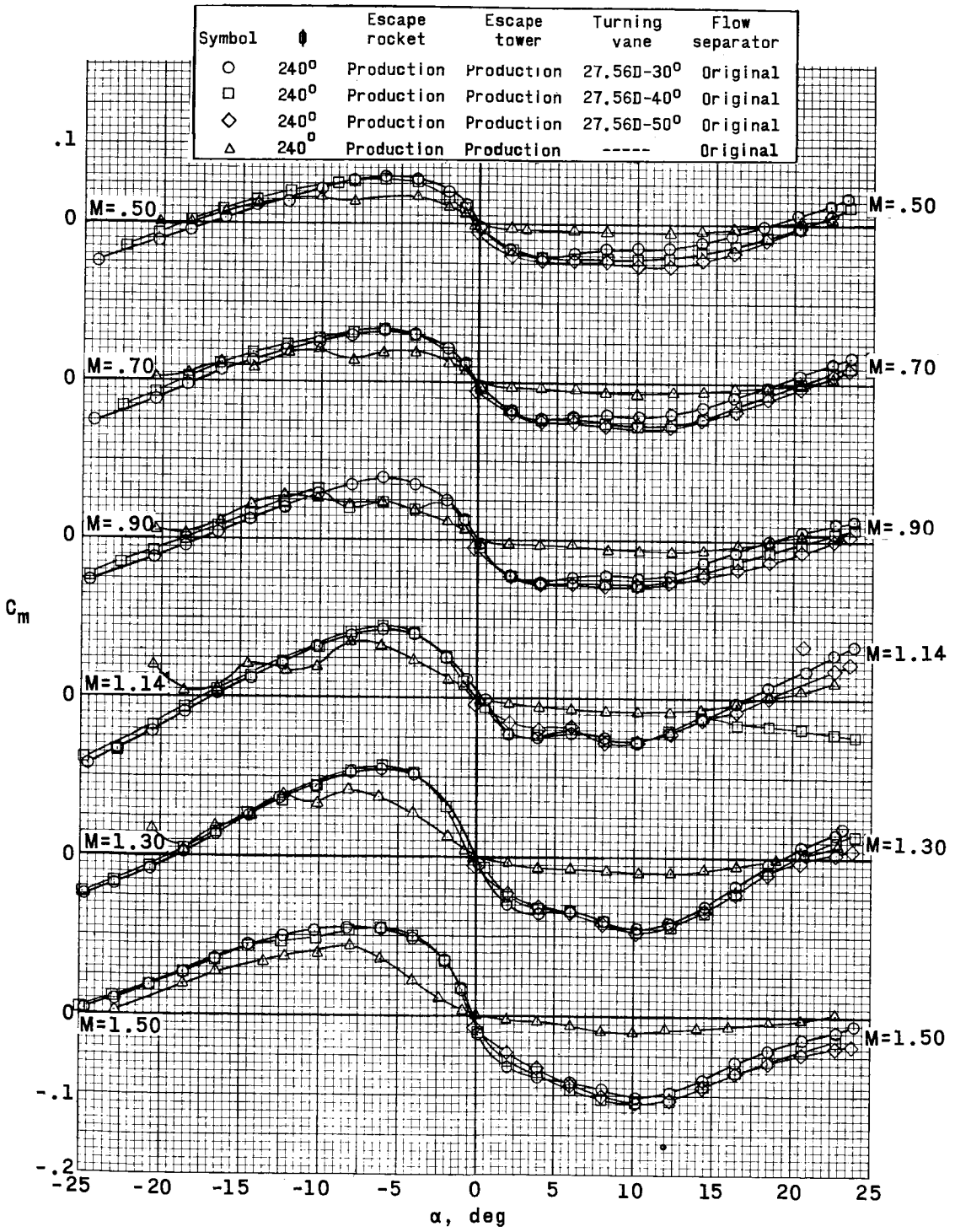

Figure 16.- Continued.

[redacted]

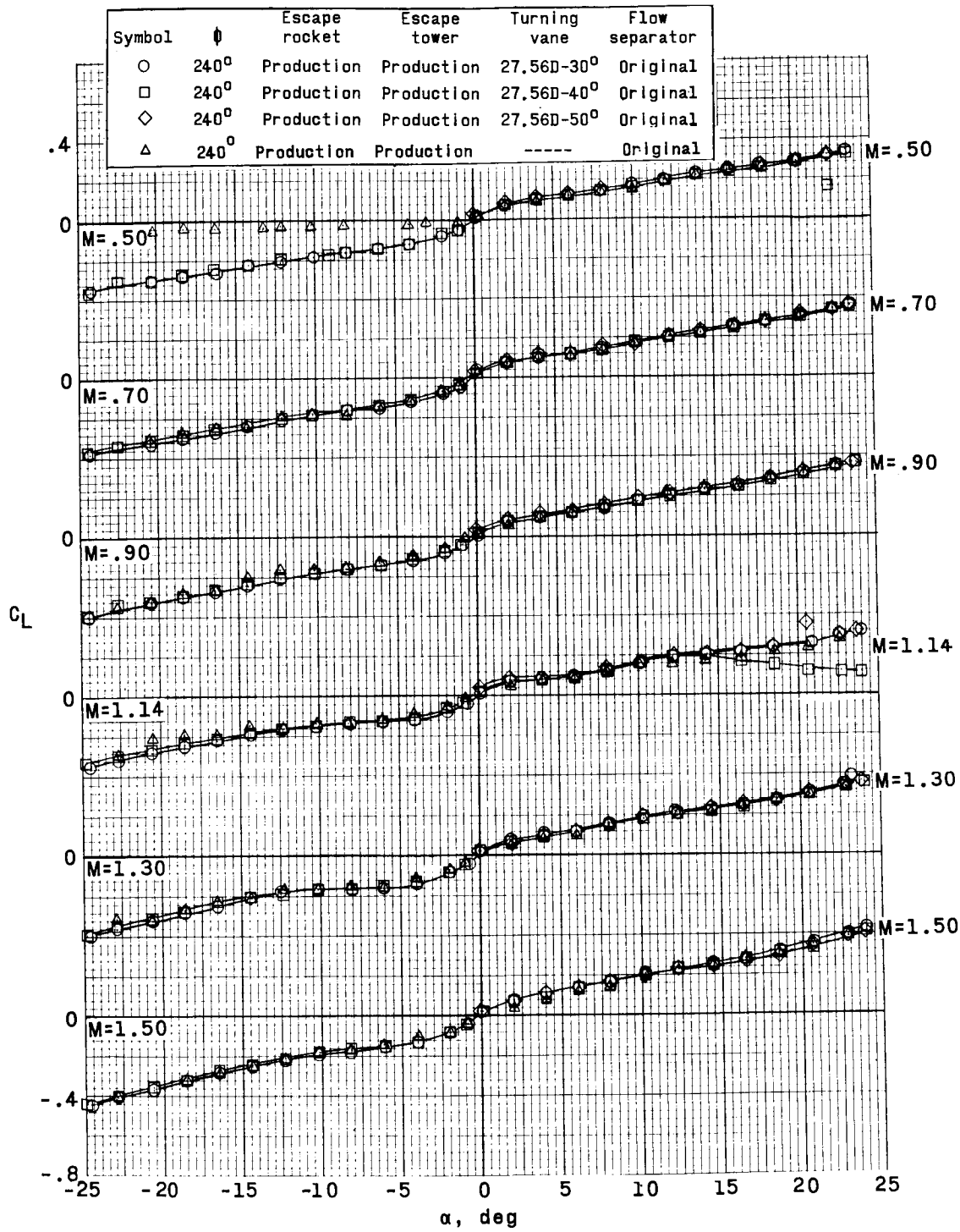

Figure 16.- Continued.

[redacted]

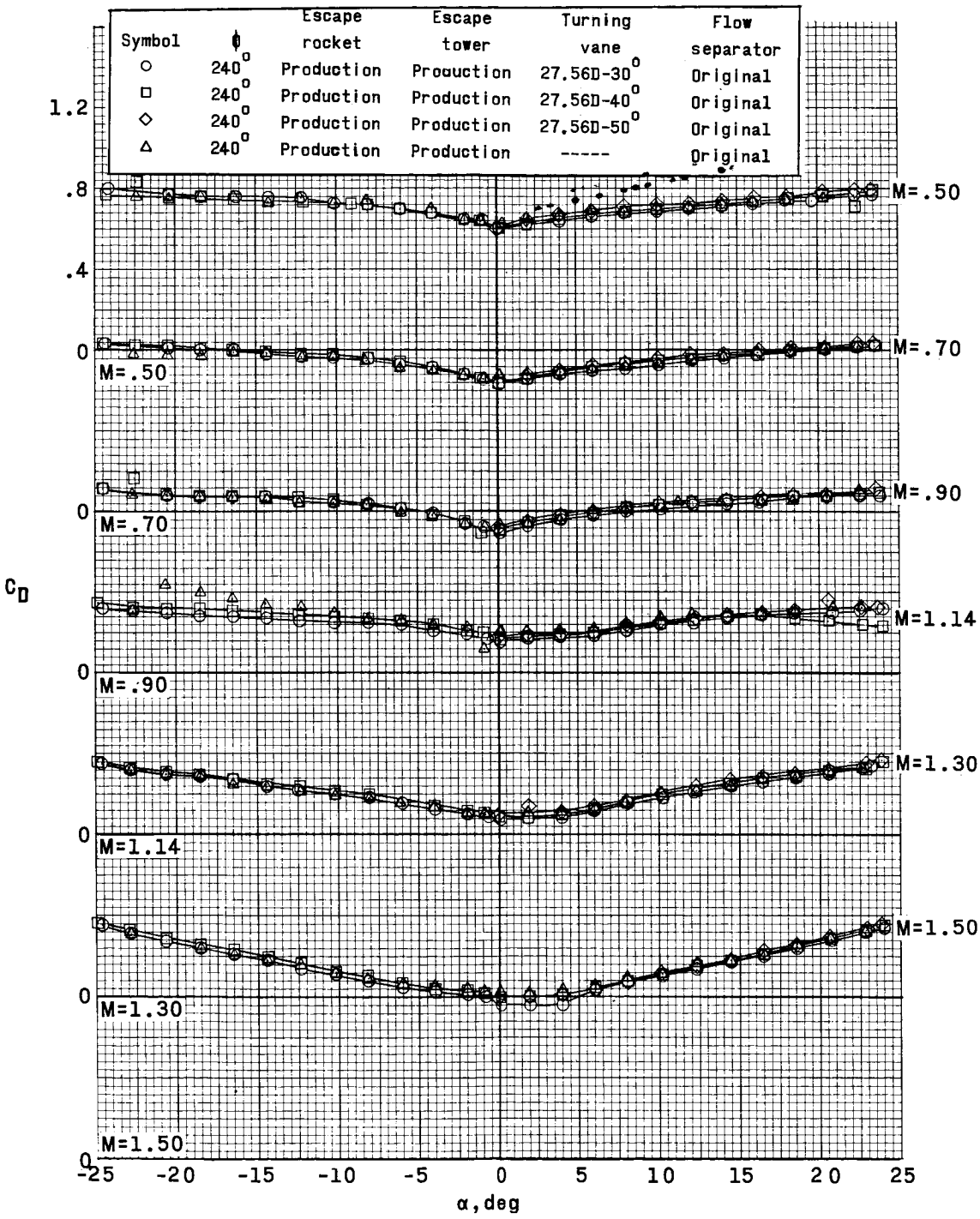

Figure 16.- Concluded.

[redacted]

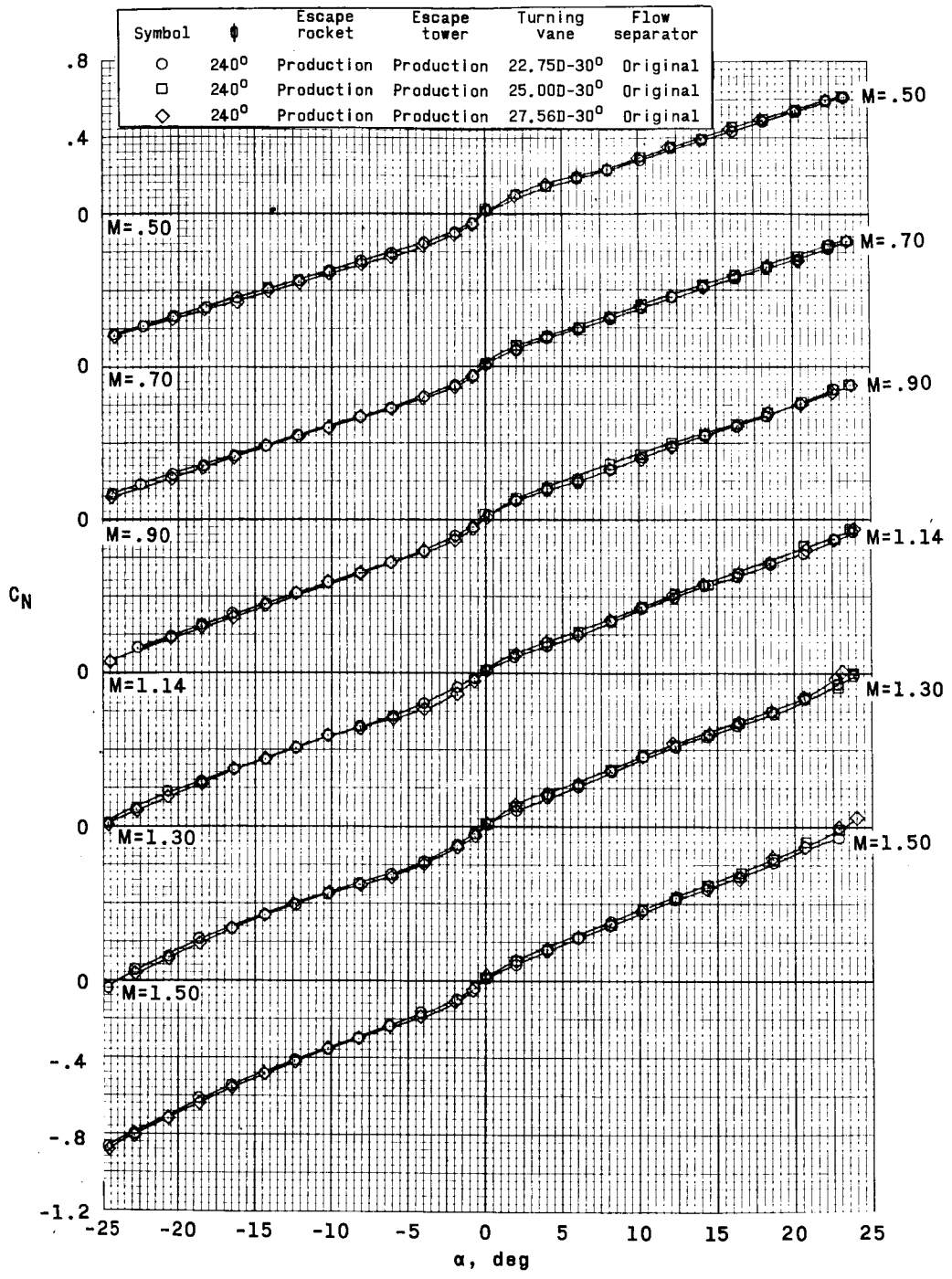

Figure 17.- Effect of escape-rocket turning-vane diameter on the aerodynamic characteristics of the escape configuration. M = 0.50 to 1.50.

[redacted]

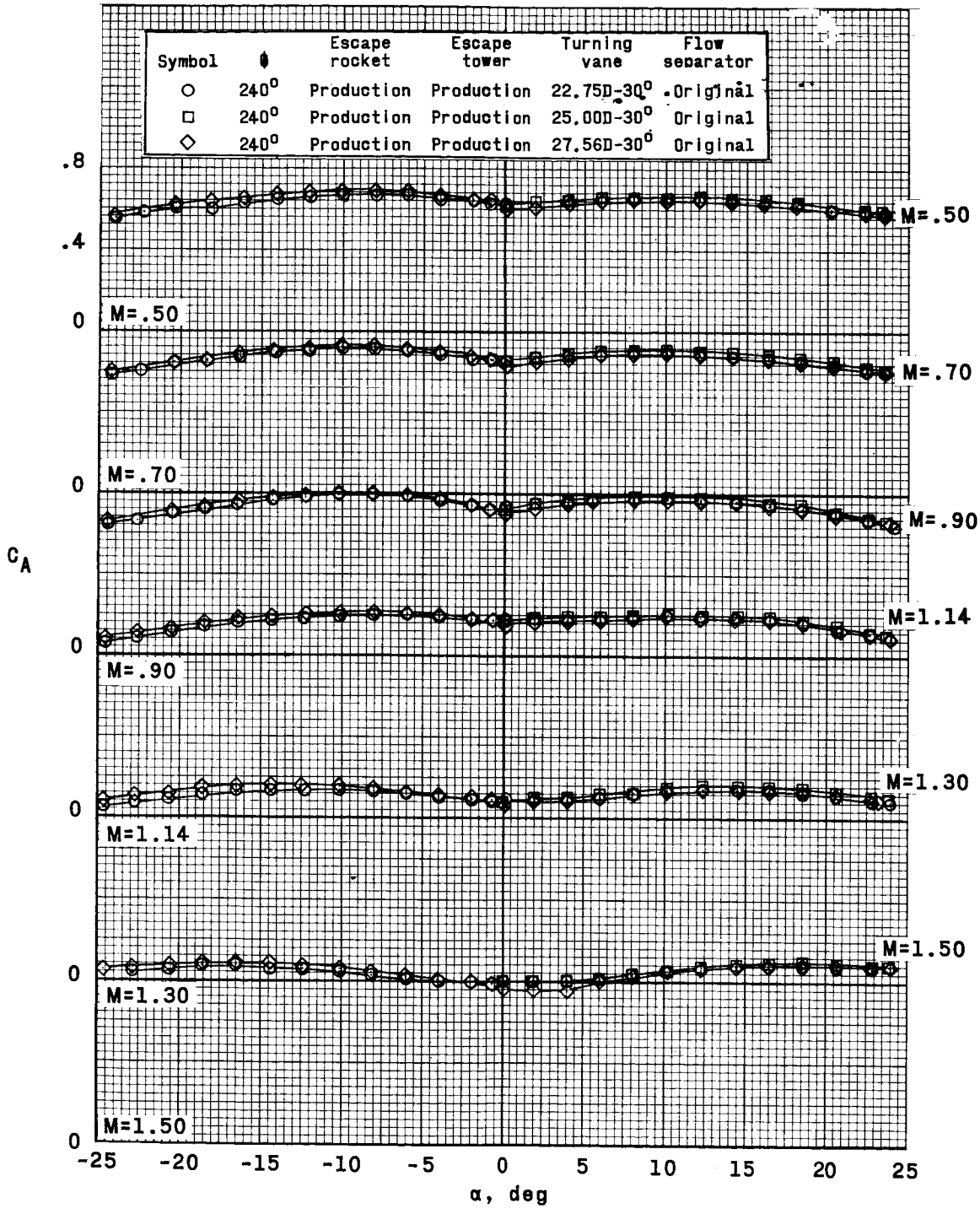

Figure 17.- Continued.

G
6

[redacted]

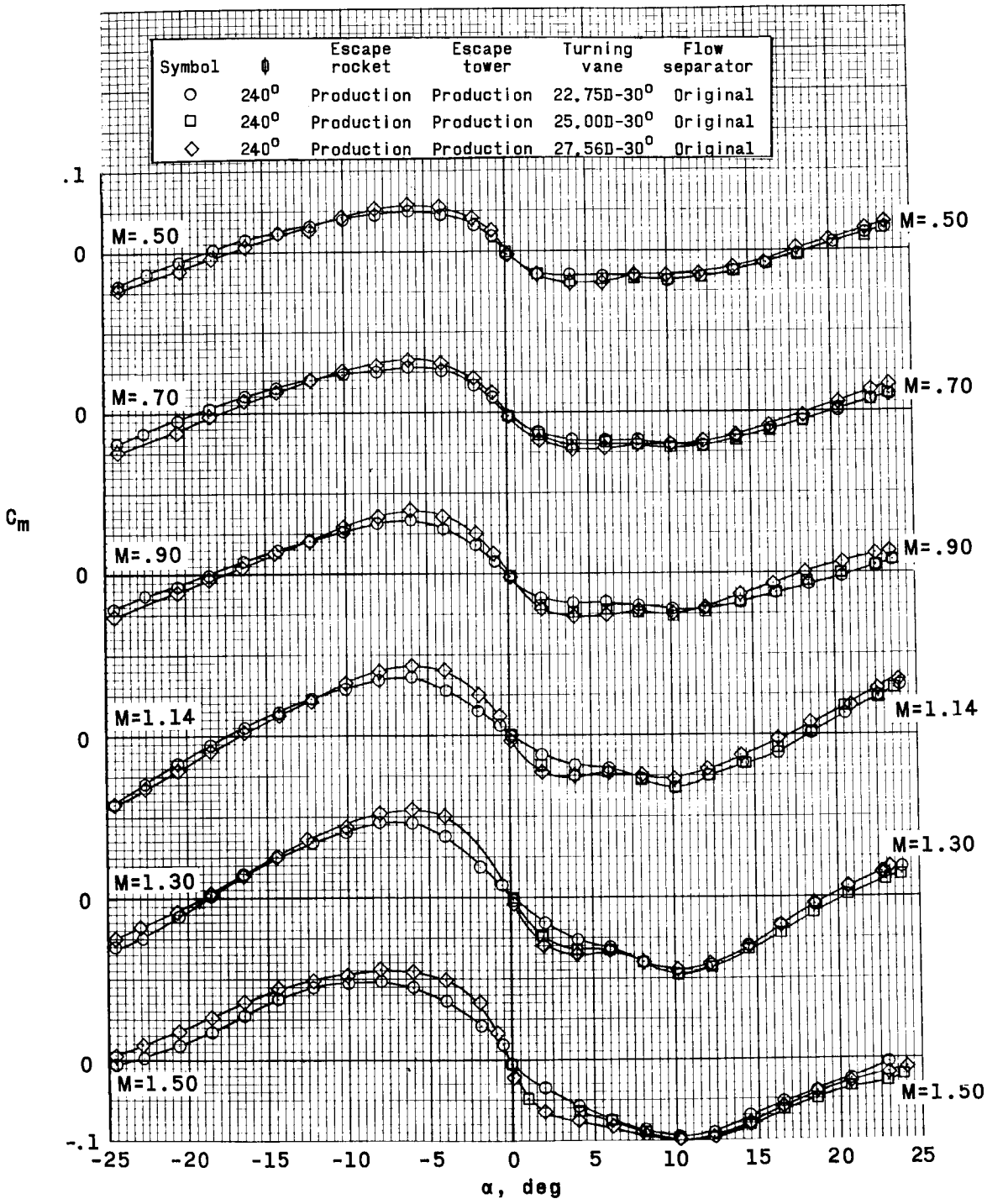

Figure 17.- Continued.

[redacted]
DECLASSIFIED

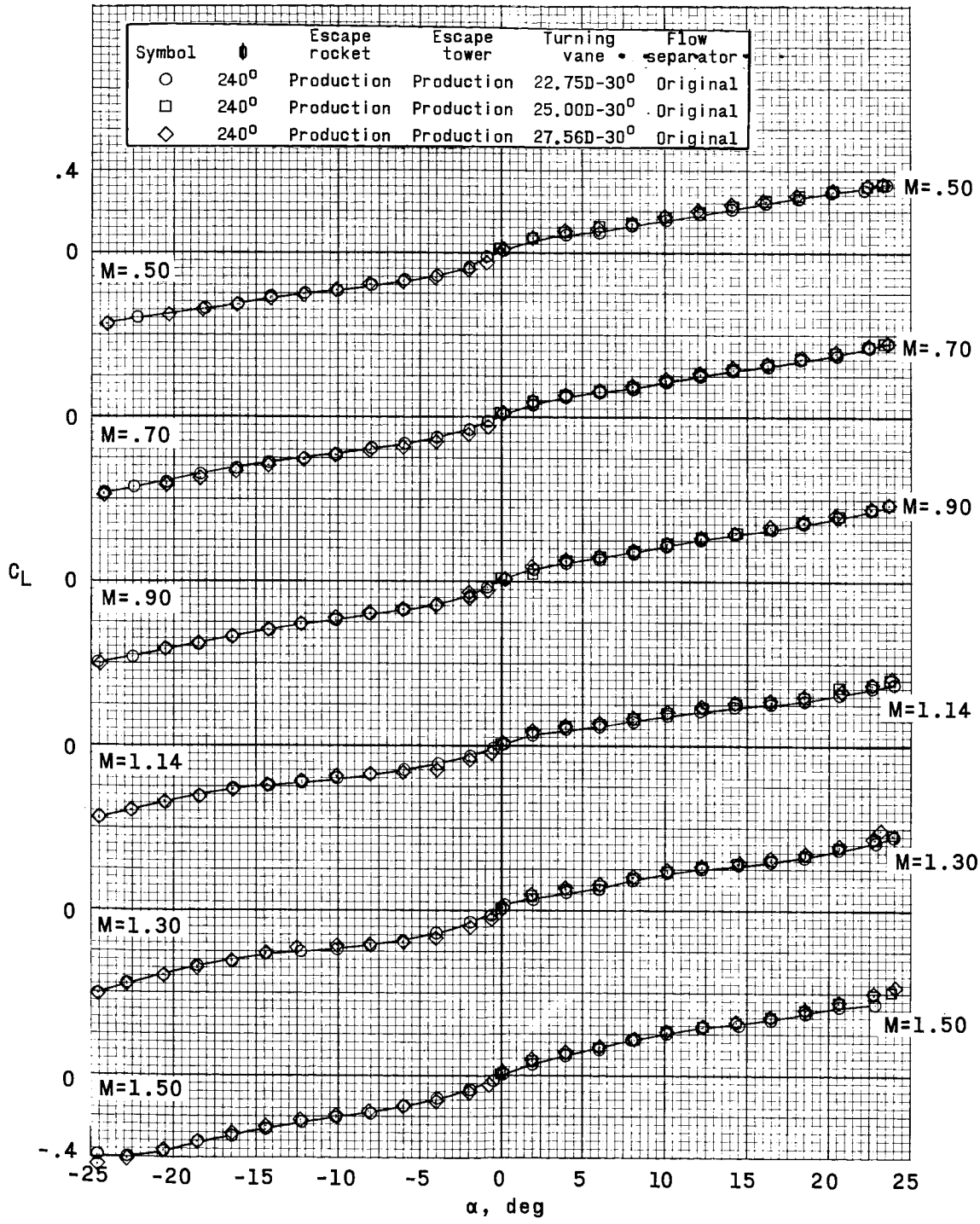

Figure 17.- Continued.

G
6

[redacted]

[redacted]

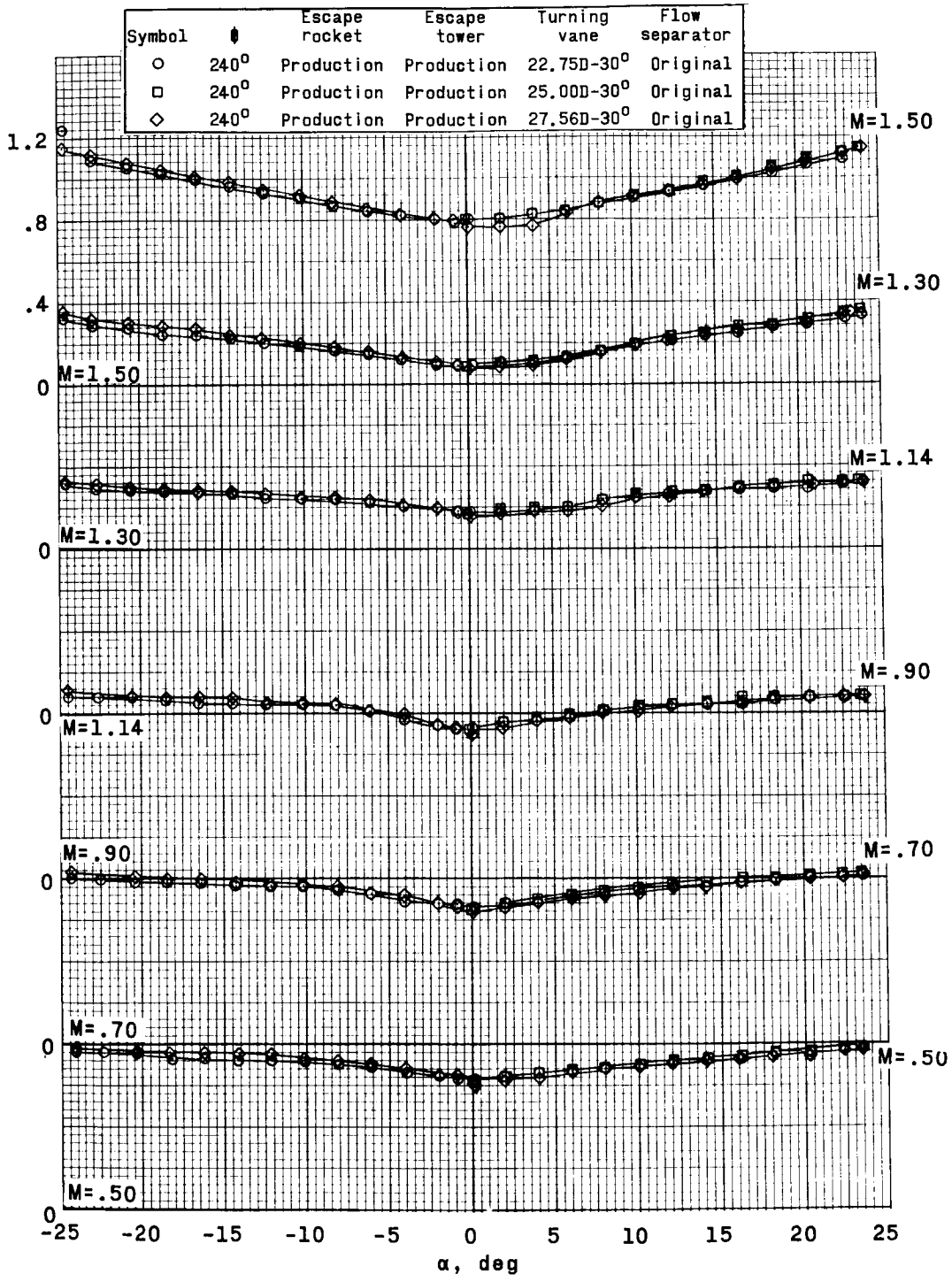

Figure 17.- Concluded.

[redacted]

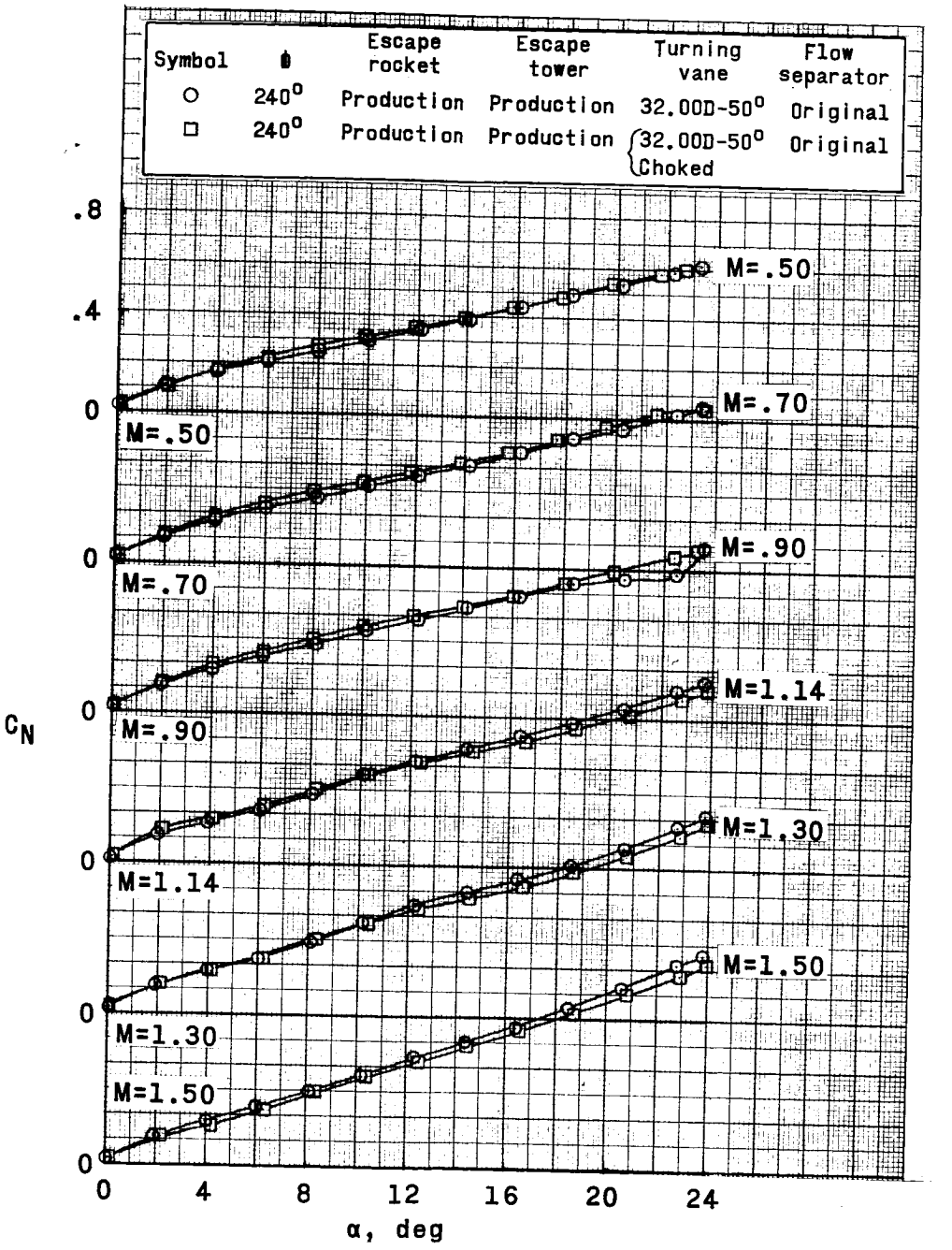

Figure 18.- Effect of escape-rocket turning-vane exit area on the aerodynamic characteristics of the escape configuration. M = 0.50 to 1.50.

[redacted]

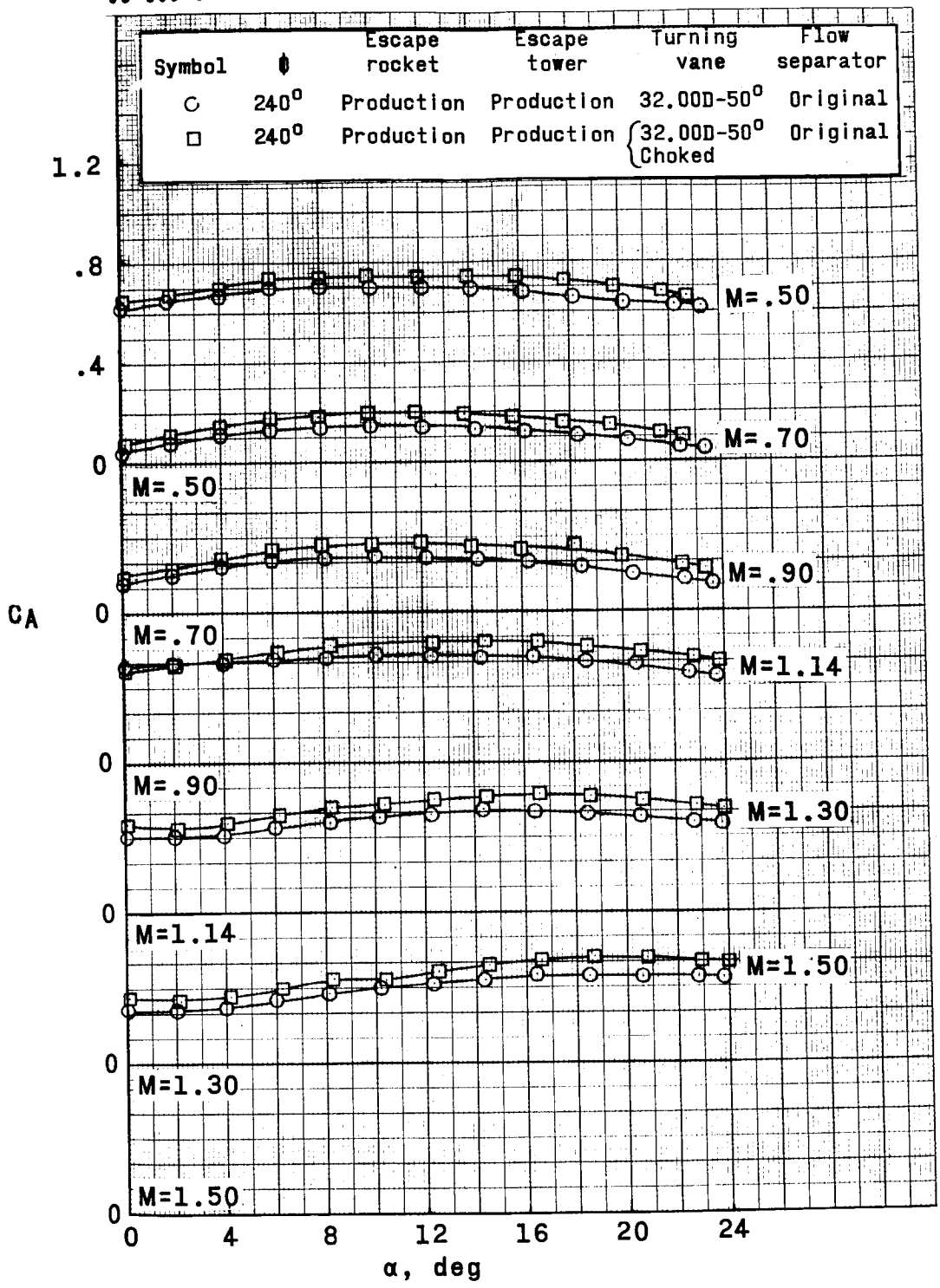

Figure 18.- Continued.

[redacted]

[redacted]

DECLASSIFIED

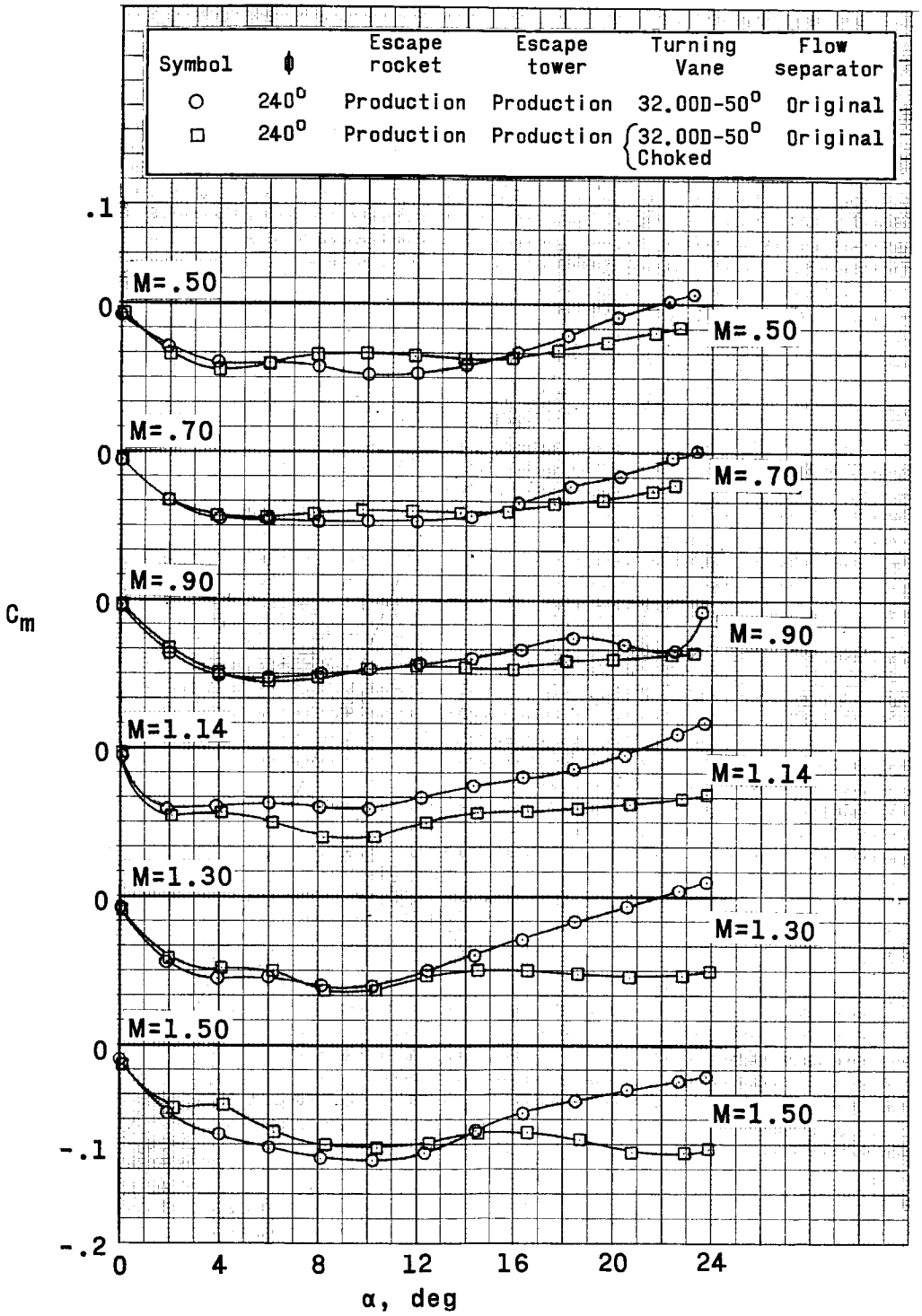

Figure 18.- Continued.

[redacted]

[redacted]

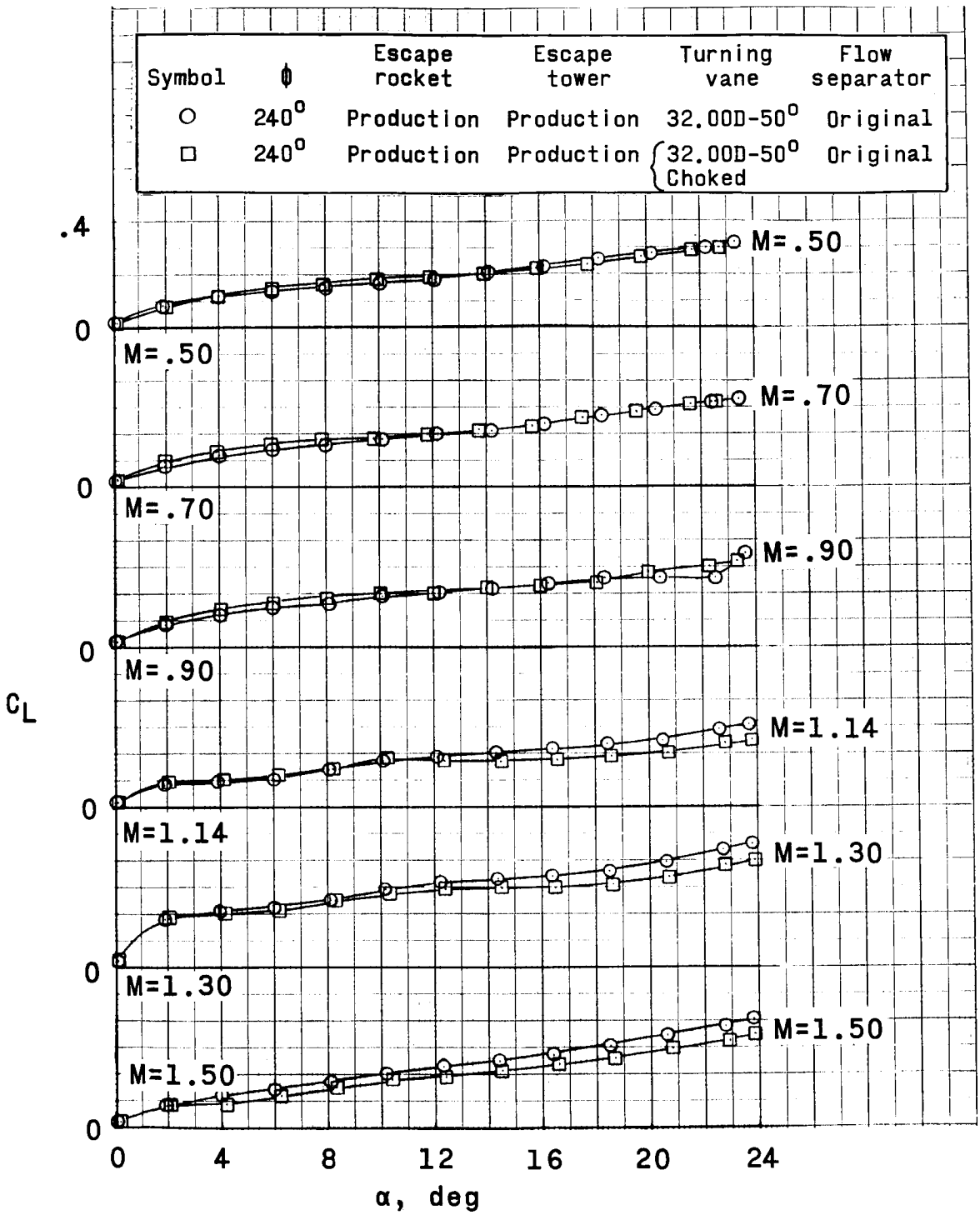

Figure 18.- Continued.

[redacted]

[redacted]
DECLASSIFIED

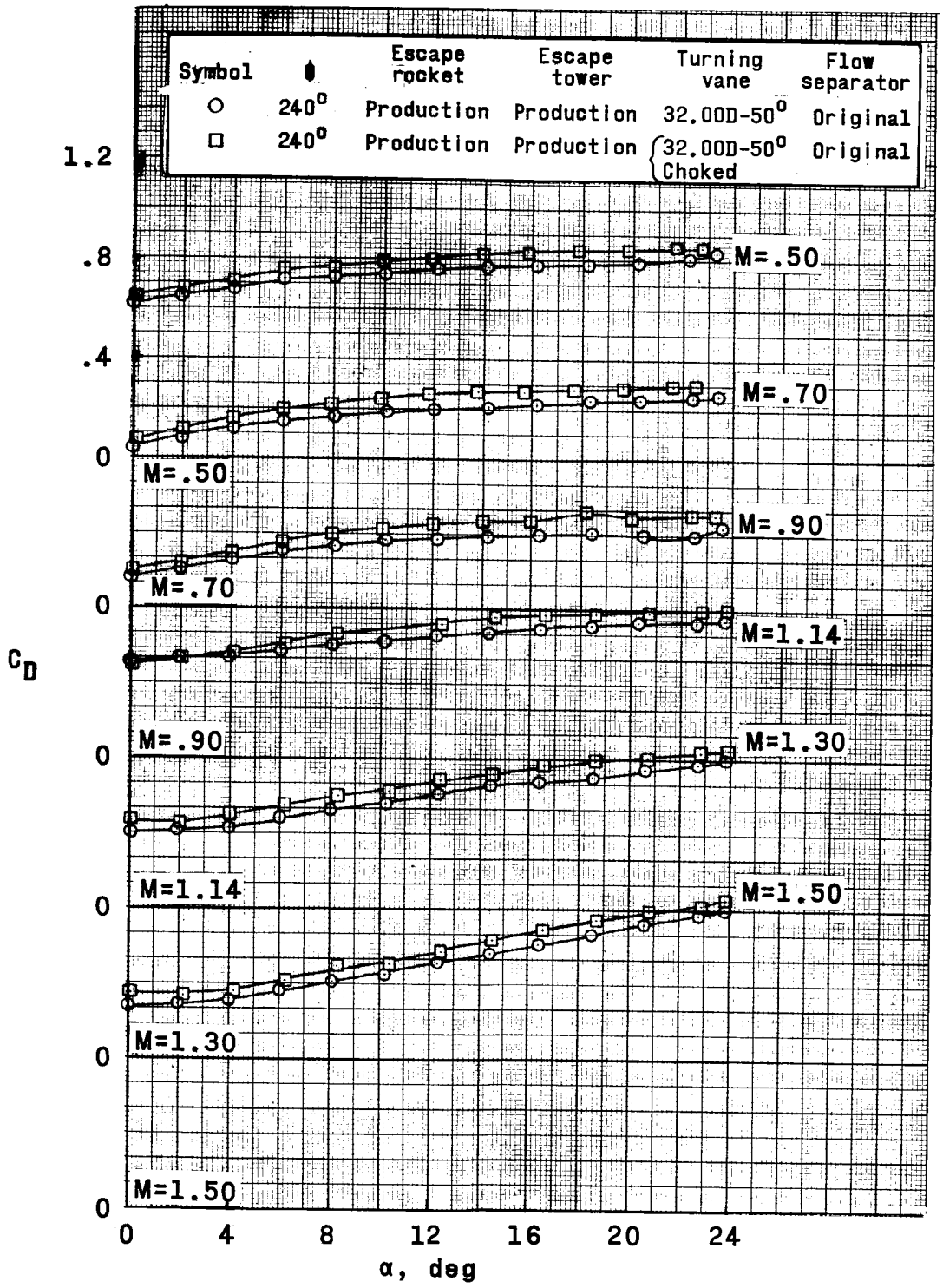

Figure 18.- Concluded.

[redacted]

[redacted]

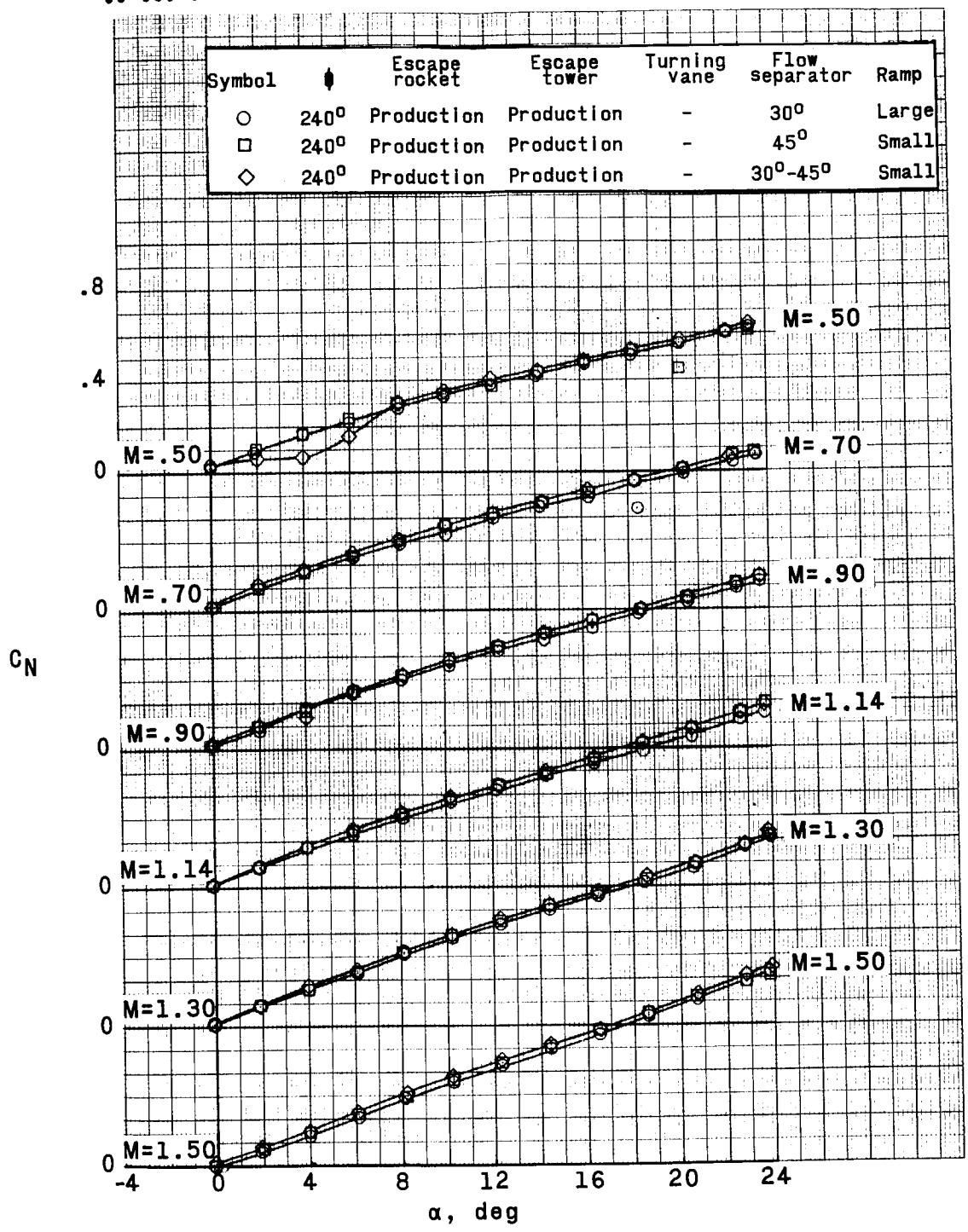

Figure 19.- Effect of various flow separators on the aerodynamic characteristics of the escape configuration (without turning vane). M = 0.50 to 1.50.

[redacted]

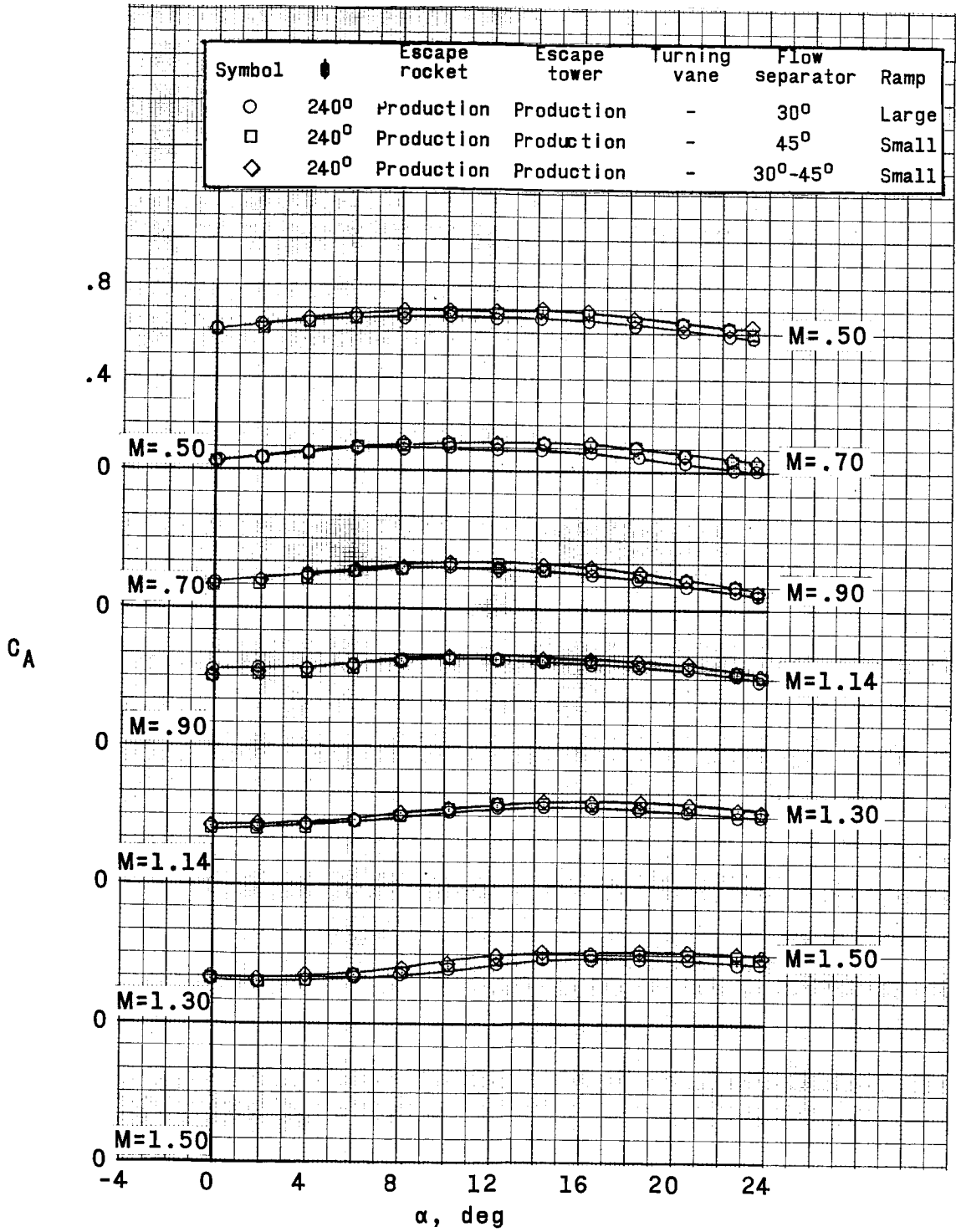

Figure 19.- Continued.

[redacted]

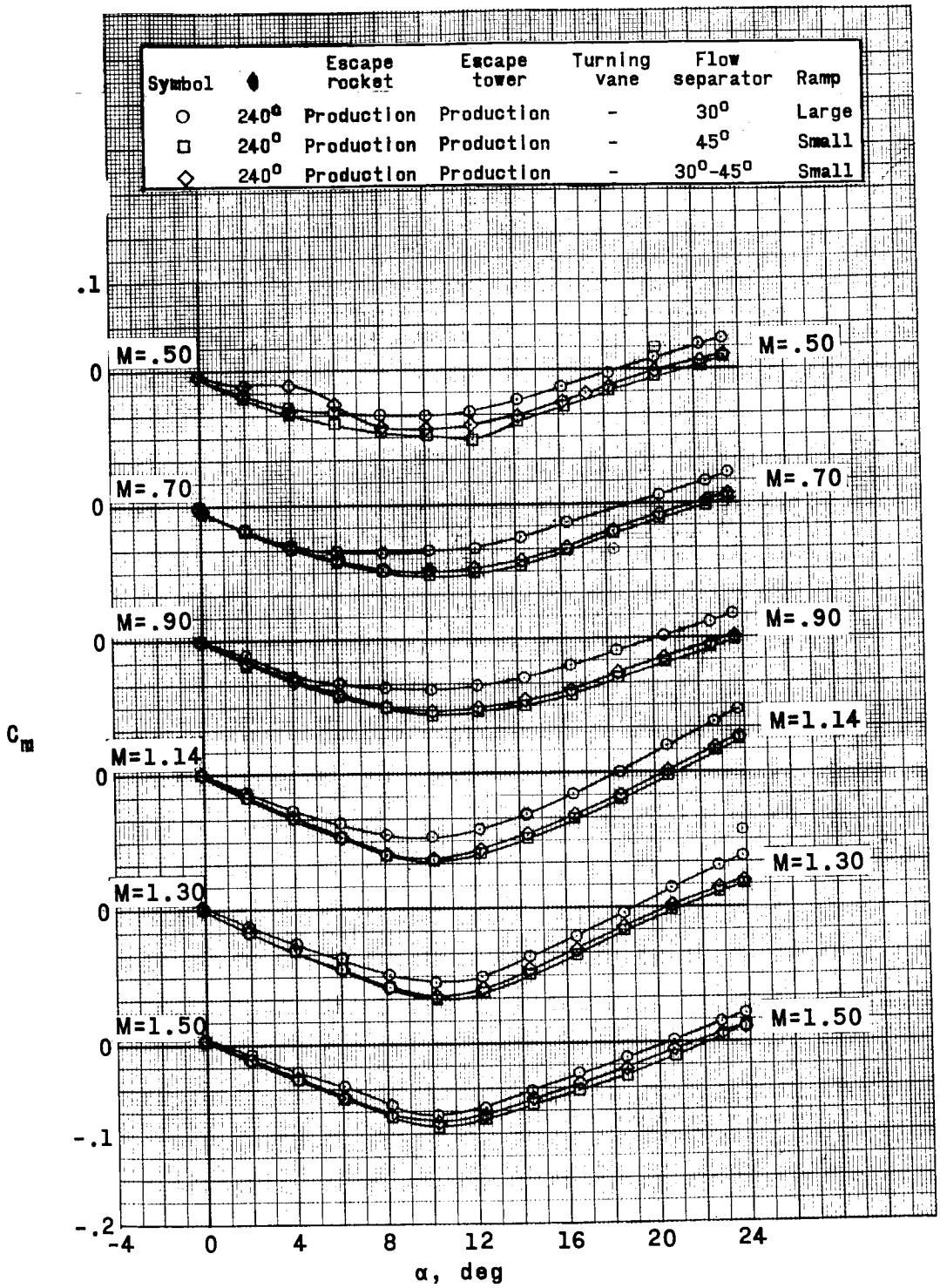

Figure 19.- Continued.

[redacted]

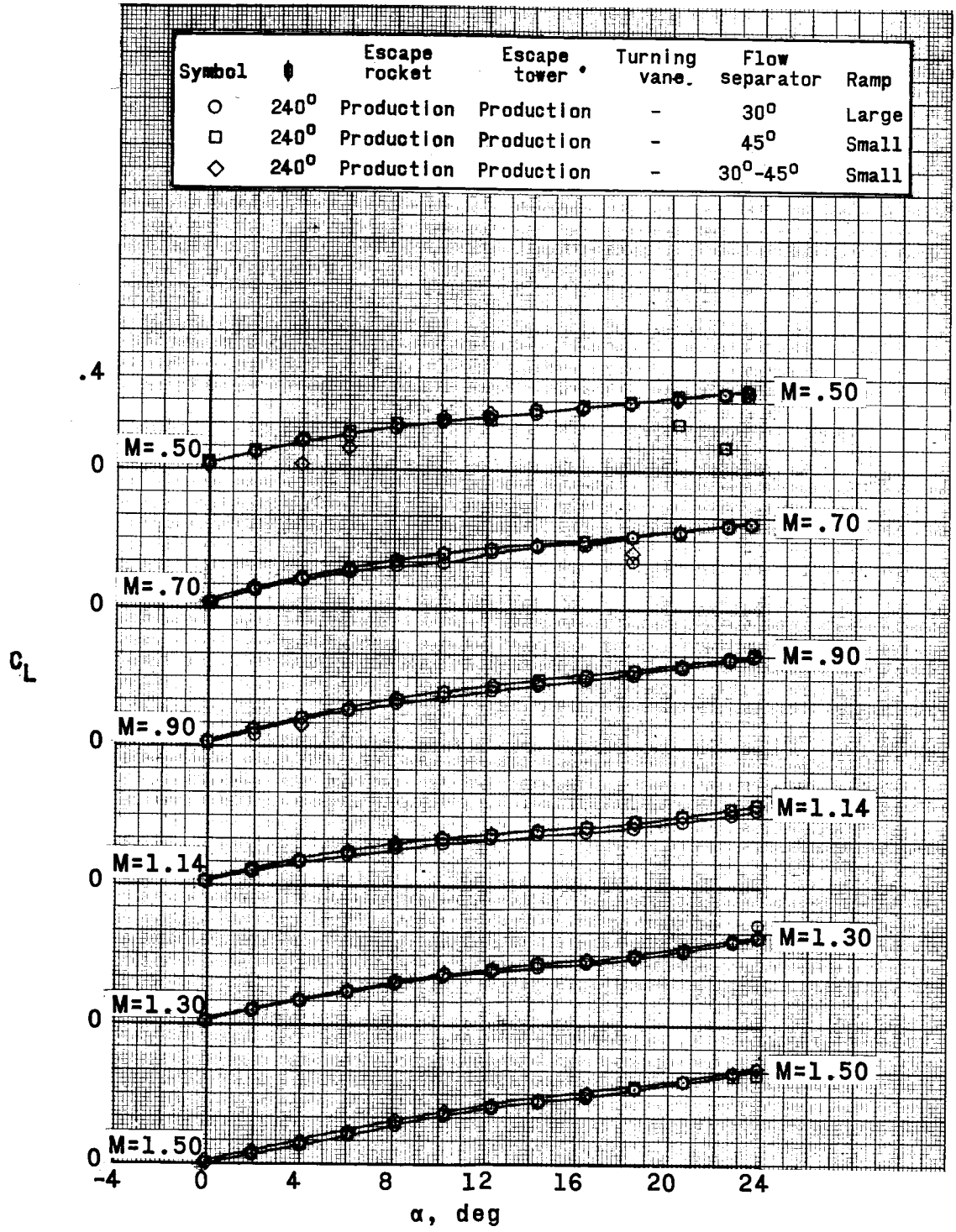

Figure 19.- Continued.

[redacted]

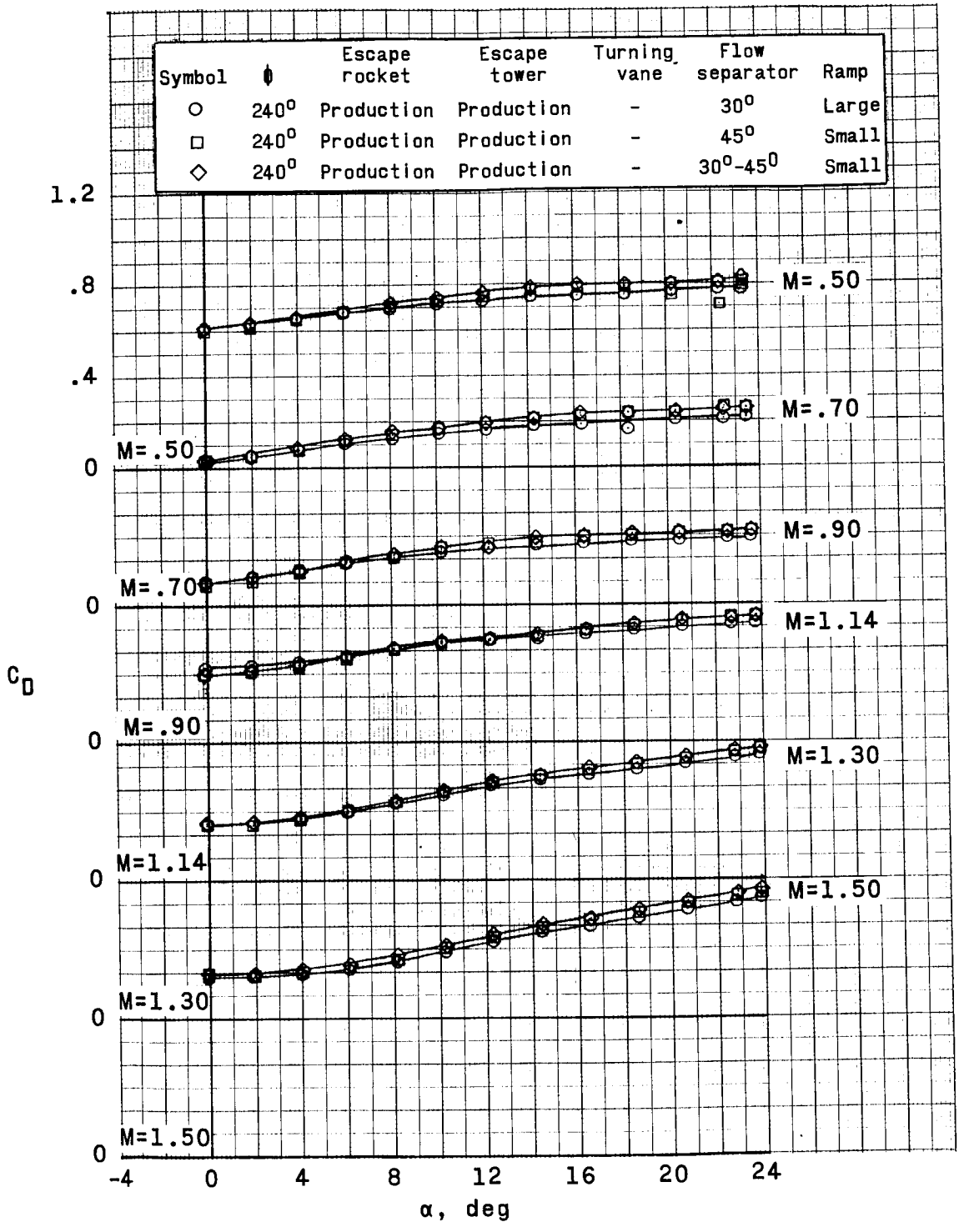

Figure 19.- Concluded.

[redacted]

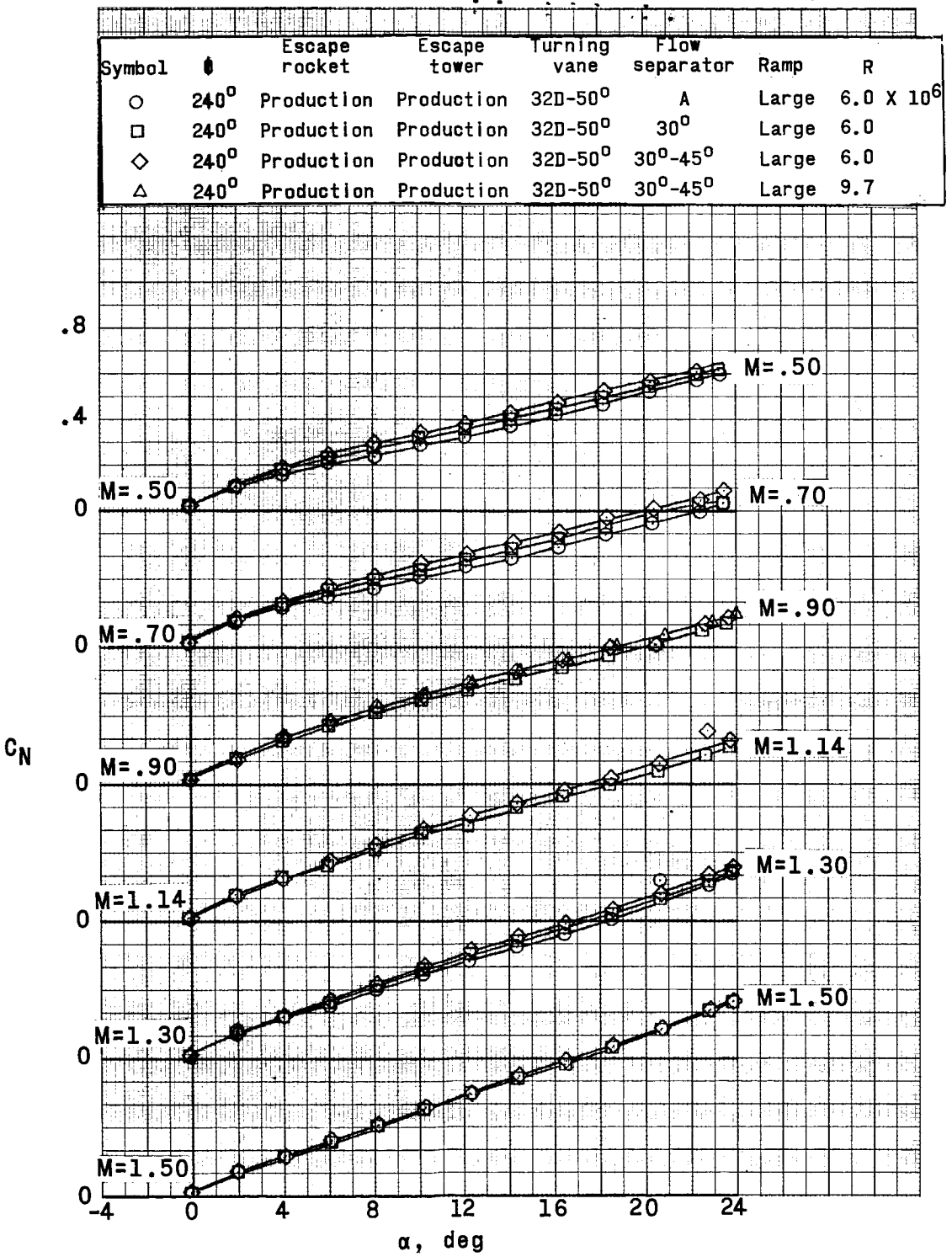

Figure 20.- Effect of various flow separators on the aerodynamic characteristics of the escape configuration (with turning vane). M = 0.50 to 1.50.

[redacted]

[redacted]

Symbol	ϕ	Escape rocket	Escape tower	Turning vane	Flow separator	Ramp	R
○	240°	Production	Production	32D-50°	A	Large	6.0×10^6
□	240°	Production	Production	32D-50°	30°	Large	6.0
◇	240°	Production	Production	32D-50°	30°-45°	Large	6.0
△	240°	Production	Production	32D-50°	30°-45°	Large	9.7

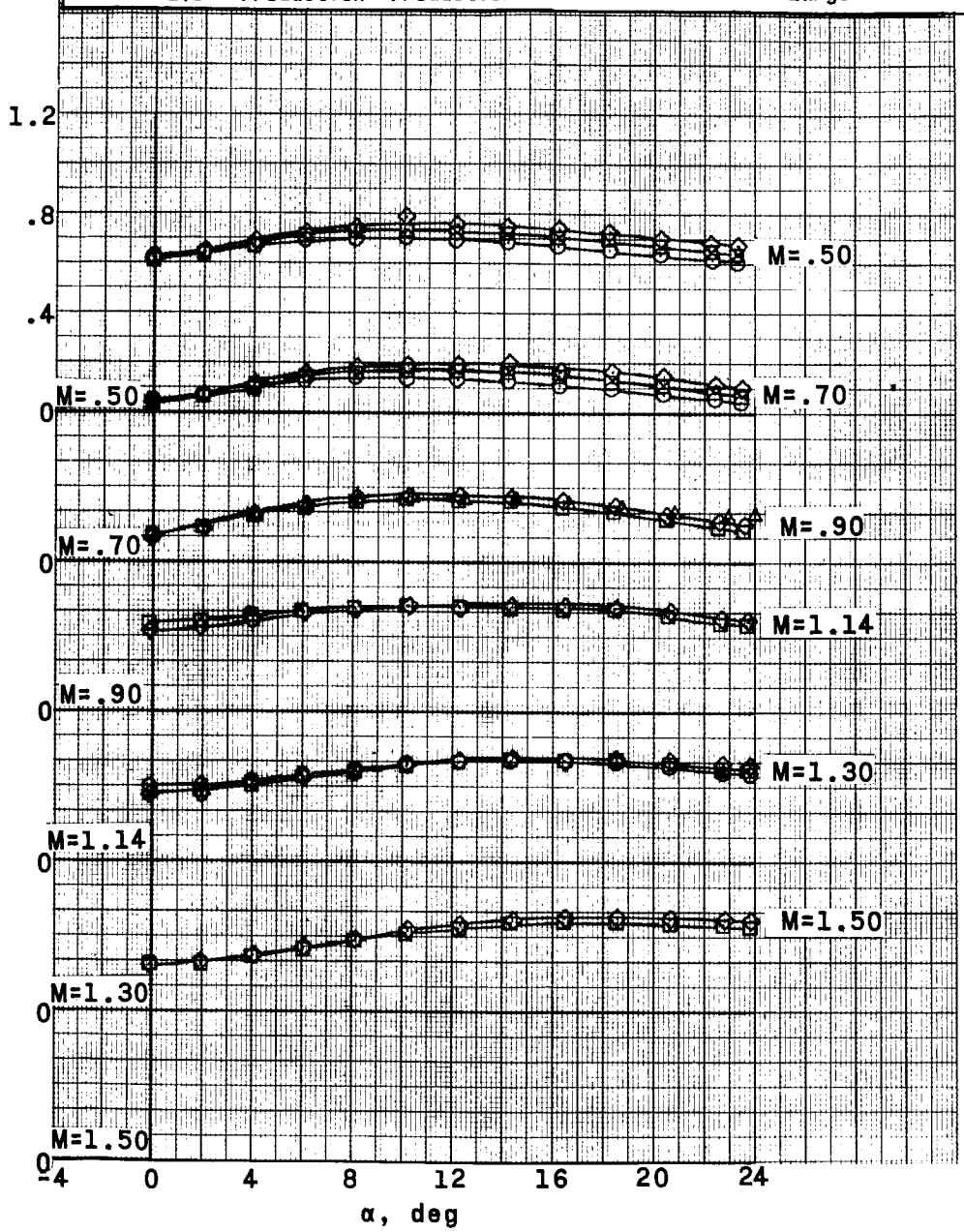

Figure 20.- Continued.

[redacted]

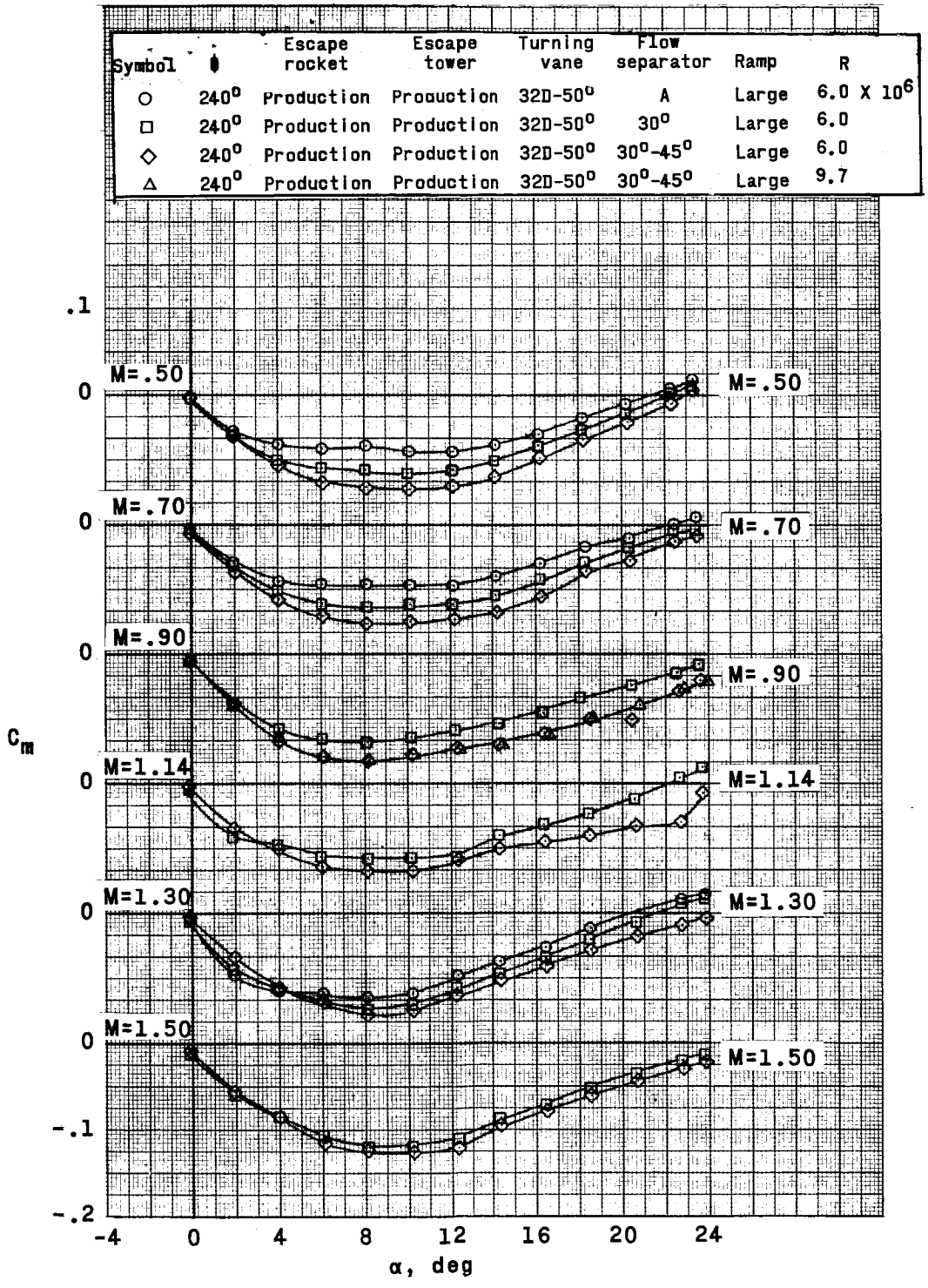

Figure 20.- Continued.

G
6

[redacted]

[redacted]

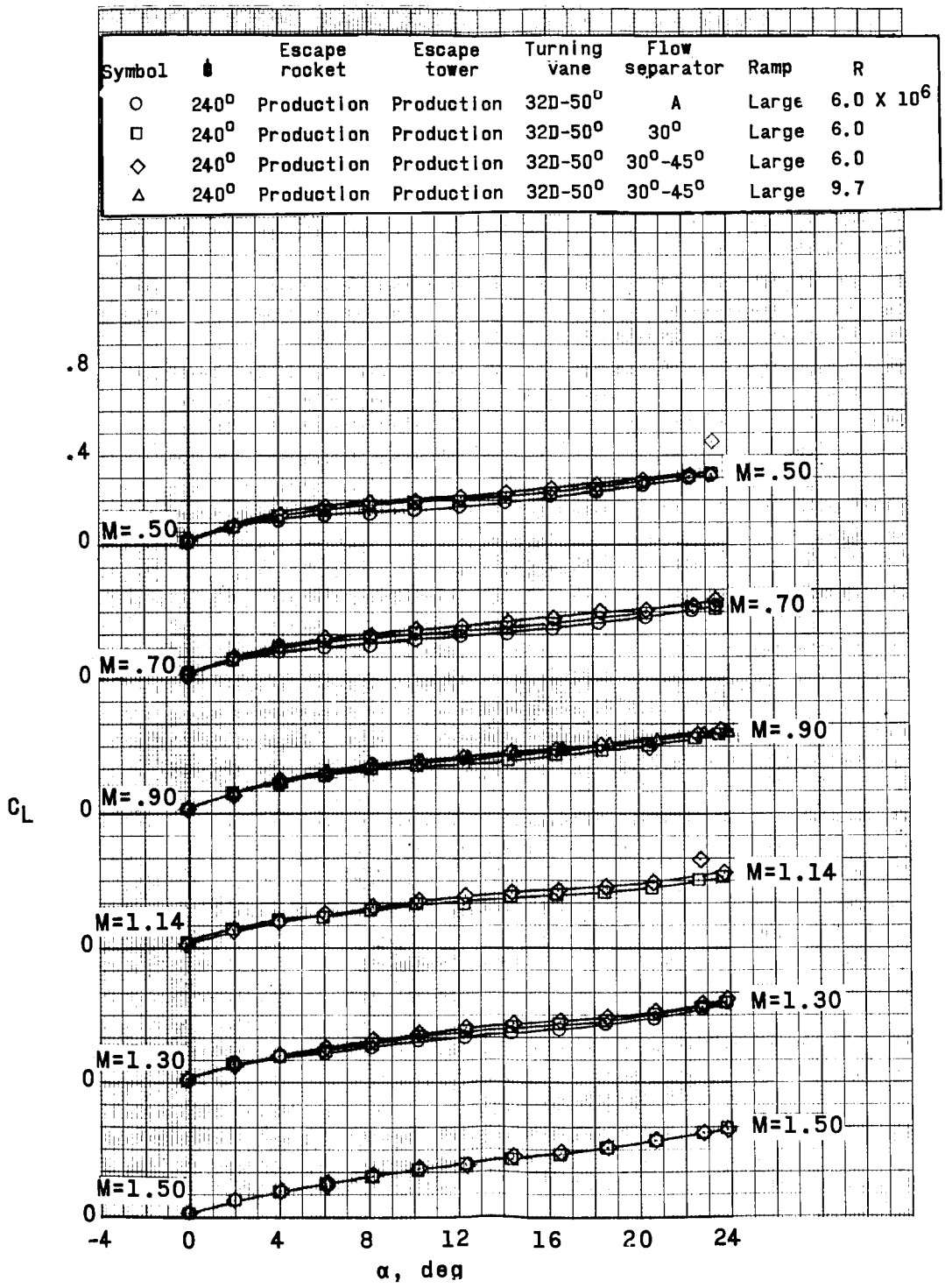

Figure 20.- Continued.

[redacted]

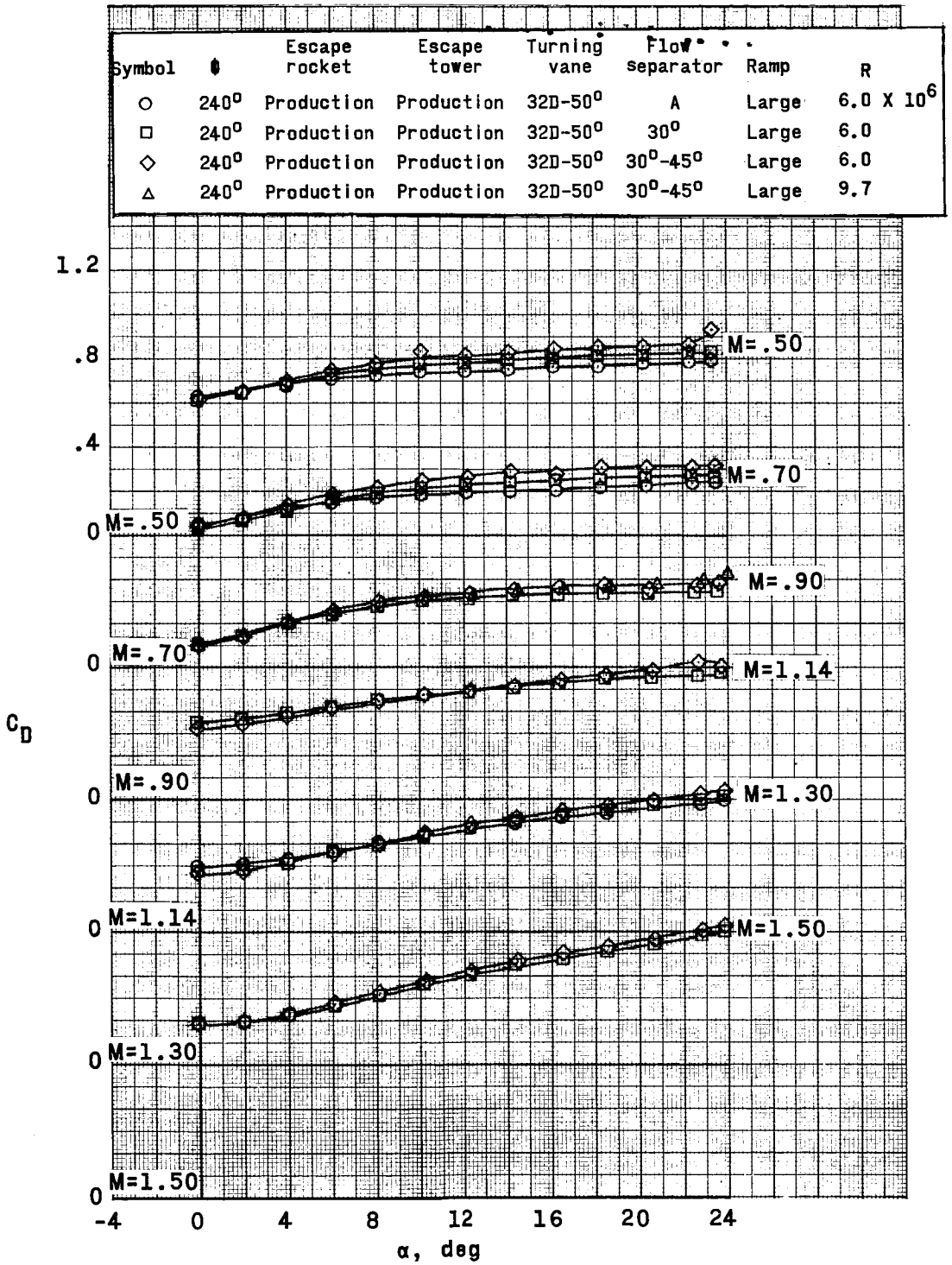

Figure 20.- Concluded.

[redacted]

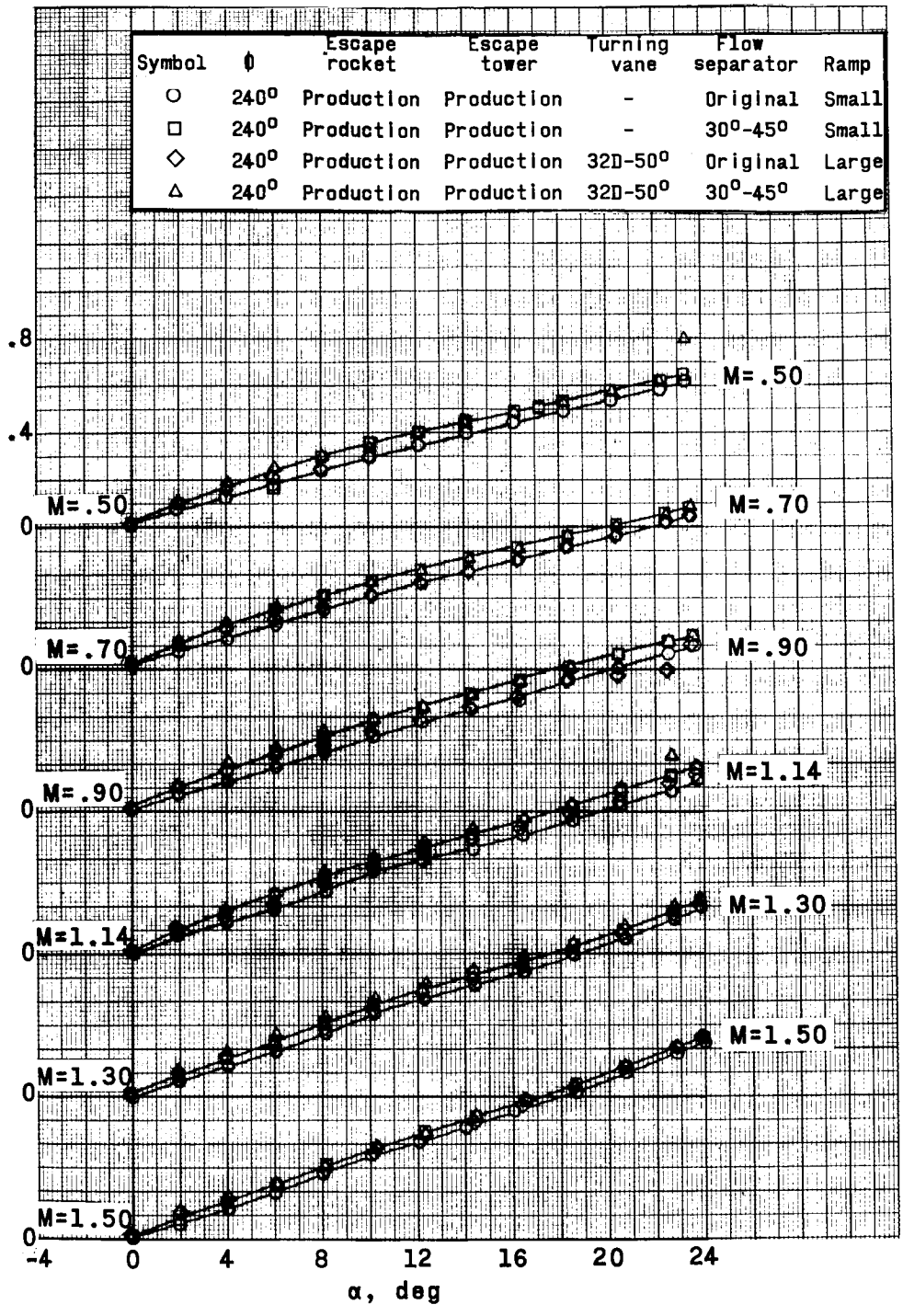

Figure 21.- Effect of turning vanes and flow separators on the aerodynamic characteristics of the escape configuration.

[redacted]

[redacted]

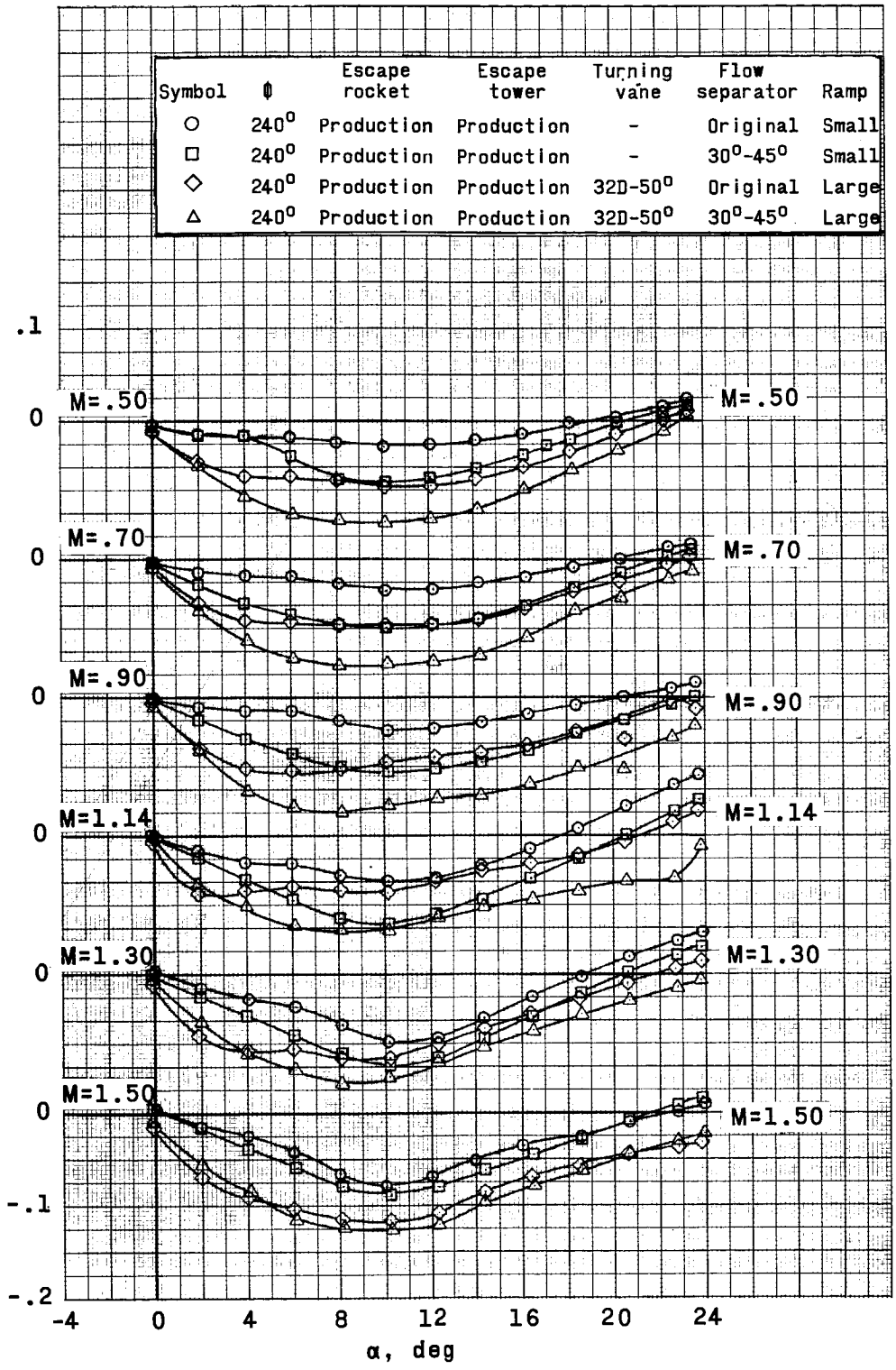

Figure 21.- Continued.

[redacted]

G
6

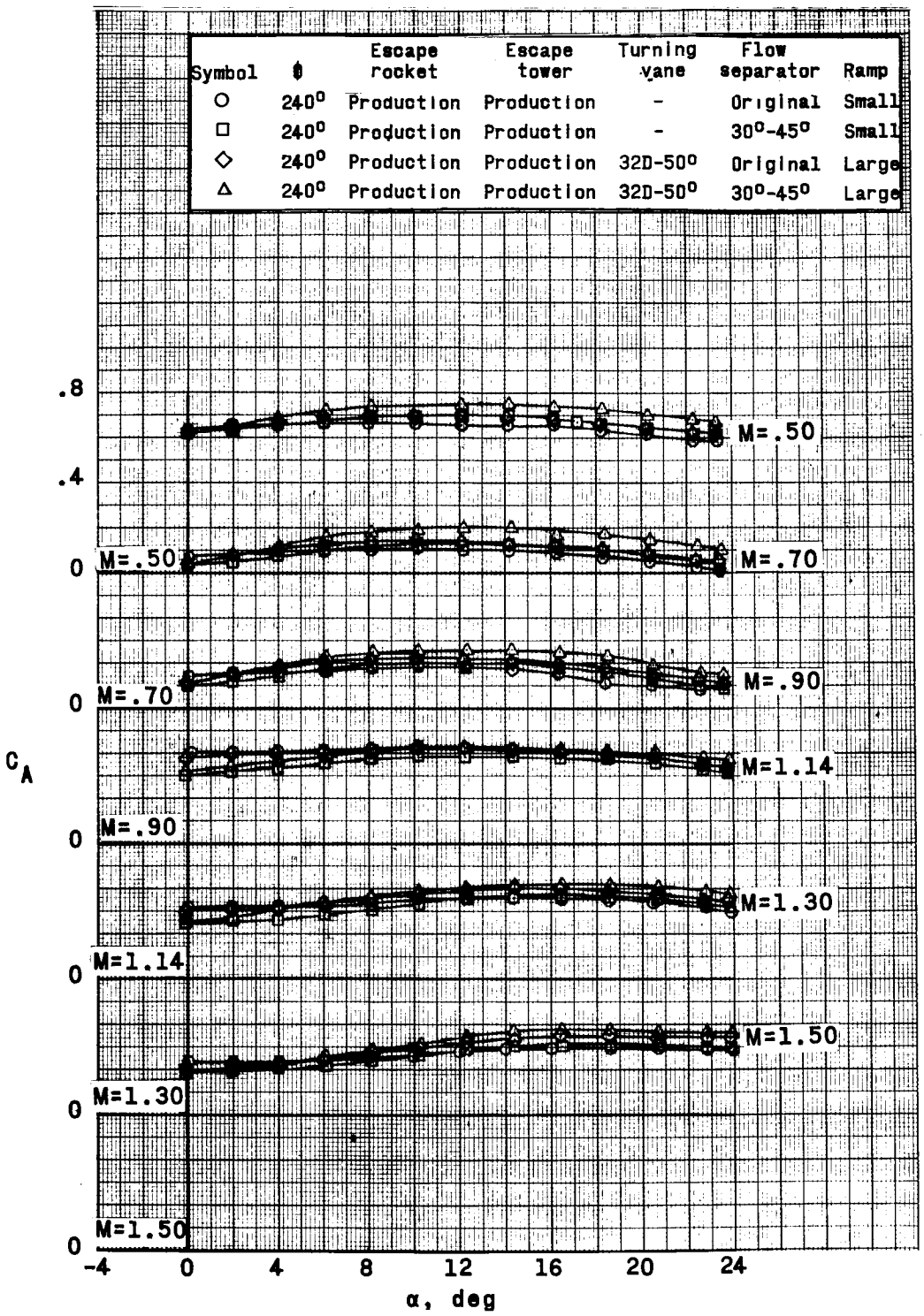

Figure 21.- Continued.

[redacted]

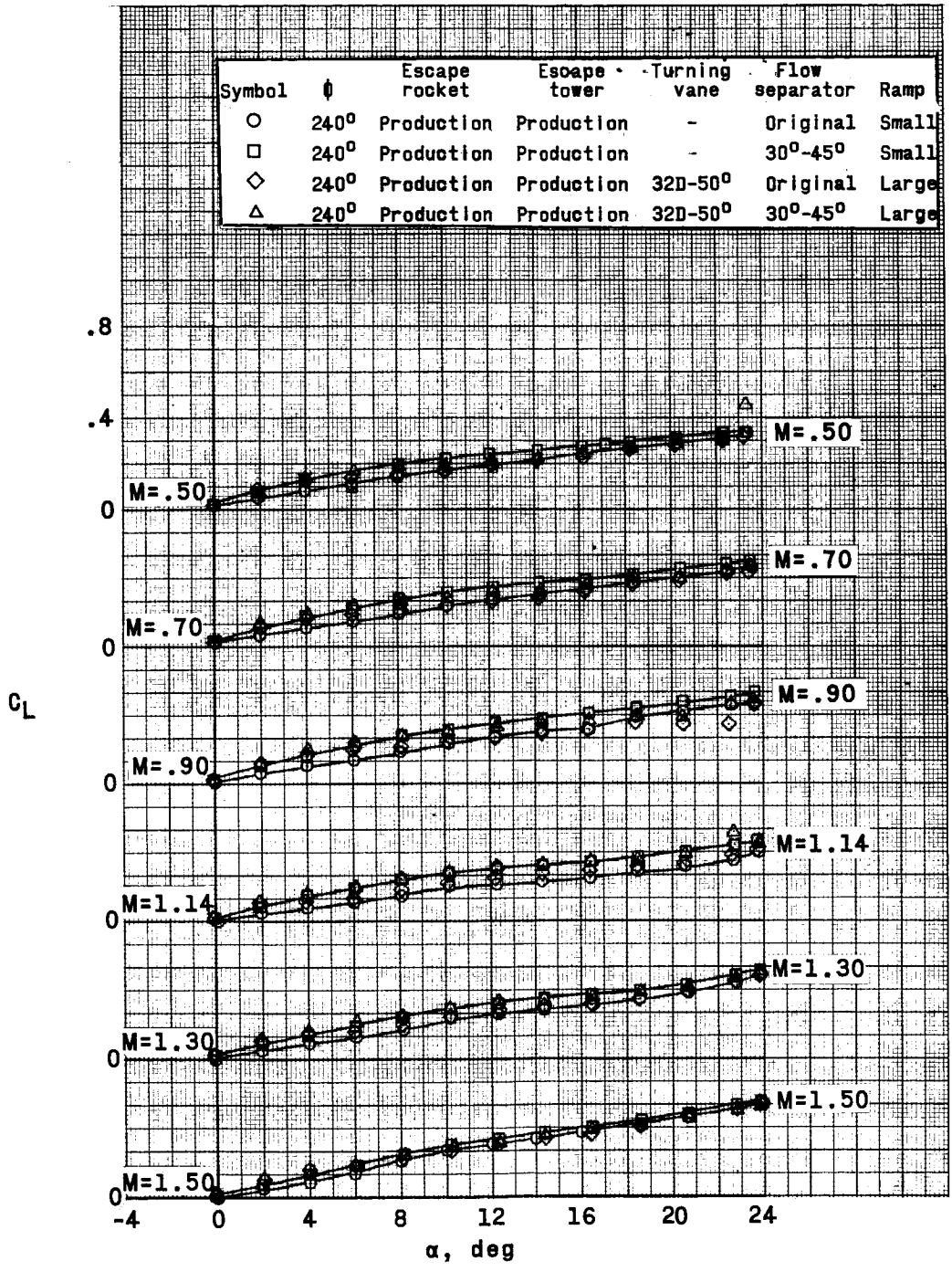

Figure 21.- Continued.

[redacted]

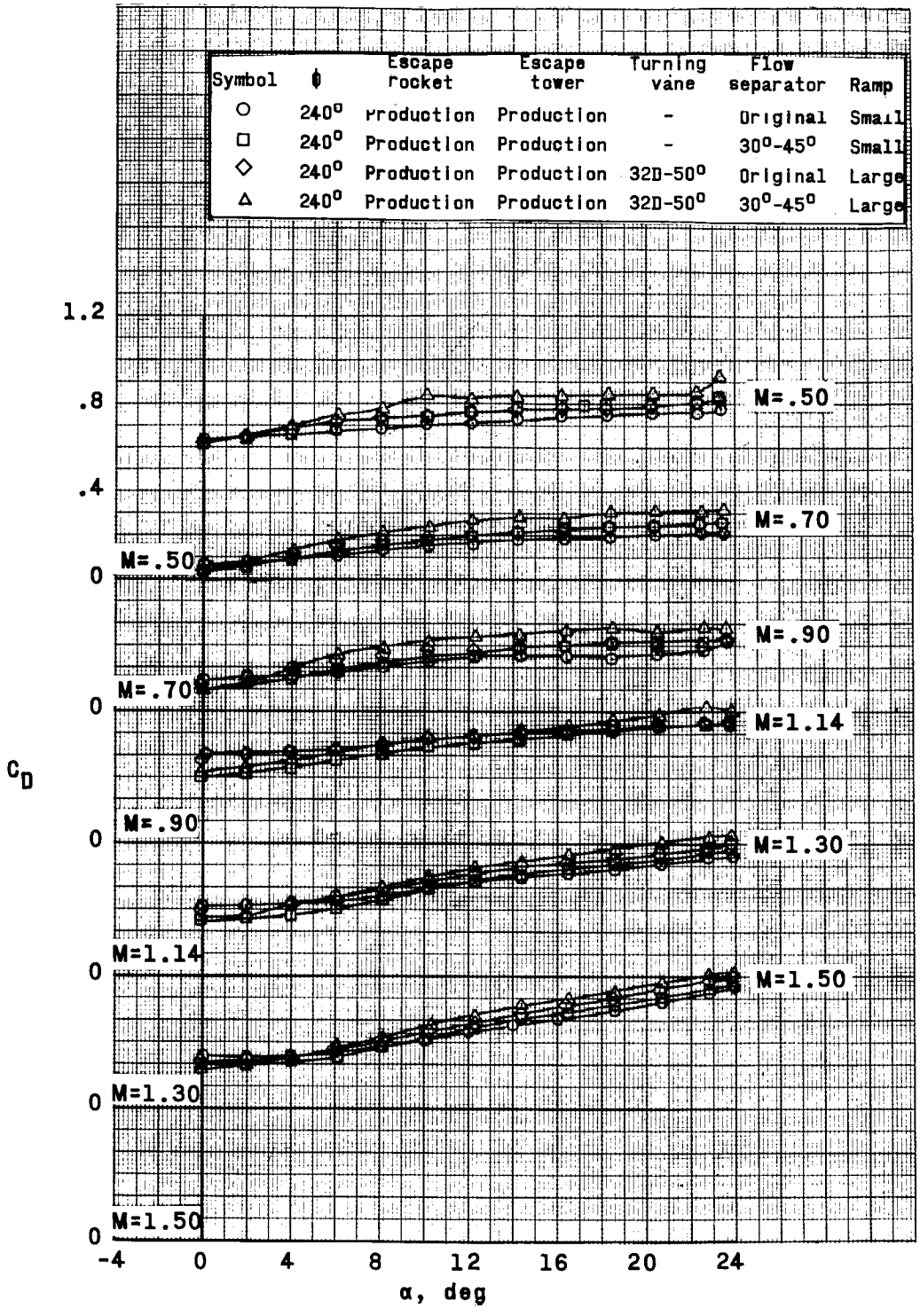

Figure 21.- Concluded.

[redacted]

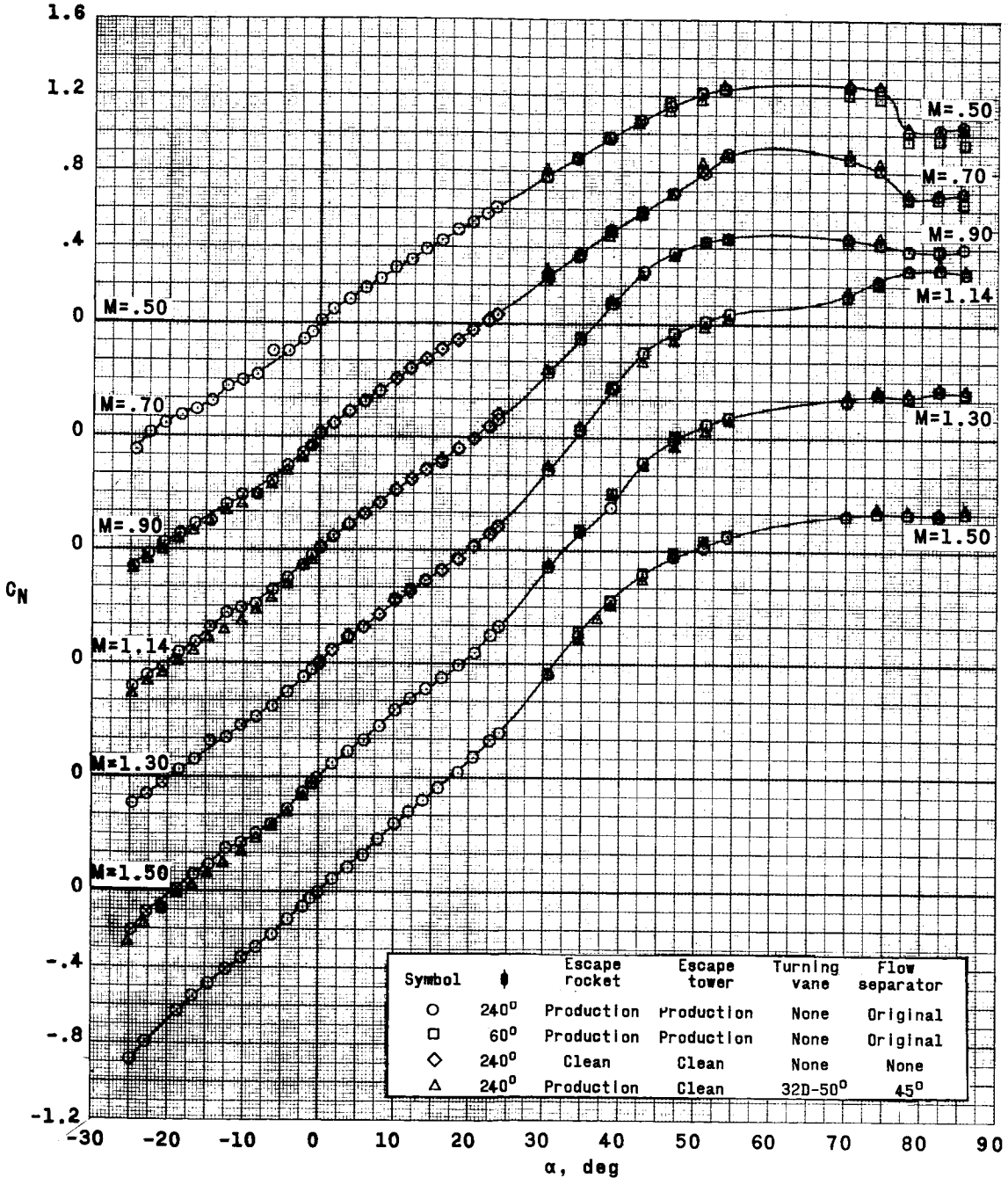

Figure 22.- Comparison of the aerodynamic characteristics of various escape configuration modifications. M = 0.50 to 1.50.

G
6

[redacted]

[redacted]

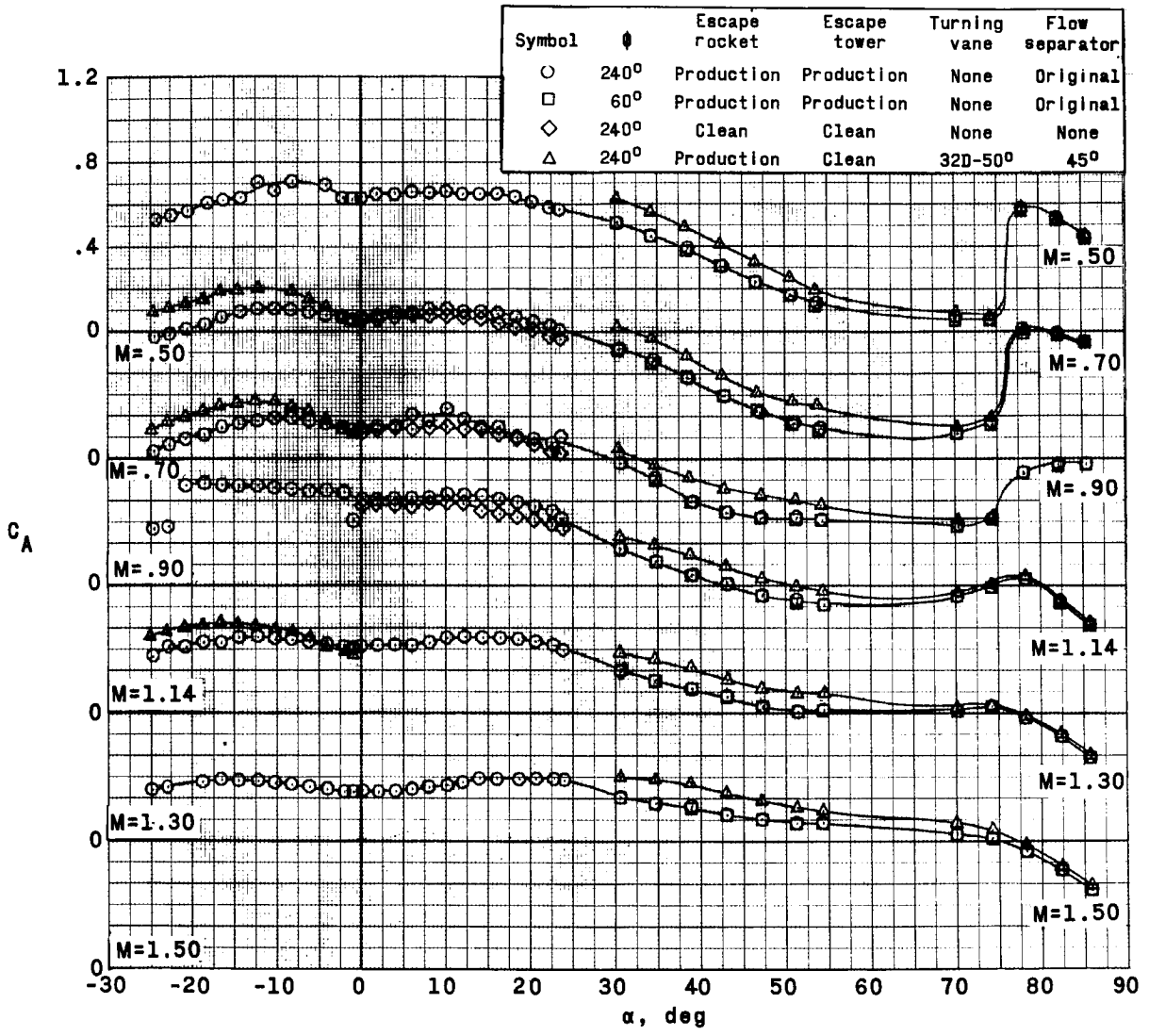

Figure 22.- Continued.

[redacted]

DECLASSIFIED
[redacted]

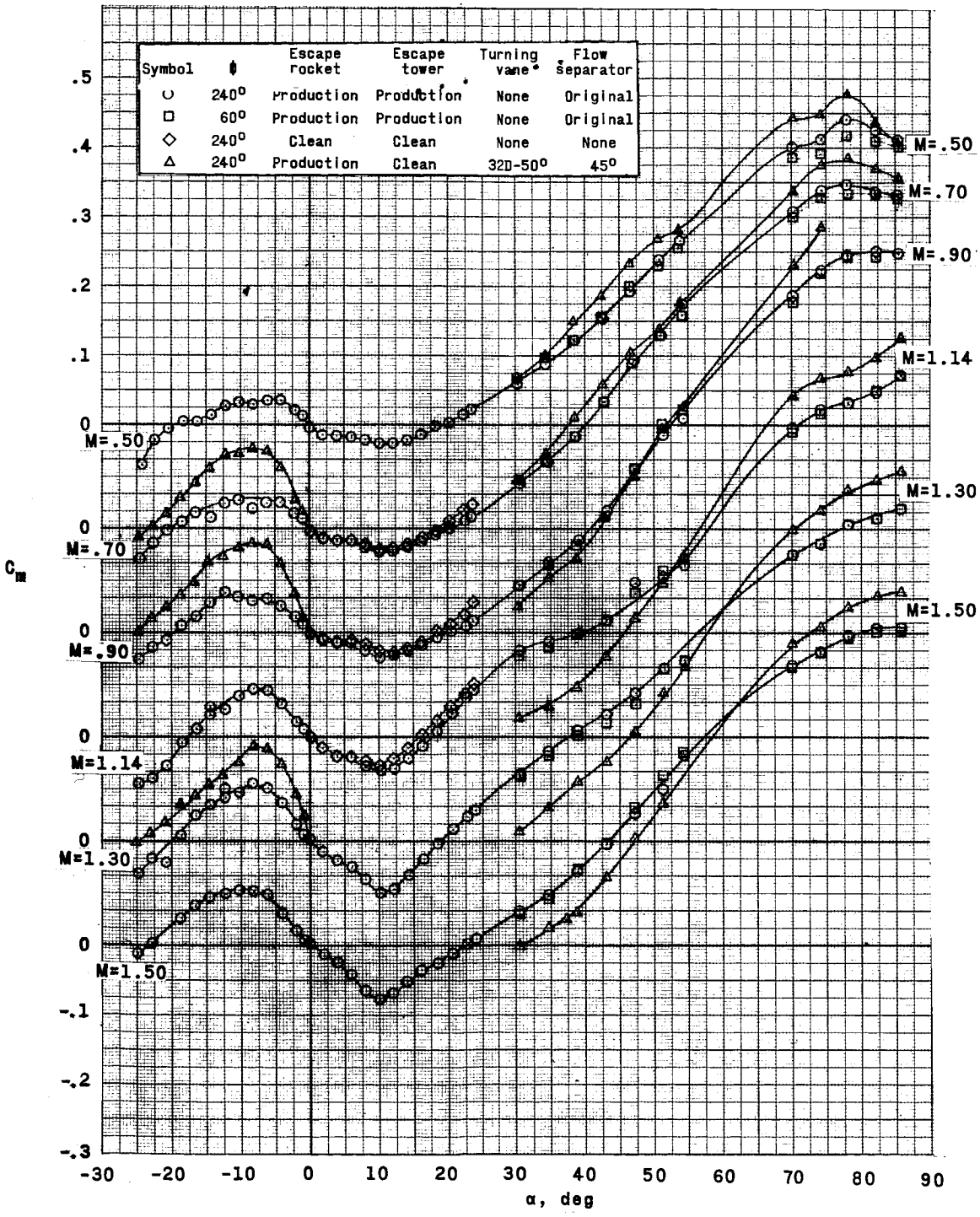

Figure 22.- Continued.

[redacted]

CONFIDENTIAL

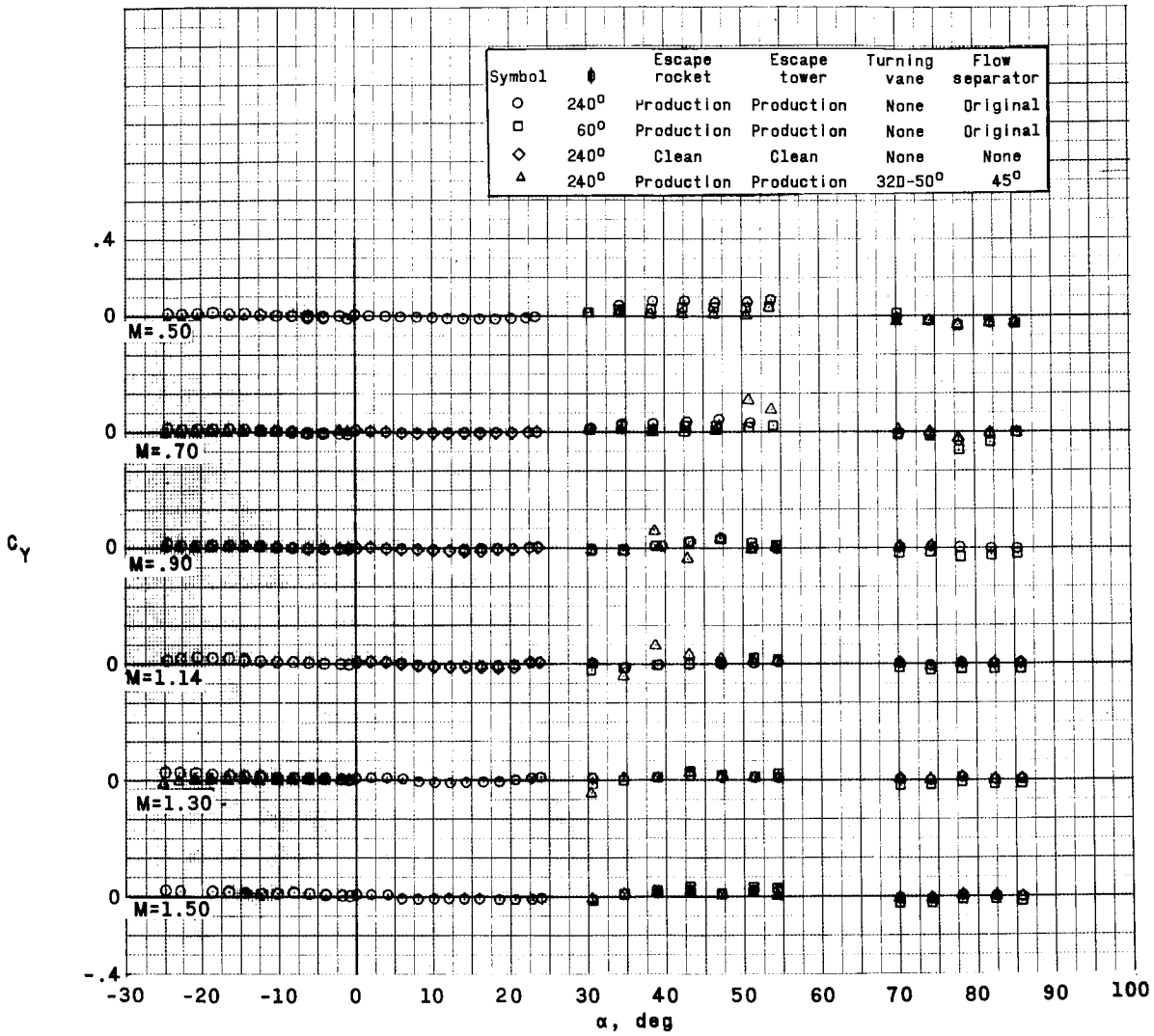

Figure 22.- Continued.

[redacted]

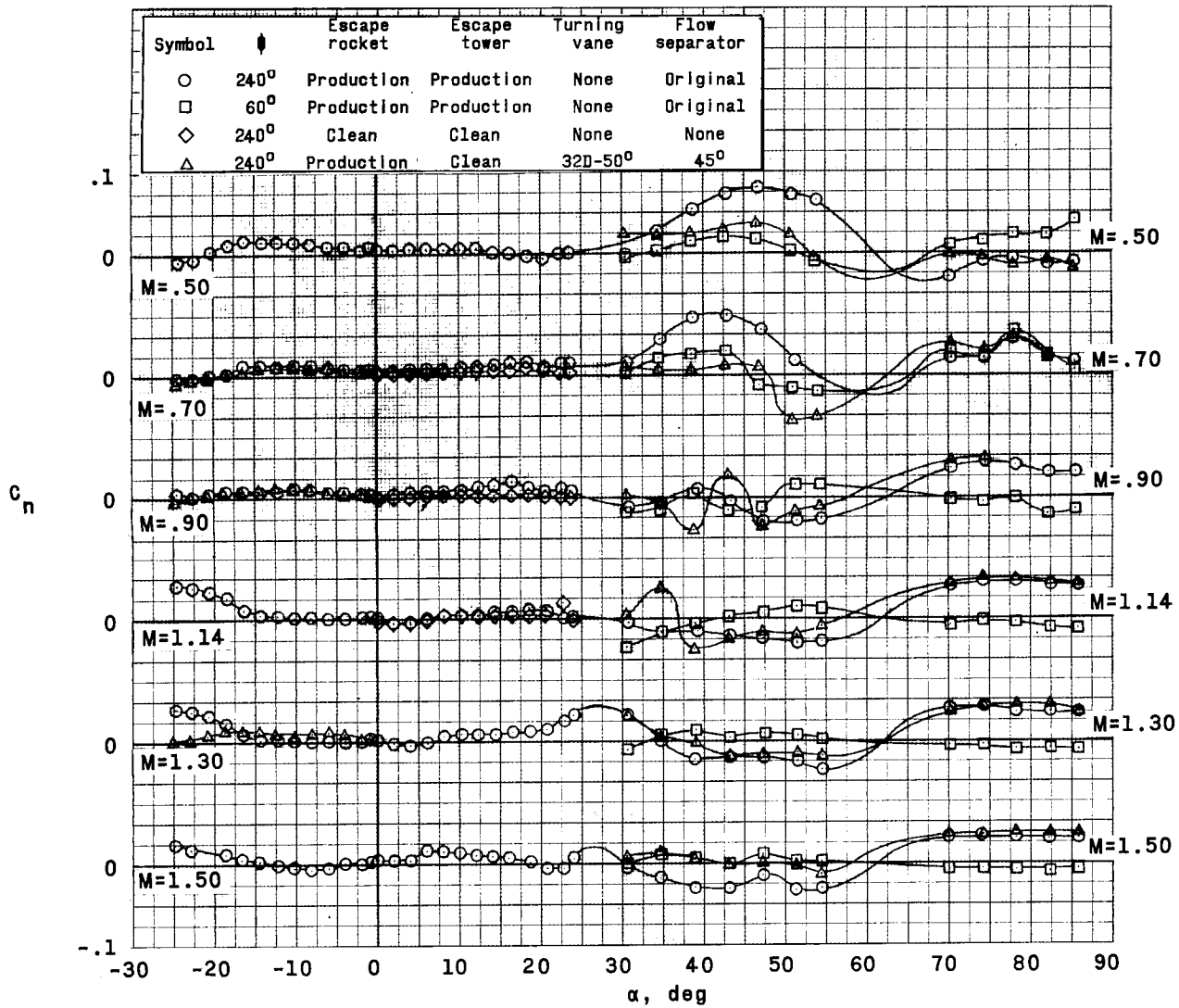

Figure 22.- Continued.

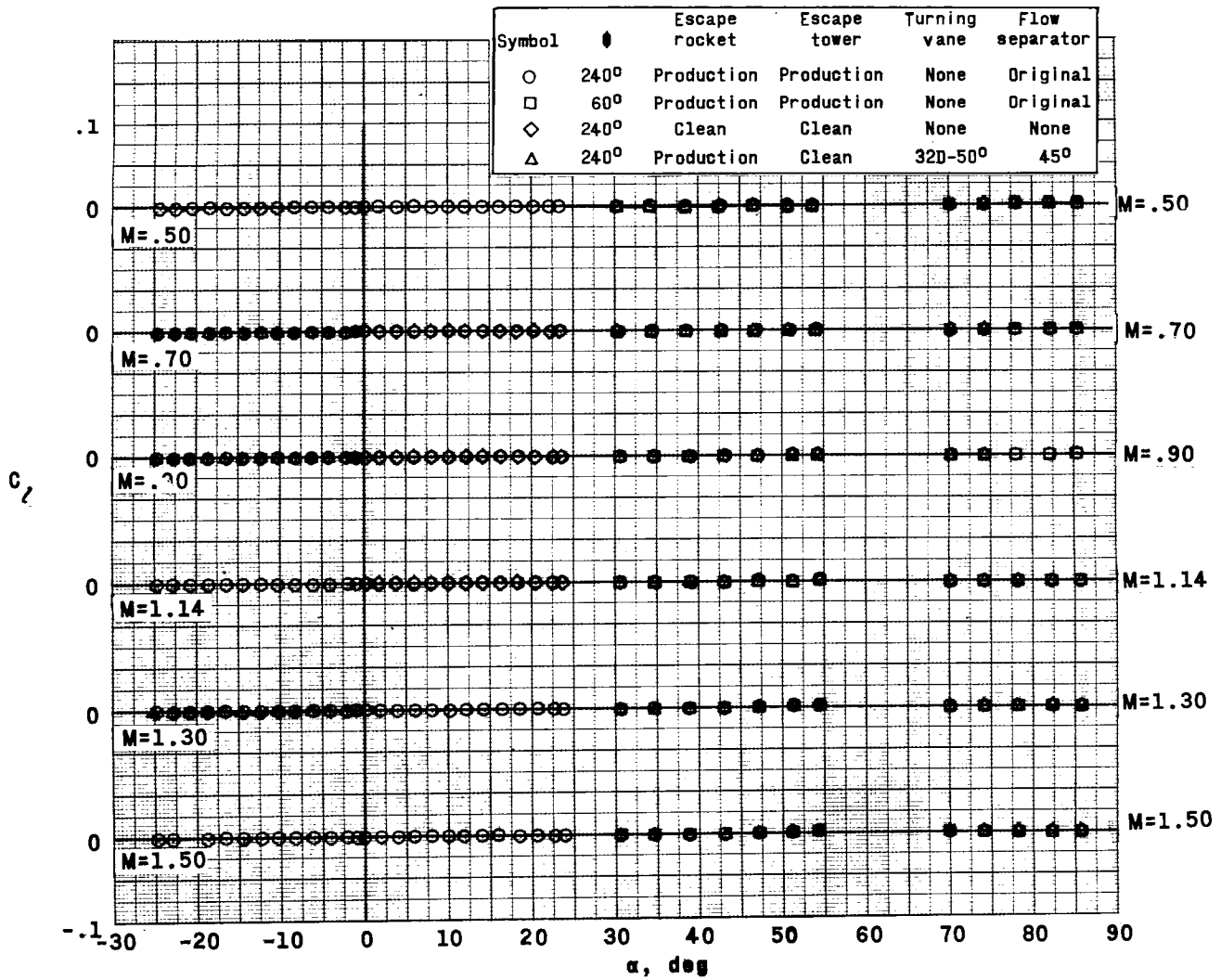

Figure 22.- Continued.

DECLASSIFIED
[redacted]

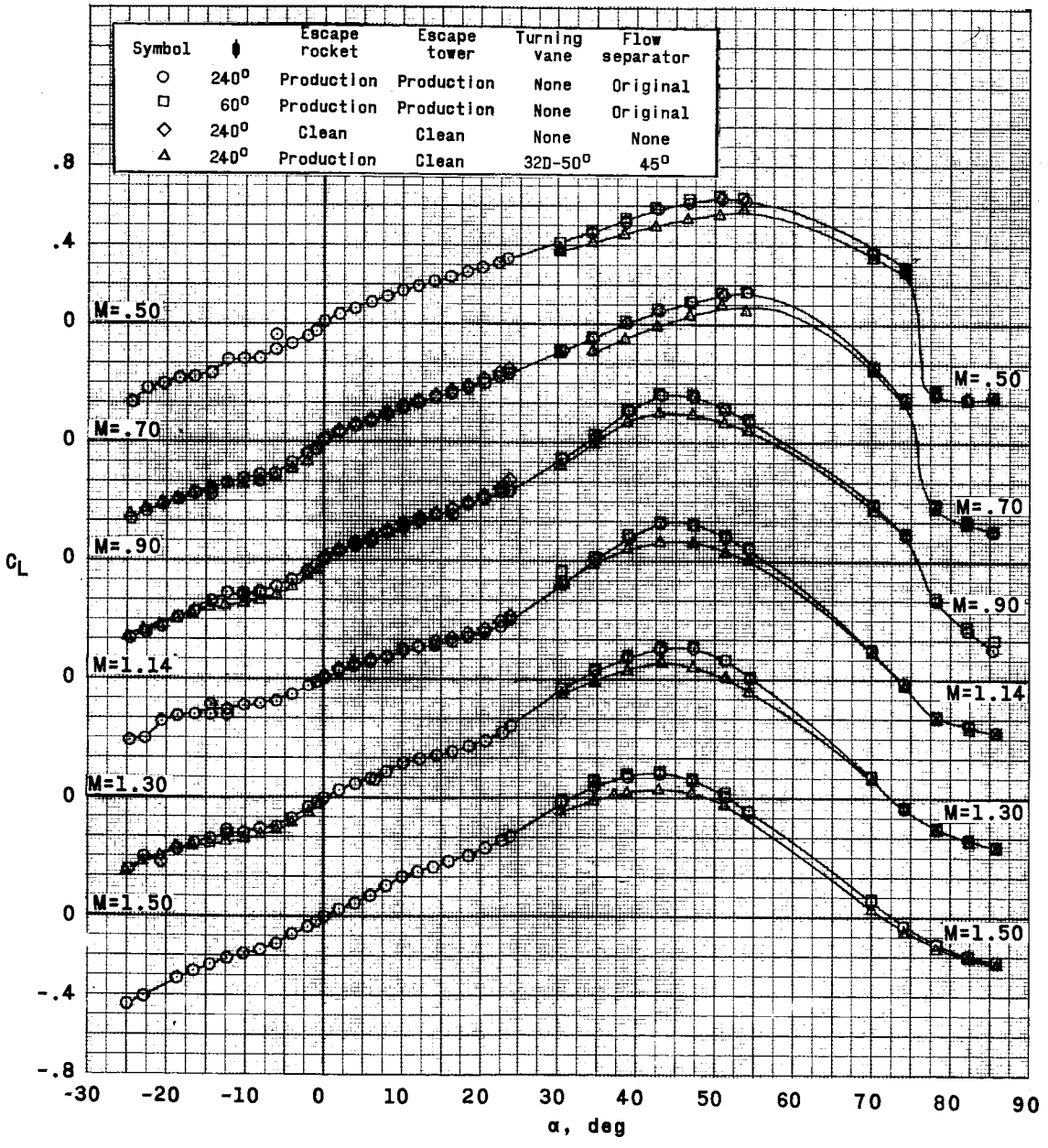

Figure 22.- Continued.

[redacted]

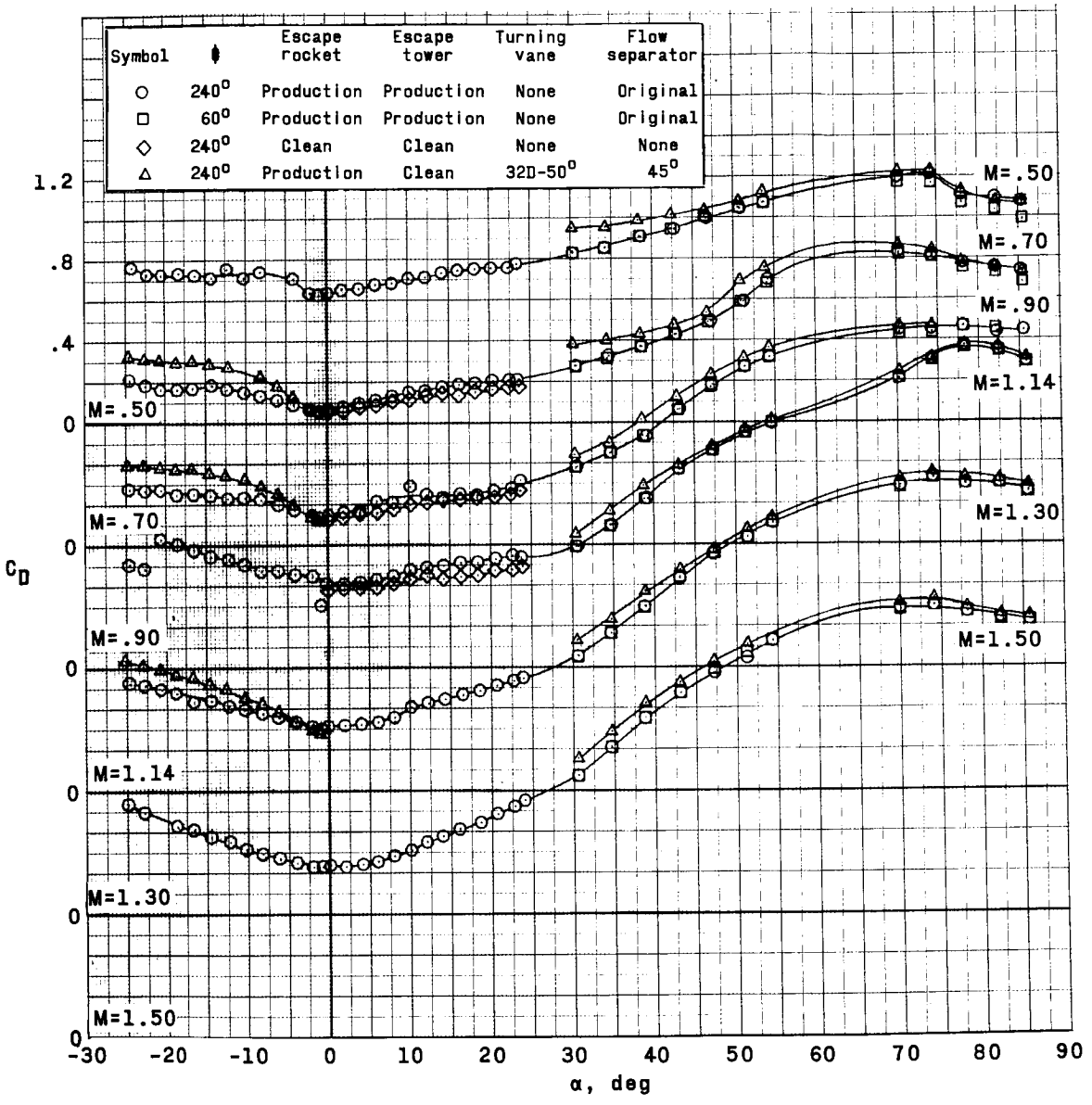

Figure 22.- Continued.

DECLASSIFIED
[redacted]

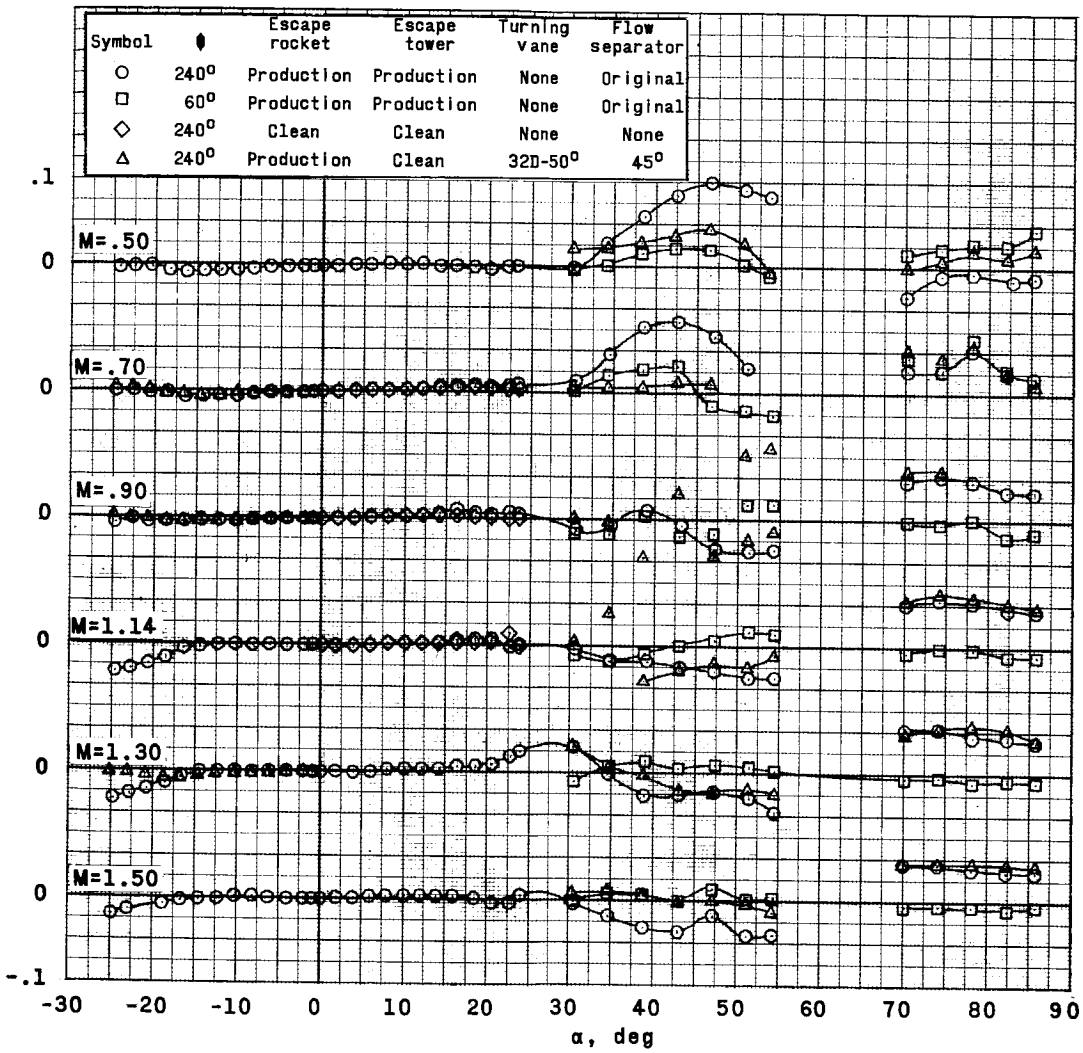

Figure 22.- Concluded.

[redacted]

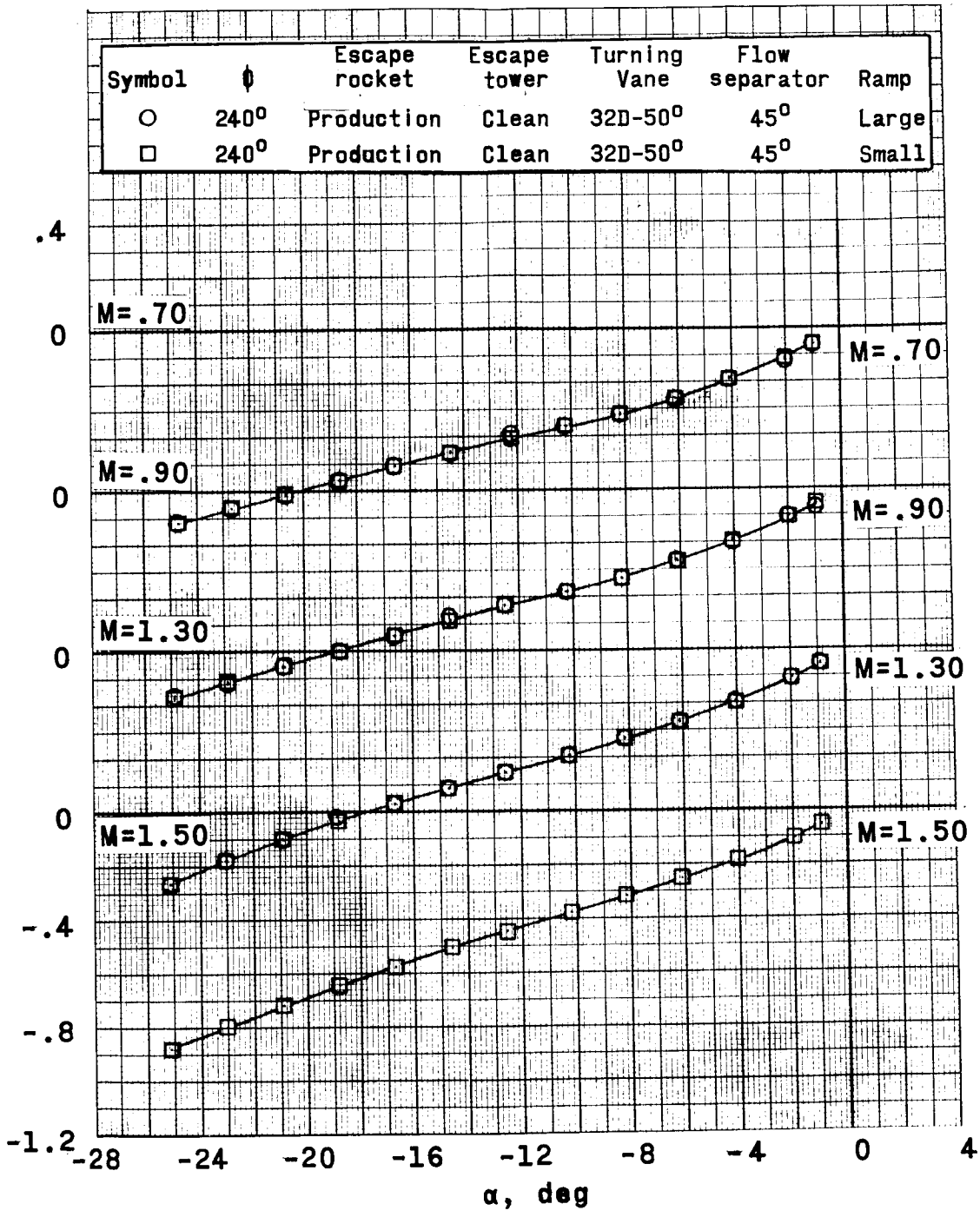

Figure 23.- Effect of ramp size at the base of the escape rocket on the aerodynamic characteristics of the escape configuration. M = 0.50 to 1.50.

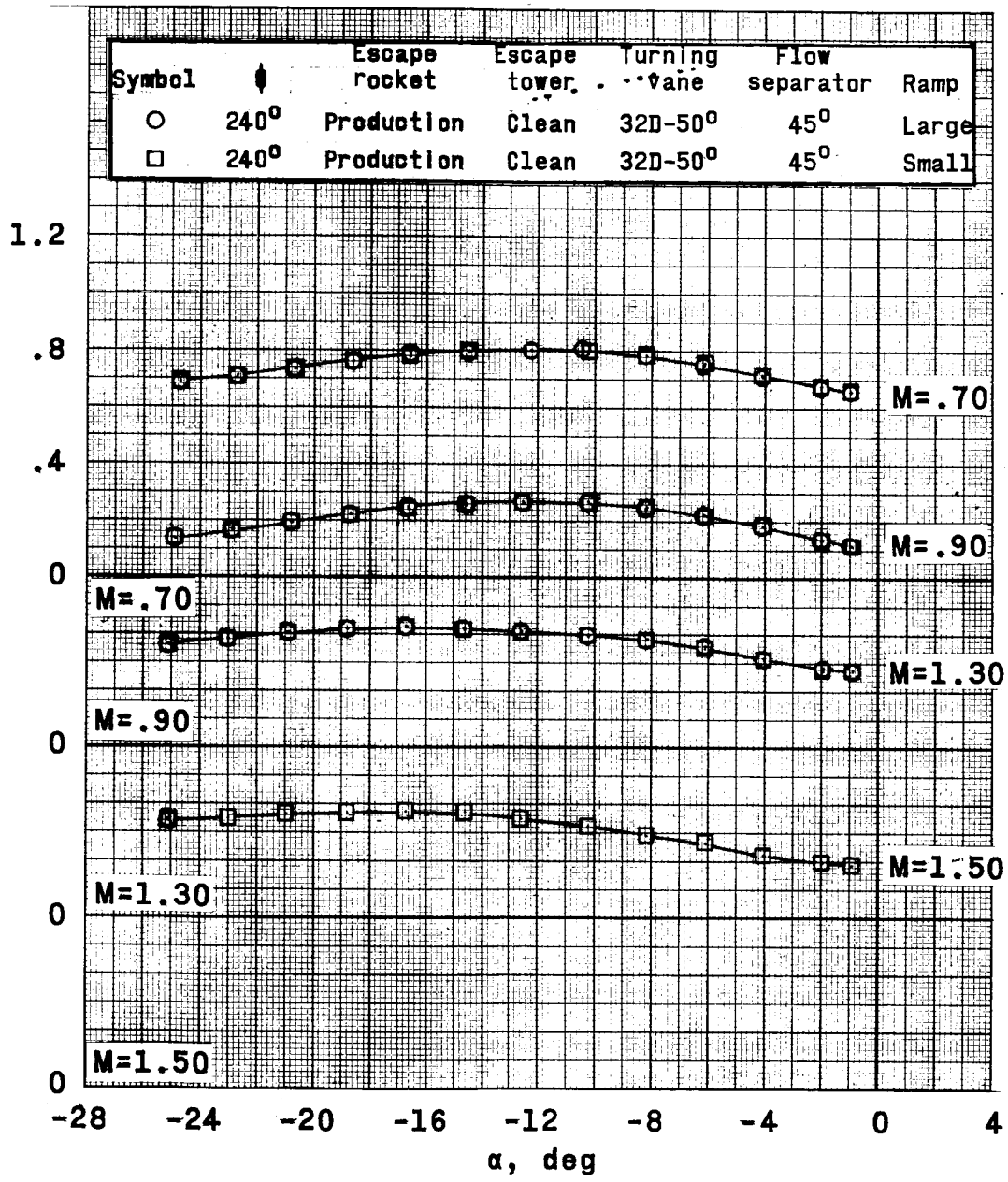

Figure 23.- Continued.

[redacted]

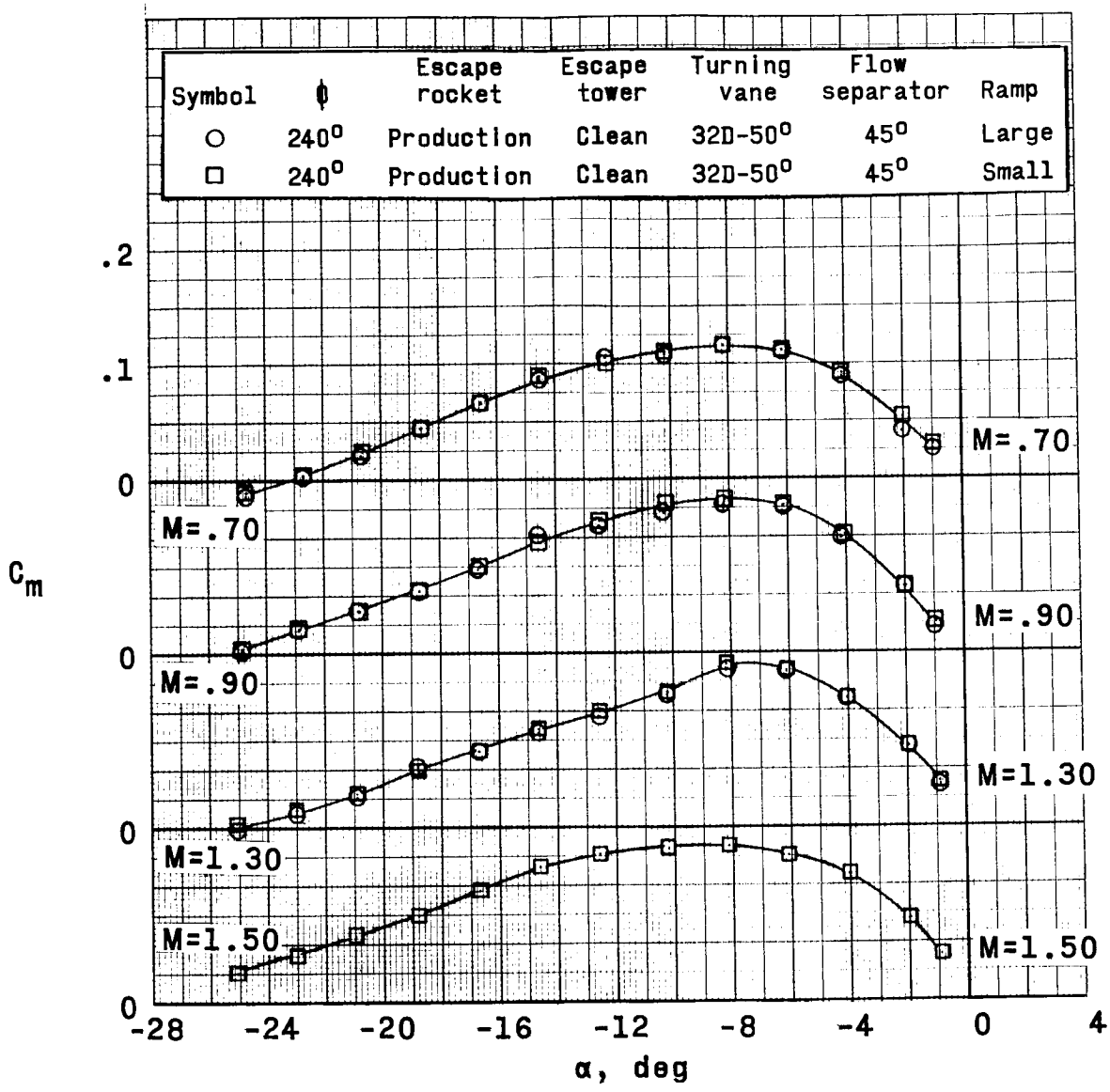

Figure 23.- Continued.

[redacted]

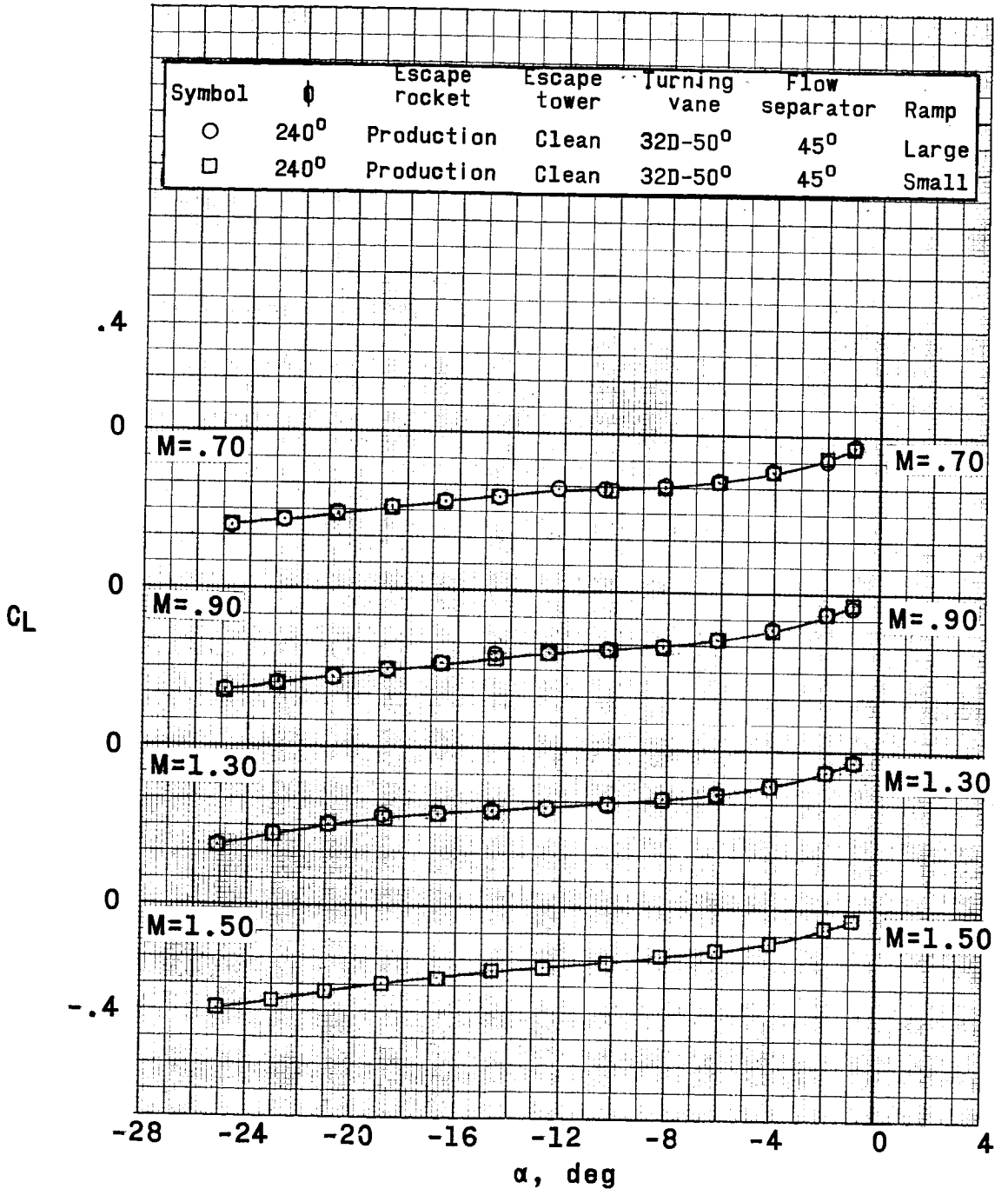

Figure 23.- Continued.

[redacted]

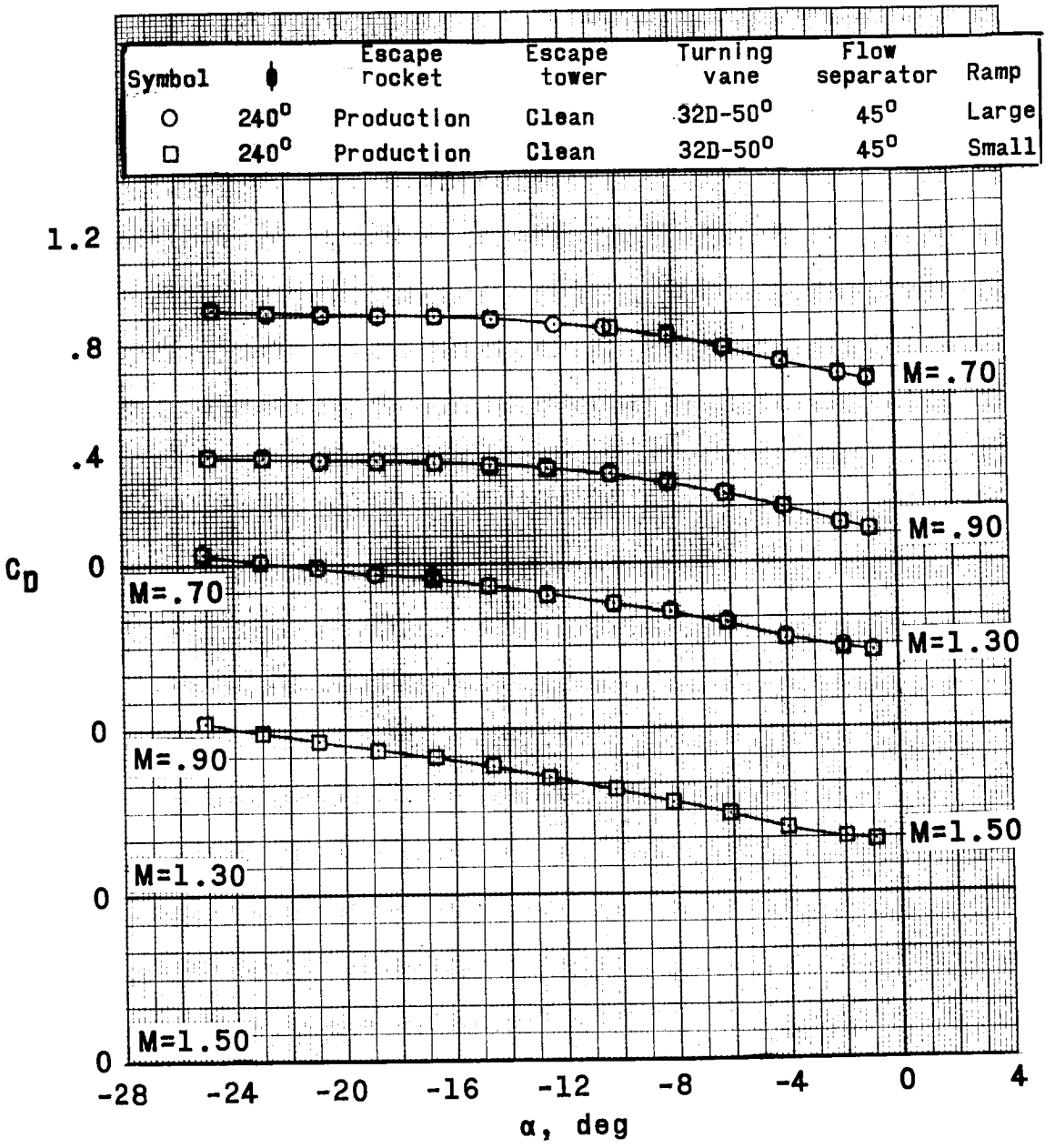

Figure 23.- Concluded.

[redacted]

DE[redacted]SIFIED

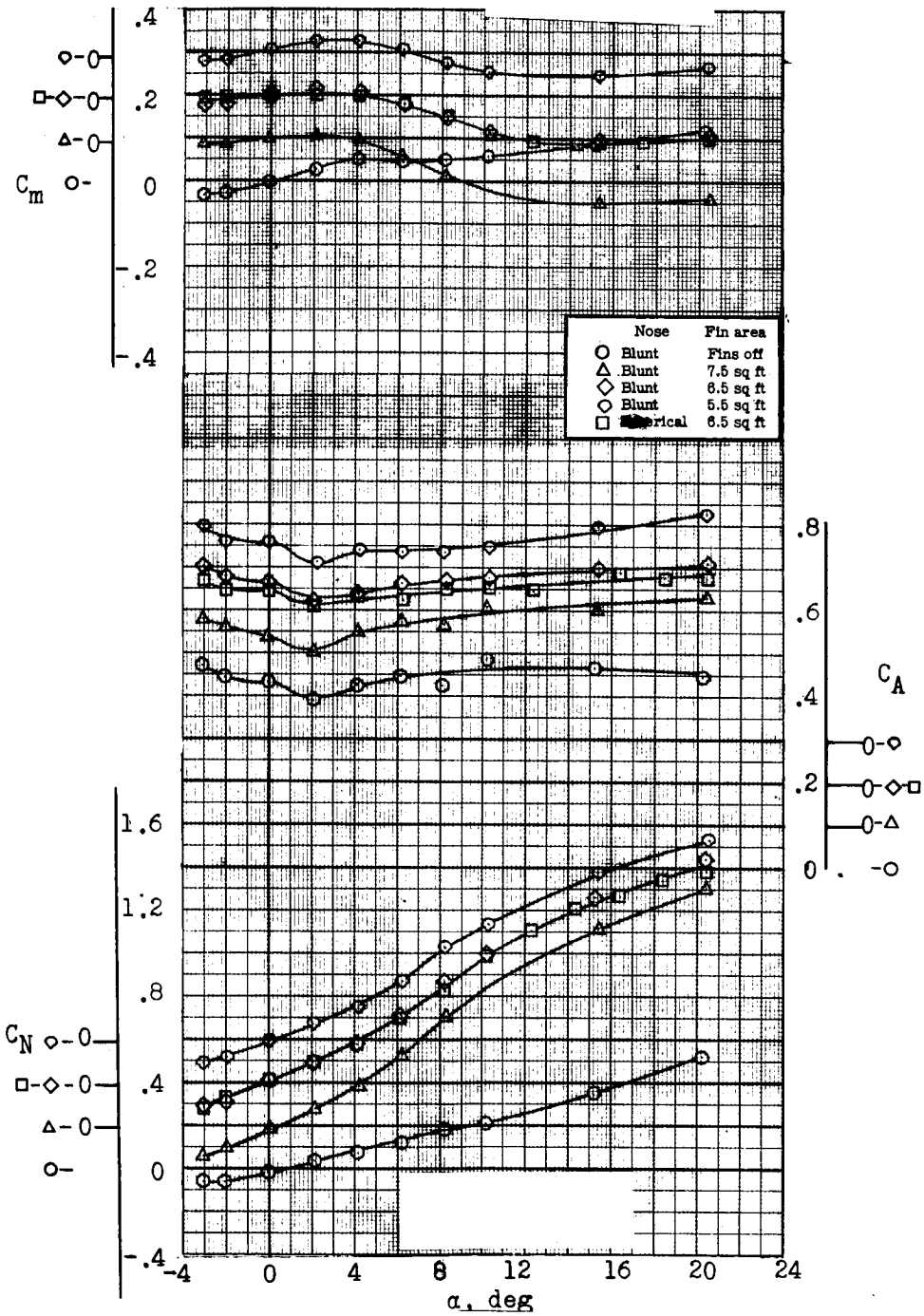

Figure 24.- Effect of fin area and nose shape on the aerodynamic characteristics of the finned-adapter escape configuration. M = 0.50.

[redacted]

[redacted]

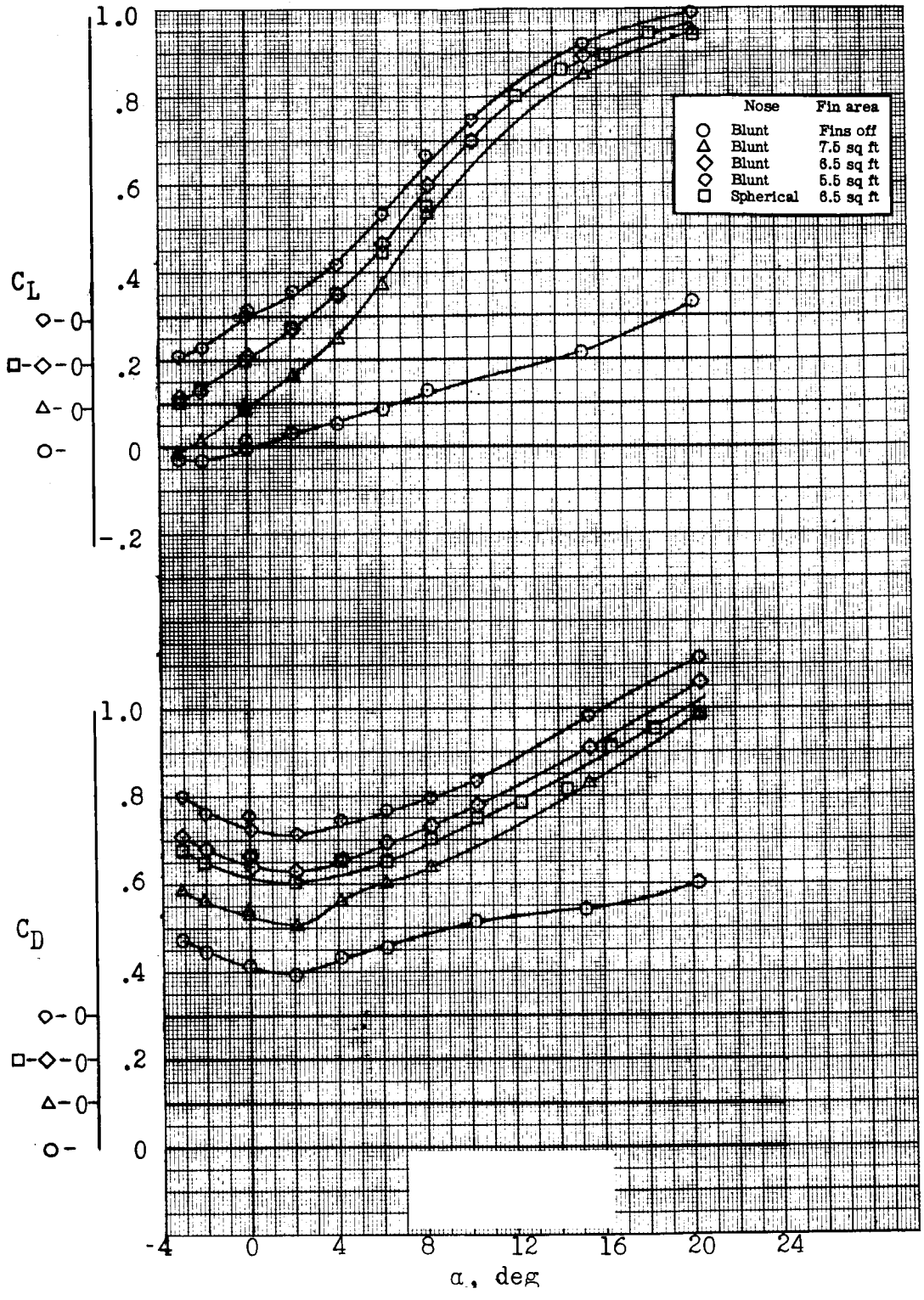

Figure 24.- Concluded.

[redacted]

DE[redacted]SIFIED

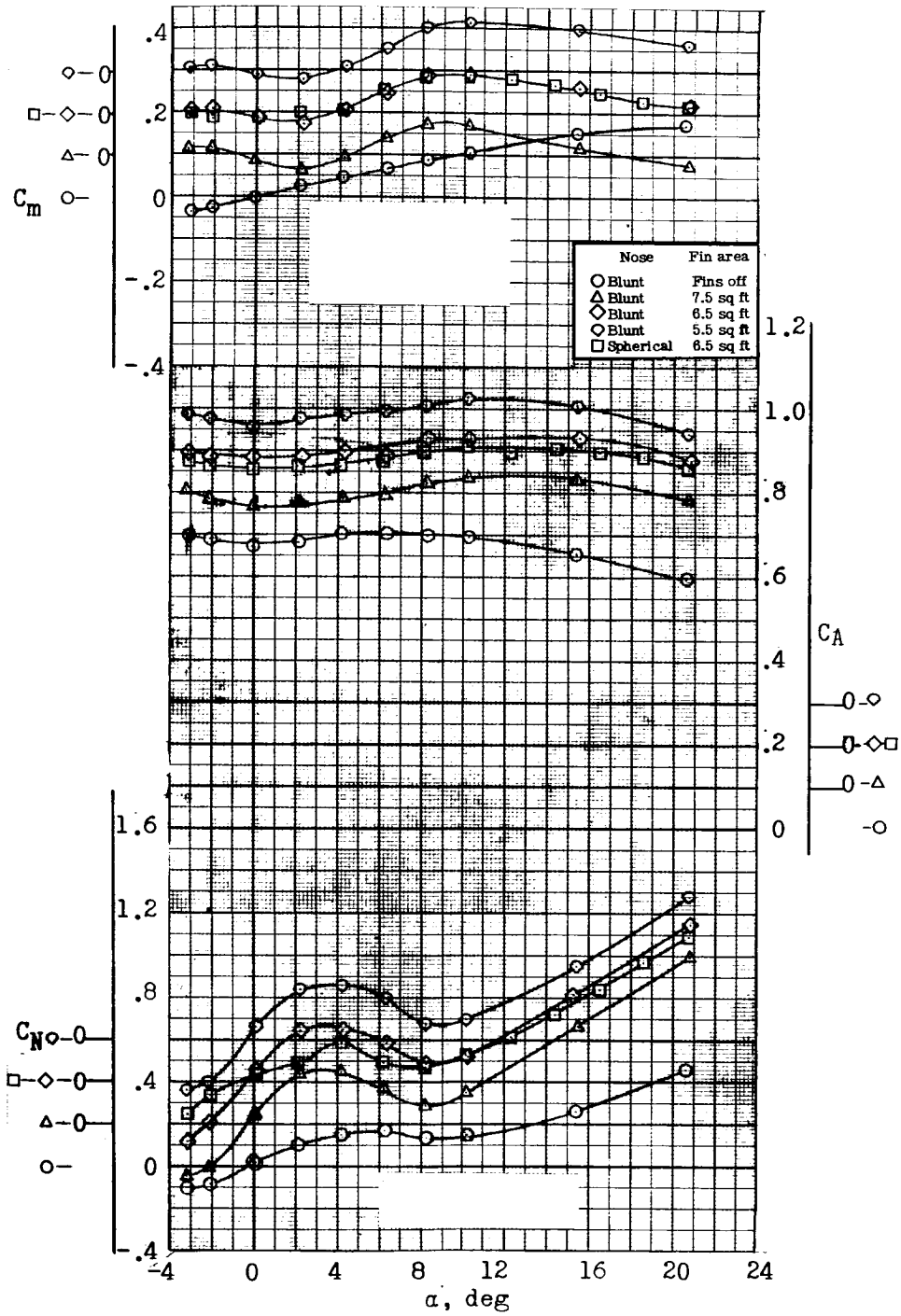

Figure 25.- Effect of fin area and nose shape on the aerodynamic characteristics of the finned-adapter escape configuration. M = 0.80.

[redacted]

[redacted]

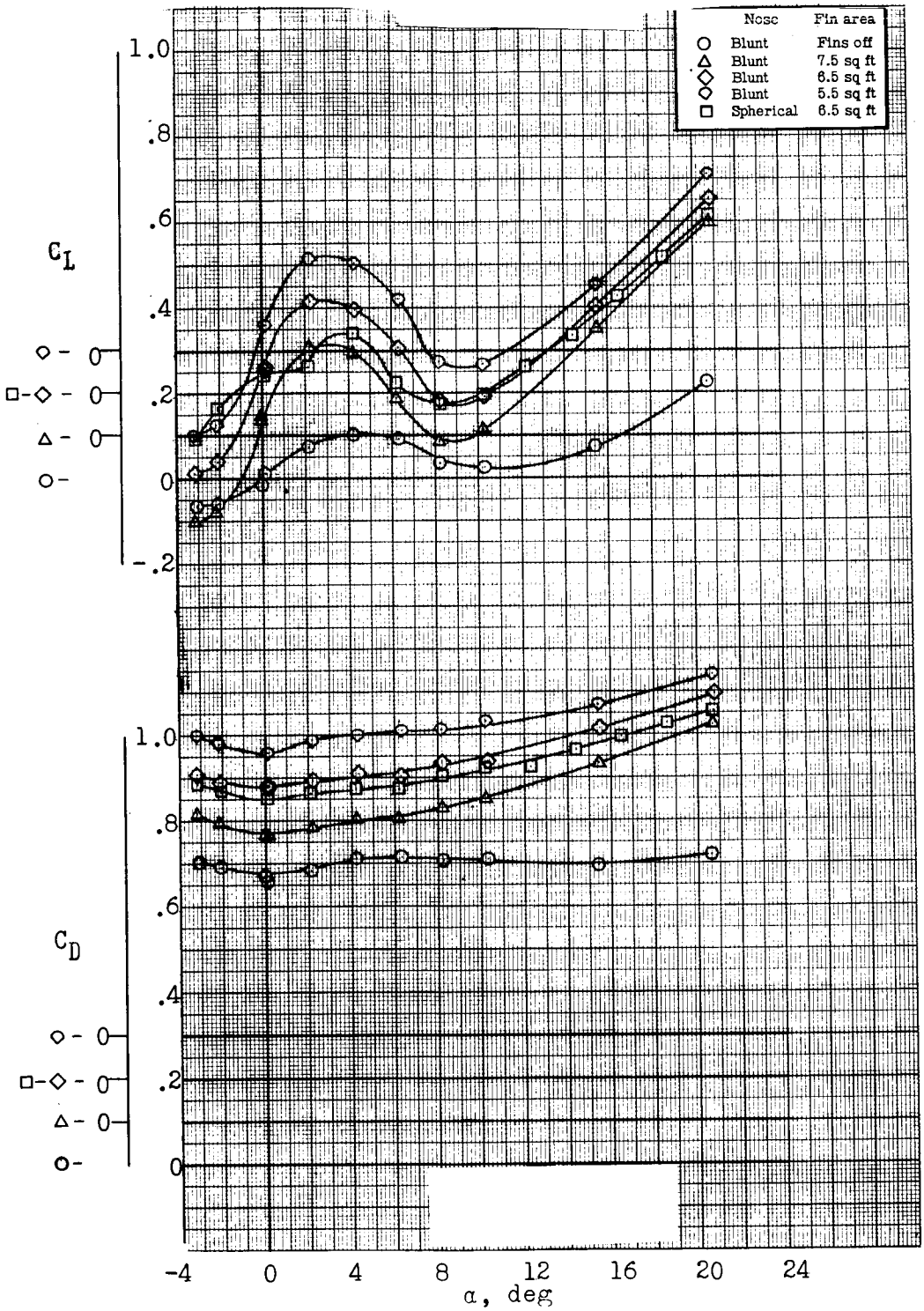

Figure 25.- Concluded.

[redacted]

DECLASSIFIED

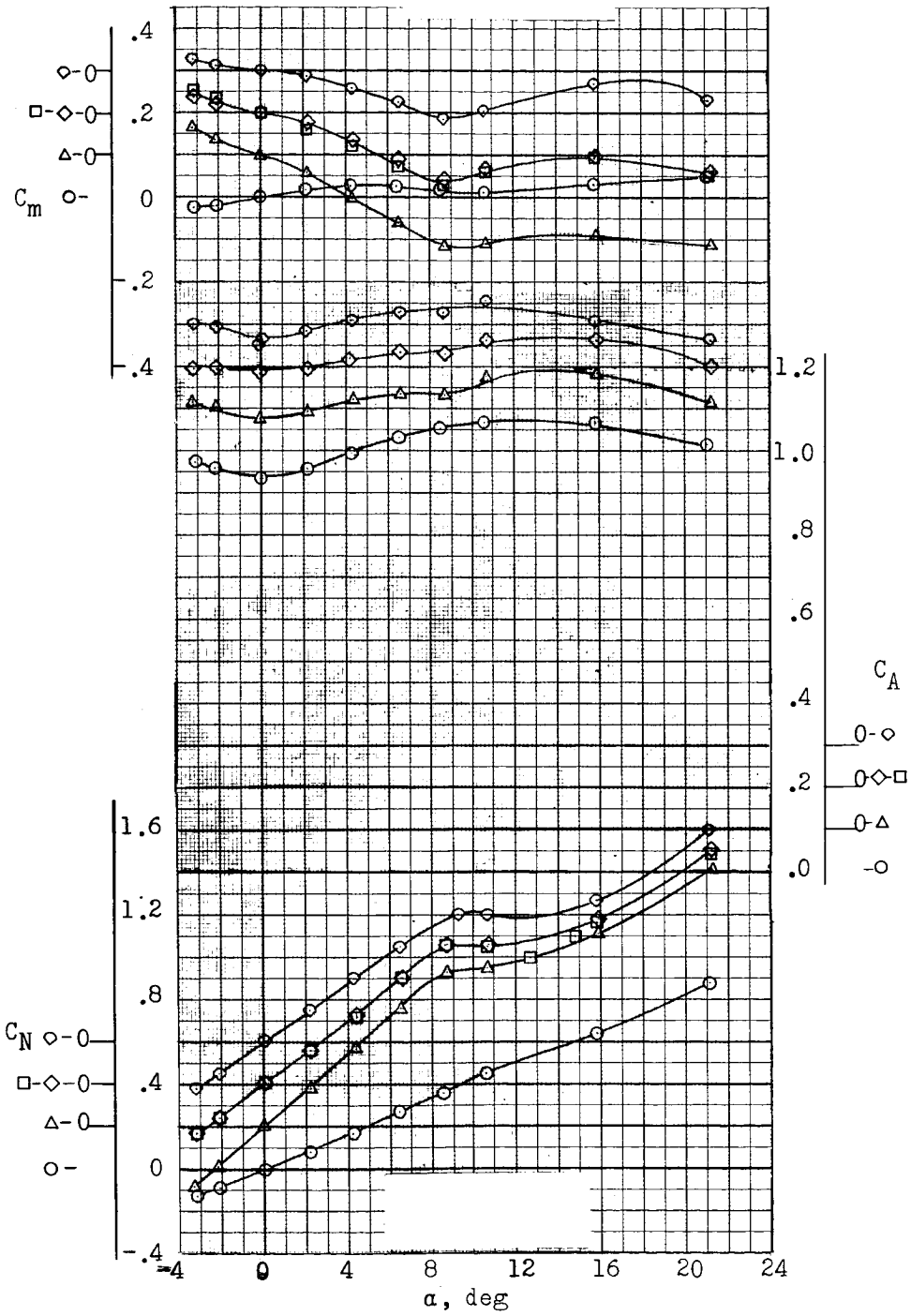

Figure 26.- Effect of fin area and nose shape on the aerodynamic characteristics of the finned-adapter escape configuration. M = 1.00.

[redacted]

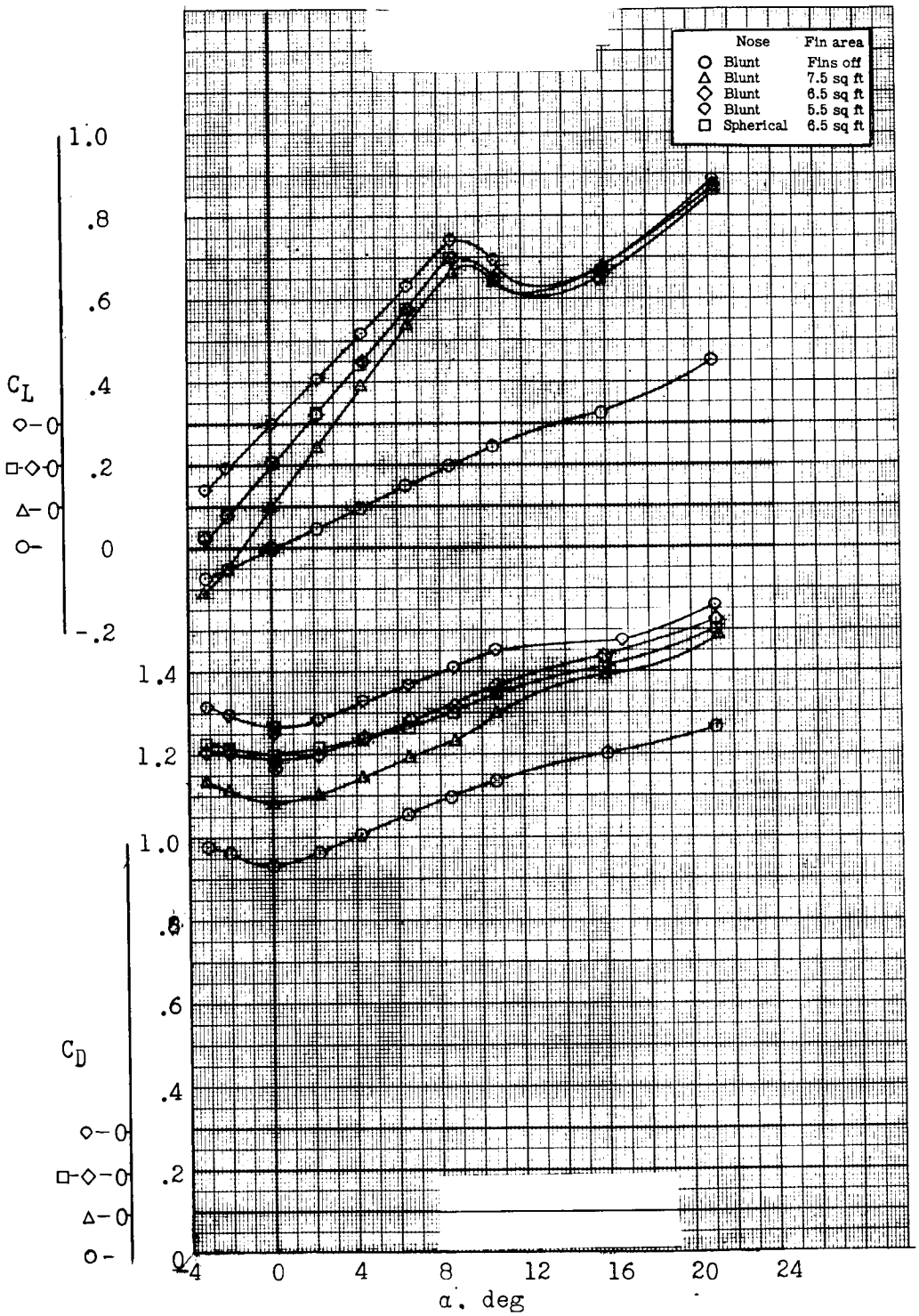

Figure 26.- Concluded.

DECLASSIFIED

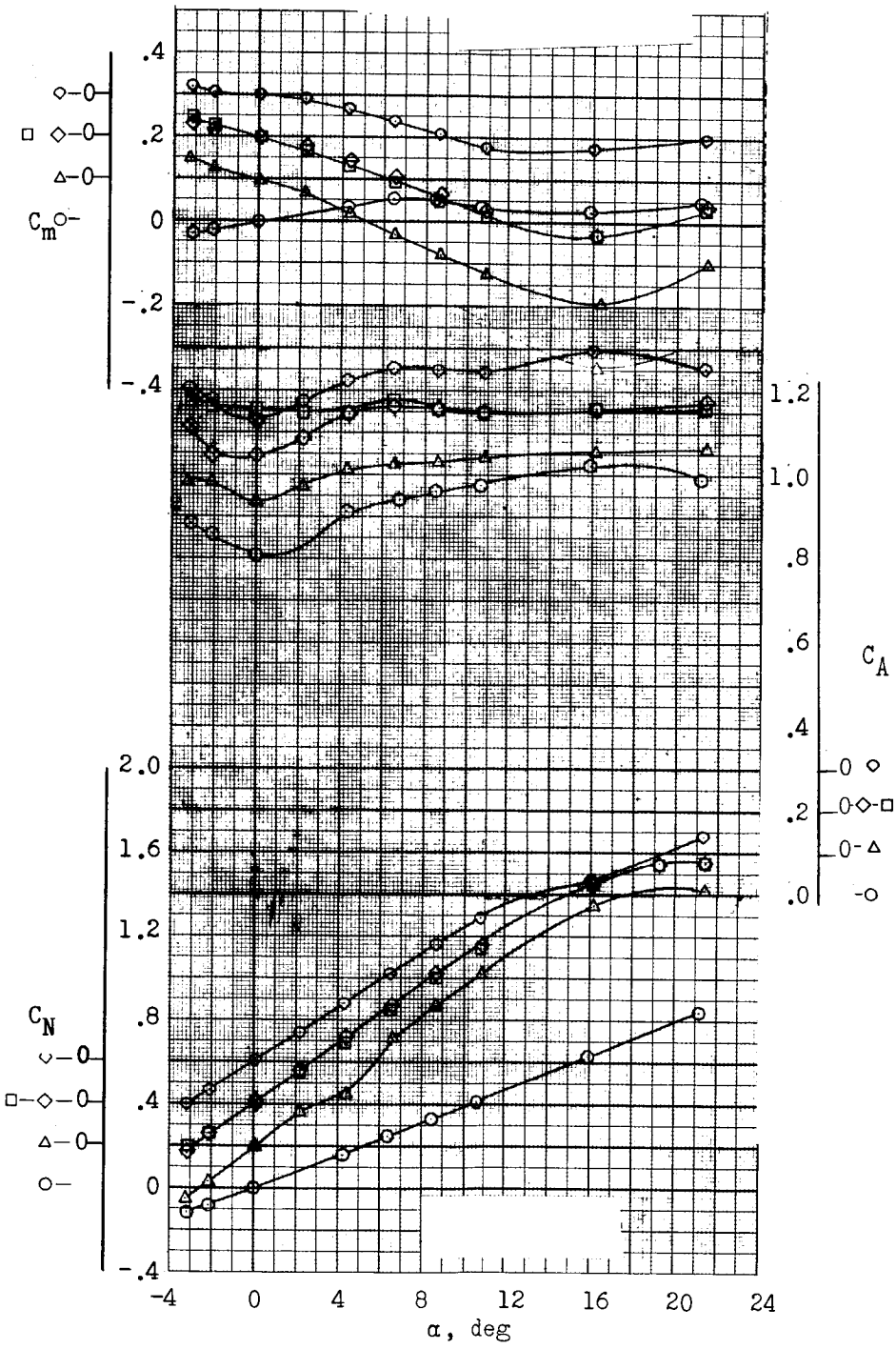

Figure 27.- Effect of fin area and nose shape on the aerodynamic characteristics of the finned-adapter escape configuration. M = 1.14.

[redacted]

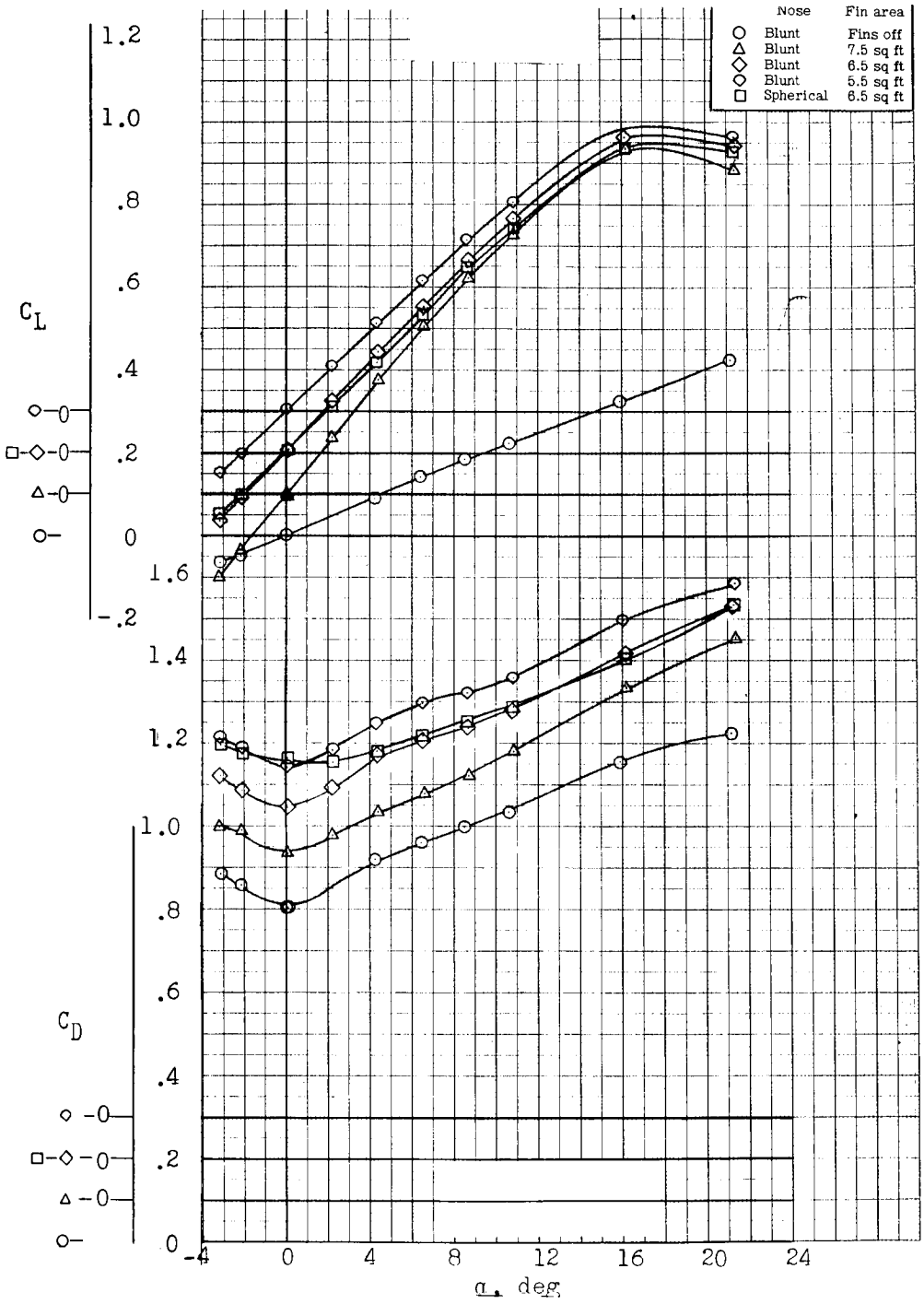

Figure 27.- Concluded.

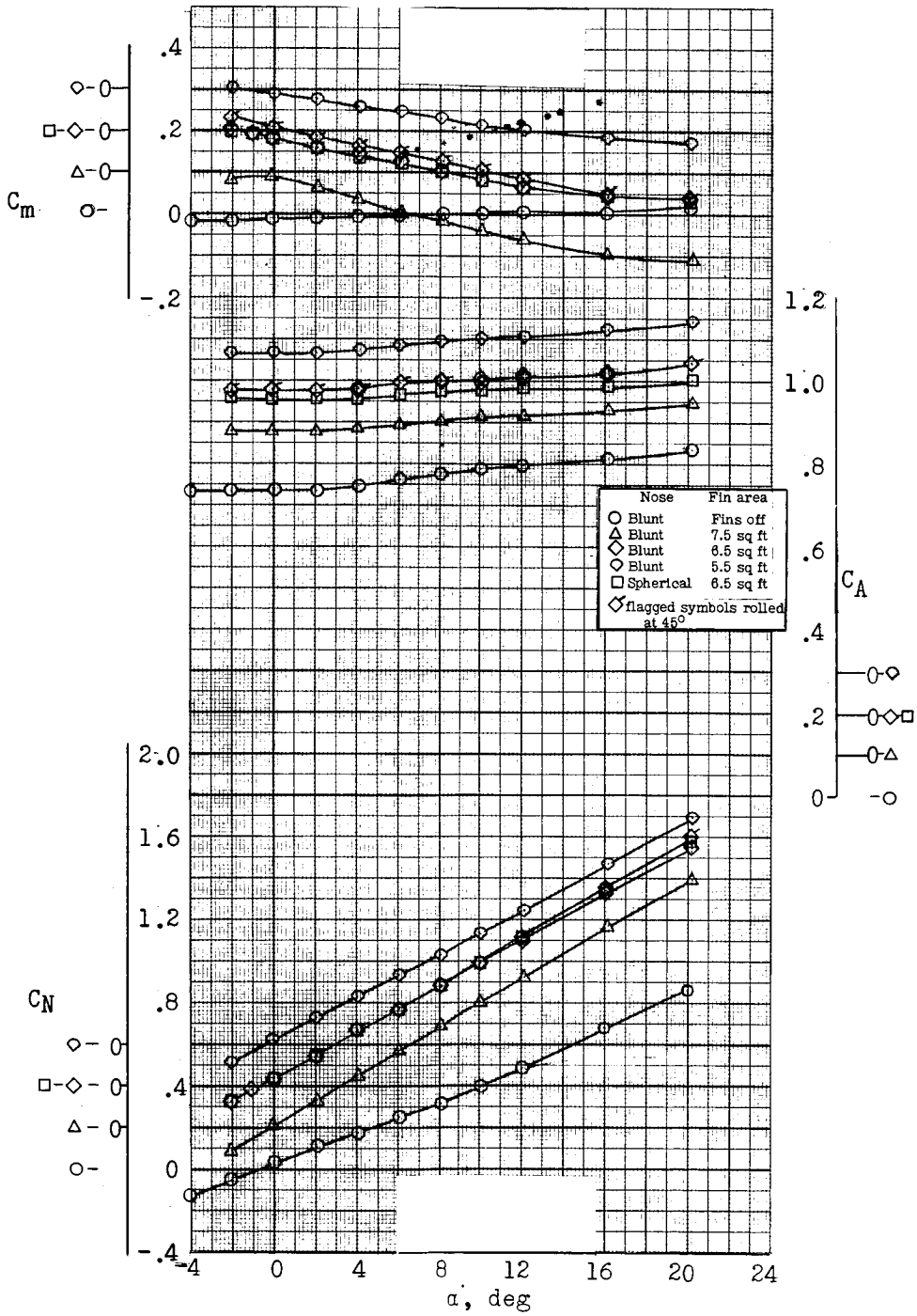

Figure 28.- Effect of fin area and nose shape on the aerodynamic characteristics of the finned-adapter escape configuration. M = 2.01.

G
6

[redacted]

[redacted]

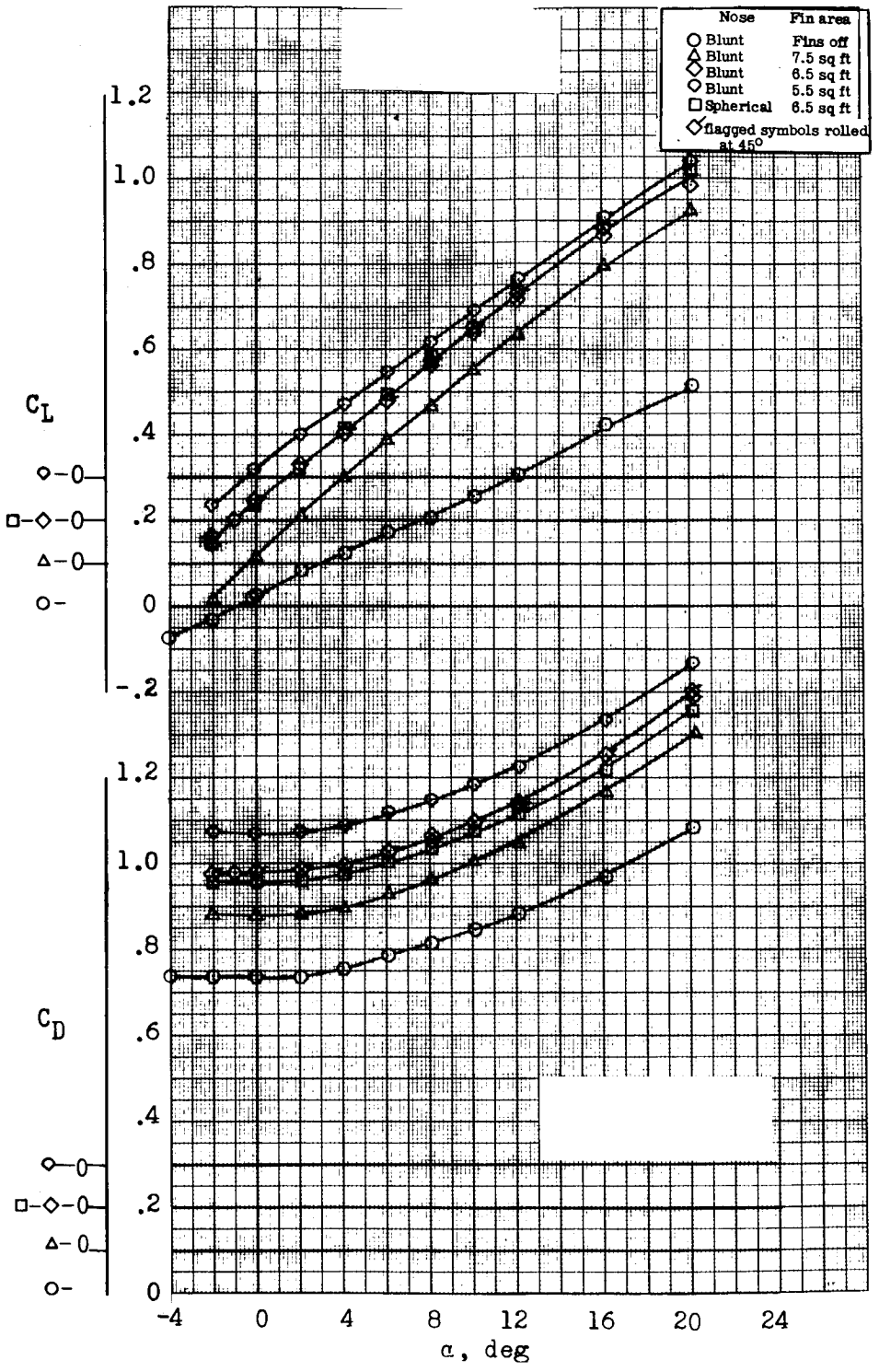

Figure 28.- Concluded.

[redacted]

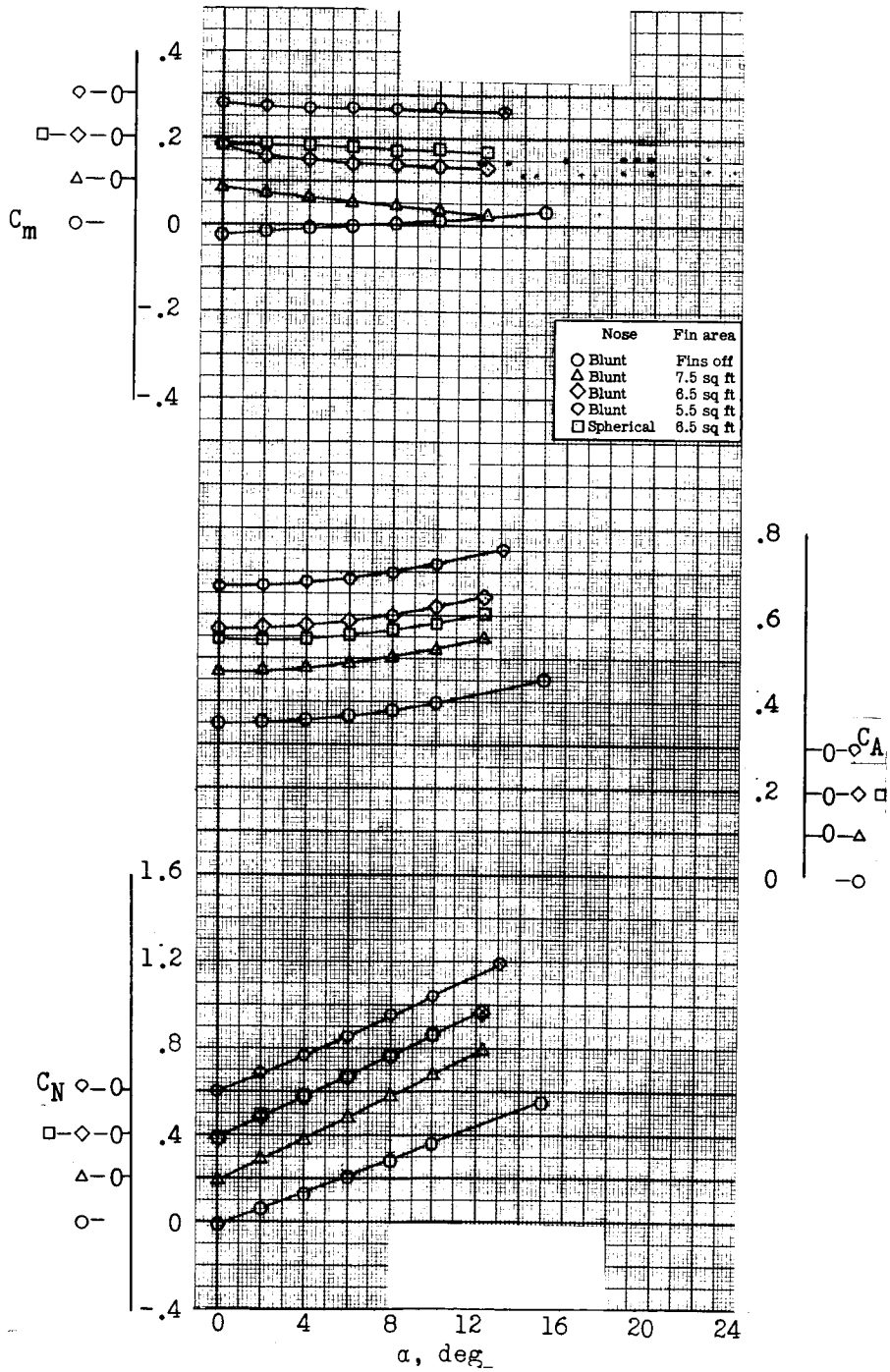

Figure 29.- Effect of fin area and nose shape on the aerodynamic characteristics of the finned-adapter escape configuration. M = 4.00.

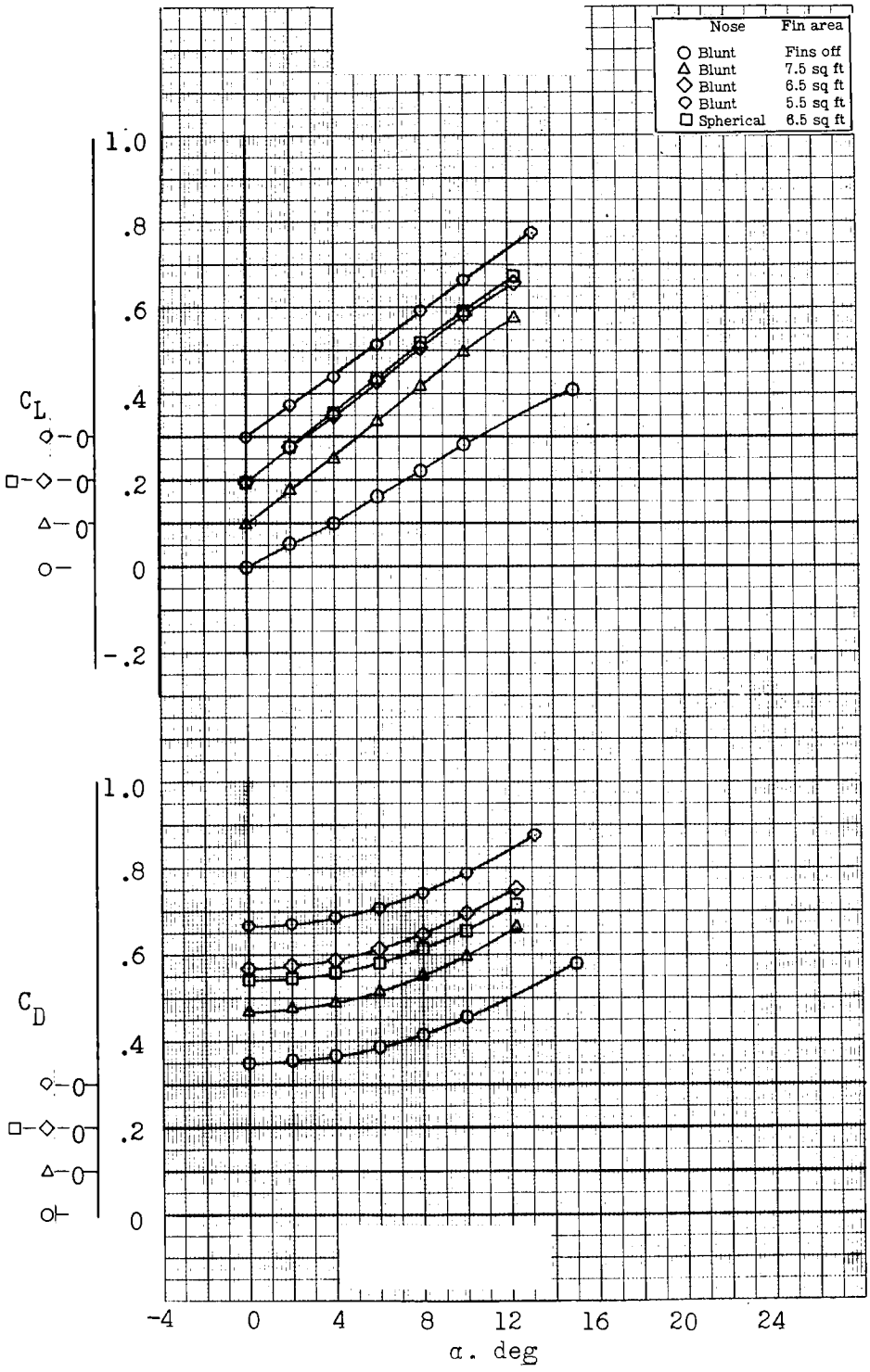

Figure 29.- Concluded.

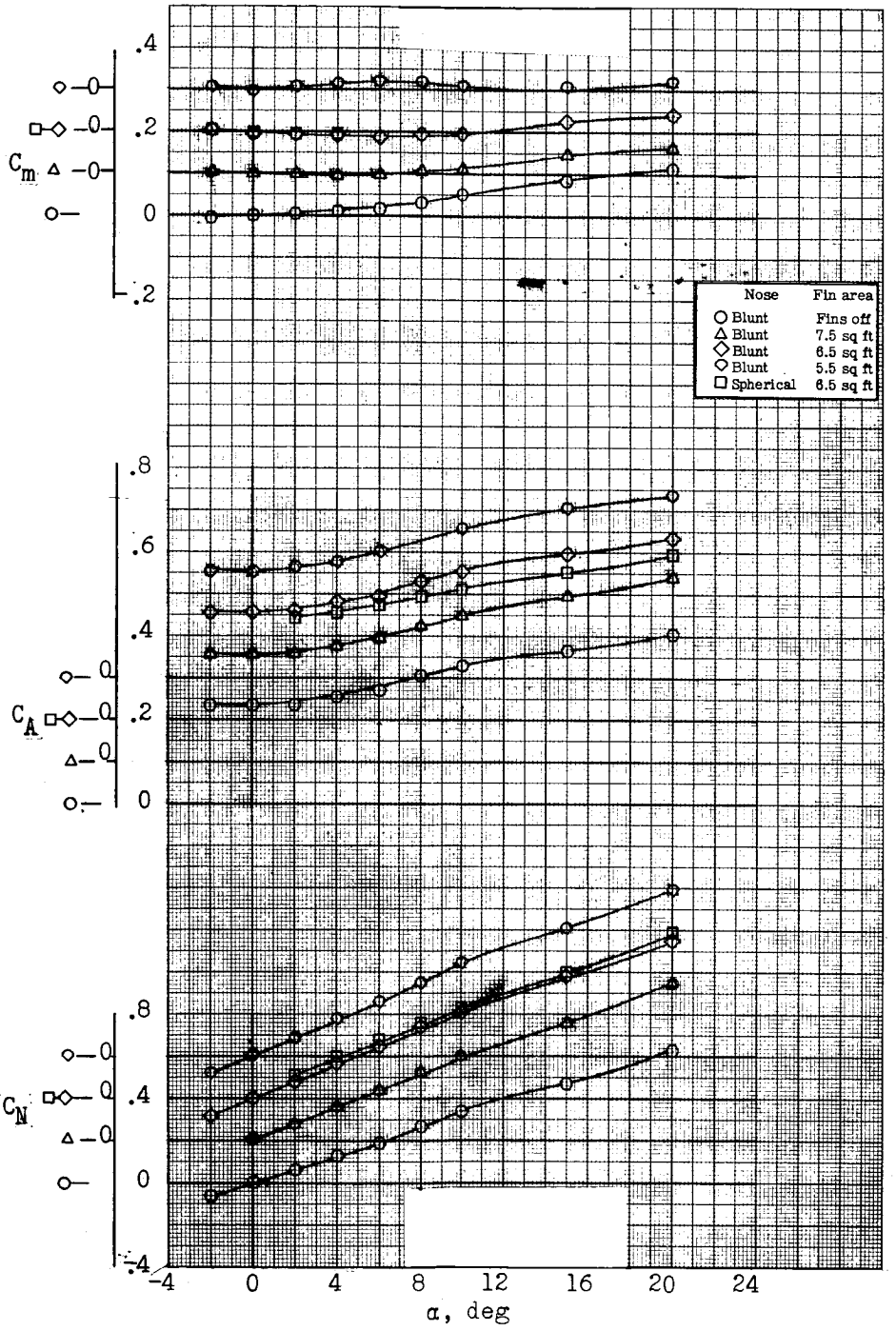

G
6

Figure 30.- Effect of fin area and nose shape on the aerodynamic characteristics of the finned-adapter escape configuration. M = 6.86.

[redacted]

[redacted]

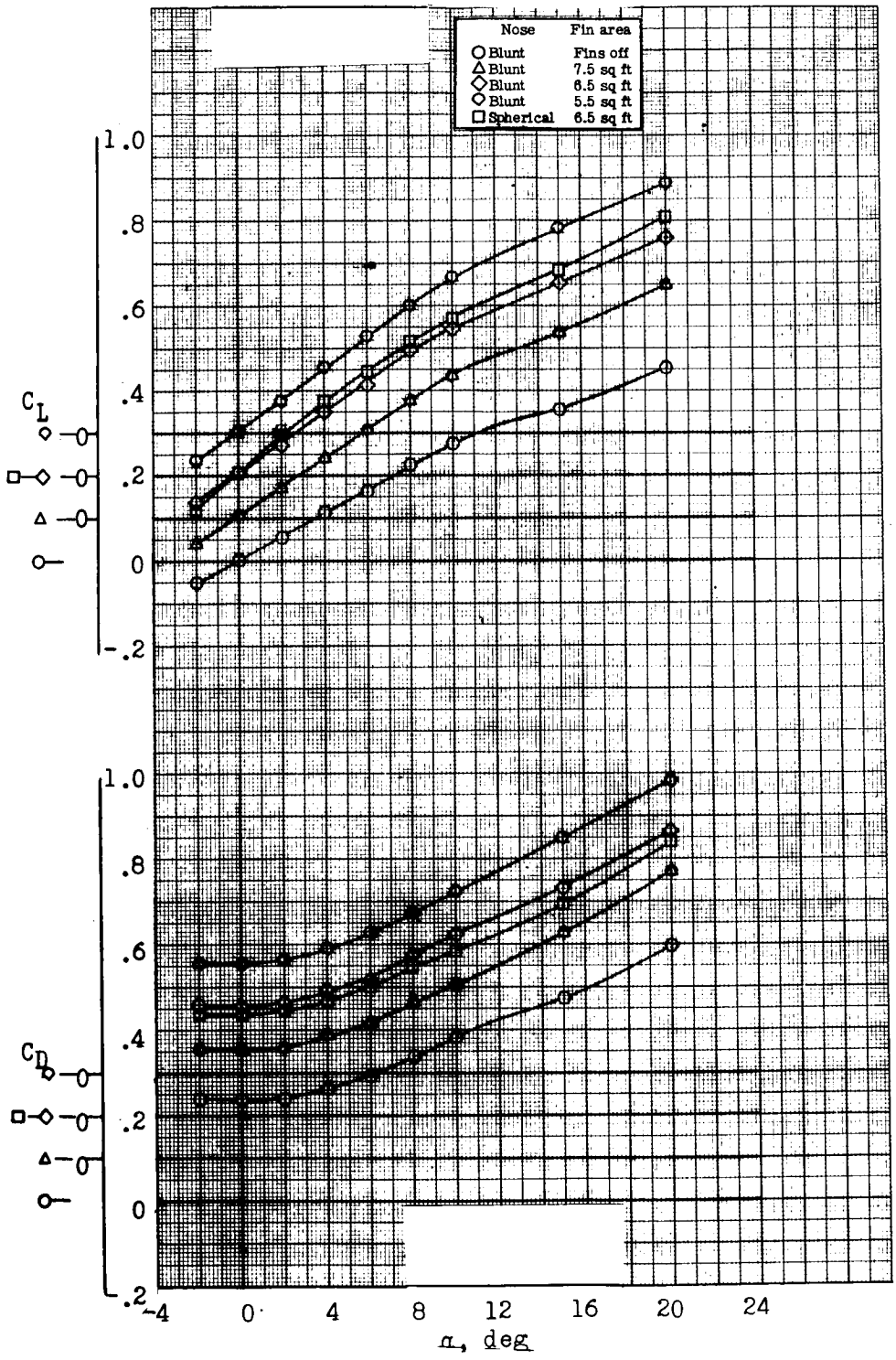

Figure 30.- Concluded.

[redacted]

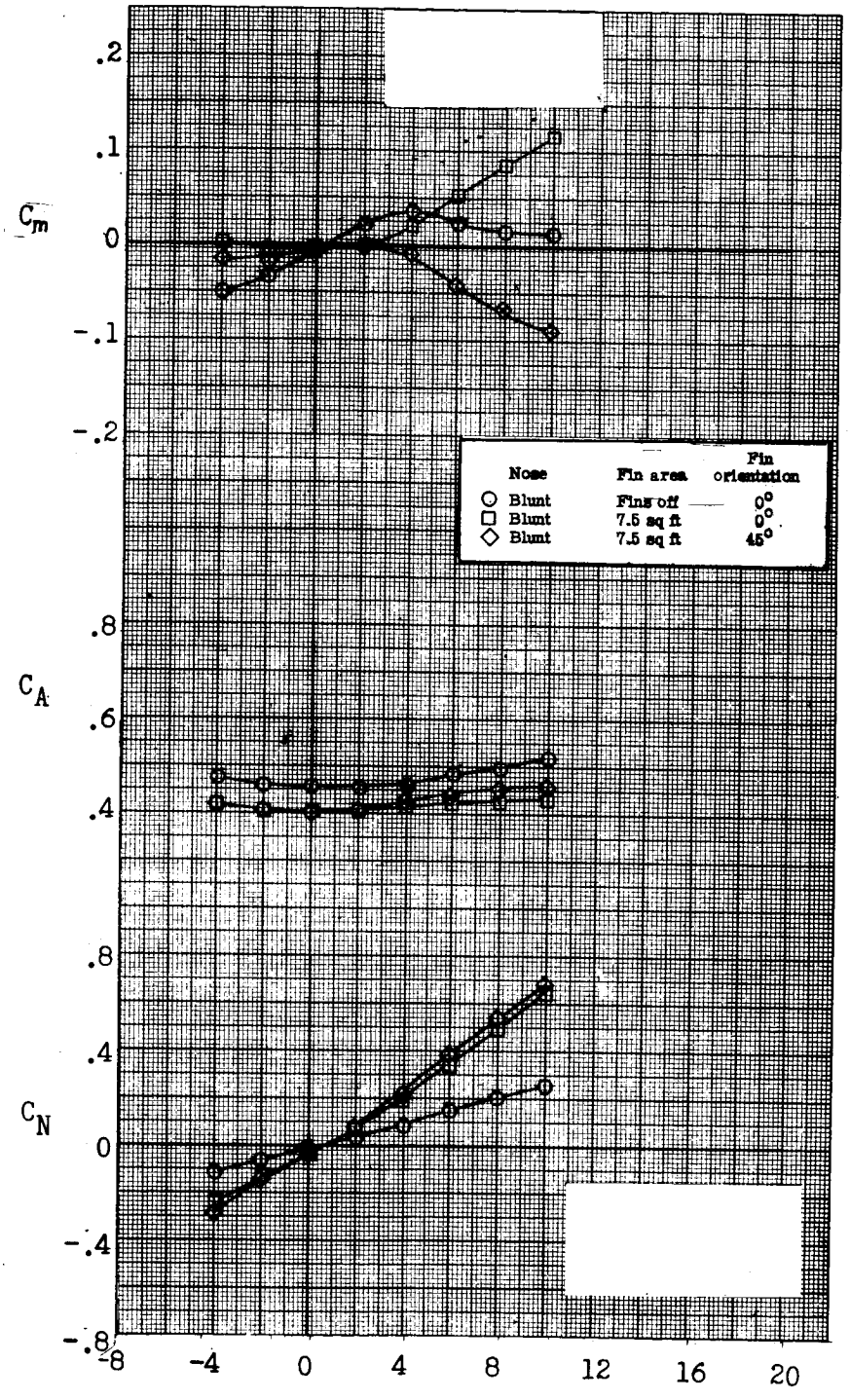

Figure 31.- Effect of fin area and fin orientation on the aerodynamic characteristics of the finned escape configuration. M = 0.50.

G
6

[redacted]

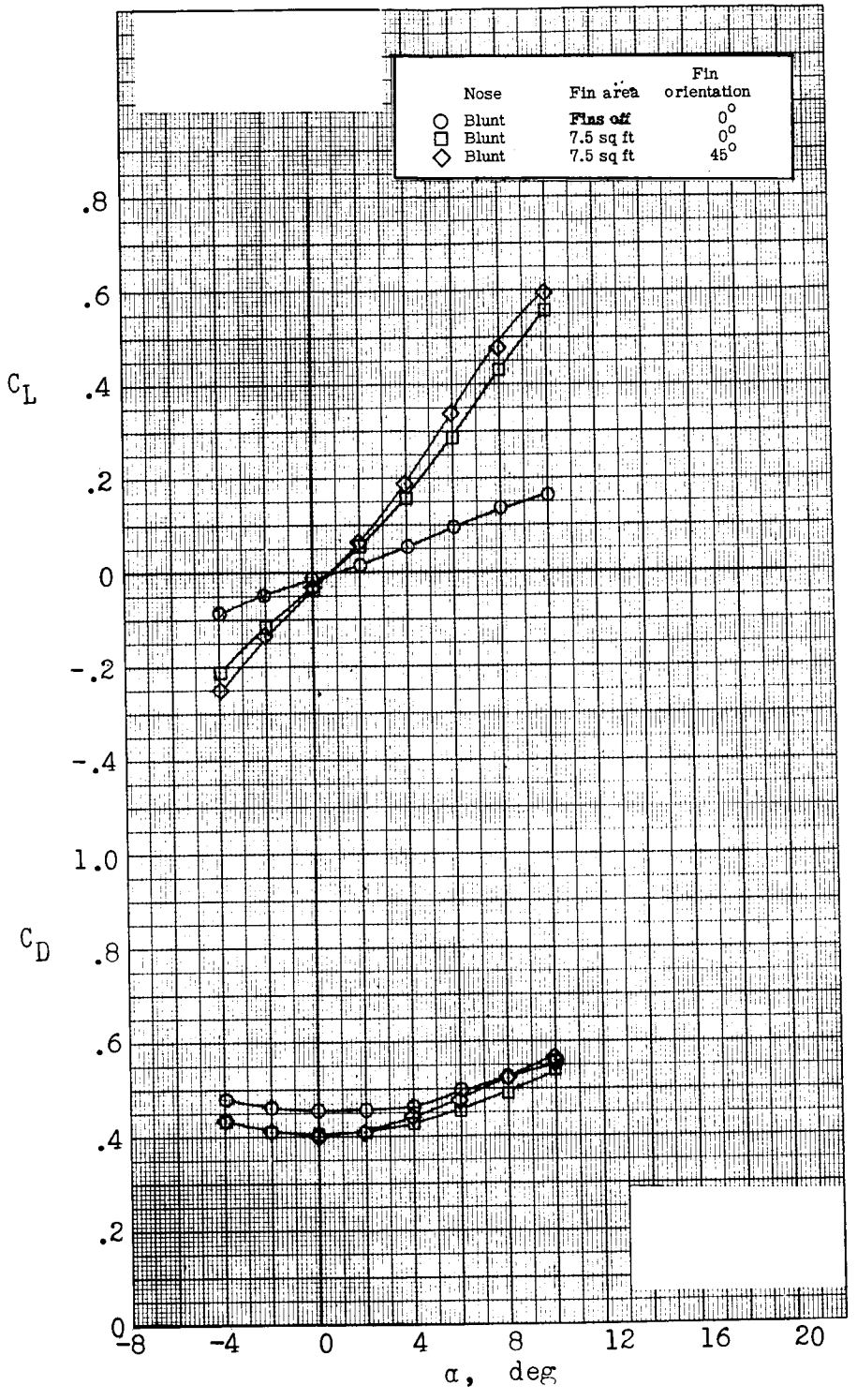

Figure 31.- Concluded.

[redacted]

11D

[redacted]
DECLASSIFIED

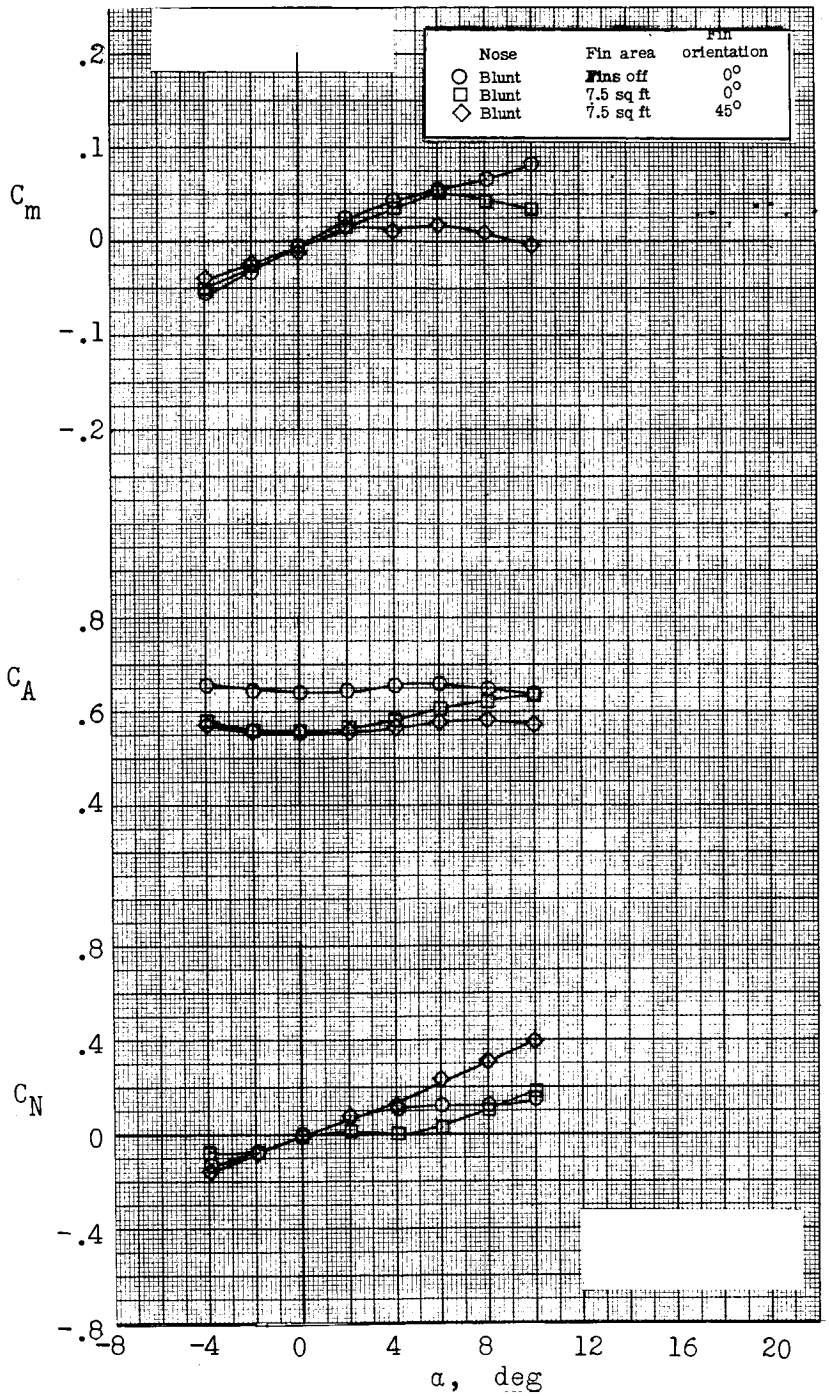

Figure 32.- Effect of fin area and fin orientation on the aerodynamic characteristics of the finned escape configuration. M = 0.70.

[redacted]

[redacted]

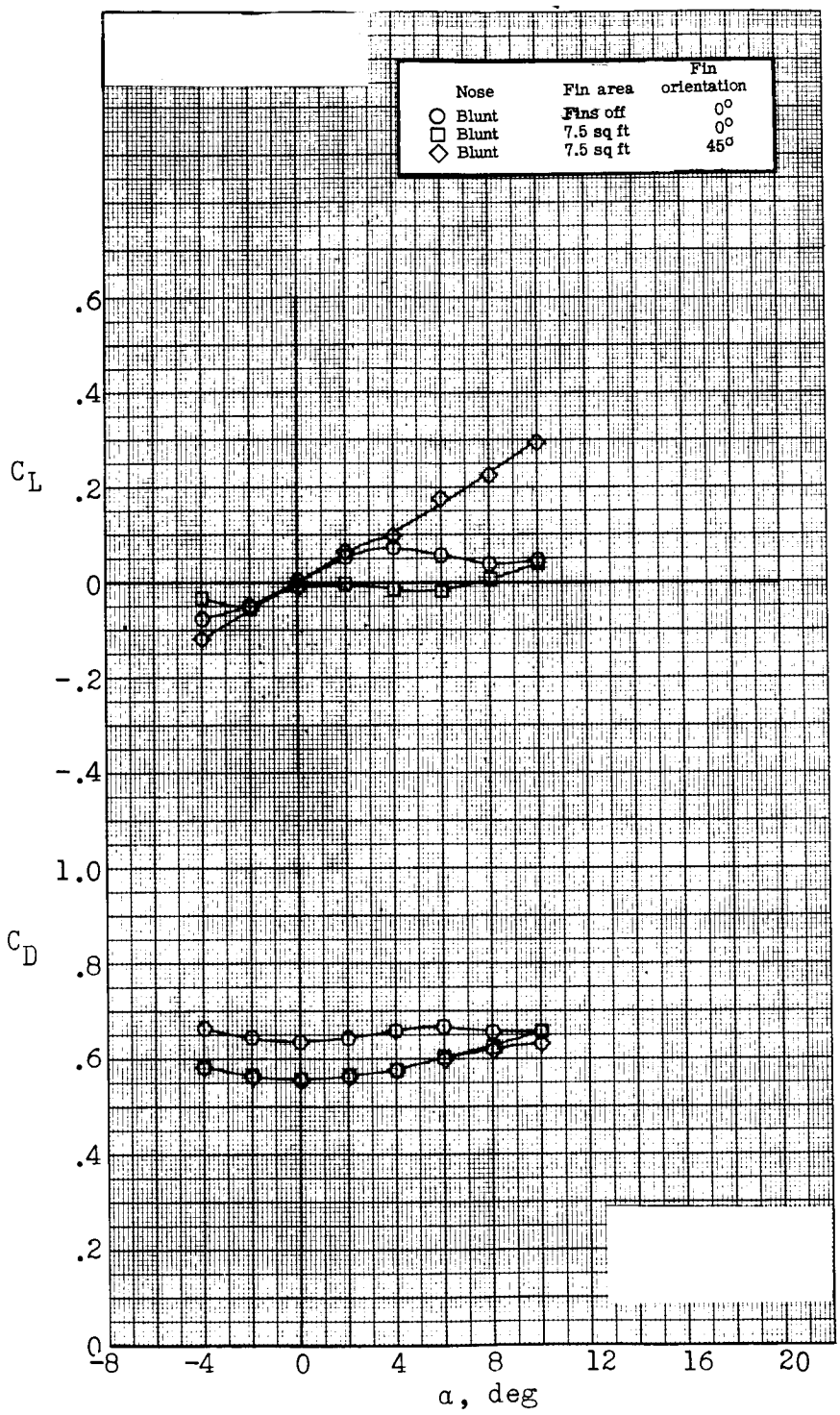

Figure 32.- Concluded.

[redacted]

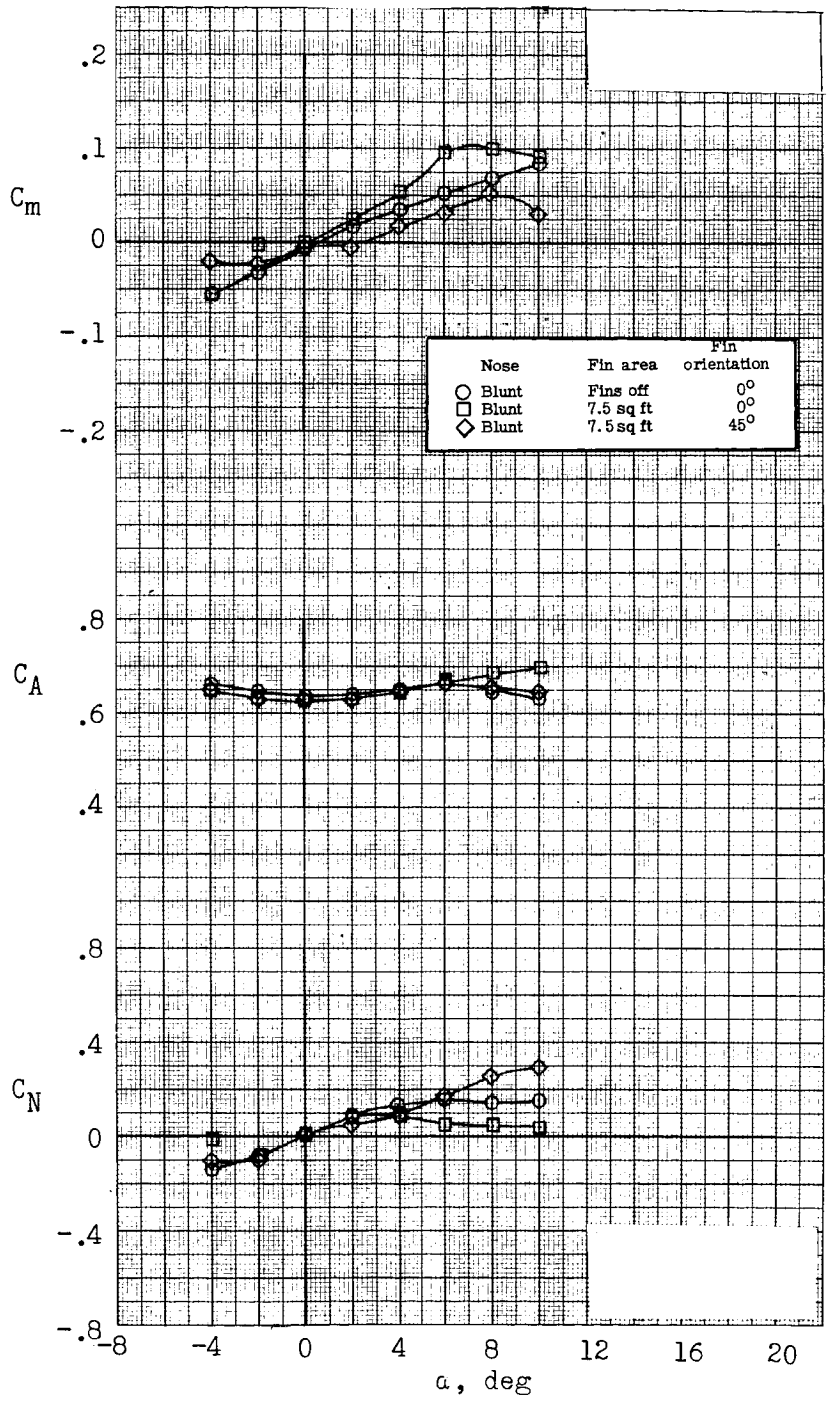

Figure 33.- Effect of fin area and fin orientation on the aerodynamic characteristics of the finned escape configuration. M = 0.80.

[redacted]

[redacted]

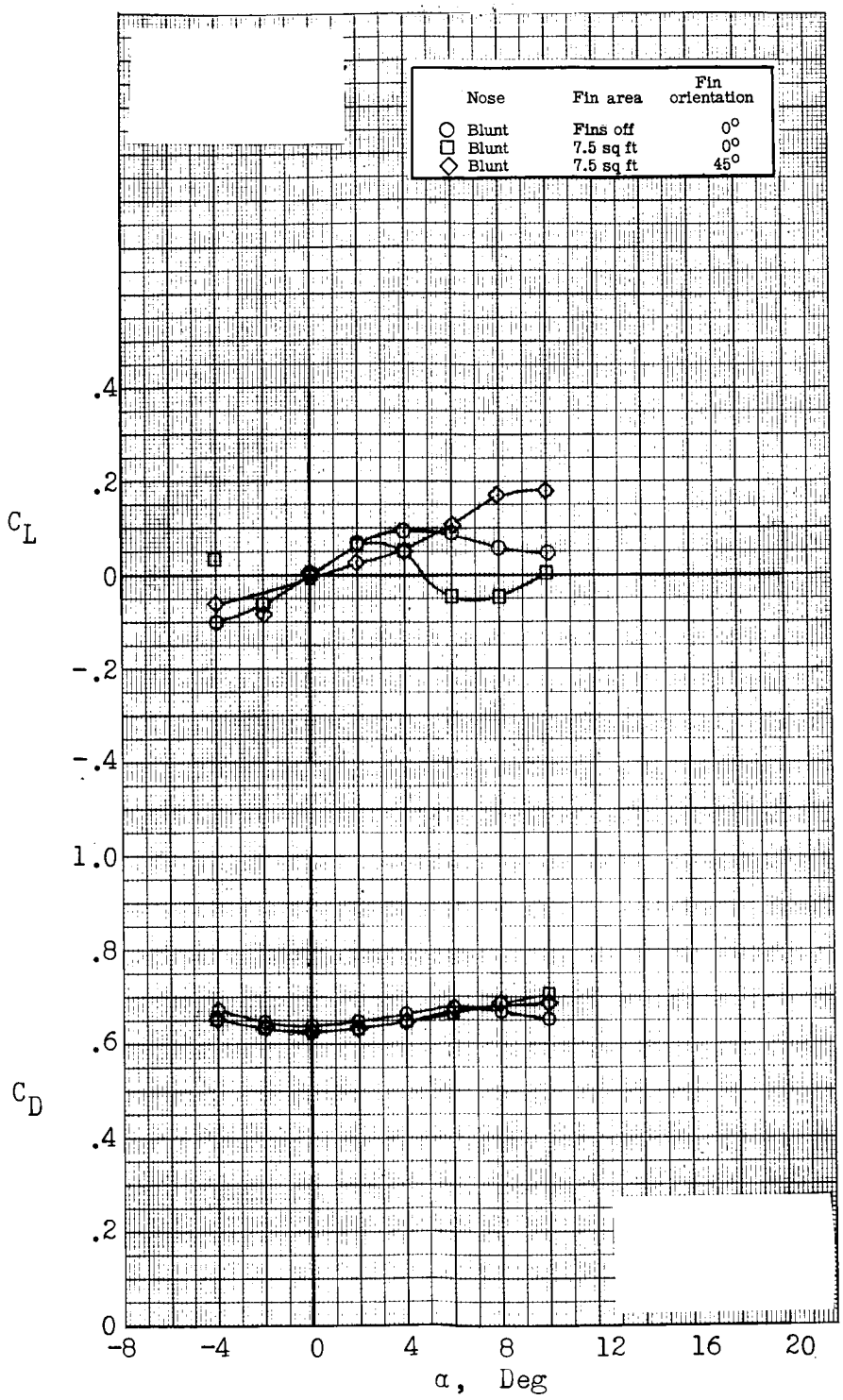

Figure 33.- Concluded.

[redacted]

DE[redacted]IFIED

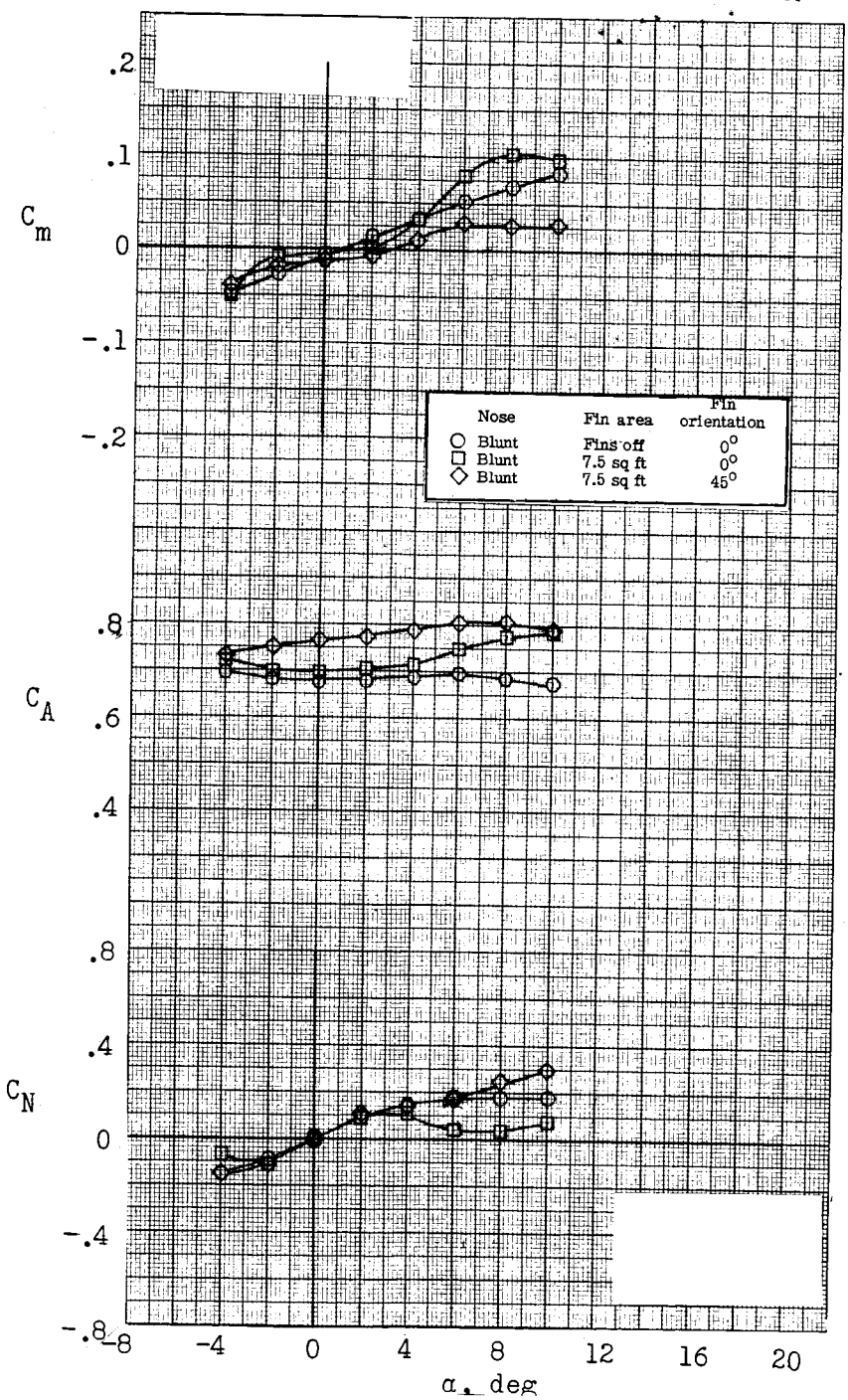

Figure 34.- Effect of fin area and fin orientation on the aerodynamic characteristics of the finned escape configuration. M = 0.90.

[redacted]

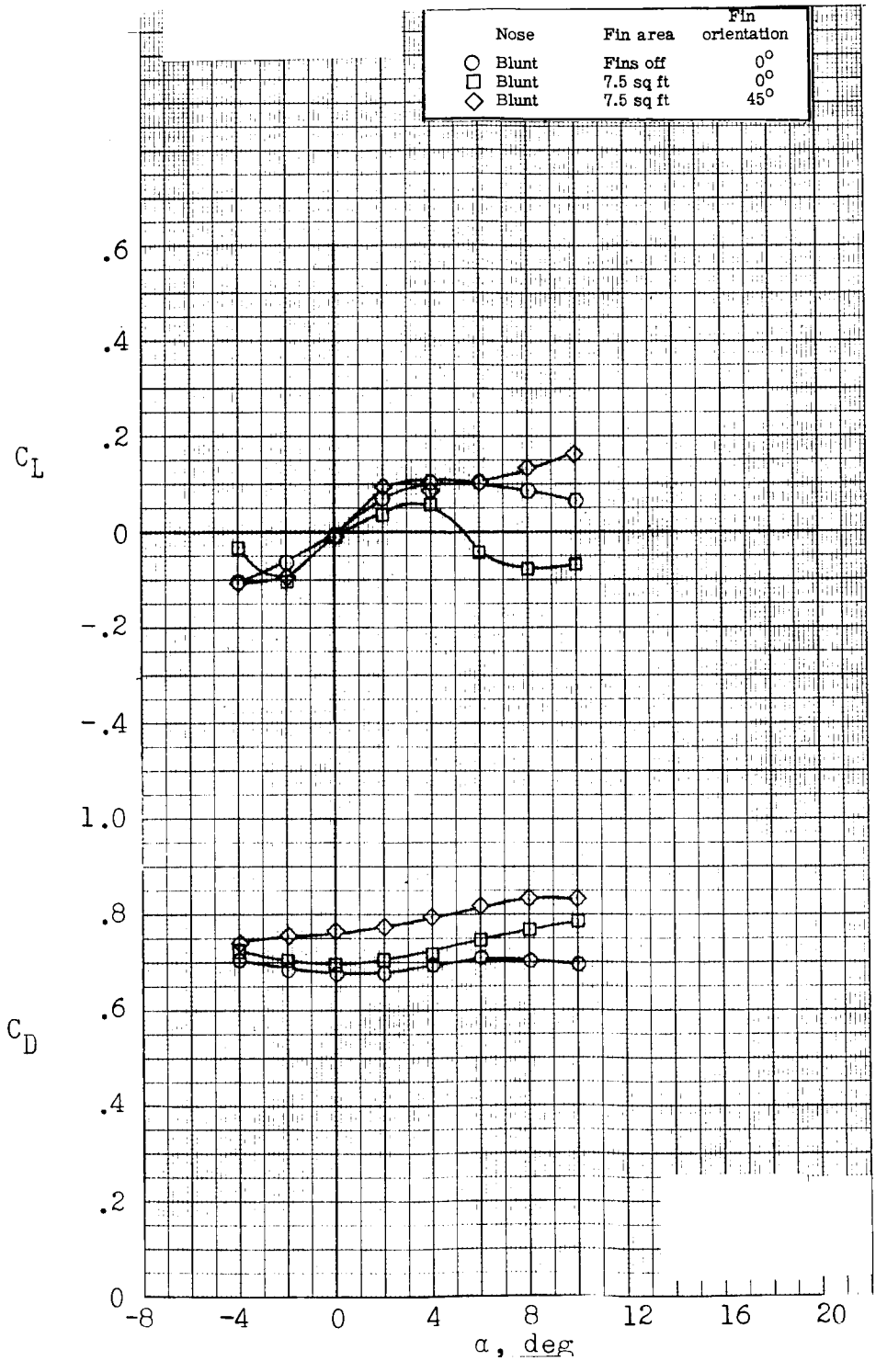

Figure 34.- Concluded.

DECLASSIFIED

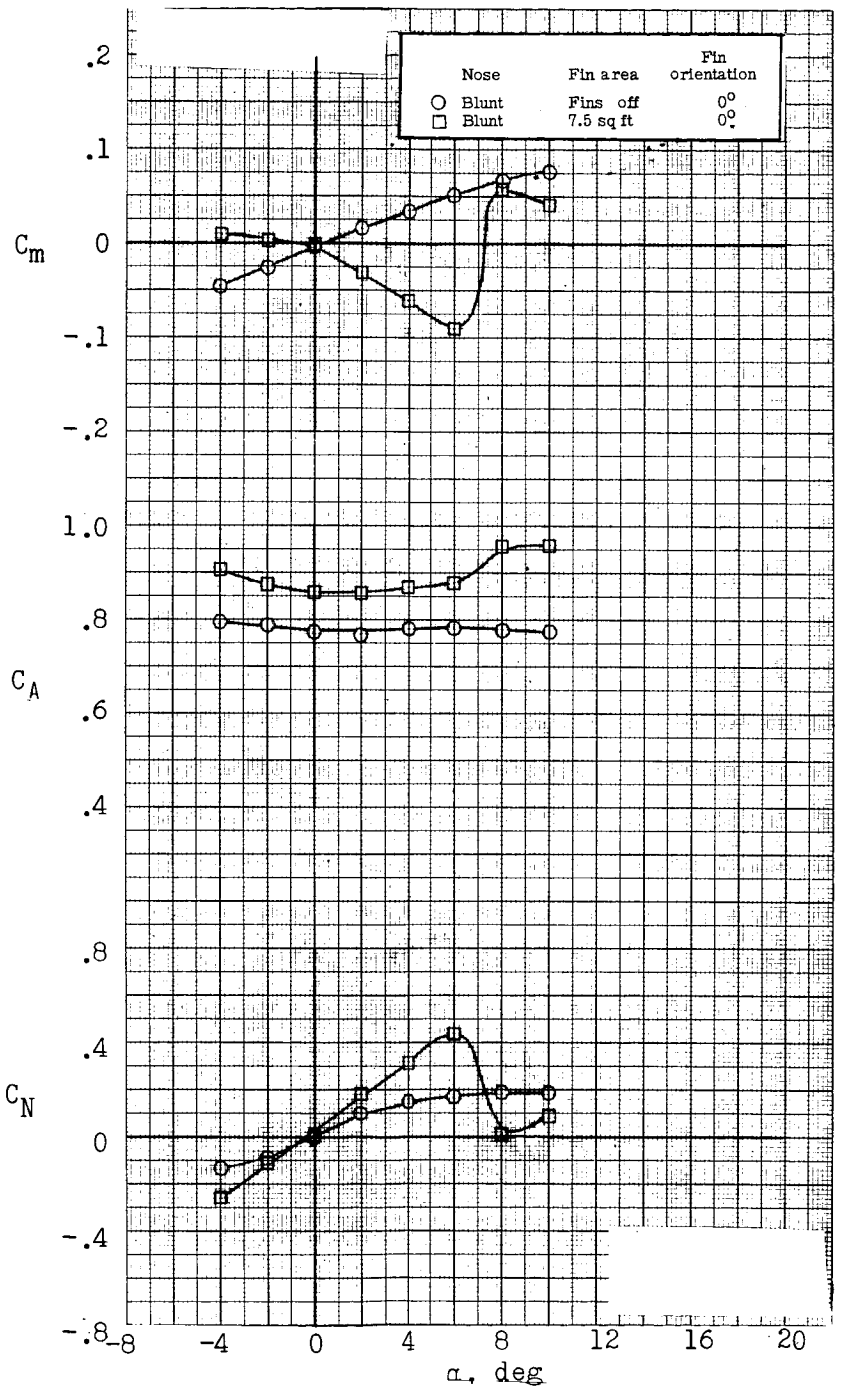

Figure 35.- Effect of fin area on the aerodynamic characteristics of the finned escape configuration. M = 1.00.

[redacted]

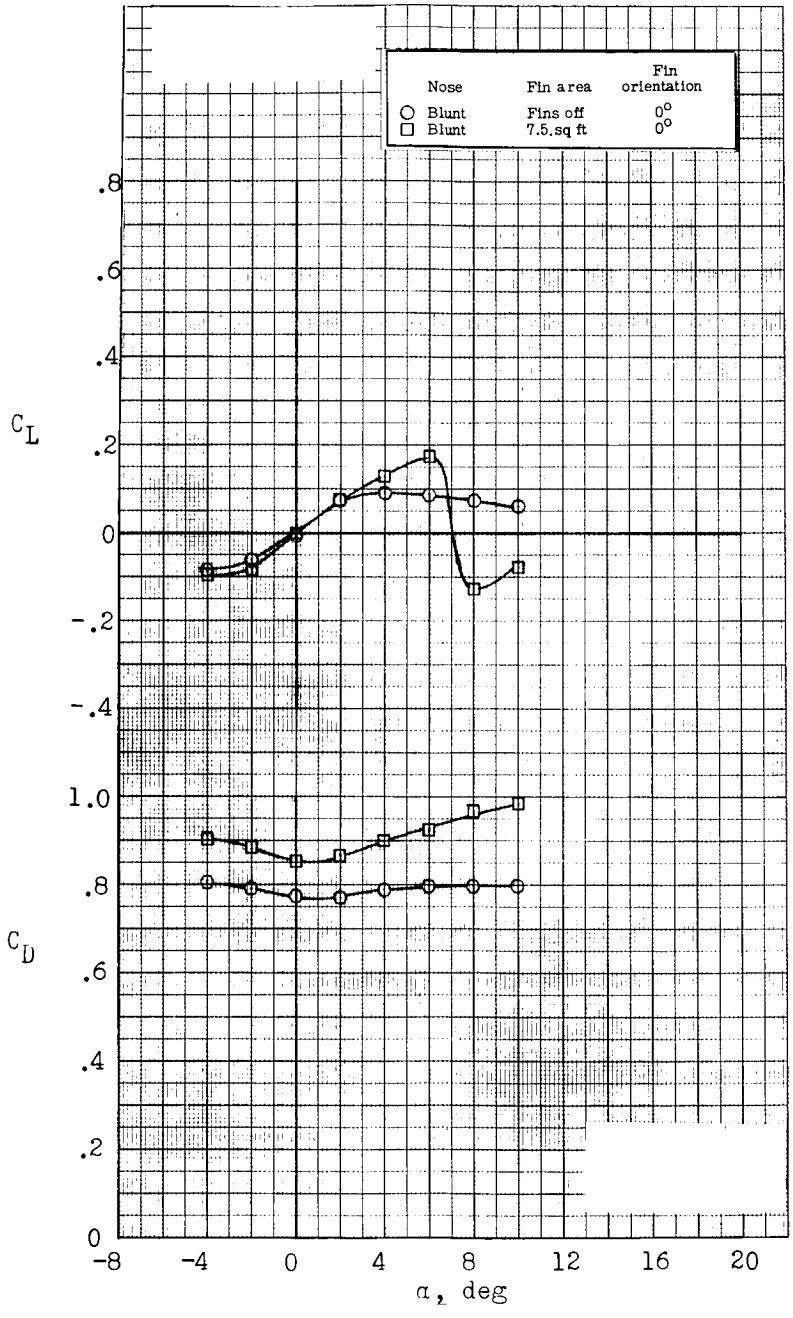

Figure 35.- Concluded.

[redacted]

DECL[redacted]IED

G
6

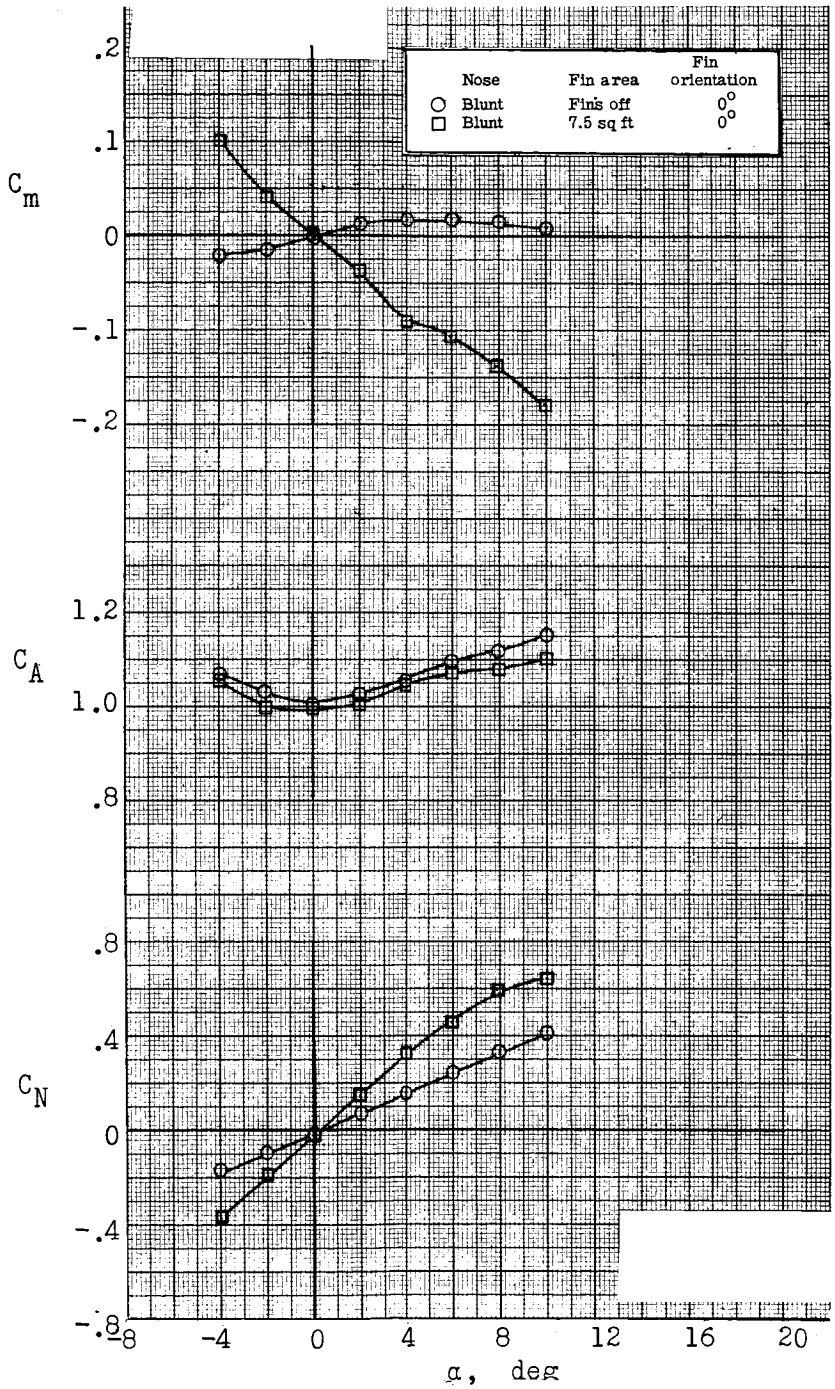

Figure 36.- Effect of fin area on the aerodynamic characteristics of the finned escape configuration. M = 1.10.

[redacted]

[redacted]

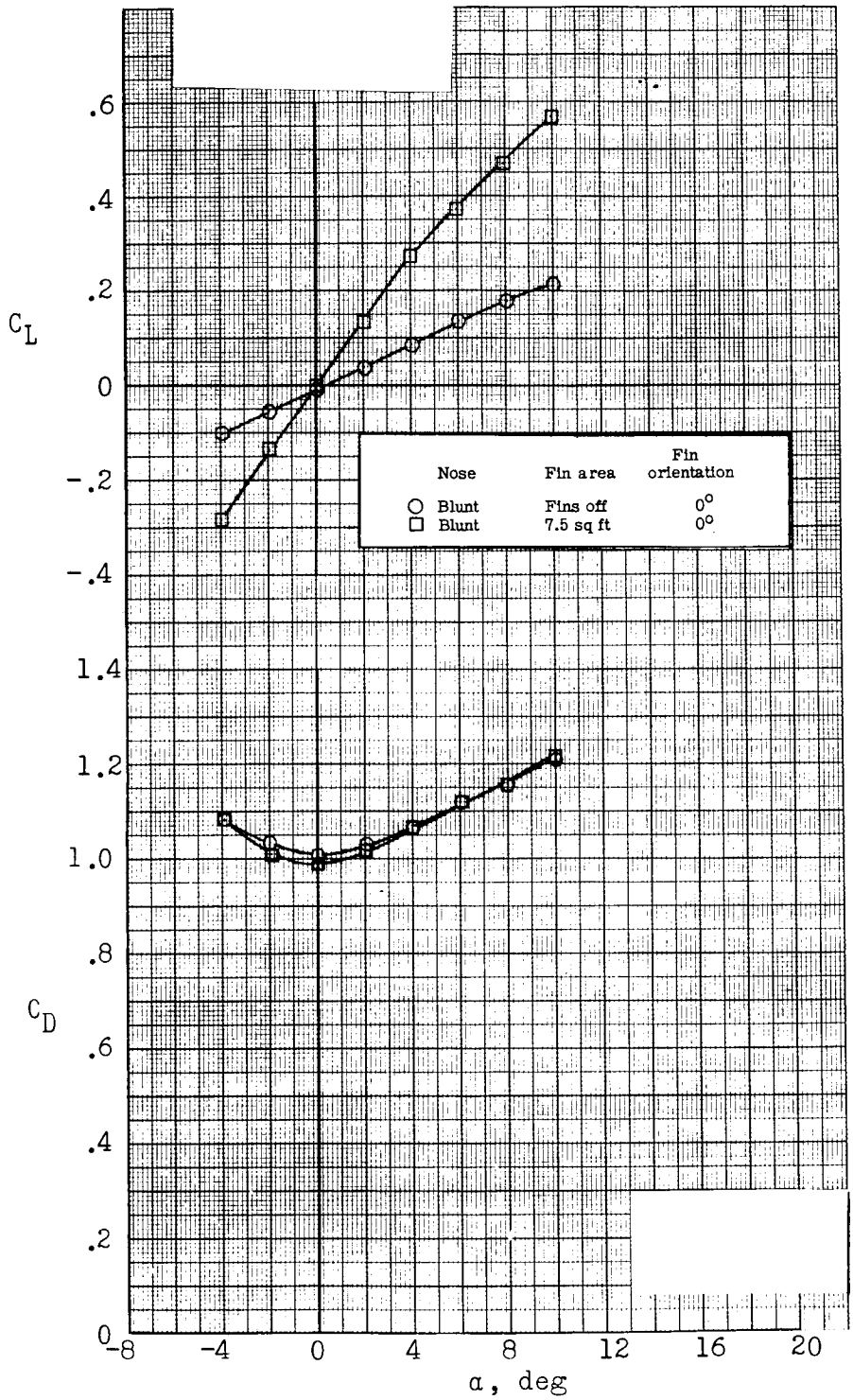

Figure 36.- Concluded.

[redacted]

DE[redacted]IED

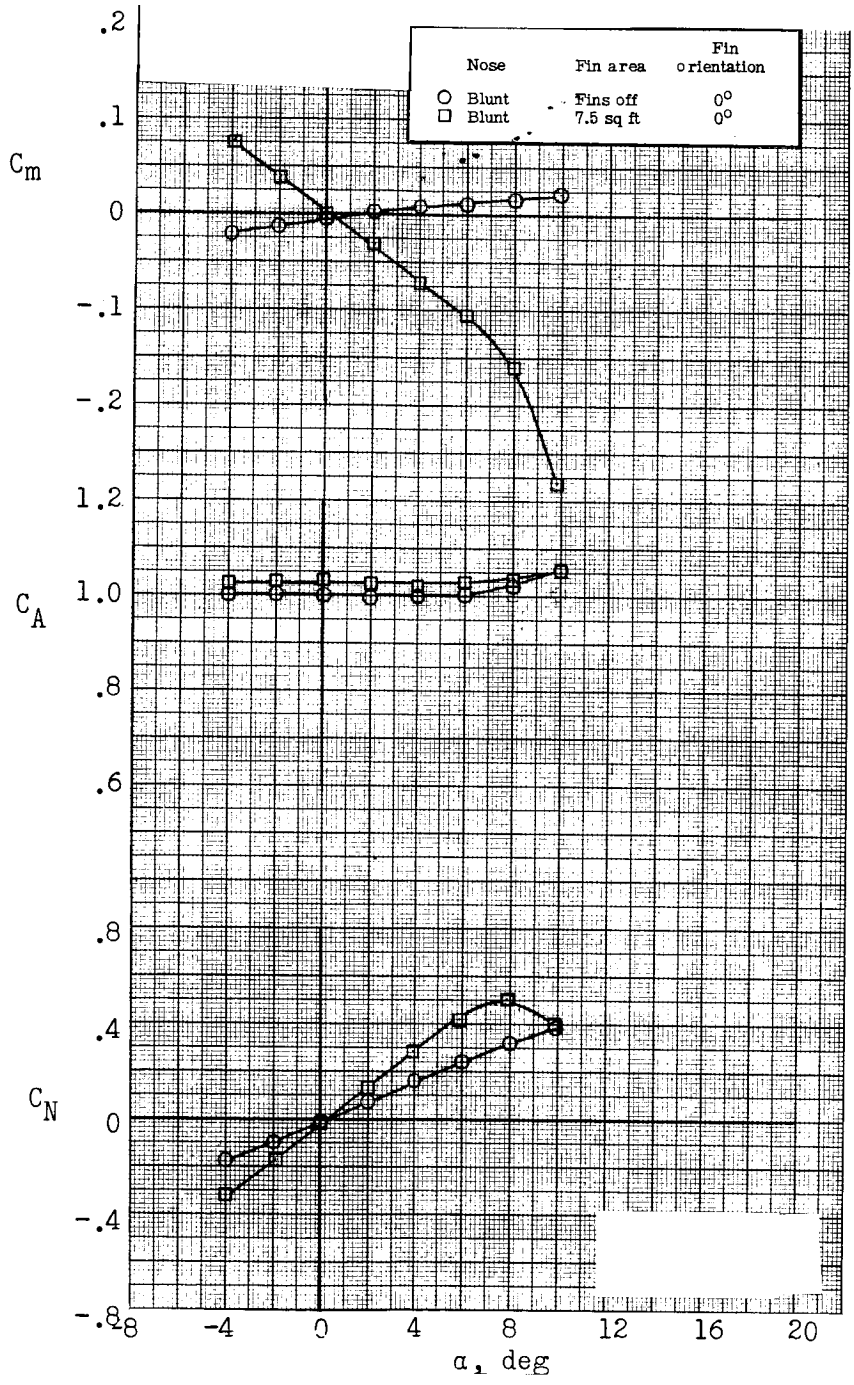

Figure 37.- Effect of fin area on the aerodynamic characteristics of the finned escape configuration. M = 1.40.

[redacted]

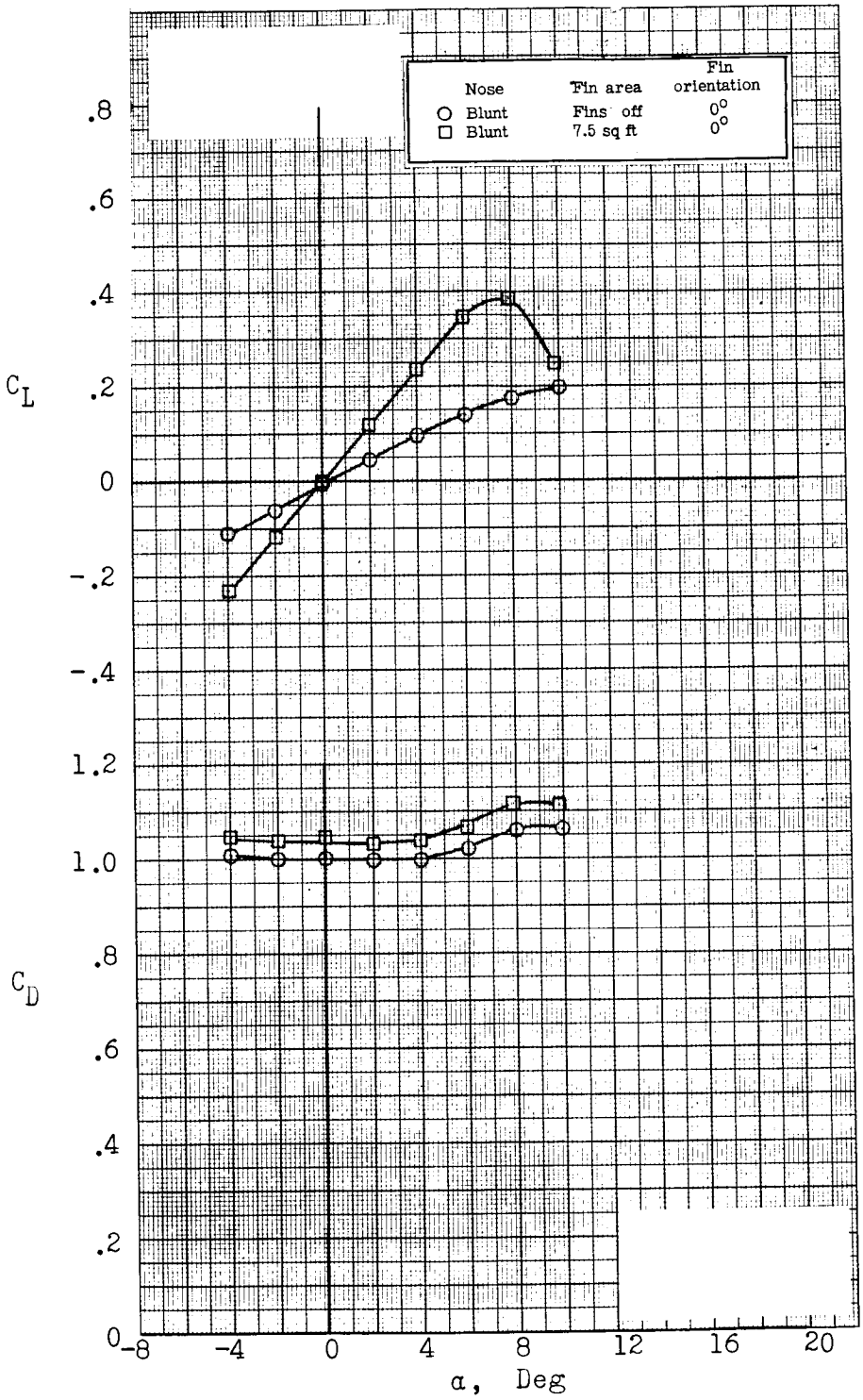

Figure 37.- Concluded.

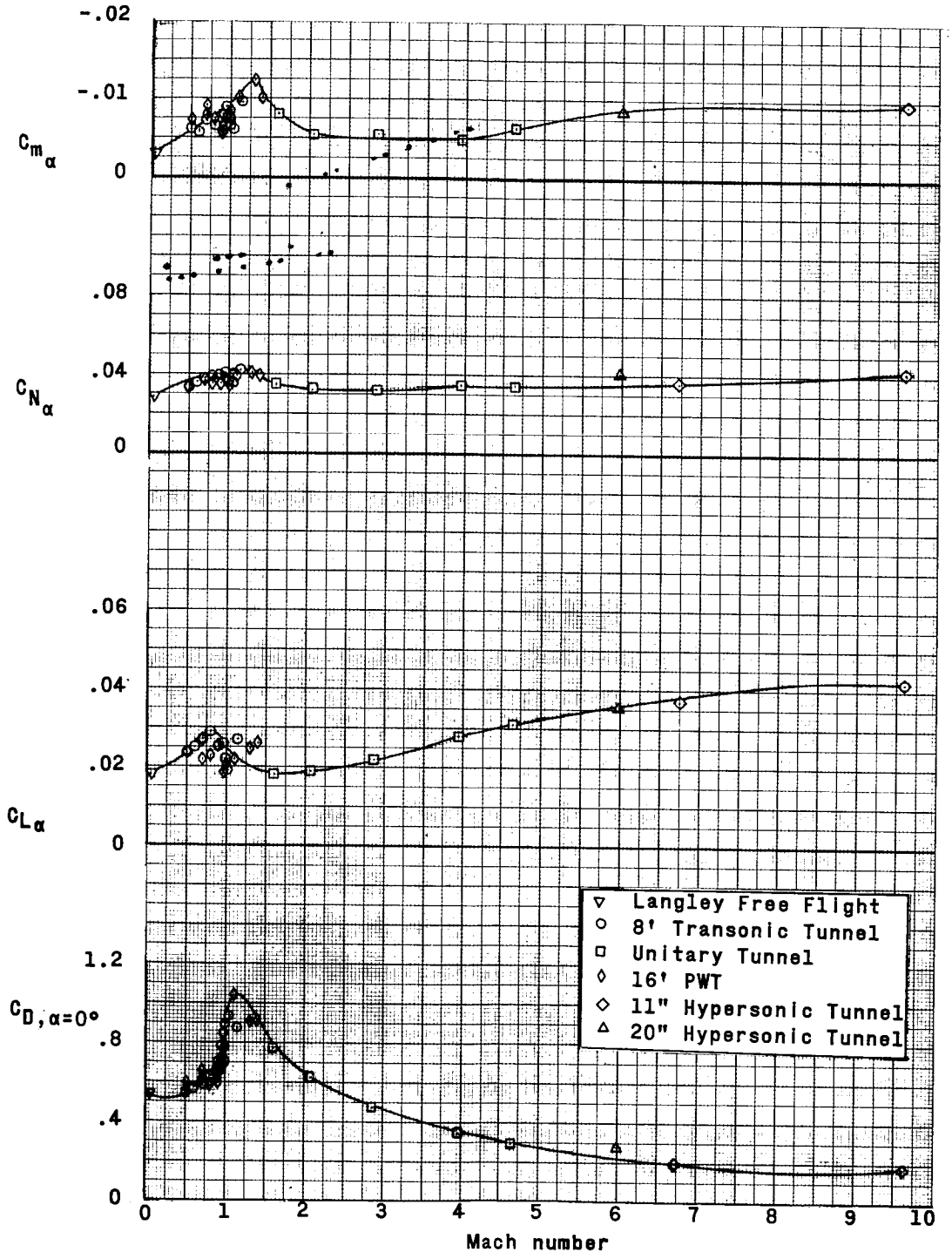

Figure 38.- Summary of the longitudinal stability characteristics of the basic escape configuration.

G
6

[redacted]

CONFIDENTIAL

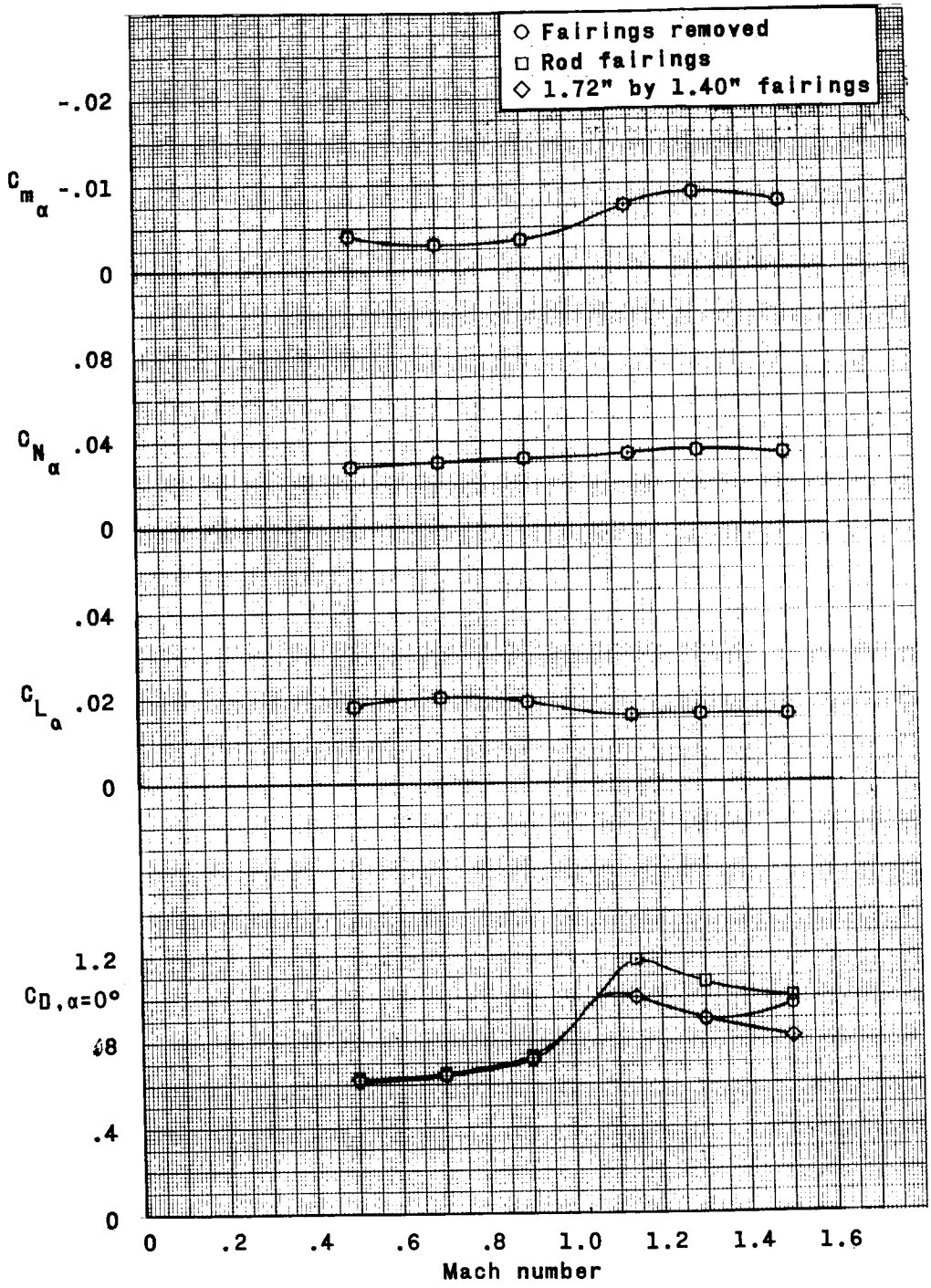

Figure 39.- Summary of the longitudinal stability characteristics of the escape configuration with and without rocket igniter-cable fairings.

[redacted]

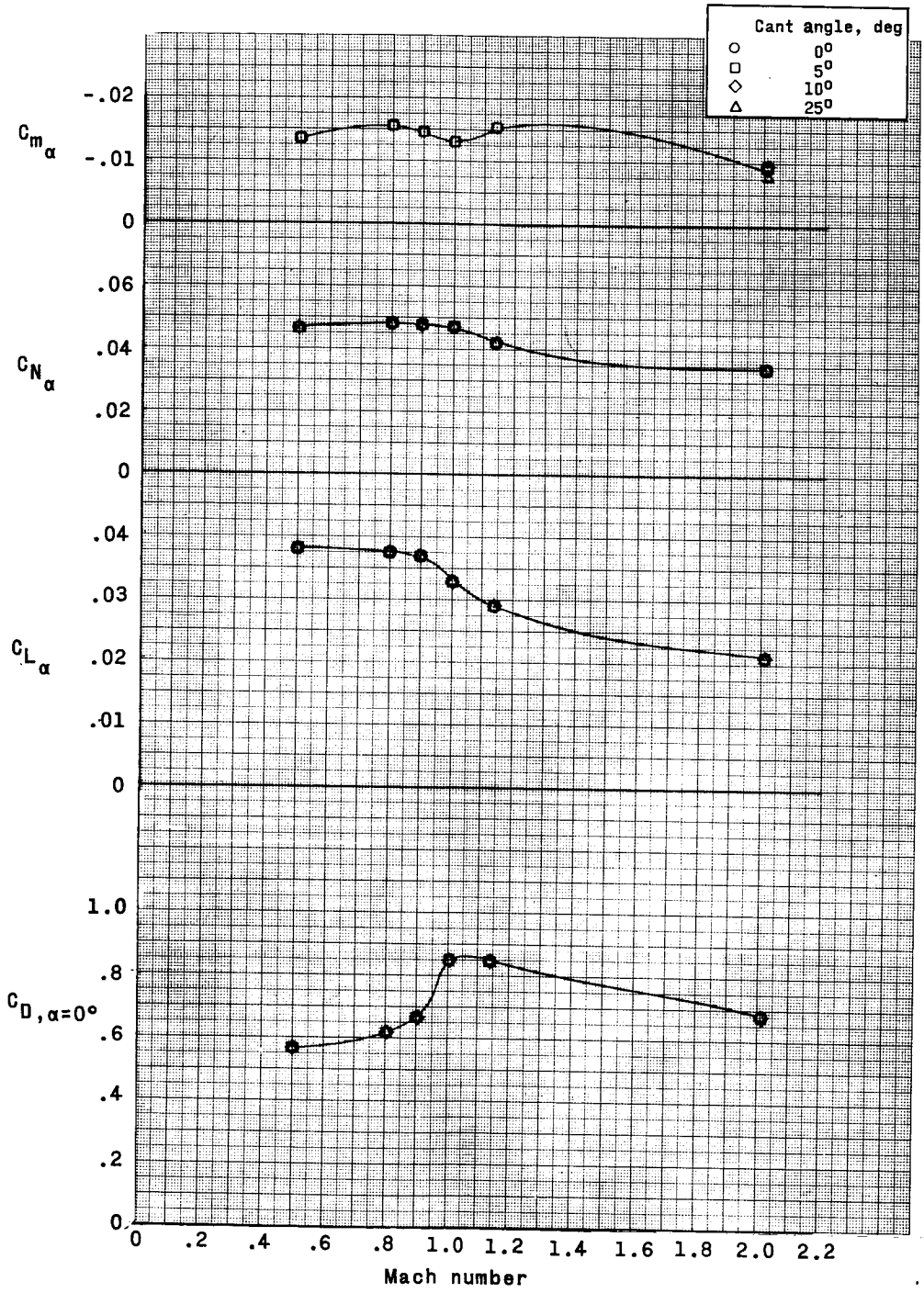

Figure 40.- Summary of the longitudinal stability characteristics of the escape configuration with and without various rocket-face cant angles.

G
6

[redacted]

[redacted]

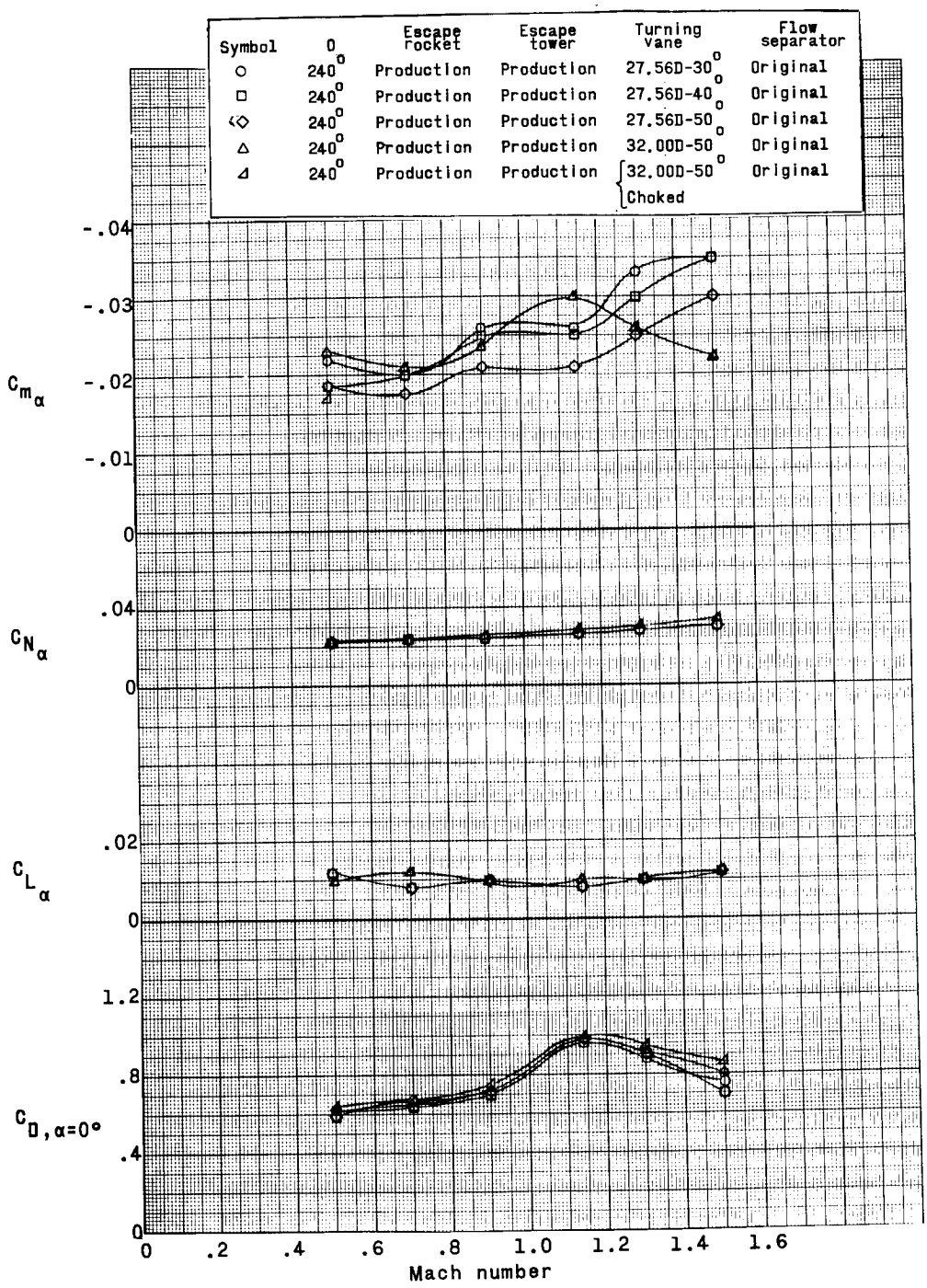

Figure 41.- Summary of the longitudinal stability characteristics of the escape configuration with various turning-vane afterbody angles.

[redacted]

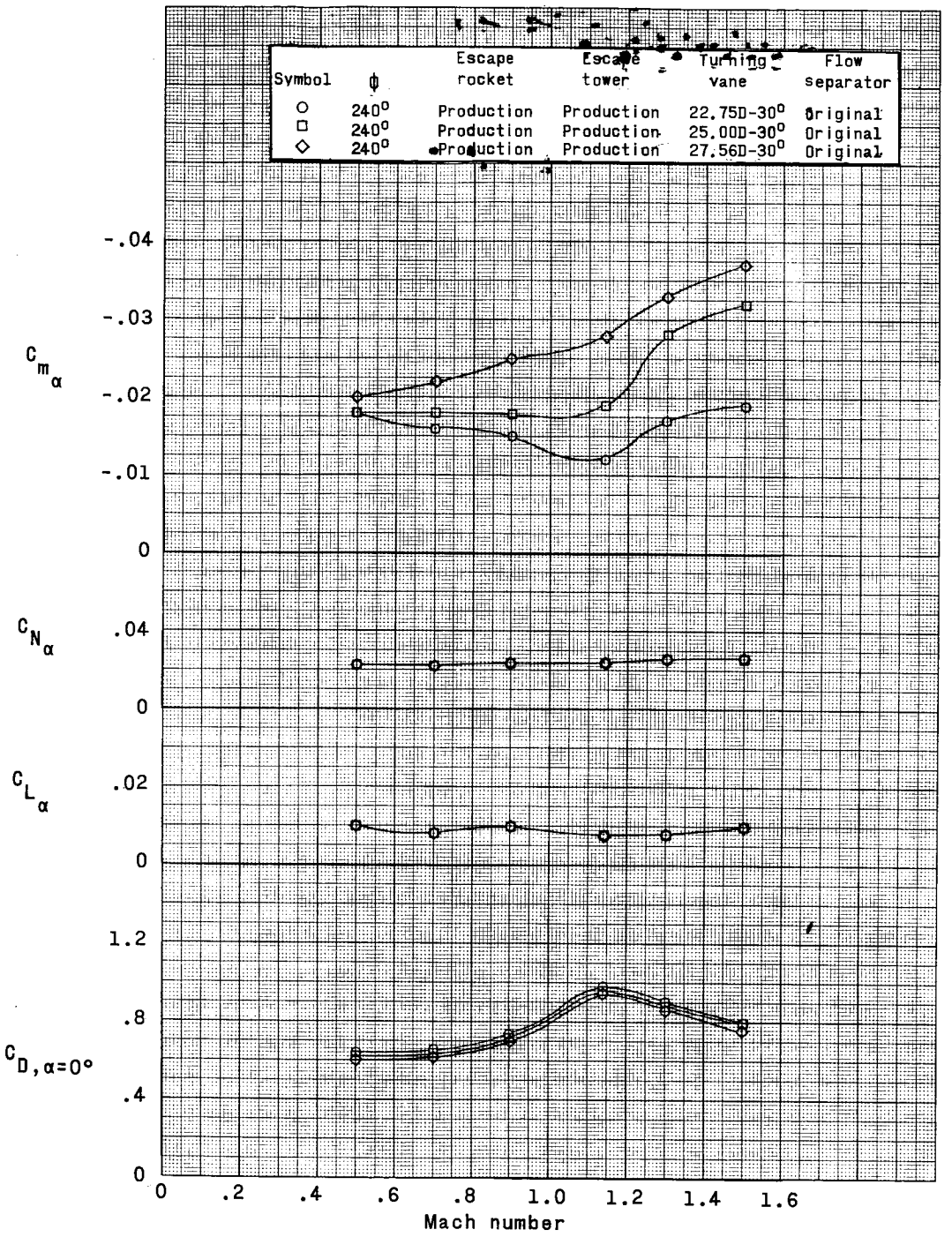

Figure 42.- Summary of the longitudinal stability characteristics of the escape configuration with various turning-vane diameters.

G
6

[redacted]

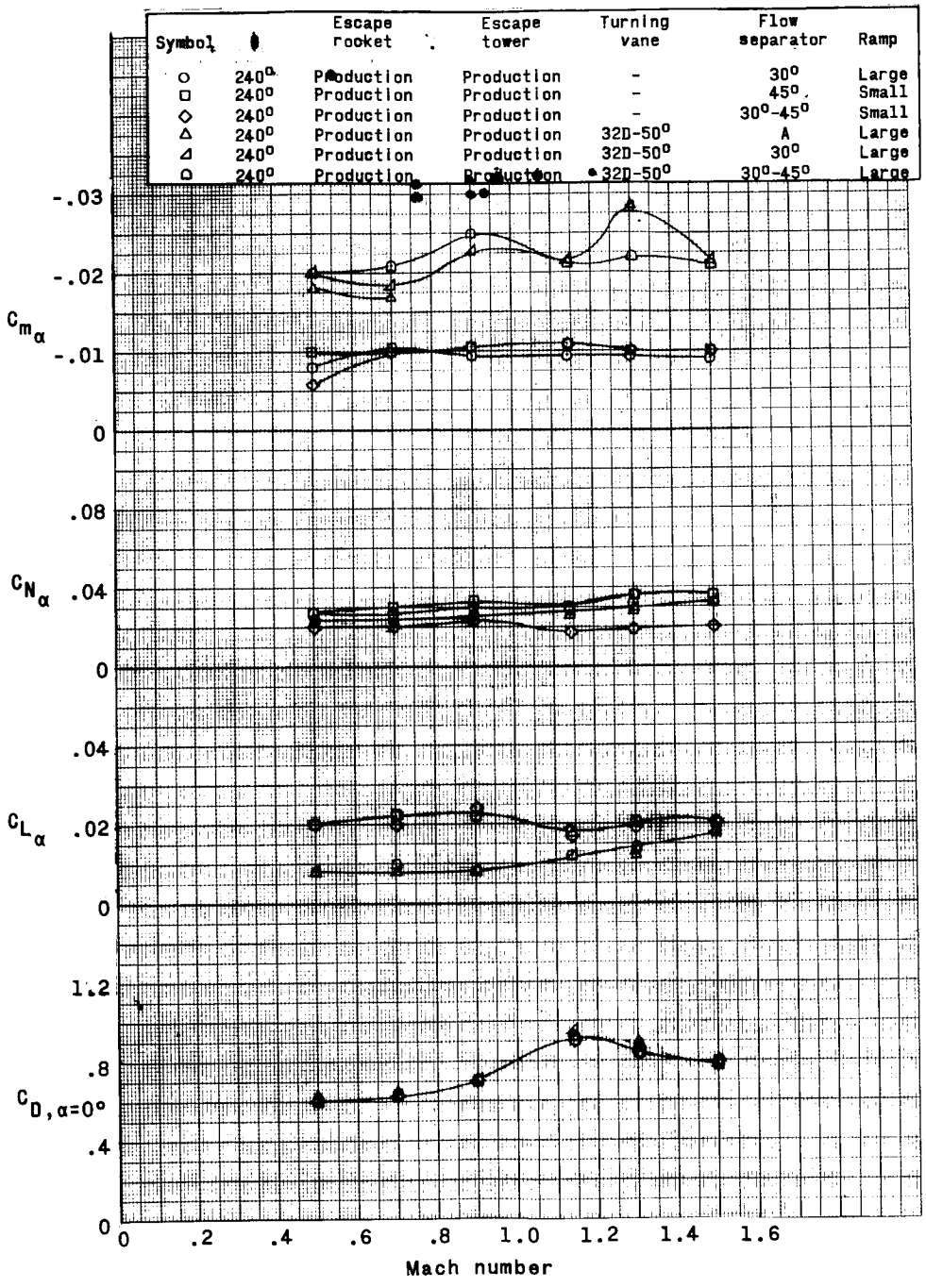

Figure 43.- Summary of the longitudinal stability characteristics of the escape configuration with various flow separators (with and without turning vanes).

[redacted]

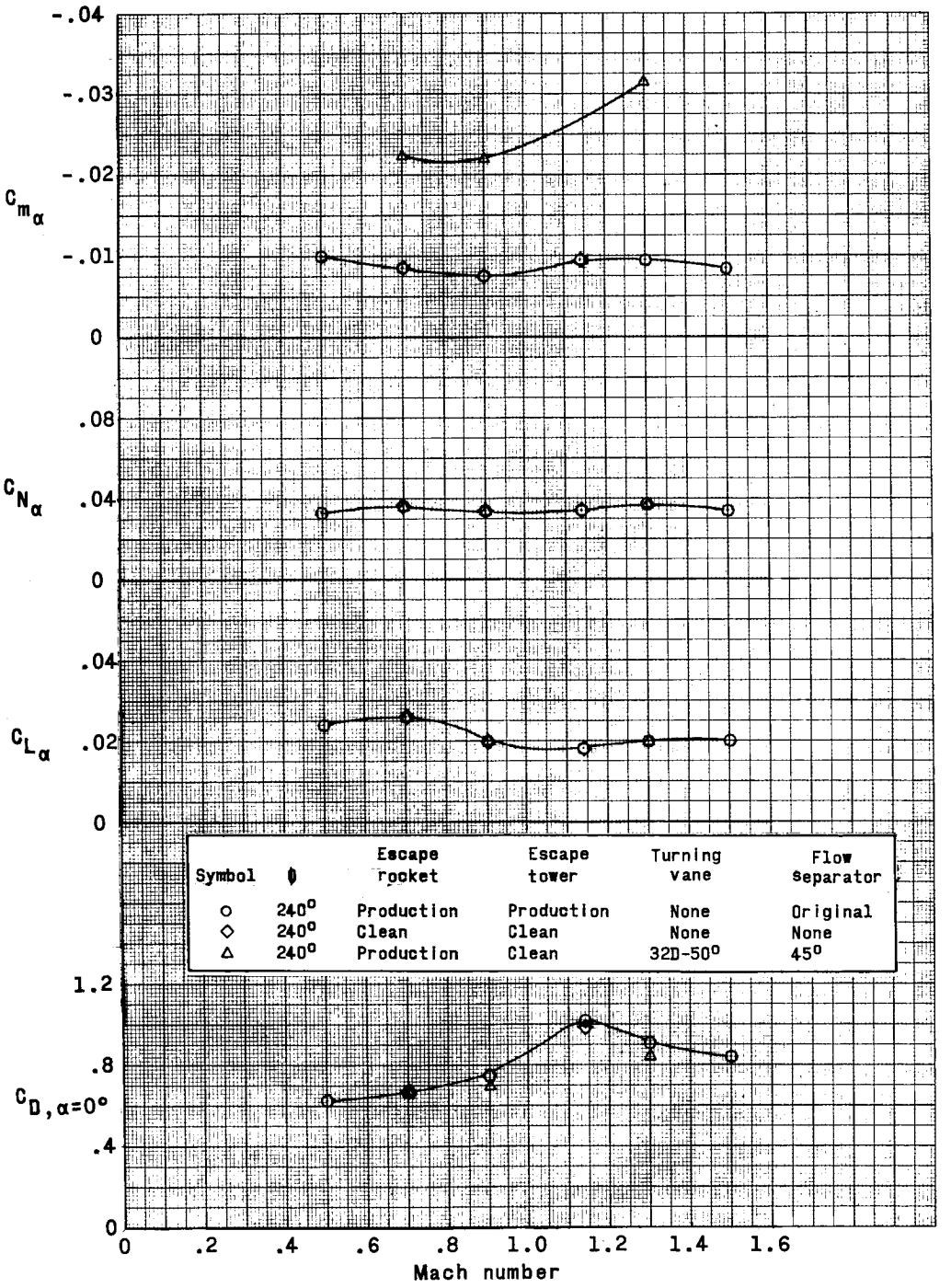

Figure 44.- Summary of the longitudinal stability characteristics of the escape configuration with various configuration modifications.

[redacted]

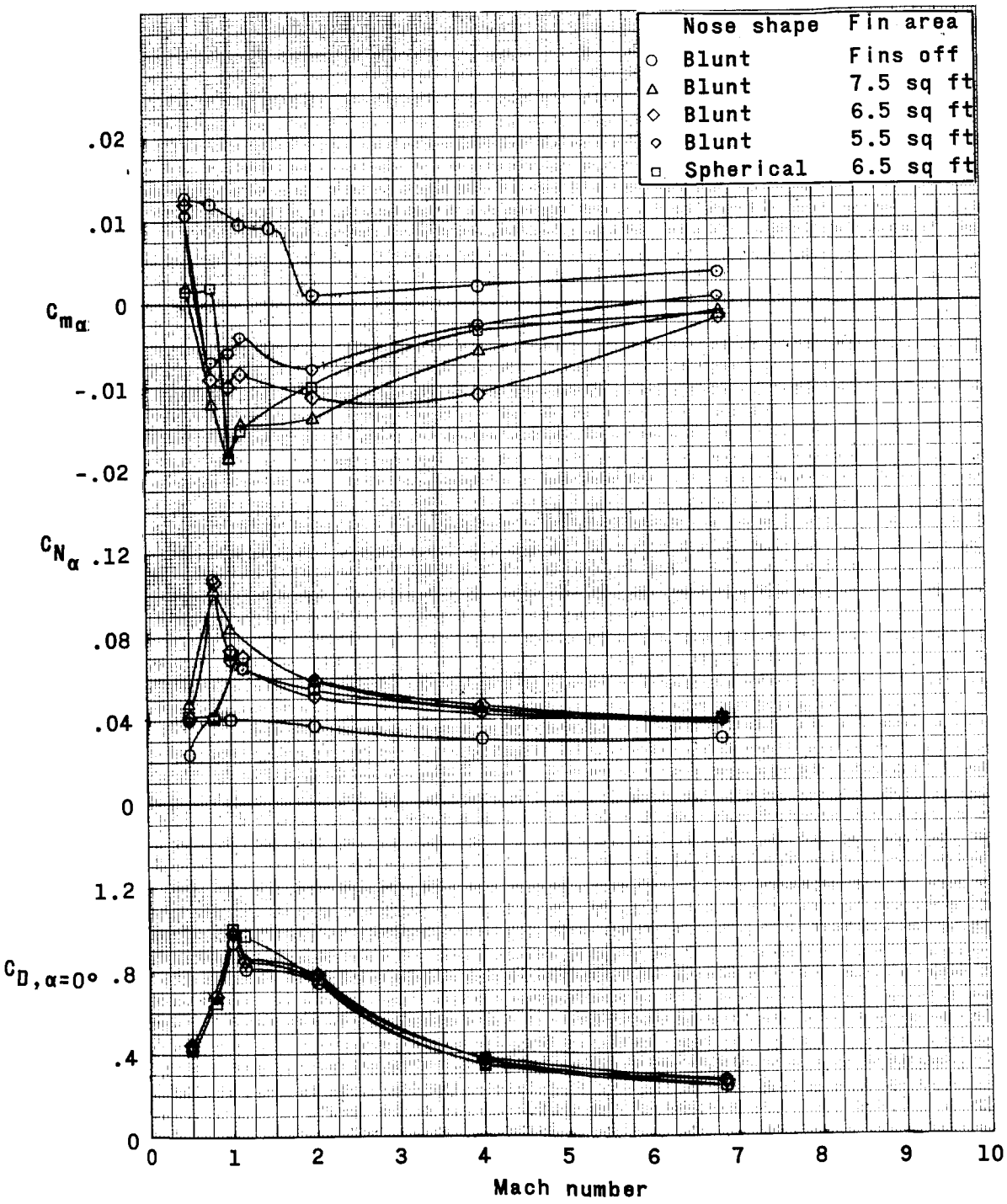

Figure 45.- Summary of the longitudinal stability characteristics of the finned-adapter escape configuration.